University of Crete
Department of Physics

Dynamic electronic and optical properties of magnetic semiconductors

Myron D. Kapetanakis

Heraklion, Greece, June 2007

Myron D. Kapetanakis

Dynamic electronic and optical properties of magnetic semiconductors

Thesis
submitted to the Department of Physics, University of Crete
for the Degree of Doctor of Philosophy in Physics

Heraklion, Greece, June 2007

Dynamic electronic and optical properties of magnetic semiconductors

Thesis author	Myron D. Kapetanakis
Thesis supervisor	Prof. Ilias Perakis
Thesis committee	N. Papanicolaou N. Tolk X. Zotos N. Kylafis V. Charmandaris J. Papadakis D. Hatzidimitriou

Department of Physics, University of Crete
Heraklion, Greece

June 2007

Contents

Chapter 1

Introduction

The interaction between itinerant carrier spins and localized magnetic moments leads to long–range ferromagnetic order in a wide variety of systems [1]. Examples include the manganese oxides (manganites) $R_{1-x}A_xMnO_3$ (R=La, Pr, Nd, Sm, $\cdots$ and A= Ca, Ba, Sr, Pb, $\cdots$) [2] and the III(Mn)V ferromagnetic semiconductors [3] such as (Ga,Mn)As and (In,Mn)As. These materials display a broad range of interesting phenomena and are of great current interest due to their novel potential applications. For example, the manganites display colossal magnetoresistance[2], where resistance can be enormously varied by small changes of the applied magnetic field. This phenomenon presents an interesting opportunity to create field effect devices, such as magnetic recording devices, based on colossal magnetoresistive materials such as the manganites. Although the manganites have been studied theoretically for years, the behavior of these material is far from well understood. Much experimental attention has recently been paid to manganese oxides due to the observation of CMR effects. Of main interest for this dissertation are the experimental investigations, related to the low–lying magnetic excitations (spin–waves). Such experiments reveal novel and anomalous properties whose origin is still unsettled despite the debate over the last decade. This system is in the strong coupling (strongly correlated) regime. The interactions are stronger than the bandwidth and the characteristic kinetic energy. Therefore correlations are expected to play an important role in describing the properties of such materials.

Furthermore, the prospect of potential applications of ferromagnetic semiconductors such as the III(Mn)V semiconductors has been recently raised. Until now, electron spin has been completely ignored in semiconductor technology which has been based solely on the charge carried by electrons. The key advance in this field is the observation of room-temperature ferromagnetism in related materials[4], which leads to the possibility of using both charge and spin in semiconductor–based devices. An emerging field in semiconductor technology, is semiconductor spintron-

ics, where is is the electron spin, instead of charge, that carries the information. The potential advantages of spin–based devices as compared with conventional semiconductor devices are indubious; increased information processing speed, decreased power consumption and increased integration densities[5](miniaturization of devices). The mean field model for carrier-induced ferromagnetism in III(Mn)V magnetic semiconductors seems to be capable of describing the thermodynamic and ground state properties. Even though in III(Mn)V semiconductors the bandwidth of the s–p valence band far exceeds the interaction energy in order to study the dynamics we need to go beyond the mean field approach and assess the role of correlations, which is a main focus of this thesis.

In materials such as that mentioned above, the magnetic and transport properties are intimately related and can be controlled by varying the itinerant carrier concentration or the dimensionality. The understanding of the magnetic excitation spectrum of such materials, beyond mean field approach, is the main emphasis of that thesis.

1.1 Spin–Waves: Magnons

In this section we discuss the collective magnetic excitations for a system of localized magnetic moments. The physical origin of these excitations, usually mentioned as magnons or spin–waves, can be understood by considering a simplified system of N local magnetic moments $\mathbf{S}_i$ with amplitude S placed on a 1D chain as in Fig. (1.1). We assume that the interactions between these magnetic moments are described by a ferromagnetic Heisenberg hamiltonian:

$$H = -\sum_{i,j} J_{ij} \mathbf{S}_i \cdot \mathbf{S}_j \tag{1.1}$$

where J_{ij} is the positive exchange interaction and i, j are indexes that run all lattice sites. A simplified Hamiltonian can be obtained from (1.1) by assuming only nearest–neighbor interactions:

$$J_{i,j} = \begin{cases} J & i = j \\ 0 & i \neq j \end{cases}$$

Within this approximation the Heisenberg hamiltonian reads:

$$H = -J \sum_i (\mathbf{S}_i \cdot \mathbf{S}_{i+1} + \mathbf{S}_{i-1} \cdot \mathbf{S}_i) \tag{1.2}$$

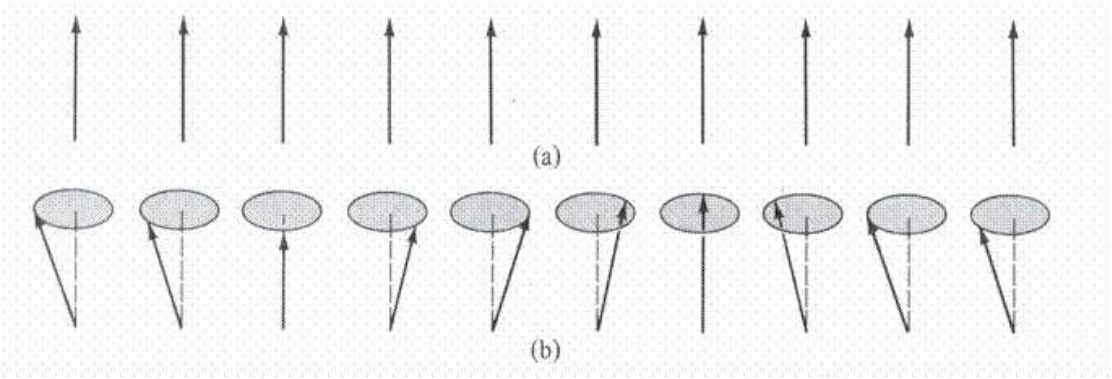

Figure 1.1: Schematic representation of the orientations in a row of spins in (a) the ferromagnetic ground state and (b) a spin wave state.

which, after using the properties for the spin operators:

$$S_i^x = \frac{1}{2}(S_i^+ + S_i^-) \tag{1.3}$$

$$S_i^y = \frac{1}{2i}(S_i^+ - S_i^-) \tag{1.4}$$

can be expressed in the form

$$H = -\frac{J}{2}\sum_i \left(S_i^z S_{i+1}^z + S_{i-1}^z S_i^z\right) \\ -\frac{J}{4}\sum_i \left(S_i^+ S_{i+1}^- + S_{i-1}^- S_i^+\right). \tag{1.5}$$

The ground state $\mid 0 >$ of a system such as the above is the ferromagnetic state, where all spins are aligned along the z-axis as illustrated in Fig. (1.1a). Using the Hamiltonian (1.5) one can calculate the ground state energy E_G and the total spin S_{tot}:

$$E_G = -JNS^2 \tag{1.6}$$

$$S_{tot} = NS. \tag{1.7}$$

A low-energy magnon can be defined in the above system as the excited state with total spin reduced by 1 as compared to the ground state. One can create such a state from the ground state (Fig. 1.1a) by first reducing the z-component of one local spin $\mathbf{S}_i$ by one:

$$\mid i >= \frac{1}{\sqrt{2S}}\mathbf{S}_i^- \mid 0 >, \tag{1.8}$$

We note that, if we act with hamiltonian (1.5) on the state $\mid i >$, we obtain a linear combination of such states:

$$H \mid i >= E_G \mid i > + JS \sum_j (\mid i > - \mid j >) \tag{1.9}$$

Therefore, the state $\mid i >$ is not an eigenstate of Hamiltonian (1.5). In order to construct an eigenstate of Heisenberg Hamiltonian we consider the following linear combination of states $\mid i >$:

$$\mid \mathbf{k} >= \frac{1}{\sqrt{N}} \sum_i e^{i\mathbf{k}\cdot\mathbf{R}_i} \mid i > \tag{1.10}$$

It can be easily shown that the state satisfies both properties of magnon eigenstate. Firstly, the total spin of the state $\mid \mathbf{k} >$ is NS-1, thus reduced by 1 as compared to the ground state $\mid 0 >$. Acting with the Heisenberg Hamiltonian on state $\mid \mathbf{k} >$ we reobtain

$$H \mid \mathbf{k} >= (E_G + \varepsilon_{\mathbf{k}}) \mid \mathbf{k} > \tag{1.11}$$

where:

$$\varepsilon_{\mathbf{k}} = SJ \sum_i (1 - e^{i\mathbf{k}\cdot\mathbf{R}_i}) \tag{1.12}$$

is the magnon energy. The physical meaning of state $\mid \mathbf{k} >$ can be understood by using the Fig. (1.1b). The reduction of S_i^z on site i creates a non-zero component $S_i^{\perp}$ perpendicular to the z-axis. Therefore, spin $\mathbf{S}_i$ now rotates around the z-axis. The superposition (1.10) of states propagates this deformation through the chain of spins like a plane wave called spin–wave or magnon. Such excitations in more complicated magnetic systems such as the manganites or the magnetic semiconductors III(Mn)V are the main focus of this thesis.

1.2 Ferromagnetism

Ferromagnetism is a macroscopic phenomenon which occurs in particular materials. A ferromagnetic material exhibits long–range magnetic order even in the absence of an external magnetic field. In these materials there are microscopic regions where the spins of individuals atoms are aligned parallel and form the well–known magnetic domains. Each one of these magnetic regions has a random orientation of its total magnetic moment. By applying an external magnetic field $\vec{B}$ however we can align the magnetic moments of the domains to be parallel with

the orientation of $\vec{B}$. Such alignment of the spins is due to interactions between the local magnetic moments and the magnetic field, which for a ferromagnet in a magnetic field $\vec{B}$ can be described to lowest order by the Hamiltonian:

$$H = -\sum_{ij} J_{ij}\mathbf{S}_i \cdot \mathbf{S}_j + g\mu_B \sum_i \mathbf{S}_i \cdot \mathbf{B} \tag{1.13}$$

where $\mathbf{S}_i$ is the total spin in region i and J_{ij} is the exchange interaction between the spins in the regions i and j. J_{ij} determines the ground state of the system described by the above hamiltonian. If the interaction between neighboring sites is positive ($J_{i,i\pm1} \geq 0$) then the ferromagnetic ground state (all spins $\uparrow$) is favored. The above model hamiltonian is commonly used to describe the properties of magnetic materials. Usually, the exchange interaction is assumed to be non–zero only between neighboring sites. Experiments in manganese oxides, a material of interest in this thesis, showed that 4^{th} nearest–neighbor interaction are important for a phenomenological description of spin–waves, while 2^{nd} and 3^{rd} order interactions are unimportant[6, 7, 8]. The physical origin of such long–range interaction, which are under debate in the literature, is the focus of chapters (3).

1.3 Long–range ferromagnetism: The key role of Double–Exchange Mechanism.

The interactions in ferromagnetic materials affect the orientation of the magnetic moments in a way that minimizes the total energy of the system. There is a variety of systems where such interactions between magnetic moments can create long–range magnetic order.

As we mentioned above, a common feature of all the systems of interest here is the strong magnetic exchange interaction between the itinerant carrier spins and the local spin–S magnetic moments. The long–range ferromagnetic order observed in magnetic systems such as the manganites and III(Mn)V magnetic semiconductors is mediated by this mechanism. A particular physical mechanism of interest here is the double–exchange mechanism which is important for manganese oxides materials such as $La_{1-x}Sr_xMnO_3$ $(0 \leq x \leq 1)$. Here x denotes hole–doping which is connected with electron–doping by $n = 1 - x$. The atomic structure of an isolated Mn atom contains five–fold degenerate 3d-orbitals. In the crystal's environment this degeneracy is partially split due to the crystall field of the surrounding atoms of oxygen. Thus we have a three-fold degenerate 3–d state, referred to as t_{2g}, and a two–fold degenerate e_g orbital, as illustrated in Fig. (1.2b). The lower energy t_{2g} orbitals contain three tightly bound electrons, which form a core

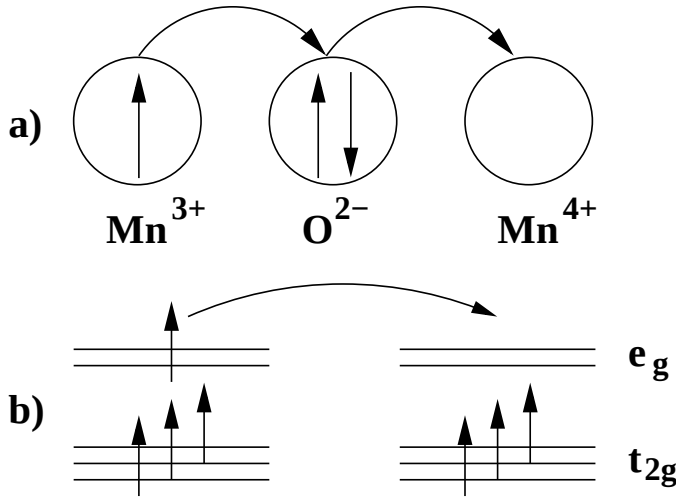

Figure 1.2: a) Schematic representation of the double–exchange mechanism b)The two bands in the manganese oxides.

spin of magnitude S=3/2, due to the large Hund's rule coupling, while e_g contains one itinerant electron. The mobility of the itinerant e_g electron is improved if all the localized spins are aligned in parallel as illustrated in Fig. (1.2b). It is not energetically favourable for an e_g electron to hop to a neighboring ion in which the t_{2g} spin is antiparallel to the spin of the e_g electron. Moreover the kinetic energy degrees of freedom further reduce the total energy. Therefore double–exchange mechanism, sketched in the Fig. (1.2a), aligns ferromagnetically the system. In Fig. 1.2a the motion of an itinerant electron from a Mn^{3+} ion to the empty e_g orbital of Mn^{4+} is shown. This hopping consists of two simultaneous motions: firstly one electron moves from the oxygen atom to Mn^{4+} and the e_g electron from the Mn^{3+} to O^{2-}. The double–exchange mechanism is named after these two motions, and is described by the Hamiltonian

$$H_{DE} = K + J \sum_i \vec{S}_i \cdot \vec{s}_i, \tag{1.14}$$

where $\vec{S}_i$ denotes a localized spin, with amplitude S and $\vec{s}_i$ an itinerant carrier. The first term in Eq. (1.14) expresses the kinetic energy of the itinerant carriers of the system. Note that only a local magnetic interaction is included in Hamiltonian (1.14). With only this term long–range ferromagnetic order is impossible, since there is no long–range coupling. The motions of the mobile carriers, described by the kinetic energy K provides such a coupling. The carriers, while hopping from one lattice site to neighboring ones, align the spins. We can understand this by viewing the crystal as a chain of wells with particles hopping from well to well.

Due to Pauli's principle, the lowest energy of this system is obtained when the mean occupancy is lower than 1. This means that only one carrier can appear at any given site each time. Moreover, these carrier spins are aligned with each other and the total carrier spin is fully polarized. Now the local magnetic–exchange interaction spreads the polarization along the lattice and therefore ferromagnetic order appears. The strength of the interaction is regulated by the parameter J. Note that the general form of Hamiltonian (1.14) can describe a variety of systems which consists of itinerant carriers and localized spins with amplitude S coupled by magnetic–exchange interaction. For the systems of interest here (1.14) can be specialized as follows. For $J < 0$ and $S = 3/2$ the above term describes double–exchange interaction in the manganites. In that case the kinetic energy K of the mobile carriers (electrons) is described by the tight binding model

$$K = -t \sum_{<ij>\sigma} c^{\dagger}_{i\sigma} c_{j\sigma}, \tag{1.15}$$

with bandwidth $t < J$ (strong coupling limit). In the case of DMS, the Mn–doping provides a hole Fermi sea and $S = 5/2$ local moments. In this way, the term K describes the kinetic energy of the valence band holes given by

$$K = \sum_{\mathbf{k}\sigma} \varepsilon_{\mathbf{k}} a^{\dagger}_{\mathbf{k}\sigma} a_{\mathbf{k}\sigma}, \tag{1.16}$$

where the s–p valence band energy $\varepsilon_{\mathbf{k}}$ is usually approximated by a quadratic formula

$$\varepsilon_{\mathbf{k}} = \frac{\hbar^2 \mathbf{k}^2}{2m_h} \tag{1.17}$$

where m_h is the effective mass of holes which in that case is $m_h = 0.5 m_e$. The above approximation is the so-called effective mass approach. More over the second term in Eq. (1.14) describes the magnetic–exchange coupling between itinerant hole and localized spin with $J > 0$. In contrast with the manganites, which are in the strong coupling regime ($t < J$), the strength J of the magnetic semiconductors is low as compared to the bandwidth (weak coupling). Therefore, in order to describe both materials we need a theory that interpolates between strong and weak coupling limit.

1.4 The materials of interest: experimental and theoretical work.

The experimental study of manganese oxides, known also as manganites, has attracted a lot of interest recently. The early experiments carried out on highly

doped samples revealed a rather trivial behavior of the magnetic excitation spectrum (spin–waves). Within this concentration regime the low–lying magnetic excitations are well described phenomenologically by the Heisenberg model which predicts a cosine–like dispersion of such excited states[9]. The striking experimental result that caused a large debate over the last 10 years was the observation of a strong deviation from Heisenberg dynamics, for intermediate electron dopings. That result, plotted in Fig. (1.3) reveals a new magnetic dynamics in manganites whose origin is not understood. The experimental measured magnon dispersion starts to deviate strongly from the fitted Heisenberg ferromagnet near to zone boundary $(0,0,\xi)$ while the effect is weaker near $(\xi,\xi,0)$ and (ξ,ξ,ξ). The understanding of the origin of this phenomenon is crucial to construct a reliable model for manganese oxides. Although a great theoretical effort has been directed to this issue, a satisfying explanation does not exist yet. Some of the mechanisms that have been proposed involve the orbital degrees of freedom, the spin–lattice interaction, the local Hubbard interaction, bandstructure effects, etc. [7, 10, 11, 12, 13]. We discuss these approximations with more details in the Chapter (2). Our contribution to this challenge is the study of the role of ubiquitous three–body correlations on the excitation spectrum of the manganites. Since the manganese oxides are strongly correlated systems, such a study is of great importance.

The main interaction which regulates ferromagnetism in such systems is the magnetic–exchange interaction between itinerant carriers and localized spins. This is ferromagnetic in the manganites. Ferromagnetic systems such as the diluted III-Mn-V magnetic semiconductors can be adequately described by a minimal model which contains only the above interaction in addition to the kinetic energy of the itinerant carriers. On the other hand, other mechanisms such as the on–site Coulomb interaction between the itinerant carriers and the super–exchange interaction between local magnetic moments are believed to participate in the dynamics of colossal magnetoresistance materials (**CMR**) such as the manganese oxides. The effects of such couplings on the magnetic excitations of the manganites is not completely understood yet, something that is one of our aims in this thesis.

Diluted magnetic semiconductors (DMS) with carrier–induced ferromagnetic order are the base of the so–call spintronic devices. In parallel with the charge–based electronics where the electron charge carries information, in spintronic technology it is the carrier's spin which plays that role. Due to the observation of room–temperature critical temperature of DMS, the potential applications of that technology is extensive. Today, room–temperature devices based on spintronics appear possible. The most promising candidate for such practical applications is the Mn–doped GaAs which Curie temperature T_C is steadily increasing over the last years reaching the maximum $T_C = 173K$ reported to date[14]. The theoretical study of magnetic semiconductors is mainly focused on the understanding of the

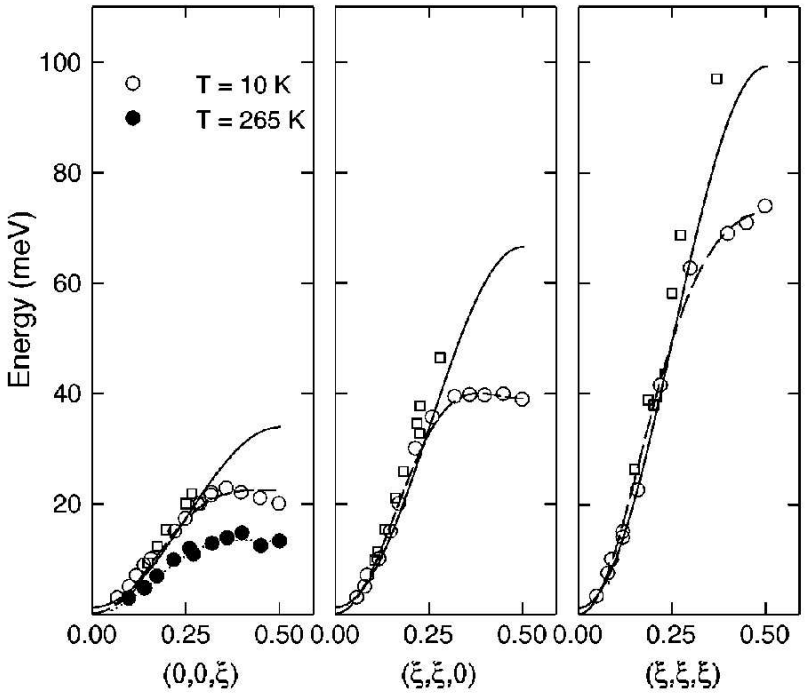

Figure 1.3: Magnon dispersion along the main directions in the Brilluin zone. Symbols: experimental results taken from Phys. Rev. Lett. **77**, 711 (1996). Solid line: fit with Heisenberg ferromagnet.

high critical temperature mechanism and the key role of doping. In this dissertation the effect of correlations is proposed to lead to an enhanced T_C of these materials and determine the magnetization dynamics important for applications. The magnetization dynamics in a ferromagnetic system such as the DMS is usually described by the phenomenological Landau–Lifshitz–Gilbert (LLG) theory[15]. In this approach the magnetization direction $\mathbf{m}$ is treated as a classical variable which obeys the well–known LLG equation

$$\frac{\partial \mathbf{m}}{\partial t} = -\gamma \mathbf{m} \times \mathbf{H}_{eff} + \alpha \mathbf{m} \times \frac{\partial \mathbf{m}}{\partial t}. \tag{1.18}$$

Here, γ is the gyromagnetic ratio and $\mathbf{H}_{eff}$ is the effective magnetic field. The latter, in general, contains the external, demagnetization and crystal–anisotropy field. The dimensionless parameter α is the so–called Gilbert damping coefficient. In the limit $\alpha = 0$, Eq. (1.18) predicts that magnetization precesses around the effective field with a frequency $\omega = \gamma H_{eff}$. On the other hand, when we switch on

damping ($\alpha > 0$) the motion of the magnetization is a spiral. After a time scale of $1/(\alpha\omega)$ $\mathbf{m}$ eventuates in a time–independent value parallel with the effective field. It is clear that the coefficient α gives a phenomenological description of the relaxation process in a ferromagnetic system. By assuming that the magnetization precesses around H_{eff} at a very small angle, which means $\omega \to 0$, we can obtain that the linear response function of such a system is of the form

$$x_{+-}(\omega \to 0) = \frac{\phi}{\omega_0 - \omega - i\alpha\omega}, \tag{1.19}$$

where $\omega_0 = \gamma H_{eff}$. Using the classical result (1.19) one can obtain a microscopic expression for α. This is achieved by comparing the classical result of Eq. (1.19) with the quantum magnetic susceptibility. The theoretical study of the physical study of constant α in III(Mn)V magnetic semiconductors has attracted considerable attention over the last years. Nevertheless, it is usually calculated within a mean field approach, where many–body effects are neglected, and its microscopic origin is not well understood. Our results of the microscopic calculation of Gilbert damping in a DMS is presented in chapter (6), where we determine the corrections on Gilbert damping coming from the ubiquitous many–body correlations.

The general outline of this thesis is briefly as follows. In the first part, containing Chapters (2–5), we focus on the study of elementary spin–wave excitations on manganese oxides. We start our study with Chapter (2) where the simple double–exchange hamiltonian is employed and a variational treatment of spin–waves is presented. The results of that chapter were published in Physical Review B **73**, 174424, (2006). Since the double–exchange mechanism is the most important coupling in strongly correlated systems, such as the manganites, a good understanding of that magnetic interaction is of major importance. Before we continue to a more realistic model it is important to understand the physics of the many–body correlations within the minimal hamiltonian. We discuss the relevance of our numerical results with the experimental observed anomalous spin–wave softening. The physical meaning of the many–body correlations is also given in that Chapter. The comparison with the experiments shows a discrepancy of the simplified double–exchange hamiltonian, something that motivates the inclusion of the local Coulomb interaction in our model Hamiltonian. The variational results of that study are presented in the Chapter (3) where a more realistic model Hamiltonian, beyond double–exchange model, is introduced. These results are published in Physical Review B, **75**, 140401(R) (2007) as a Rapid Communications. In this chapter we study the role of the on–site Coulomb and super–exchange coupling on spin–wave excitation spectrum. The local Coulomb repulsion between itinerant electrons is the largest energy scale in the manganites. Therefore, such a coupling can not be neglected in a reliable description of the magnetic excitation spectrum in the manganites. A more detailed paper with our full results is in preparation.

In the next two chapters (4–5) we introduce the green's function formalism. The application of that method allows us to determine the finite lifetime of the magnetic excitations on the manganites, which is of great importance for for understanding spin–wave and magnetization dynamics (in preparation for publishing in Physical Review B). The Green's function method demands a approximate way of terminating the infinite chain of equations of motion. We devise a decoupling scheme that reproduces the results of the previous chapters and allows us to study magnon damping. We discuss this in detail in chapter (4). The latter motivates us to apply the same method to the other material of interest here; the diluted magnetic semiconductors DMS. This is the focus of the next chapter (6). In this chapter we concentrate on the long–wavelength spin–waves which regulate the dynamics of such materials. We examine here how the many–body correlations (beyond mean field) can affect the critical temperature and spinwave stiffness of DMS. The other issue addressed in this chapter is the role of correlations on the dynamics of the magnetization relaxation process regulated by the phenomenological Gilbert damping as described above. The results of this chapter (in preparation for publishing in Physical Review **B**) give insights into the role of many–body effects in DMS, an issue that is currently under debate.

Chapter 2

Three–body correlation effects on the spin dynamics of double–exchange ferromagnets.

2.1 Introduction

Given the wide variety of ferromagnetic systems, it is important to understand the properties of the minimal Hamiltonian that describes their common properties and spin dynamics. Examples of such systems range from ferromagnetic semiconductors such as EuO, EuS, chrome spinels, or pyrochlore [1] to dilute III(Mn)V and II-VI magnetic semiconductors[19, 20]. To accomplish this goal, as well as calculate the effects of correlations beyond the mean field approximation, it is often necessary to neglect particularities of the individual systems, such as chemical structure and crystal environment. The most basic model that applies to all such materials is considered to be the Kondo lattice or double exchange Hamiltonian

$$H = K + H_{exch} + H_{super} + H_U, \tag{2.1}$$

where

$$K = -t \sum_{<ij>\sigma} c^{\dagger}_{i\sigma} c_{j\sigma}, \tag{2.2}$$

is the kinetic energy of the itinerant carriers. Here, the symbol <> means that the sum runs only over nearest neighbors, so that mobile electrons can hop from a particular lattice site i to all neighboring ones. Alternatively, the above kinetic

energy can be written in momentum space as follows:

$$K = \sum_{\mathbf{k}\sigma} \varepsilon_{\mathbf{k}} c^{\dagger}_{\mathbf{k}\sigma} c_{\mathbf{k}\sigma}. \tag{2.3}$$

In the manganites, with chemical structure ($R_{1-x}A_xMnO_3$), $n = 1 - x$ itinerant electrons per Mn atom occupy the band of Mn d–states with e_g symmetry. Following other authors, we simplify the calculation of the three–body correlations of interest here by considering a single tight–binding band of cubic symmetry and neglect the bandstructure and the degeneracy of the e_g states (which may be lifted by external perturbations). The operator $c^{\dagger}_{\mathbf{k}\sigma}$ creates an electron with momentum $\mathbf{k}$, spin σ and kinetic energy:

$$\varepsilon_{\mathbf{k}} = -2t \sum_{i=1}^{d} \cos k_i a, \tag{2.4}$$

where $d = 1, 2, 3$ is the system dimensionality and a is the lattice constant. From now on we take $a = 1$ and measure the momenta in units of $\hbar/a$.

A common feature of all the systems of interest here is the strong magnetic exchange interaction between the itinerant carrier spins $\boldsymbol{\sigma}_i$ and the local spin–S magnetic moments $\mathbf{S}_i$, which are located at the N^d lattice sites $\mathbf{R}_i$. This interaction is expressed by

$$H_{exch} = -J \sum_{i} \mathbf{S_i} \cdot \boldsymbol{\sigma}_i, \tag{2.5}$$

where the itinerant carrier spin operator has second quantization expression

$$\boldsymbol{\sigma}_i = \frac{1}{2} \sum_{\sigma\sigma'} c^{\dagger}_{i\sigma} \sigma_{\sigma\sigma'} c_{i\sigma'}. \tag{2.6}$$

In the manganites, the localized $\mathbf{S_i}$ S=3/2 spins are due to the three electrons in the tightly bound t_{2g} orbitals. Introducing the collective localized spin operator

$$\mathbf{S_q} = \frac{1}{\sqrt{N}} \sum_{j} \mathbf{S}_j e^{-i\mathbf{q}\mathbf{R}_j}, \tag{2.7}$$

and the corresponding spin lowering operator

$$S^{-}_{\mathbf{q}} = S^{x}_{\mathbf{q}} - iS^{y}_{\mathbf{q}}, \tag{2.8}$$

we express the magnetic exchange interaction in momentum space as follows:

$$\begin{aligned} H_{exch} \;=\; & -\frac{J}{2\sqrt{N}} \sum_{\mathbf{kq}\sigma} \sigma\, S^{z}_{\mathbf{q}}\; c^{\dagger}_{\mathbf{k}-\mathbf{q}\sigma} c_{\mathbf{k}\sigma} \\ & -\frac{J}{2\sqrt{N}} \sum_{\mathbf{kq}} \left(S^{-}_{\mathbf{q}}\; c^{\dagger}_{\mathbf{k}-\mathbf{q}\uparrow} c_{\mathbf{k}\downarrow} + h.c. \right), \end{aligned} \tag{2.9}$$

where $\sigma = \pm 1$. In the manganites, $J > 0$ describes the ferromagnetic Hund's rule coupling between the local and itinerant spins on each lattice site. H_{super} is the weak antiferromagnetic direct super–exchange interaction between the spins localized in neighboring sites, while H_U describes the local Coulomb (Hubbard) repulsion among the itinerant electrons in the same lattice site. The precise values of the parameters entering in the above Hamiltonian are hard to calculate for strongly coupled many–body systems such as the manganites. Although the parameter estimates vary in the literature, typical values are $t \sim 0.2$-0.5 eV and $J \sim$ 2eV, which corresponds to $4 \leq J/t \leq 10$ [22]. On the other hand, the antiferromagnetic super–exchange interaction is weak, $\sim 0.01t$. The electron concentration, $n = (N_e/N)^d = 1 - x$ where N_e is the number of electrons, varies from 0 to 1. Ferromagnetism in the metallic state of the manganites is observed within a concentration range $0.5 \leq n \leq 0.8$ in both 3D and quasi–2D (layered) systems. In this chapter we neglect the effects of H_{super} and H_U in order to focus on the role of double–exchange interaction. This is the minimal model considered by many authors as the first step towards describing the properties of the manganites. The role of these interactions will be examined in the next chapter of this dissertation.

Given the questions raised in the literature about the adequacy of the simple double exchange model for explaining the magnetic and transport properties of the manganites [22], it is important to treat the Hamiltonian H in a controlled way in the parameter regime relevant to the manganites. Such a treatment would allow us to assess the accuracy of the commonly used approximations and understand the successes and limitations of the very basic model in explaining the experiments.

Given the large values of J/t in most of the systems of interest, a widely used approximation is the $J \to \infty$ limit (double exchange ferromagnet) [23]. In this strong coupling limit, the itinerant carrier is allowed to hop on a site only if its spin is parallel to the local spin on that site. The kinetic energy is then reduced when all itinerant and local spins are parallel, which favors a ferromagnetic ground state (double exchange mechanism). We denote this fully polarized half–metallic state by $|F\rangle$

$$|F\rangle = \prod_{\nu \leq k_F} c^\dagger_{\nu\uparrow}|v\rangle \bigotimes |S, S, \cdots\rangle, \tag{2.10}$$

and note that it is an exact eigenstate of our model Hamiltonian H. This state describes local spins with $S_z = S$ on all lattice sites and a Fermi sea of spin–$\uparrow$ itinerant electrons occupying all momentum states with $\varepsilon_{\mathbf{k}} \leq E_F$, where E_F is the Fermi energy of the system.

Another approximation commonly used in the literature is to treat the local spins as classical ($S \to \infty$ limit) [22]. The ferromagnetism can then be described by an effective nearest neighbor Heisenberg model with ferromagnetic interaction.

The quantum effects are then often taken into account perturbatively in 1/S. This 1/S expansion can be implemented systematically by using the Holstein–Primakoff bosonization method [11, 24, 1]. To $O(1/S)$, this method gives noninteracting Random Phase Approximation (RPA) magnons, whose dispersion is determined by the exchange interaction [51, 25]. In the strong coupling limit $J/t \to \infty$, this RPA dispersion coincides with that of the nearest neighbor Heisenberg ferromagnet, discussed in the introduction. The $O(1/S^2)$ correction to the spin wave dispersion however deviates from this Heisenberg form. This deviation comes from the scattering of the RPA magnon with the spin–$\uparrow$ electron Fermi sea. The $O(1/S^2$ approximation corresponds to treating this to lowest order in the electron–magnon interaction strength (Born approximation). [11, 24] In order to assess the success of the minimal Hamiltonian in describing the manganites beyond $O(1/S^2)$, it is important to study the role of correlations. So far, the role of nonperturbative carrier–magnon correlations (beyond $O(1/S^2)$) has been studied by exact diagonalization of small and 1D systems [26, 27] or by using variational wavefunctions [29, 31] inspired by the Hubbard model and the Gutzwiller wavefunction [32, 62, 33, 34]. The variational calculations of Refs.[29, 31] treat the local correlations expected to dominate in the strong coupling limit [62]. The ferromagnetic (Nagaoka) state $|F\rangle$ was shown to become unstable with increasing electron concentration due to the softening of either single particle spin excitations [33] or long wavelength spin wave excitations (negative stiffness)[29, 31]. The spin wave dispersion deviated from the Heisenberg form for very small electron concentrations[31]. In the concentration range $0.5 \leq n \leq 0.8$ relevant to the manganites, Wurth *et.al.* [31] found small deviations from the Heisenberg form. A similar conclusion was reached based on the 1/S expansion[24]. For $n \sim 0.7$, the $O(1/S^2)$ magnon dispersion showed a relative hardening at the zone boundary in the strong coupling limit [24].

Due to the interplay between the spin and charge degrees of freedom, a good understanding of the spin dynamics is important for understanding the physics of colossal magnetoresistance and transport in the manganites. In order to understand the spin dynamics, the excitations of the spin degrees of freedom must be studied experimentally. Several such experimental studies of the spin wave excitation spectrum have been reported in the literature. Heisenberg–like magnons were observed in the ferromagnetic regime for high electron concentrations (typically $n > 0.7$) [9]. This observation is consistent with the spin wave spectrum obtained in the classical spin limit or by using the strong coupling RPA. However, most importantly for our purposes here, for lower electron concentrations $0.5 \leq n \leq 0.7$, unexpectedly strong deviations from the short range Heisenberg magnon dispersion were observed in several different manganites [35, 36, 37, 38, 7, 39, 40]. Most striking is the pronounced softening of the spin wave dispersion and short magnon life-

time close to the zone boundary, which indicate a new spin dynamics in the metallic ferromagnetic phase for intermediate electron concentrations $0.5 \leq n \leq 0.7$. The physical origin of this dynamics remains under debate despite many years of theoretical work. It has been conjectured that the coupling to additional degrees of freedom not included in the double exchange Hamiltonian H is responsible for this new spin dynamics. Some of the mechanisms that have been proposed involve the orbital degrees of freedom, the spin–lattice interaction, the local Hubbard interaction, bandstructure effects, etc. [7, 10, 11, 12, 13].

In this chapter we study variationally the low energy spin excitations of the half–metallic fully polarized state $|F\rangle$. Our focus is on the role of correlations described by the minimal Hamiltonian and assess whether they might by responsible for the experimentally observed anomaly. Our theory treats exactly up to three–body correlations between a magnon and a Fermi sea pair by using the most general variational wavefunction that includes up to one Fermi sea pair excitations. As already noted in the context of the Hubbard model, [62, 34] the Gutzwiller wavefunction, which treats local correlations, [31, 29] is a special case of our wavefunction. Here we treat both local and long–range correlations on equal footing in momentum space in order to interpolate between the weak and strong coupling limits with the same formalism. We show that it is important for describing realistic systems to depart from the strong coupling limit. We treat nonperturbatively in a variational way the multiple electron–magnon and hole–magnon scattering processes that lead to vertex corrections of the carrier–magnon interaction. The above two scattering channels are *coupled* by three–body correlations. We show that this coupling is important for the intermediate electron concentrations and exchange interactions relevant to the manganites, while for small (large) n the electron–magnon (hole–magnon) scattering channel dominates. In the case of the 1D Hubbard model, a similar three–body treatment gave excellent agreement with the exact results [41]. Analogous calculations were performed to describe the electron–Fermi sea pair local Hubbard interactions [41, 62, 34] and the valence (or core) hole–Fermi sea pair interactions that lead to the Fermi Edge (X–ray Edge) Singularity [42, 43].

Our variational wavefunction offers several advantages. While local correlations [31, 29] dominate in the strong coupling limit, long range correlations become important as J/t decreases [62]. The phenomenogical fits to the experimental results indicate the importance of long range correlations. By working in momentum space, we treat both long and short range correlations while addressing both the weak and strong coupling limits with the same formalism. We therefore expect that our results interpolate well for the intermediate values of J/t relevant to the manganites. [62] Our wavefunction satisfies momentum conservation automatically, which reduces the number of independent variational parameters. Further-

more, our results become exact in the two limits of $N_e = 1$ and $N_e = N^d$. We therefore expect that they interpolate well for intermediate electron concentrations $0 < n < 1$. Our variational equations contain previously used approximations such as the RPA ($O(1/S)$), ladder diagram approximation, and $O(1/S^2)$ results as special cases. Finally, our results converge with increasing system size N and thus apply to the thermodynamic limit. The only restriction is that we neglect contributions from two or more Fermi sea pair excitations. Such multipair contributions are however suppressed for large S, while their contribution in the case of the 1D Hubbard model was shown to be small [41, 43].

Here we address a number of issues regarding the effects of up to three–body carrier–magnon correlations on the spin dynamics predicted by the simplest double exchange Hamiltonian. First, by comparing to the 1/S expansion, RPA, and ladder approximation results, we show that vertex corrections and long range three–body magnon–Fermi sea pair correlations, which couple the electron–magnon and hole magnon scattering channels, play an important role on the spin dynamics in the parameter regime relevant to the manganites. We find large deviations from the strong coupling double exchange spin wave dispersion, including a strong magnon softening at the zone boundary in the intermediate electron concentration and exchange interaction regime. On the other hand, for small electron concentrations (relevant e.g. in III(Mn)V semiconductors [19, 20]), the electron-magnon multiple scattering processes dominate. However, even in this regime the deviations from the RPA and $O(1/S^2)$ magnon dispersions can be strong.

Second, by using an unbiased variational wavefunction, we determine the change in the ferromagnetic phase boundary due to the three–body correlations and carrier–magnon vertex corrections (not included to $O(1/S^2)$). The variational nature of our calculation allows us to rigorously conclude that the ferromagnetic state $|F\rangle$ is unstable when its energy exceeds that of the variational spin wave energy. In addition to the long wavelength softening and eventual instability, which occurs in all dimensions, we find another instability for momenta close to the zone boundary while the stiffness remains positive. This instability only occurs in 2D and 3D for intermediate electron concentrations ($0.4 \leq n \leq 0.7$ for the 2D three–body calculation). This effect is exacerbated by the three–body correlations. One should contrast the above instability to the spin wave softening (but not instability) at the zone boundary that occurs for small $n < 0.3$ [24, 11, 31].

Third, we study the deviations from the Heisenberg spin wave dispersion induced by the three–body correlations and vertex corrections. This comparison is important given the experimental observation of pronounced deviations for $n \leq 0.7$ [35, 36, 37, 38, 7, 39, 40]. Deviations from Heisenberg behavior already occur to $O(1/S^2)$, or even to $O(1/S)$ for finite J/t, but in most cases correspond to magnon hardening[24]. By comparing our results to the Heisenberg dispersion with the

same stiffness, we show that, for values of J/t relevant to the manganites and such that the ferromagnetic state is stable up to $n \sim 0.8$ or higher, the three–body correlations in the 2D system give magnon hardening at the zone boundary for $n \leq 0.4$ followed by strong magnon softening for $0.4 < n \leq 0.7$ and then small magnon hardening for $n > 0.7$. This behavior is similar to the experiment.

The outline of this Chapter is as follows. In Section 2.2 we discuss the four approximations we use to calculate the effects of the carrier–magnon correlations on the spin wave dispersion. In Subsection 2.2.1 we obtain variationally the well–known RPA magnon dispersion. In Subsection 2.2.2 we discuss the variational wavefunction that treats the three–body correlations. The variational equations that determine the spin wave dispersion are presented in Subsection 2.2.3. In Subsection 2.2.4 we establish the connection between the above variational results and the 1/S expansion results[24, 11]. We show, in particular, that the $O(1/S^2)$ magnon dispersion can be obtained from our variational equations by treating the carrier–magnon scattering to lowest order in the corresponding interaction strength (Born approximation). In Subsection 2.2.5 we discuss the two–body ladder approximation, obtained from our variational results by neglecting the coupling between the electron–magnon and hole–magnon scattering channels. In Subsection 2.2.6 we discuss the approximation of carrier–localized spin scattering and show that this variational treatment improves on the RPA while making the numerical calculation of three–body effects feasible in much larger systems. In Section 2.3 we present our numerical results for the spin wave dispersion, ferromagnetic phase diagram, and deviations from Heisenberg dispersion in the 1D, 2D, and 3D systems and compare between the different approximations. Finally we end with the conclusions in Section 2.4.

2.2 Calculations

In this section we discuss the four approximations that we use to treat the effects of the carrier–magnon correlations. From now on we measure the energies $\omega_{\mathbf{Q}}$ of the spin wave states with respect to that of the fully polarized (half–metallic) ferromagnetic state $|F\rangle$, whose stability and low energy spin excitations we wish to study. We note that $|F\rangle$ is an exact eigenstate of the Hamiltonian H with maximum spin value and total spin z–component $N(S + n/2)$. To study the stability of this state in a controlled way, it is important to use approximations that allow us to draw definite conclusions. This is possible with the variational principle, which allows us to conclude that a negative excitation energy $\omega_{\mathbf{Q}}$ means instability of $|F\rangle$, driven by the spin wave of momentum $\mathbf{Q}$. Our variational states have the form $|\mathbf{Q}\rangle = M^{\dagger}_{\mathbf{Q}}|F\rangle$, where the operator $M^{\dagger}_{\mathbf{Q}}$ conserves the total momentum,

lowers the z–component of the total spin by 1, and includes up to one Fermi sea pair excitations. A spin wave has total spin z–component of $N(S+n/2)-1$, which corresponds to one reversed spin as compared to $|F\rangle$. This spin reversal can be achieved either by lowering the localized spin z–component by 1 or by coherently promoting an electron from the spin–$\uparrow$ band to the spin–$\downarrow$ band. The spin reversal can be accompanied by the scattering (shakeup) of Fermi sea pairs. From now on we use the indexes $\nu, \mu, \cdots$ to denote single electron states inside the Fermi surface and $\alpha, \beta, \cdots$ to denote states outside the Fermi surface. For a more detailed presentation of our variational theory see appendix 8.1.

2.2.1 The RPA result

We start the discussion of the approximations by showing firstly that the well known RPA magnon dispersion [51, 25] can be obtained variationally for any value of J/t by neglecting in $M^{\dagger}_{\mathbf{Q}}$ all Fermi sea pair excitations. The most general such operator has the form:

$$M^{\dagger}_{\mathbf{Q}RPA} = S^{-}_{\mathbf{Q}}|F\rangle + \frac{1}{\sqrt{N}}\sum_{\nu} X^{\mathbf{Q}RPA}_{\nu} c^{\dagger}_{\mathbf{Q}+\nu\downarrow}c_{\nu\uparrow}, \tag{2.11}$$

The explicit form of the variational equations within RPA is obtained easily after some algebra. The variational equations for the N_e amplitudes X^{RPA}_{ν} and for the magnon energy are given by

$$\omega^{RPA}_{\mathbf{Q}} = \frac{Jn}{2} - \frac{J}{2N}\sum_{\nu} X^{\mathbf{Q}RPA}_{\nu}, \tag{2.12}$$

$$X^{\mathbf{Q}RPA}_{\nu} = \frac{JS}{JS + \varepsilon_{\nu+\mathbf{Q}} - \varepsilon_{\nu} - \omega^{RPA}_{\mathbf{Q}}}. \tag{2.13}$$

This full RPA result can also be obtained as the zeroth order contribution to an expansion in powers of 1/n, where n is the number of electron flavors and corresponding degenerate electron bands. [47] In the strong coupling limit $JS \to \infty$, $X^{RPA} \to 1$ and $M^{\dagger}_{\mathbf{Q}RPA}$ reduces to the total spin operator. To lowest order in t/JS we obtain from Eqs. (2.12) and (2.13) that the RPA dispersion then reduces to the Heisenberg dispersion

$$\omega^{RPA}_{\mathbf{Q}} = \frac{1}{2N}\frac{1}{S+n/2}\sum_{\nu<k_F}(\varepsilon_{\mathbf{v}\nu+\mathbf{Q}} - \varepsilon_{\nu}) + O(t/JS). \tag{2.14}$$

The $O(1/S)$ magnon dispersion [24, 51] is obtained from the above strong coupling RPA result by replacing the total spin prefactor $S+n/2$ by S.

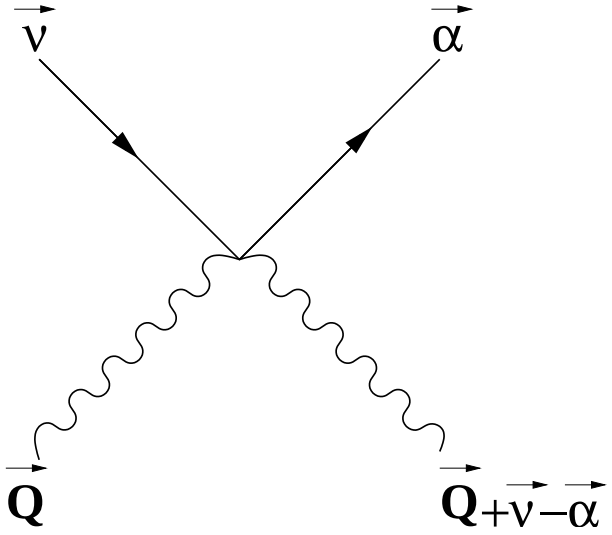

Figure 2.1: The scattering between an electron and a magnon as described by wavefunction (2.15). solid line: itinerant electron, wave line: magnon.

2.2.2 Three–body Correlations

We now include in $M^{\dagger}_{\mathbf{Q}}$ the most general contribution of the one Fermi sea pair states:

$$M^{\dagger}_{\mathbf{Q}} = S^{-}_{\mathbf{Q}} + \frac{1}{\sqrt{N}} \sum_{\nu} X^{\mathbf{Q}}_{\nu}\ c^{\dagger}_{\mathbf{Q}+\nu\downarrow} c_{\nu\uparrow} + \sum_{\alpha\mu} c^{\dagger}_{\alpha\uparrow} c_{\mu\uparrow} \times$$

$$\left[\Psi^{\mathbf{Q}}_{\alpha\mu}\ S^{-}_{\mathbf{Q}+\mu-\alpha} + \frac{1}{2\sqrt{N}} \sum_{\nu} \Phi^{\mathbf{Q}}_{\alpha\mu\nu} c^{\dagger}_{\mathbf{Q}+\mu-\alpha+\nu\downarrow} c_{\nu\uparrow} \right], \qquad (2.15)$$

where the amplitudes $X^{\mathbf{Q}}_{\nu}$, $\Psi^{\mathbf{Q}}_{\alpha\mu}$ and $\Phi^{\mathbf{Q}}_{\alpha\mu\nu}$ are all determined variationally; we do not use the RPA results for $X^{\mathbf{Q}}$. As compared to previous calculations, we do not assume any particular form or momentum dependence for the above variational amplitudes. This allows us to treat in an unbiased way the long range correlations for any value of J/t. The first two terms on the rhs of Eq.(2.15) create a magnon of momentum $\mathbf{Q}$. The last two terms describe the scattering of a momentum $\mathbf{Q}$ magnon to momentum $\mathbf{Q} + \nu - \alpha$ with the simultaneous scattering of a Fermi sea electron from momentum $\mu < k_F$ to momentum $\alpha > k_F$ and the creation of electron–hole pair. This scattering is shown schematically in the Fig. (2.1). Our wavefunction Eq. (2.15) becomes exact in the two limits of $N_e = 1$ and $N_e = N^d$. To see this, we note that, for $N_e = 1$, the Fermi sea consists of a single electron. As a result, multipair excitations do not contribute, while $\Phi^{\mathbf{Q}} = 0$. In the half–filling limit $N_e = N^d$, all lattice sites are occupied by one spin–$\uparrow$ electron and the

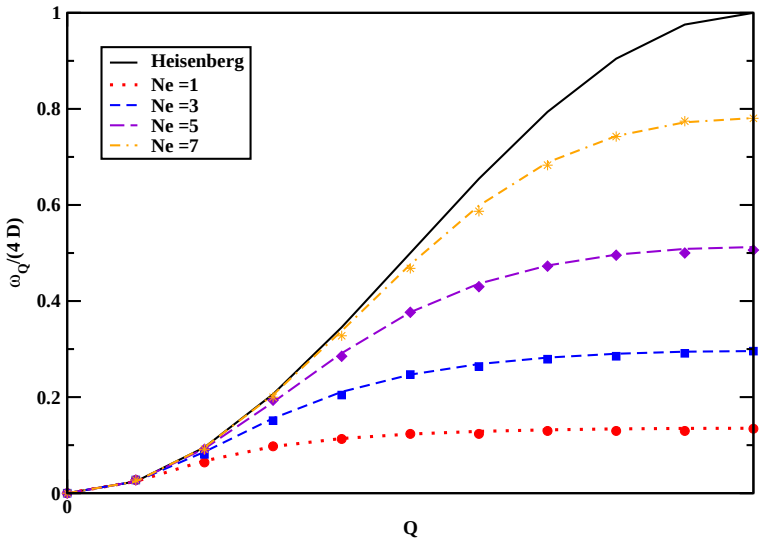

Figure 2.2: Spin-wave dispersion at the $J \to \infty$ limit in a 1D system with N =20, S =1/2 and for number of electrons Ne =1, 3, 5, 7. The points in the figure show exact results.

Fermi sea occupies all momentum states up to the zone boundary. As a result, the RPA wavefunction Eq. (2.11) becomes exact. Eq. (2.15) also gives the exact wavefunction in the atomic limit $t = 0$, $\varepsilon_k = 0$, where the variational amplitudes do not depend on the electron momenta. To see this, we note that, due to the Pauli principle, $\Phi^{\mathbf{Q}}_{\alpha\mu\nu}$ must be antisymmetric with respect to the exchange of the Fermi sea electron momenta ν and μ. In the atomic limit, $\Phi^{\mathbf{Q}}$ therefore vanishes since it is independent of the momenta. For the same reason, all multipair amplitudes vanish as well and Eq.(2.15) gives the exact result. The above exact results give us confidence that our wavefunction and variational calculations provide an adequate way for interesting parameter regions where exact results are not possible. Further confidence in our results is provided by the fact that we reproduce exact numerical calculations of such systems made by exact diagonalization of small 1D system [26, 27]. Fig (2.2) shows this comparison. We see that our results are in very good agreement with the exact calculations.

2.2.3 The variational equations

In this section we present the variational equations that determine the wavefunction amplitudes $X^{\mathbf{Q}}$, $\Psi^{\mathbf{Q}}$, and $\Phi^{\mathbf{Q}}$ for the simple double–exchange hamiltonian.

These are obtained by minimizing the variational energy $\langle F|M_{\mathbf{Q}}HM_{\mathbf{Q}}^{\dagger}|F\rangle$, where $M_{\mathbf{Q}}^{\dagger}$ is given by Eq.(2.15), with respect to the above variational amplitudes. The normalization condition $\langle F|M_{\mathbf{Q}}M_{\mathbf{Q}}^{\dagger}|F\rangle = 1$ is enforced via a Lagrange multiplier, which coincides with the variational magnon energy $\omega_{\mathbf{Q}}$. Similar to the three–body Fadeev equations, the resulting variational equations are equivalent to solving the Schrödinger equation within the subspace spanned by the states $S_{\mathbf{Q}}^{-}|F\rangle$ and $c_{\mathbf{Q}+\nu\downarrow}^{\dagger}c_{\nu\uparrow}|F\rangle$, which describe all possible configurations with one reversed spin and no Fermi sea excitations, and the magnon–Fermi sea pair states $c_{\alpha\uparrow}^{\dagger}c_{\nu\uparrow}S_{\mathbf{Q}+\nu-\alpha}^{-}|F\rangle$ and $c_{\alpha\uparrow}^{\dagger}c_{\nu\uparrow}c_{\mathbf{Q}+\mu+\nu-\alpha\downarrow}^{\dagger}c_{\mu\uparrow}|F\rangle$ to which a magnon or spin flip excitation can scatter with the simultaneous excitation of a Fermi sea pair. We note that the above momentum space basis ensures the conservation of momentum and total spin. The explicit form of the variational equations is obtained after straightforward algebra by projecting the Schrödinger equation $[H, M_{\mathbf{Q}}^{\dagger}]|F\rangle = \omega_{\mathbf{Q}}|F\rangle$ in the above basis after calculating the commutator $[H, M_{\mathbf{Q}}^{\dagger}]$ by using Eq.(2.15) for $M_{\mathbf{Q}}^{\dagger}$ and noting that $H|F\rangle = 0$ (we take the energy of $|F\rangle$ as zero). The variational equation that gives the energy $\omega_{\mathbf{Q}}$ reads

$$\omega_{\mathbf{Q}} = \frac{Jn}{2} - \frac{J}{2N}\sum_{\nu} X_{\nu}^{\mathbf{Q}} + \frac{J}{2N}\sum_{\alpha\nu}\Psi_{\alpha\nu}^{\mathbf{Q}}. \tag{2.16}$$

The last term in the above equation describes the contribution due to the carrier–magnon scattering. The first two terms on the rhs give the RPA magnon energy if $X_{\nu}^{\mathbf{Q}}$ is substituted by its RPA value, obtained for $\Psi^{\mathbf{Q}} = 0$. The carrier–magnon scattering however renormalizes $X_{\nu}^{\mathbf{Q}}$ as compared to the RPA result:

$$\left(JS + \varepsilon_{\nu+\mathbf{Q}} - \varepsilon_{\nu} - \omega_{\mathbf{Q}}\right) X_{\nu}^{\mathbf{Q}} = JS\left[1 + \sum_{\alpha}\Psi_{\alpha\nu}^{\mathbf{Q}}\right]. \tag{2.17}$$

The first term on the rhs of the above equation gives the RPA contribution to $X_{\nu}^{\mathbf{Q}}$, while the second term, as well as the correlation contribution to the magnon energy $\omega_{\mathbf{Q}}$, describe the effects of the magnon–carrier scattering. Note that the RPA result Eqs. (2.12) and (2.13) is obtained from Eqs. (2.16) and (2.17) after setting $\Psi = \Phi = 0$. The scattering amplitude $\Psi^{\mathbf{Q}}$ is determined by the variational equation

$$\begin{aligned}\left(\omega_{\mathbf{Q}} - \frac{Jn}{2} + \varepsilon_{\nu} - \varepsilon_{\alpha}\right)\Psi_{\alpha\nu}^{\mathbf{Q}} &= \frac{J}{2N}\left(1 - X_{\nu}^{\mathbf{Q}}\right) \\ +\frac{J}{2N}\sum_{\alpha'}\Psi_{\alpha'\nu}^{\mathbf{Q}} - \frac{J}{2N}\sum_{\nu'}\Psi_{\alpha\nu'}^{\mathbf{Q}} &- \frac{J}{2N}\sum_{\nu'}\Phi_{\alpha\nu'\nu}^{\mathbf{Q}}.\end{aligned} \tag{2.18}$$

The first term on the rhs of the above equation gives the Born scattering approximation contribution to the carrier–magnon scattering amplitude, which is the

only one that contributes to $O(1/S^2)$ in magnon energy Eq. (2.16). The next two terms describe the effects of the multiple electron–magnon (second term) and hole magnon (third term) scattering. Finally, the last term comes from the electronic contribution to the scattered magnon, i.e. from the coherent excitation of a spin–$\uparrow$ electron to the spin–$\downarrow$ band. The amplitude Φ^Q of the latter contribution to Eq.(2.15) is given by the variational equation

$$\left(JS + \varepsilon_{\mathbf{Q}+\mu+\nu-\alpha} - \varepsilon_\mu + \varepsilon_\alpha - \varepsilon_\nu - \omega_{\mathbf{Q}}\right) \Phi^{\mathbf{Q}}_{\alpha\nu\mu} = JS\left(\Psi^{\mathbf{Q}}_{\alpha\nu} - \Psi^{\mathbf{Q}}_{\alpha\mu}\right). \tag{2.19}$$

We note that, in the strong coupling limit $J \to \infty$, $\Phi^{\mathbf{Q}}_{\alpha\nu\mu} \to \Psi^{\mathbf{Q}}_{\alpha\nu} - \Psi^{\mathbf{Q}}_{\alpha\mu}$ and the last two terms in Eq. (2.15) describe the scattering of a Fermi sea pair with the strong coupling RPA magnon created by the total spin lowering operator $S^-_{\mathbf{Q}} + \frac{1}{\sqrt{N}} \sum_\nu c^\dagger_{\mathbf{Q}+\nu\downarrow} c_{\nu\uparrow}$. Our general wavefunction Eq. (2.15) does not assume an RPA magnon and includes corrections to the strong coupling limit results that we show are important for the values of J/t relevant to the manganites. One can see by conjecturing the corresponding matrix elements that multipair contributions wavefunction Eq. (2.15) contribute to $O(1/S^3)$ or higher. Therefore, our calculation reproduces the $O(1/S^2)$ results however treats vertex correlations variationally to all orders in $1/S$. This variational nature allows us to draw define conclusions we discuss below.

A closed equation for the carrier–magnon scattering amplitude $\Psi^{\mathbf{Q}}$ can be obtained by substituting in Eq. (2.18) the expressions for $\Phi^{\mathbf{Q}}$ and $X^{\mathbf{Q}}$ obtained from Eqs. (2.19) and (2.17). Defining the excitation energy

$$\begin{aligned} \Delta^{\mathbf{Q}}_{\alpha\nu} &= \omega_{\mathbf{Q}} + \varepsilon_\nu - \varepsilon_\alpha \\ &- \frac{J}{2N} \sum_{\nu'} \frac{\varepsilon_{\mathbf{Q}+\nu'+\nu-\alpha} - \varepsilon_{\nu'} + \varepsilon_\alpha - \varepsilon_\nu - \omega_{\mathbf{Q}}}{JS + \varepsilon_{\mathbf{Q}+\nu'+\nu-\alpha} - \varepsilon_{\nu'} + \varepsilon_\alpha - \varepsilon_\nu - \omega_{\mathbf{Q}}}, \end{aligned} \tag{2.20}$$

we thus obtain the following equation:

$$\begin{aligned} \Delta^{\mathbf{Q}}_{\alpha\nu} \Psi^{\mathbf{Q}}_{\alpha\nu} &= \frac{J}{2N} \frac{\varepsilon_{\nu+\mathbf{Q}} - \varepsilon_\nu - \omega_{\mathbf{Q}}}{JS + \varepsilon_{\nu+\mathbf{Q}} - \varepsilon_\nu - \omega_{\mathbf{Q}}} \left[1 + \sum_{\alpha'} \Psi^{\mathbf{Q}}_{\alpha'\nu}\right] \\ &- \frac{J}{2N} \sum_{\nu'} \Psi^{\mathbf{Q}}_{\alpha\nu'} \frac{\varepsilon_{\mathbf{Q}+\nu+\nu'-\alpha} - \varepsilon_{\nu'+\varepsilon_\alpha-\varepsilon_\nu} - \omega_{\mathbf{Q}}}{JS + \varepsilon_{\mathbf{Q}+\nu+\nu'-\alpha} - \varepsilon_{\nu'} + \varepsilon_\alpha - \varepsilon_\nu - \omega_{\mathbf{Q}}}. \end{aligned} \tag{2.21}$$

The above equation describes up to three–body correlations between the magnon and a Fermi sea pair. The first term on the rhs describes the bare carrier–magnon scattering amplitude. This is renormalized by the multiple scattering of a Fermi sea electron (second term on the rhs) and a Fermi sea hole (last term on the rhs). These two contributions describe vertex corrections of the carrier–magnon interaction. In Fig. (2.3) we give a schematic representation of the physical processes including in

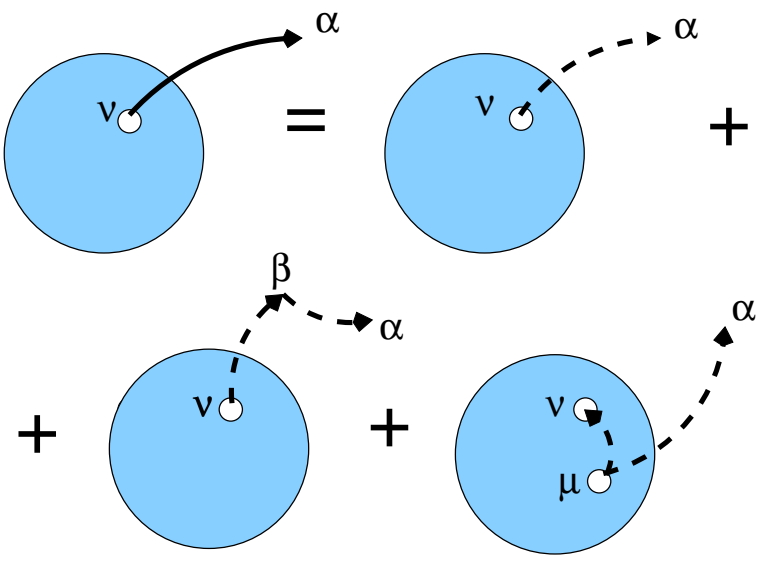

Figure 2.3: The creation of a electron–hole pair due to scattering with the magnon as described by variational amplitude Ψ. All the 3–body processes are also presented.

Eq. (2.21). In this Figure, the Fermi sea is illustrated as a blue circle, an electron–hole pair excitation by a solid line vector, and the electron magnon interaction by dashed line. The creation of an electron–hole pair can take place with three different processes. First, the Fermi pair $\nu - \alpha$ can be created by a direct scattering of an electron ν from momentum ν inside the Fermi sea to momentum α out of the Fermi sea. The latter process described by the first term in Fig. (2.3). However, this creation of an electron or a hole can be accompanied by scattering via the electron magnon interaction. Such rescattering processes are described by the participation of the rest holes $\beta \neq \alpha$ and electrons $\mu \neq \nu$ provides two new processes expressed by the second and third term respectively of Fig. (2.3). To obtain the spin–wave spectrum numerically, Eqs.(2.16) and (2.21) were solved iteratively until convergence for the spin wave energy was reached.

Now we identify the three–body correlation contribution to the carrier–magnon scattering amplitude $\Psi^{\mathbf{Q}}$, Eq. (2.21), and distinguish it from the two–body multiple scattering contributions. We note from Eq. (2.21), that $\Psi^{\mathbf{Q}}$ has the form

$$\Psi^{\mathbf{Q}}_{\alpha\nu} = \frac{J}{2N\Delta^{\mathbf{Q}}_{\alpha\nu}} \frac{\varepsilon_{\nu+\mathbf{Q}} - \varepsilon_{\nu} - \omega_{\mathbf{Q}}}{JS + \varepsilon_{\nu+\mathbf{Q}} - \varepsilon_{\nu} - \omega_{\mathbf{Q}}} + \frac{\Gamma^{e}_{\nu} - \Gamma^{h}_{\alpha\nu}}{\Delta^{\mathbf{Q}}_{\alpha\nu}}, \tag{2.22}$$

where we introduced the electron vertex function

$$\Gamma^{e}_{\nu} = \frac{J}{2N} \frac{\varepsilon_{\nu+\mathbf{Q}} - \varepsilon_{\nu} - \omega_{\mathbf{Q}}}{JS + \varepsilon_{\nu+\mathbf{Q}} - \varepsilon_{\nu} - \omega_{\mathbf{Q}}} \sum_{\alpha'} \Psi^{\mathbf{Q}}_{\alpha'\nu}, \tag{2.23}$$

and the hole vertex function

$$\Gamma^h_{\alpha\nu} = \frac{J}{2N}\sum_{\nu'}\Psi_{\alpha\nu'}\frac{\varepsilon_{\mathbf{Q}+\nu+\nu'-\alpha}+\varepsilon_\alpha-\varepsilon_\nu-\varepsilon_{\nu'}-\omega_{\mathbf{Q}}}{JS+\varepsilon_{\mathbf{Q}+\nu+\nu'-\alpha}-\varepsilon_{\nu'}+\varepsilon_\alpha-\varepsilon_\nu-\omega_{\mathbf{Q}}}, \tag{2.24}$$

Substituting Eq. (2.22) into Eq. (2.23) we obtain after some algebra that

$$\begin{aligned}\Gamma^e_\nu \;=\; & \left[1-\frac{J}{2N}\frac{\varepsilon_{\nu+\mathbf{Q}}-\varepsilon_\nu-\omega_{\mathbf{Q}}}{JS+\varepsilon_{\nu+\mathbf{Q}}-\varepsilon_\nu-\omega_{\mathbf{Q}}}\sum_{\alpha'}\frac{1}{\Delta^{\mathbf{Q}}_{\alpha'\nu}}\right]^{-1}\times \\ & \left[\frac{J^2}{4N^2}\left(\frac{\varepsilon_{\nu+\mathbf{Q}}-\varepsilon_\nu-\omega_{\mathbf{Q}}}{JS+\varepsilon_{\nu+\mathbf{Q}}-\varepsilon_\nu-\omega_{\mathbf{Q}}}\right)^2\sum_{\alpha'}\frac{1}{\Delta^{\mathbf{Q}}_{\alpha'\nu}}\right. \\ & \left.-\frac{J}{2N}\frac{\varepsilon_{\nu+\mathbf{Q}}-\varepsilon_\nu-\omega_{\mathbf{Q}}}{JS+\varepsilon_{\nu+\mathbf{Q}}-\varepsilon_\nu-\omega_{\mathbf{Q}}}\sum_{\alpha'}\frac{\Gamma^h_{\alpha'\nu}}{\Delta^{\mathbf{Q}}_{\alpha'\nu}}\right].\end{aligned} \tag{2.25}$$

The first factor on the rhs of the above equation comes from the electron–magnon two–body ladder diagrams summed to infinite order. The last term in the second factor describes the coupling of the electron–magnon and hole–magnon scattering channels. This coupling comes from the three–body correlations. An analogous equation for Γ^h can be obtained by substituting Eq.(2.22) into Eq. (2.24). In the case of the simpler variational wavefunction $\Phi = 0, \Psi \neq 0$ discussed below, which describes the carrier–localized spin scattering contribution, the calculation of Γ^h simplifies by noting from Eq.(2.18) and the definition Eq.(2.22) that $\Gamma^h_\alpha = \Gamma^h_{\alpha\nu}$. The corresponding variational equation can be obtained by setting $\Phi^{\mathbf{Q}} = 0$ in Eq. (2.18):

$$\begin{aligned}\Gamma^h_\alpha = & \left[1+\frac{J}{2N}\sum_{\nu'}\frac{1}{\Delta^{\mathbf{Q}}_{\alpha\nu'}}\right]^{-1}\times \\ & \left[\frac{J^2}{4N^2}\sum_{\nu'}\frac{\varepsilon_{\nu'+\mathbf{Q}}-\varepsilon_{\nu'}-\omega_{\mathbf{Q}}}{JS+\varepsilon_{\nu'+\mathbf{Q}}-\varepsilon_{\nu'}-\omega_{\mathbf{Q}}}\frac{1}{\Delta^{\mathbf{Q}}_{\alpha\nu'}}+\frac{J}{2N}\sum_{\nu'}\frac{\Gamma^e_{\nu'}}{\Delta^{\mathbf{Q}}_{\alpha\nu'}}\right].\end{aligned} \tag{2.26}$$

The first factor on the rhs comes from the hole–magnon ladder diagrams, while the coupling to Γ^e comes from the three–body correlations. The magnon energy is obtained from Eq. (2.16) after substituting Eq. (2.17):

$$\omega_{\mathbf{Q}} = \frac{J}{2N}\sum_\nu\frac{\varepsilon_{\nu+\mathbf{Q}}-\varepsilon_\nu-\omega_{\mathbf{Q}}}{JS+\varepsilon_{\nu+\mathbf{Q}}-\varepsilon_\nu-\omega_{\mathbf{Q}}}+\sum_\nu\Gamma^e_\nu. \tag{2.27}$$

The first term in Eq.(2.27) gives the RPA contribution to the magnon energy. The second term is the carrier–magnon self energy contribution, determined exclusively by the electron vertex function Γ^e. The latter satisfies Eq.(2.25), which

describes the multiple electron–magnon scattering contribution (ladder diagrams, two–body correlations) as well as the coupling to the hole vertex function, Eq. (2.24), due to the three–body correlations. Below we discuss three contributions to the full Γ^e: $O(1/S^2)$ (Born scattering approximation), ladder diagram (two–body carrier–magnon correlations), and the contribution due to carrier scattering with the localized spins.

2.2.4 1/S Expansion

In this section we make the connection with the Holstein–Primakoff bosonization treatment of the quantum effects[11, 24]. In particular, we show that the $O(1/S^2)$ magnon dispersion [11, 24] can be obtained by solving Eq.(2.25) perturbatively, to lowest order in the carrier–magnon interaction and 1/S.

First, we recall that classical spin behavior is obtained in the limit $S \to \infty$ with the band splitting JS kept finite. By expanding Eqs (2.21), (2.23) and (2.24) in powers of the small parameter 1/S (JS= finite) we see that $\Psi^{\mathbf{Q}} = O(1/S)$, $\Gamma^e = O(1/S^2)$, and $\Gamma^h = O(1/S^2)$. In particular, we obtain from Eq.(2.25) to lowest order in 1/S

$$\Gamma^e_\nu = -\frac{J^2}{4N^2}\left(\frac{\varepsilon_{\nu+\mathbf{Q}} - \varepsilon_\nu}{JS + \varepsilon_{\nu+\mathbf{Q}} - \varepsilon_\nu}\right)^2 \sum_\alpha \frac{1}{\varepsilon_\alpha - \varepsilon_\nu}, \tag{2.28}$$

and from Eq.(2.27)

$$\begin{aligned} \omega_{\mathbf{Q}} &= \frac{J}{2N}\sum_\nu \frac{\varepsilon_{\nu+\mathbf{Q}} - \varepsilon_\nu - \omega_{\mathbf{Q}}}{JS + \varepsilon_{\nu+\mathbf{Q}} - \varepsilon_\nu - \omega_{\mathbf{Q}}} \\ &\quad -\frac{J^2}{4N^2}\sum_{\alpha\nu} \frac{\left(\varepsilon_{\nu+\mathbf{Q}} - \varepsilon_\nu\right)^2}{\left(JS + \varepsilon_{\nu+\mathbf{Q}} - \varepsilon_\nu\right)^2\left(\varepsilon_\alpha - \varepsilon_\nu\right)}. \end{aligned} \tag{2.29}$$

The last term in the above equation comes from the lowest order magnon–electron scattering contribution. The $O(1/S)$ spin wave dispersion [51] is obtained from the first term by neglecting $\omega_{\mathbf{Q}} = O(1/S)$ in the denominator. The spin wave energy to $O(1/S^2)$ is obtained by expanding the first term to this order. This corresponds to keeping only the 1^{st} contribution of the figure (2.3) while the rescattering terms are neglected. We recover the strong coupling $O(1/S^2)$ results of Refs [11, 24], obtained by using the bosonization technique, by further expanding Eq.(2.29) in the limit $JS \to \infty$.

It is important to note that he $O(1/S^2)$ magnon dispersion is not variational. As a result, we cannot definitely conclude instability of the ferromagnetic state

if we find a negative magnon energy to $O(1/S^2)$. On the other hand, the three–body calculation outlined in the previous section treats the magnon–Fermi sea pair interaction variationally rather than perturbatively (as in the 1/S expansion), while recovering the $O(1/S^2)$ results as a special case. The n–pair contributions to Eq.(2.15) have amplitudes of order $O(1/S^n)$. Therefore, the shake–up of multipair excitations is suppressed for large S. Our three–body calculation thus puts the $O(1/S^2)$ results on a more quantitative (variational) basis by treating fully rather than perturbatively all contributions of the one Fermi sea pair states.

2.2.5 Two–body Ladder Approximation

To go beyond the Born approximation ($O(1/S^2)$) result, we first consider the two–body correlation contributions to the Fermi sea pair amplitude $\Psi^{\mathbf{Q}}$ while still neglecting the three–body correlations. This is equivalent to treating the ladder diagrams that describe the multiple electron–magnon and hole–magnon scattering, while neglecting the coupling between these two scattering channels. Noting that the magnon dispersion is determined by Γ^e only Eq. (2.27). The ladder approximation dispersion is thus obtained from Eq. (2.25) by setting $\Gamma^h = 0$ and Eq.(2.27):

$$\omega_{\mathbf{Q}} = \frac{J}{2N}\sum_{\nu}\frac{\varepsilon_{\nu+\mathbf{Q}} - \varepsilon_{\nu} - \omega_{\mathbf{Q}}}{JS + \varepsilon_{\nu+\mathbf{Q}} - \varepsilon_{\nu} - \omega_{\mathbf{Q}}}$$
$$+\frac{J^2}{4N^2}\sum_{\nu}\frac{\left(\frac{\varepsilon_{\nu+\mathbf{Q}}-\varepsilon_{\nu}-\omega_{\mathbf{Q}}}{JS+\varepsilon_{\nu+\mathbf{Q}}-\varepsilon_{\nu}-\omega_{\mathbf{Q}}}\right)^2 \sum_{\alpha'} 1/\Delta^{\mathbf{Q}}_{\alpha'\nu}}{1 - \frac{J}{2N}\frac{\varepsilon_{\nu+\mathbf{Q}}-\varepsilon_{\nu}-\omega_{\mathbf{Q}}}{JS+\varepsilon_{\nu+\mathbf{Q}}-\varepsilon_{\nu}-\omega_{\mathbf{Q}}}\sum_{\alpha'} 1/\Delta^{\mathbf{Q}}_{\alpha'\nu}}, \qquad (2.30)$$

where $\Delta^{\mathbf{Q}}$ is given by Eq.(2.20). A diagrammatic representation of the Ladder approximation is given by removing the last term in Fig. (2.3), i.e. the Fermi sea hole rescattering process. We note that, similar to the 1/S expansion, the above ladder approximation result is not variational. A similar approximation was used in the context of the Fermi Edge Singularity [42, 43]. There it was shown that at least three–body correlations are necessary in order to describe the unbinding of the discrete exciton bound state[42, 43]. In the case of the Hubbard model, the ladder approximation was shown to overestimate the electron self energy [41].

The difference between the spin wave dispersions Eq.(2.30) and the full three–body calculation comes from the three–body correlations. By comparing the corresponding curves in the next section we can therefore judge the role of these correlations on the spin dynamics.

2.2.6 Carrier–localized spin scattering ($\Phi = 0, \Psi \neq 0$)

To describe the three–body correlations, the coupled equations for Γ^e and Γ^h must be solved. Although this is possible in 1D and 2D for fairly large systems, in 3D the numerical solution of the full variational equations is challenging, due to the dependence of $\Gamma^h_{\alpha\nu}$ on six momentum components. On the other hand, Γ^e_ν depends on one momentum only. The dependence of $\Gamma^h_{\alpha\nu}$ on the momentum ν can be eliminated by considering a simpler variational wavefunction, obtained from Eq.(2.15) by setting $\Phi = 0$. This corresponds to treating fully the scattering of the electron with the localized spins while neglecting the electronic contribution to the scattered magnon. This approximation becomes exact in the two limits $N_e = 1$ and $N_e = N^d$ and also recovers the $O(1/S^2)$ and RPA results. Its main advantage is that it improves the RPA by allowing us to treat variationally three-body carrier–localized spin correlations in a large system. The corresponding spin wave dispersion is obtained by solving the coupled Eqs.(2.25) and (2.26) and then substituting Γ^e in Eq.(2.27).

2.3 Numerical results

In this section we present the results of our numerical calculations. We perform an extensive spin of the full parameter space and establish the importance of correlations. To draw conclusions on the role of the correlations, we compare the different approximations discussed in the previous section for a d–dimensional lattice with N^d sites. We performed our calculations for d=1, 2, and 3. The dimensionality of the system affects the quantum fluctuations and correlation effects. Quantum fluctuations are expected to be most pronounced in the 1D system, where we show that the 1/S expansion can lead to spurious features. The calculation of the 1D magnon dispersion could also be relevant to quasi–1D materials with chain structures. Our 2D magnon dispersion is relevant to the quasi–2D layered manganites, [44, 45] where a pronounced spin wave softening and deviations from the Heisenberg dispersion similar to the 3D system [35, 36, 37, 38, 7] were observed experimentally[39, 40]. The similarity of the spin dynamics in the 3D and 2D systems indicates that the relevant physical mechanisms are generic and do not depend crucially on the particularities of the individual systems. In 2D, the full three–body variational calculation can be performed in fairly large systems ($N \sim 20 - 30$), while in 3D it could only be performed for $N \sim 10$. Therefore, the 2D system also offers computational advantages. On the other hand, the rest of the approximations discussed here can be performed in very large systems (up to $N \sim 200$), until full convergence with increasing N is reached.

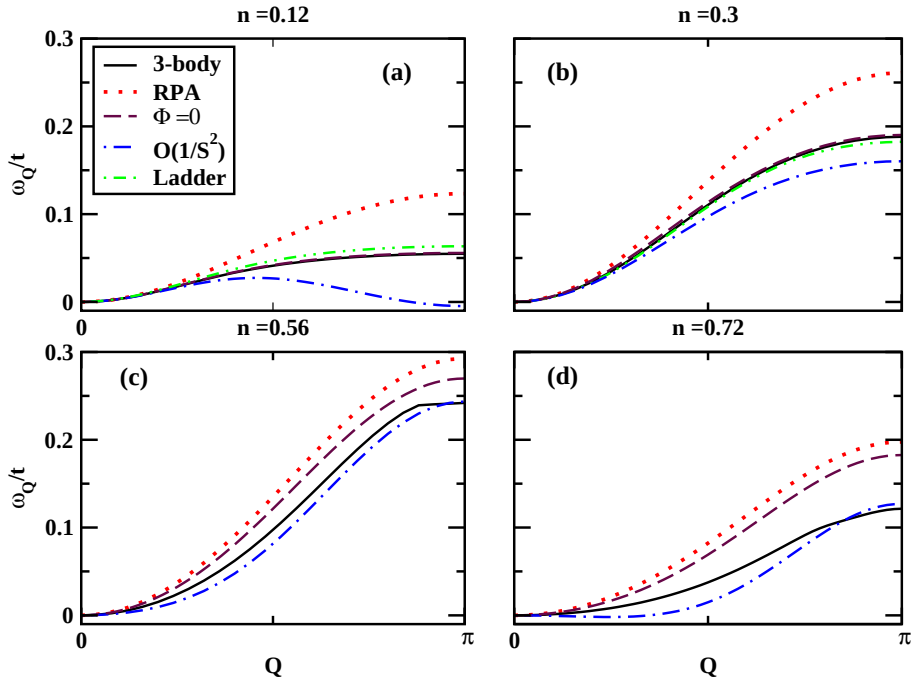

Figure 2.4: Spin-wave dispersion in the 1D system: comparison of the full three–body variational calculation (solid curve) to the different approximations discussed in the text. $J/t = 10$.

We start with the dependence of the spin wave excitation spectrum on the electron concentration n. Figs. (2.4) and (2.5) show the magnon dispersion in the 1D and 2D systems respectively for a fixed exchange interaction, $J/t = 10$, and four different values of n. The 2D dispersion (Fig. (2.5)) was calculated along the Brillouin zone direction $(0,0) \rightarrow (\pi,0)$ $(\Gamma - X)$, where the discrepancies between the different approximations are maximized.

For very small electron concentrations ($n = 0.12$ in Figs. (2.4) and (2.5), the carrier–magnon scattering tends to soften the spin wave dispersion close to the zone boundary, consistent with previous results[31, 24]. This can be seen by comparing in Figs. (2.4a) and (2.5a) the RPA dispersion with the different calculations of the carrier–magnon scattering effects. It is important to note that, despite the softening, the spin wave dispersion does not become negative (unstable) close to the zone boundary for very low concentrations. This softening may be interpreted as a remnant in the thermodynamic limit of the failure of the RPA for $N_e = 1$, where Eq. (2.15) gives the exact solution.

Indeed, for $N_e = 1$, the magnon energy is of $O(1/N^2)$, while the RPA gives $O(1/N)$ energies. Furthermore, for low concentrations, the $\Phi \neq 0, \Psi \neq 0$ and $\Phi = 0, \Psi \neq 0$ variational calculations give results similar to the ladder approximation (the corresponding curves almost overlap in Figs. (2.4a) and (2.5a). This indicates that the three–body correlations are weak for very low concentrations. This result can be understood by noting that the last term in Eq. (2.21) (and Eq. (2.20)), which describes the hole–magnon multiple scattering contribution, is suppressed for small n. Indeed, with decreasing n and Fermi energy E_F, the phase space available for the hole to scatter decreases relative to the phase space available for electron scattering. As a result, the electron–magnon scattering channel (electron ladder diagrams) dominates. On the other hand, the difference between the above dispersions and the RPA is strong, while the differences from the $O(1/S^2)$ (Born scattering) result are noticeable even for very small n (Figs. 2.4a and 2.5a). The latter differences come from the multiple electron–magnon and hole–magnon scattering processes. In 1D, the $O(1/S^2)$ result fails qualitatively for very low ($n = 0.12$ in Fig. (2.4) and very high ($n \geq 0.8$) electron concentrations. For such concentrations, the $O(1/S^2)$ dispersion becomes negative (unstable) at the zone bondary. This zone boundary instability persists even in the strong coupling limit $J \to \infty$ but is absent in all our variational results.

With increasing electron concentration, the spin wave energies and stiffness initially increase (compare the $n = 0.12$ and $n = 0.3$ dispersions in Figs. (2.4) and (2.5). Fig. (2.6) shows $D(n)$, obtained by fitting the quadratic behavior $D(n)Q^2$ to the long wavelength numerical dispersions, for finite exchange interaction $J/t = 10$. As can be seen in Fig. (2.6), the RPA predicts an initial increase of the spin wave stiffness with n followed by a decrease. However, the carrier–magnon scattering reduces the spin wave stiffness and changes the above concentration dependence significantly, especially in 2D and 3D (see Fig. (2.6). The difference from the RPA behavior is particularly striking for the $O(1/S^2)$ contribution to $D(n)$. The latter is significantly suppressed as compared to the rest of the approximations of carrier–magnon scattering. This particularly strong softening indicates that the $O(1/S^2)$ result significantly underestimates T_c and the stability of the fully polarized ferromagnetic state. We note that, due to the variational nature of the full three–body calculation, the exact stiffness will be smaller (softer) than the corresponding results of Fig. (2.6) (solid curve).

As the electron concentration increases, we see from Figs. (2.4) and (2.5) that the different approximations start to deviate substantially from each other. This is clear for the 2D system (Fig. 2.5), while in 1D the differences develop for higher electron concentrations. Compared to the full three–body variational calculation ($\Phi \neq 0, \Psi \neq 0$), the ladder and $O(1/S^2)$ (non-variational) approximations give softer spin wave energies, while the variational $\Phi = 0, \Psi \neq 0$ and RPA

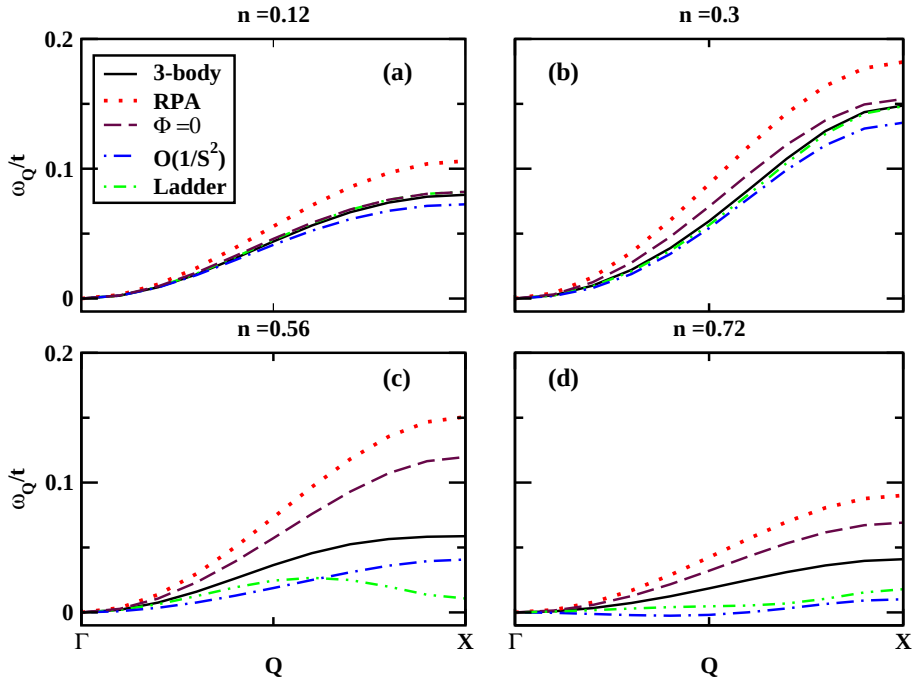

Figure 2.5: Spin-wave dispersion in the 2D system along the direction $\Gamma - X$ for the same parameters as in Fig. 2.4: comparison of the full three–body variational calculation (solid curve) to the different approximations discussed in the text.

($\Phi = \Psi = 0$) wavefunctions give higher spin wave energies. The large differences between the above dispersions point out the important role of carrier–magnon correlations for such electron concentrations. The difference between the full three–body calculation (or the $\Phi = 0, \Psi \neq 0$ calculation) and the ladder approximation in Figs. (2.5c) and (2.5d) shows that the three–body correlations are significant, while the differences from the $O(1/S^2)$ result show the importance of the multiple carrier–magnon scattering processes (vertex corrections). One can conclude from the above comparisons that the Fermi sea hole–magnon scattering cannot be neglected for such concentrations. Furthermore, as can be seen in Fig. (2.5), the different approximations bound the full three–body result. This is particularly useful for the 3D system, where the full three–body variational calculation could only be performed for relatively small N^d lattices with $N \sim 10$ (due to the large number of variational parameters $\Psi^{\mathbf{Q}}_{\alpha\nu}$). On the other hand, Fig. 5 shows the spin wave dispersions for a rather large (50^3) 3D lattice, obtained by using the RPA, $O(1/S^2)$, and $\Phi = 0, \Psi \neq 0$ approximations. By comparing the spin wave dispersions in Figs. (2.7) and (2.5), obtained for the same parameters, we see that

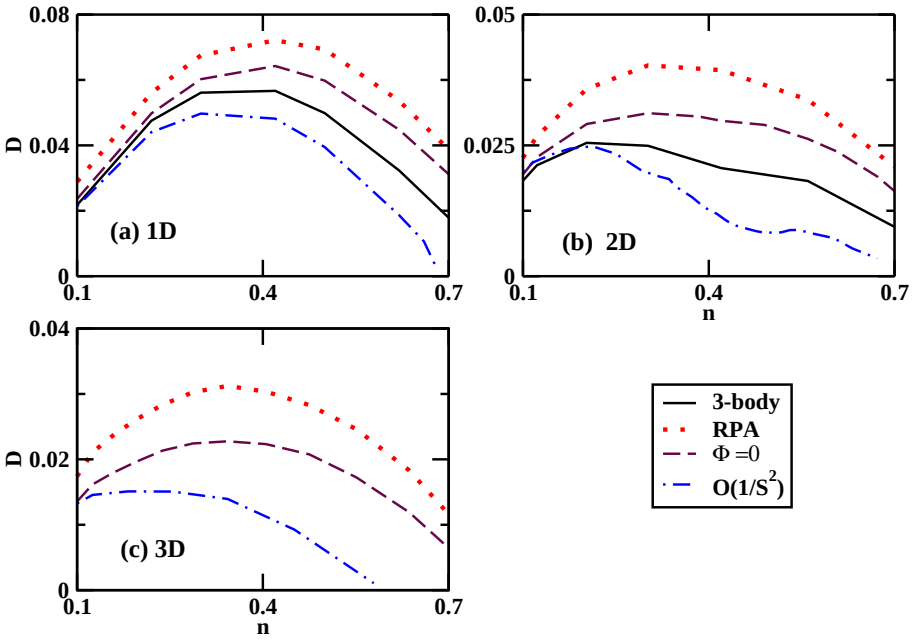

Figure 2.6: Spin wave stiffness for $J = 10t$ as function of electron concentration and system dimensionality.

the trends as function of n are qualitatively similar in the 2D and 3D systems.

The differences between the approximations studied here (which are due to the correlations) are very pronounced in the electron concentration range $0.5 \leq n \leq 0.8$ for intermediate exchange interaction values, i.e. in the parameter regime relevant to the manganites. This can be seen more clearly in Fig. (2.8), which shows the 2D spin wave dispersions obtained with the different approximations along the main directions in the Brillouin zone for the typical parameters $n = 0.7, J = 8t$. Fig. (2.8) compares the dispersions along the directions $(0,0) \rightarrow (\pi,0)$ $(\Gamma - X)$, $(\pi,0) \rightarrow (\pi,\pi)$ $(X - M)$, and along the diagonal $(0,0) \rightarrow (\pi,\pi)$ $(\Gamma - M)$. The discrepancies between the different approximations are very large along $\Gamma - X$ but much smaller along the other directions. For example, the RPA fails completely along the direction $\Gamma - X$, where the full three–body calculation shows a striking spin wave softening that is most pronounced close to the X point. Such a strong effect, much stronger than the softening at small n, only occurs for intermediate electron concentrations $0.4 < n \leq 0.7$ and is underestimated by the $\Phi = 0, \Psi \neq 0$ variational calculation. On the other hand, the $O(1/S^2)$ dispersion for the parameters of Fig. 5 shows instability at long wavelengths (negative stiffness) rather than softening at the zone boundary.

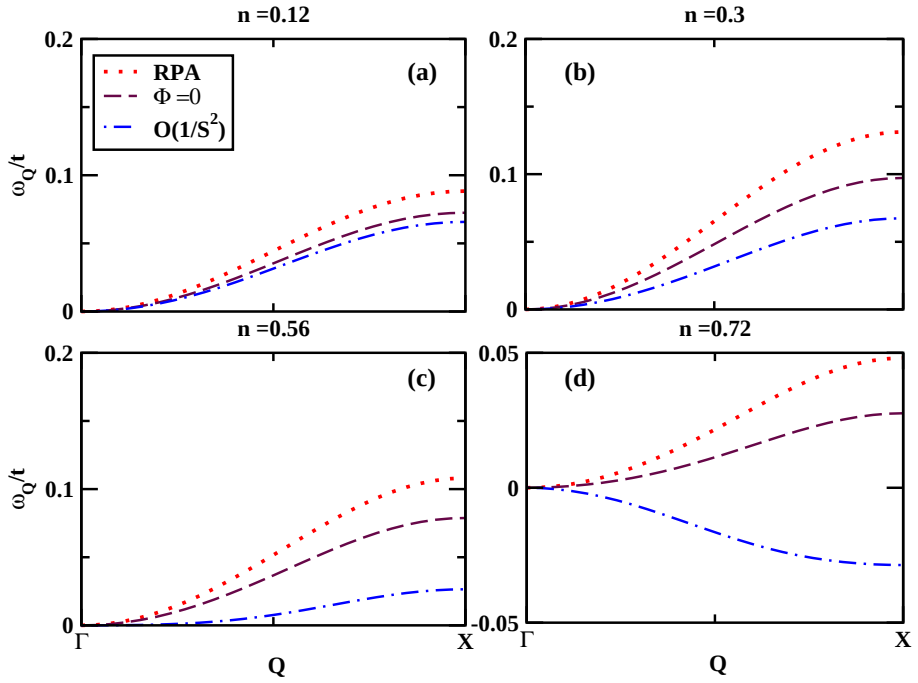

Figure 2.7: Spin wave dispersions in 3D for $J/t = 10$ and electron concentrations similar to Figs. (2.4) and (2.5).

To see the origin of the above spin wave softening, we show in Fig. (2.9) the spin wave dispersion for a slightly smaller J/t than in Fig (2.8). The spin wave energy now becomes negative in the vicinity of the X point, while the magnon stiffness remains positive. This variational result allows us to conclude instability of the fully polarized ferromagnetic state due to the X point magnons. The strong zone boundary softening is a precursor to this instability. Fig. (2.9) also compares the full three–body and RPA calculations for two different values of N with fixed n. For $n = 0.7$, our results have converged reasonably well even for $N \sim 10$ and thus reflect the behavior in the thermodynamic limit.

The above zone boundary instability occurs in 2D and 3D for intermediate electron concentrations ($0.4 \leq n \leq 0.7$ for the 2D three–body calculation), where a strong magnon softening and short magnon lifetimes were observed in the manganites [35, 36, 37, 38, 7, 39, 40]. Although the other approximations can also give an instability, this occurs within a more limited range of n and J than for the full three–body calculation (discussed further below). The magnitude and concentration dependence of the softening also depends on the local Hubbard repulsion (H_U) and direct super–exchange (H_{super}) interactions and the bandstructure (to

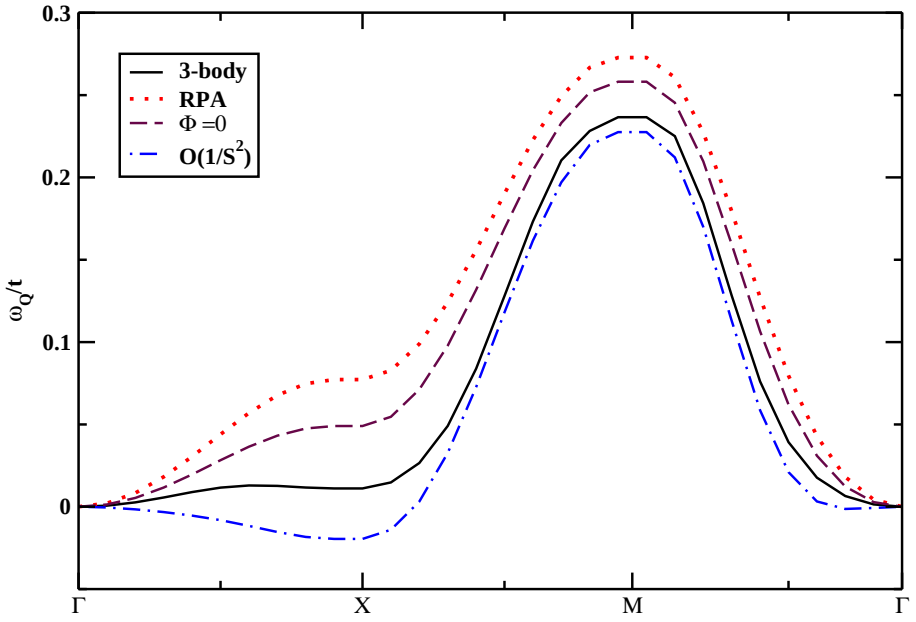

Figure 2.8: Spin wave dispersion along the different directions in Brillouin zone for $n = 0.7, J = 8t$: Comparison of the different approximations.

be considered elsewhere). We note that spin wave softening at the zone boundary of electronic origin was obtained before within the one–orbital Hamiltonian for finite values of J/t by including these additional effects [11, 13]. The main difference here is that our calculation is variational (and thus allows us to draw definite conclusions by guaranteeing that the exact magnon energies are even softer than the calculated values) and our effect was obtained by using the simplest possible Hamiltonian ($H_U = H_{super} = 0$).

It is important to note here that the strong magnon softening and instability only occur for finite values of J/t and disappear in the strong coupling limit $J \to \infty$. This can be seen in Fig. (2.10), which compares the 2D magnon dispersions for $n = 0.7$ and different values of $J/t > 1$ with the result obtained by expanding Eqs.(2.21) and (2.27) in the limit $J \to \infty$. As can be seen in Fig. (2.10), the zone boundary magnon softening disappears with increasing J/t. The magnon dispersions converge slowly to the strong coupling result, which is reached only for $J/t \sim 1000$. Since the typical exchange interaction values in the manganites are of the order of $J/t \leq 10$, we conclude that the manganites are far from the $J \to \infty$ limit. Noting in Fig.8 that the zone boundary magnon softening has disappeared completely for $J/t \geq 20$, we see that the finite J/t effects play an important role

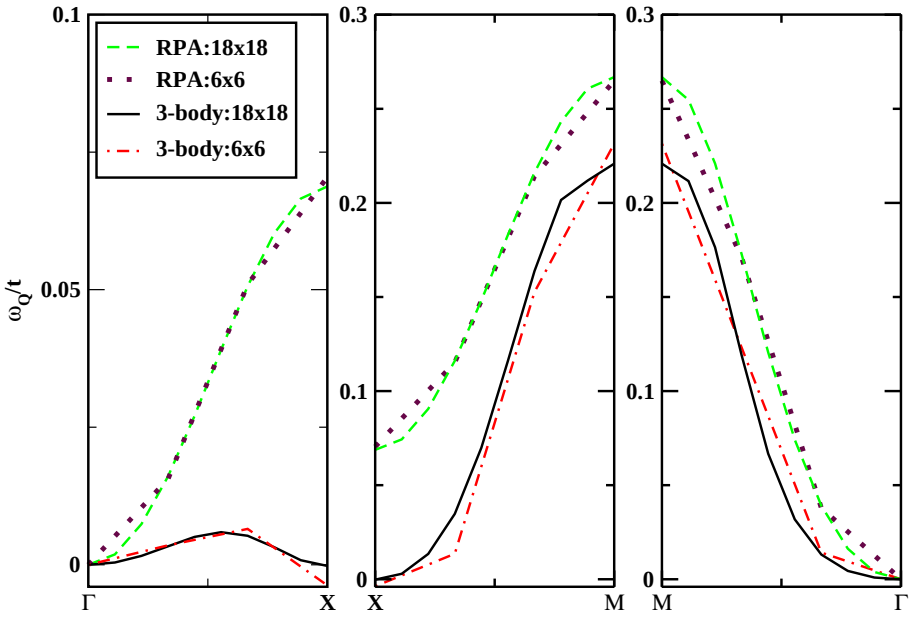

Figure 2.9: Spin wave dispersion for a $N \times N$ 2D lattice along different directions ($n = 0.7, J = 7.5t$). Convergence with system size N is very good for this n.

in the manganite spin dynamics.

We now turn to the 3D system, where the full three–body variational calculation faces computational difficulties due to the large number of variational parameters $\Psi^{\mathbf{Q}}_{\alpha\nu}$. As can be seen in Fig. (2.9), in the 2D system the magnon dispersion results for $n = 0.7$ have already converged reasonably well for $N \sim 10$. We therefore expect that, in 3D, a calculation for a $N \times N \times N$ lattice with $N \sim 10$ should give reasonable results. Fig.(2.11) show the 3D magnon dispersions obtained this way for $N = 8$, $n \sim 0.7$, and $J/t = 14$ using the different approximations. Fig. 9 shows similar 3D magnon behavior as in the 2D system (Fig. 2.7): magnon softening close to the X point and significant deviations between the different approximations along $\Gamma - X$ even for this relatively large $J/t = 14$. Similar to the 2D and 1D systems, the $O(1/S^2)$ dispersion and the carrier–localized spin scattering ($\Phi = 0, \Psi \neq 0$) variational results bound the full three–body magnon dispersion.

Next we turn to the stability of the fully polarized half metallic ferromagnetic state. Our results show two different instabilities due to the exchange interaction ($H_U = H_{super} = 0$). The first is the X–point zone boundary instability discussed above, which occurs in 2D and 3D for intermediate electron concentrations. For low or high electron concentrations (for all concentrations in 1D), we find a second

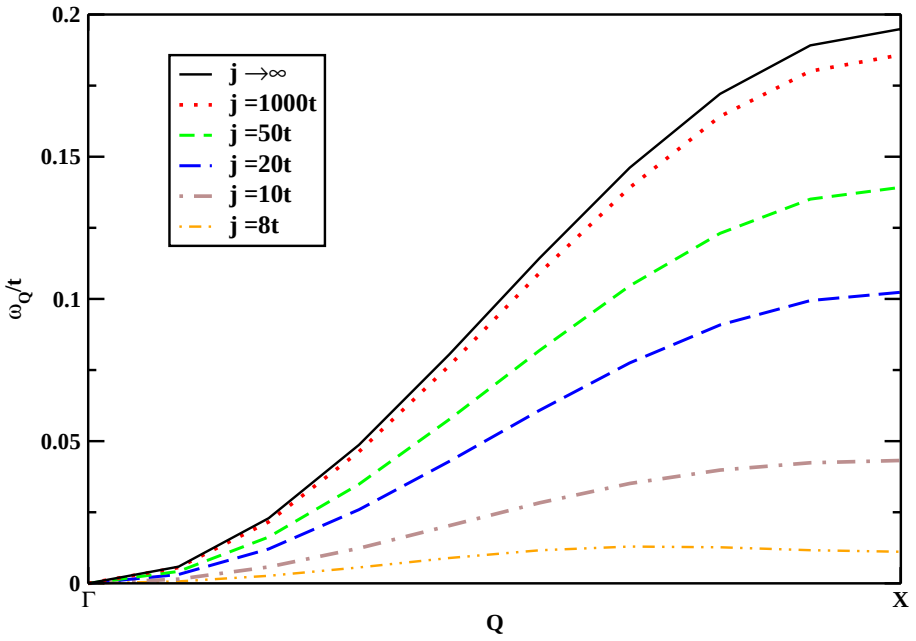

Figure 2.10: Spin wave dispersion in 2D, obtained from the full three–body calculations, for $n = 0.7$ and increasing values of J/t. Convergence to the strong coupling limit is slow.

instability with respect to long wavelength spin waves (negative magnon stiffness) similar to previous calculations. In this case, the minimum magnon energy occurs at a finite momentum value instead of $\mathbf{Q} = 0$. This momentum increases with n and becomes π at $n = 1$ (antiferromagnetic order at half filling). This result implies instability to a spiral state, while the system can further lower its energy by phase separating [22, 47]. Due to the variational nature of our calculation, it is guaranteed that, if the magnon energy becomes negative for $J = J_c(n)$, the ground state of the Hamiltonian H for all $J < J_c(n)$ is not the half metallic state $|F\rangle$. The phase diagrams of Fig. (2.12) describe the stability of this state against spin wave excitations. The most striking feature in Fig. (2.12) is the large shift (increase) of the ferromagnetic phase boundary, $J_c(n)$, as compared to the RPA, due to the carrier–magnon scattering. Furthermore, the different approximations of the carrier–magnon scattering lead to significant differences in $J_c(n)$. By comparing the shape of $J_c(n)$ between the 1D and 2D/3D systems, we see that, in the latter case, $J_c(n)$ develops a plateau–like shape within an intermediate concentration regime (see Fig. (2.12d). This feature is absent in the 1D system, where there is no zone boundary instability. This plateau occurs for $0.4 < n \leq 0.7$ in 2D (full

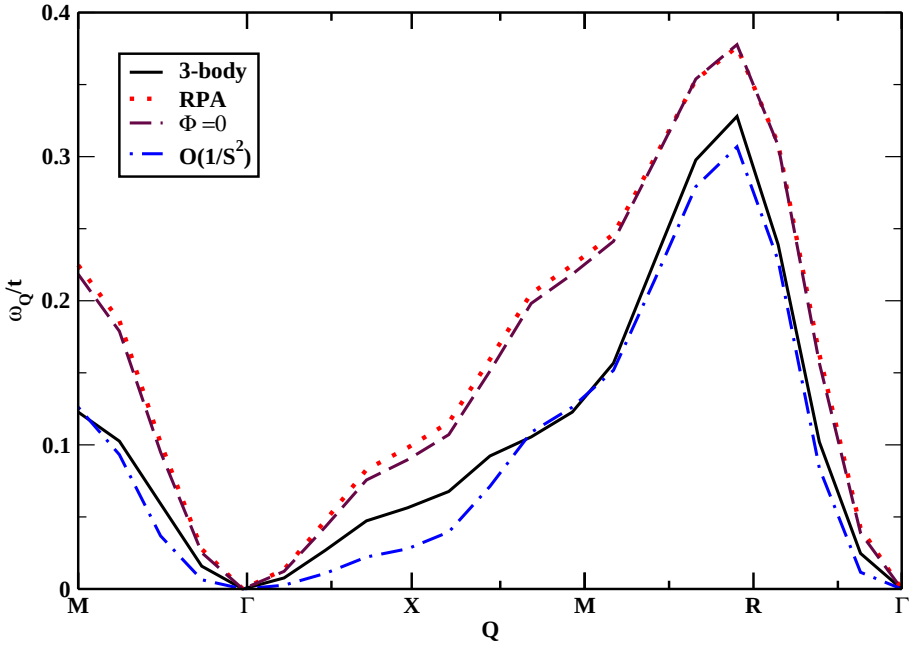

Figure 2.11: Spin wave dispersion for a $N \times N \times N$ 3D lattice along different directions ($n = 0.7, J = 14t$, and $N = 8$). $\Gamma = (0,0,0), X = (\pi,0,0), M = (\pi,\pi,0), R = (\pi,\pi,\pi)$.

three–body calculation) and for $0.25 < n < 0.6$ in 3D ($\Phi = 0, \Psi \neq 0$ three–body calculation). It is much less pronounced for the $O(1/S^2)$ and RPA calculations

For small n, $J_c(n)$ is small, implying enhanced stability of the ferromagnetic state in the concentration regime relevant, e.g., to III-Mn-V semiconductors[19, 20]. This stability is a remnant of the fact that, in the exactly solvable limit $N_e = 1$, the ferromagnetic state $|F\rangle$ is the ground state for all values of J/t. $J_c(n)$ increases more slowly with n in 1D than in 2D and 3D. This implies enhanced stability of the fully polarized ferromagnetic state, partly due to the lack of zone boundary instability in 1D. Fig. 10(d) shows the 2D phase diagrams for the electron concentrations relevant to the manganites. The full three–body variational calculation gives $J_c(n) \sim 7 - 8t$ in this regime, close to the high end of the values quoted in the literature[22]. Therefore, the simple double exchange Hamiltonian predicts that the manganites lie in a regime that is close to the instability of the ferromagnetic state. In this regime, the correlations, vertex corrections, and finite J effects play an important role in the spin dynamics.

Fig. (2.12) also compares the phase diagrams obtained by using the different

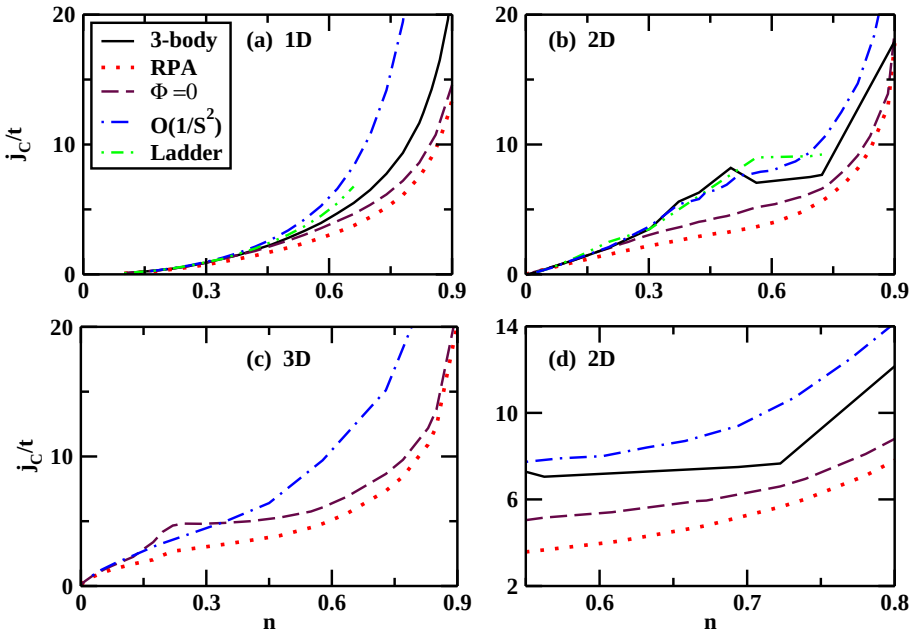

Figure 2.12: Phase diagram due to the spin wave instability and comparison between the different approximations discussed in the text. (a) 1D system, (b) 2D system, (c) 3D system, and (d) 2D system in the electron concentration range relevant to the manganites.

approximations implemented here. The $O(1/S^2)$ calculation underestimates the stability of the fully polarized ferromagnetic state, while the RPA and carrier–localized spin scattering ($\Phi = 0, \Psi \neq 0$) variational results overestimate the stability. For low concentrations $n \leq 0.3$, all the different treatments of the carrier–magnon scattering predict a similar ferromagnetic phase boundary. It is clear from Fig. (2.12d) that, in the electron concentration regime $0.5 \leq n \leq 0.8$ relevant to the manganites, the RPA significantly overestimates the stability of the ferromagnetic state. For example, for $n \sim 0.5$, the RPA underestimates $J_c(n)$ by 100% as compared to the full three–body variational calculation. Finally, close to half filling $n = 1$, the two variational results give magnon energies similar to the RPA, which becomes exact for $n = 1$. On the other hand, the $O(1/S^2)$ approximation fails in this high concentration regime.

Finally we discuss the relevance of our calculation based on this minimal Hamiltonian of the spin wave dispersion observed experimentally in the quasi–2D and 3D manganites. The experimental results are typically analyzed by fitting the short range Heisenberg dispersion to the long wavelength experimental dispersion and

then comparing the two close to the zone boundary [9, 35, 36, 37, 38, 7, 45, 39, 40]. This comparison showed that the Heisenberg model fails to describe the experimental results in the over–doped manganites (typically for $0.5 \leq n \leq 0.7$), but fits well in the under–doped samples ($n > 0.7$). This failure is due to the strong magnon softening close to the zone boundary (X–point) [35, 36, 37, 38, 7, 39, 40], whose physical origin is currently under debate [35, 36, 37, 38, 7, 39, 40, 10, 12, 13]. Here we compare our numerical results with the Heisenberg dispersion $\omega_{\mathbf{Q}}^{Heis}$, obtained by fitting to the long wavelength numerical results, by introducing the parameter $\Delta = \omega_X^{Heis}/\omega_X - 1$, where ω_X^{Heis} and ω_X are the Heisenberg and numerical magnon energies calculated at the X–point. $|\Delta|$ thus measures the magnitude of the deviations from Heisenberg behavior at the zone boundary. For example, $|\Delta| \sim 1$ means 100% deviation, $\Delta > 0$ means magnon softening at the zone boundary, as compared to the Heisenberg dispersion with the same stiffness, while $\Delta < 0$ implies zone boundary hardening. Fig. (2.13) compares $\Delta(n)$ obtained from our different approximations. With the exception of small values of J/t, the RPA gives small deviations from Heisenberg behavior, mostly a hardening at the zone boundary ($\Delta < 0$, see Fig. (2.12), and predicts a weak concentration dependence of $\Delta(n)$. This similarity between the RPA and Heisenberg dispersions is expected for $J \gg t$ since the two coincide in the strong coupling limit $J \to \infty$ (see Eq.(2.14)).

The magnon–electron scattering leads to larger deviations from Heisenberg ferromagnet spin dynamics and enhances $\Delta(n)$ (see Figs. (2.13a) and (2.13b) for 2D and 3D respectively). In order to compare with the experiment, the value of J/t must be chosen so that $|F\rangle$ is stable up to $n \sim 0.8$, where a metallic ferromagnetic state is observed experimentally. For $J/t \sim 10$, this is the case for the full three–body calculation, while larger values of J/t are required to achieve stability for $n \sim 0.8$ with respect to the $O(1/S^2)$ magnons. Figs. (2.13a) and (2.13b) compare the behavior of $\Delta(n)$ for the different approximations in the 2D and 3D systems respectively. The $O(1/S^2)$ calculation gives magnon *hardening* rather than softening in the concentration range of interest, similar to the strong coupling results of Ref. [24]. This is in contrast to $\Delta(n)$ obtained by using the full three–body calculation, shown in Fig. (2.13a) for the 2D system. In this case, the magnon hardening for $n < 0.5$ ($\Delta < 0$) changes to magnon softening for $0.5 < n < 0.7$ ($\Delta > 0$) and then back to a small magnon hardening for $n > 0.7$. This behavior with n is consistent with the experimental trends. Although magnon softening at the X point can be obtained using other approximations, the full three–body calculation gives such an enhanced effect within the range of intermediate electron concentrations of interest and for values of J/t such that the fully polarized ferromagnetic state is stable for $0.5 \leq n \leq 0.8$ (where it is observed experimentally). The above behavior of $\Delta(n)$ is not reproduced in the strong coupling limit $J \to \infty$, where magnon hardening is obtained. It arises from the interplay of the

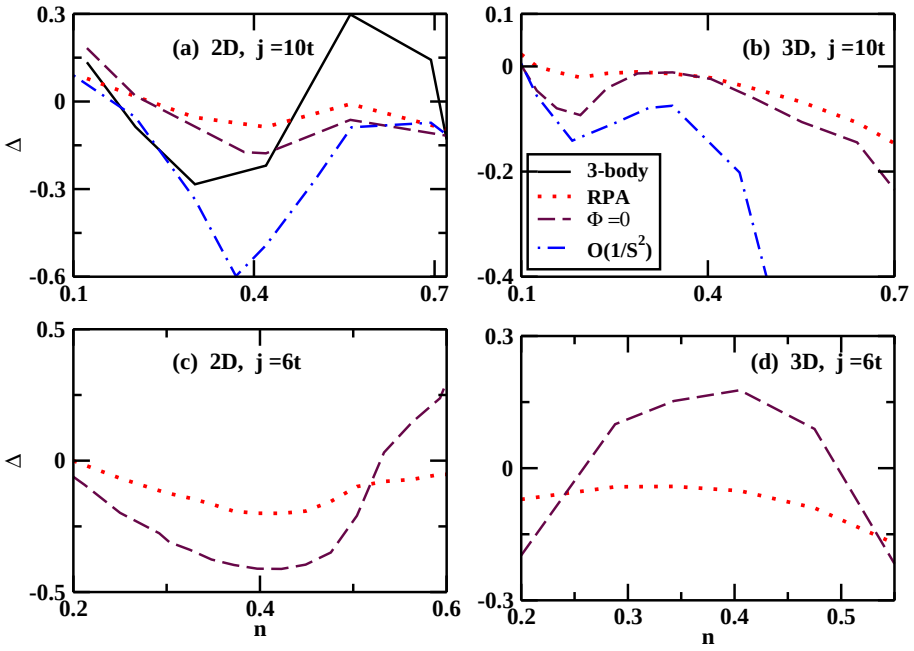

Figure 2.13: Deviation $\Delta(n)$, defined in the text, from Heisenberg ferromagnet spin dynamics in the 2D and 3D systems for fixed $J/t = 10$ and different electron concentrations.

X–point instability and the plateau–like shape of $J_c(n)$, Fig. (2.12), induced by the correlations. On the other hand, for $J = 10t$, the carrier–localized spin scattering approximation ($\Phi = 0, \Psi \neq 0$ variational wavefunction) gives $\Delta(n)$ that, more or less, follows the RPA behavior (see Figs. (2.13a) and (2.13b). As J/t decreases, magnon softening, $\Delta > 0$, can also be obtained with this approximation over a range of electron concentrations in both 2D and 3D (see Figs. (2.13c) (2D) and (2.13d (3D)). However, for such J/t, the ferromagnetic state is unstable for $n > 0.6$, i.e. in a regime where ferromagnetism is observed experimentally. We expect that the precise behavior of $\Delta(n)$ in the realistic materials will also depend on H_U, H_{super}, and the bandstructure effects (to be studied elsewhere). Here we point out that at least three–body correlations must be included for a meaningful comparison to the experiment.

2.4 Conclusions

In this chapter we presented a nonperturbative variational calculation of the effects of magnon–Fermi sea pair correlations on the spin wave dispersion for the simplest possible double exchange Hamiltonian. Our theory treats exactly all three–body long range correlations between an electron, a Fermi sea hole, and a magnon excitation. We achieved this by using the most general variational wavefunction that includes up to one Fermi sea pair excitations. Since the contribution of multipair Fermi sea excitations is suppressed by powers of $1/S$, one could alternatively think of our calculation as putting the $O(1/S^2)$ result, which treats the one Fermi sea pair contribution perturbatively within the Born approximation, on a variational nonperturbative basis. Our theory (i) becomes exact in the two limits of one and N^d electrons and should therefore interpolate well between the low concentration and half filling limits,(ii) converges well with system size and thus applies to the thermodynamic limit, (iii) becomes exact in the atomic limit (t=0), conserves momentum exactly, and treats both short and long range correlations on equal basis; it should therefore interpolate well between the strong and weak coupling limits, which is important given the relatively small values of J/t in the manganites. and (iv) contains the well known $O(1/S^2)$ and RPA results as limiting cases. In this chapter we studied, among others, (i) the shape of the spin wave dispersion and ferromagnetic phase boundary for different system dimensionalities (1D, 2D, and 3D), (ii) the deviations from the strong coupling double exchange limit, and (iii) the role of up to three–body correlations and nonperturbative vertex corrections on the spin dynamics. By comparing the full three–body variational calculation to a number of approximations (RPA, 1/S expansion, ladder diagram treatment of two-body correlations, and carrier–localized spin rather than carrier–magnon scattering), we showed that the correlations play an important role on the spin excitation spectrum, the stability of the ferromagnetism, and the shape of the ferromagnetic phase boundary in the parameter range relevant to the manganites. Importantly, the correlations lead to spin dynamics that differs strongly from that of the short range Heisenberg ferromagnet for intermediate electron concentrations.

Our main results can be summarized as follows. First, the different approximations lead to substantial differences in the spin wave dispersion and ferromagnetic phase boundary for electron concentrations above $n \sim 0.3$ and intermediate values of J/t, which includes the parameter range relevant to the manganites. These large differences come from the correlations, which cannot be neglected, and imply that variational calculations should be used if possible in order to draw definite conclusions. Second, we find that, depending on n, there are two possible instabilities of the ferromagnetic state toward spin wave excitations: instability driven by a negative spin stiffness and instability at large momenta, close to the X–point

zone boundary, with positive stiffness. The latter instability only occurs in the 2D and 3D systems, for electron concentrations $n \leq 0.7$ and finite values of J. The three–body carrier–magnon correlations enhance this effect. As a precursor to the above zone boundary instability, we find a strong magnon softening at the X–point, which should be accompanied by short magnon lifetimes. Third, by comparing to the Heisenberg dispersion obtained by fitting to the long wavelength numerical results, we find strong deviations from the spin dynamics of the short range Heisenberg model. By choosing the exchange interaction so that the fully polarized ferromagnetic state is stable up to $n > 0.8$ as in the experiment, we show that the full three–body 2D calculation gives strong magnon softening at the X point for $0.5 \leq n \leq 0.7$, which changes into a small hardening for $n > 0.7$. This is similar to the behavior observed in the manganites. Our work provides new insight into the spin dynamics in the manganites and can be extended to treat related ferromagnetic systems (such as e.g. the III-Mn-V magnetic semiconductors) that are far from the double exchange strong coupling limit. Our calculations imply that the metallic ferromagnetic state in the manganites should be viewed as a strongly correlated state. Finally, the carrier–magnon correlations studied here can also play an important role in the ultrafast relaxation dynamics of itinerant ferromagnetic systems, which is beginning to be explored by using ultrafast magneto-optical pump–probe spectroscopy[48, 49, 50].

Chapter 3

Non–Heisenberg spin dynamics of double–exchange ferromagnets with Hubbard Repulsion.

3.1 Introduction

In the previous chapter we examined the spin–wave dispersion using the simple double–exchange hamiltonian $H_U = 0 = H_{AF}$ as our model hamiltonian. However, it is believed that this simple model is not adequate to describe the manganese oxides. The on-site Coulomb interaction must be included in a realistic model since it is the larger energy parameter in systems such as manganites. Having examined the simplest double–exchange model and clarified the role of correlations, in this chapter we study the concentration dependence of the spinwave dispersion predicted by the model Hamiltonian

$$H = K + H_{exch} + H_U + H_{AF}, \tag{3.1}$$

with a single e_g orbital per lattice site[11, 2, 58]. The question is whether the largest energy scale on the system, the local Hubbard repulsion U, changes qualitatively the physical processes and correlation effects predicted by the minimal Hamiltonian. Our main focus again is on the zone boundary spinwave softening and how U affects this. In a recent paper[11] it was suggested that perhaps U plays an important role and introduces effects absent in the minimal Hamiltonian. However, this paper presents a mean–field treatment with only partial results that could not explain the experiment. As already suggested by Golosov, the role of correlations induced by U absent in the minimal model, must be studied before conclusion can be drawn. Here we use a three–body variational wavefunction simi-

lar to the previous chapter to treat exactly the long–range magnon–Fermi sea pair three–body correlations induced by the interplay between H_U, H_{exch}, and H_{AF} (nonperturbatively in $1/S$). This approach interpolates between the strong/weak coupling and n=0/n=1 limits with the same formalism and can therefore be used to address the regime of intermediate interactions and n relevant to the manganites. At the same time, it recovers the 1/S expansion and exact numerical results [60, 41] as special cases. The recovery of such exact results gives us confidence on the validity of our method. As discuss below, we find that the magnon–pair correlations result in a pronounced spinwave softening at the zone boundary, which increases with hole doping x and depends strongly on the interaction parameters. However, we find that the physical origin of that softening differs. In particular, we identify correlations due to U absent in the minimal model which we show are mainly responsible for the softening Our variational calculation allows us to draw definite conclusions regarding the magnitude of this softening. We also show that the above correlations affect strongly the stability of the ferromagnetic order.

The rest of this chapter is organized as follows. First, in section 3.2 we discuss the method we use to calculate the spinwave dispersion. In subsection 3.2.1 we obtain the spin–wave dispersion when all the three–body correlations are included. The calculation of the RPA magnon energy is also presented in this subsection. The numerical calculation is more challenging with U because additional momentum dependencies are introduced. The set of our variational equations is transformed to a form convenient for the numerical calculation, by reducing the number of momentum components. This is very important for treating large systems and assessing the convergence to the thermodynamic limit. Moreover this allow us to provide a physical explanation of the origin of our numerical results. In subsection 3.2.2 the expansion in powers of the spin–polarized band splitting energy $J_S = SJ + nU$ is discussed. The spin–wave energy is expanded up to first order with respect to J_S. In this way we reproduce previous results. As we mentioned above the Hubbard repulsion parameter U is the largest energy scale in systems such as the manganites. For this reason this interaction is considered to be very large and thus the $U \to \infty$ limit is relevant. In subsection 3.2.3 we present the results we obtain in this limit and compare with our finite U results. Second, in section 3.3 we present our numerical results that are mainly focused on the role of the Hubbard repulsion and the super–exchange interaction. The significance of the spin–exchange interaction was already discussed in the previous chapter. In order to study the role of the interaction parameters U/t and J_{AF}/t we fix the spin–exchange parameter J/t. We perform our numerical calculations in fairly large 2D systems which are relevant to quasi–layered manganese oxides materials.

3.2 Method

In this section we present the variational equations that determine the wavefunction amplitudes $X^{\mathbf{Q}}$, $\Psi^{\mathbf{Q}}$, and $\Phi^{\mathbf{Q}}$ for the full hamiltonian Eq. (3.1). These are obtained by applying the same variational method described in the previous chapter. Because of the Hubbard repulsion and super–exchange interaction term included in the model hamiltonian Eq. (3.1) the system of variational equations is complicated as compared with the one obtained using the simple double–exchange hamiltonian ($H_U = 0 = H_{AF}$) in the previous chapter.

3.2.1 The three–body correlations equations

The variational equation that gives the magnon energy $\omega_{\mathbf{Q}}$ reads

$$\omega_{\mathbf{Q}} = \frac{Jn}{2} - \frac{J}{2N}\sum_{\nu} X_{\nu}^{\mathbf{Q}} + 2J_{AF}S\left(\gamma_{\mathbf{Q}} - \gamma_0\right) + \frac{J}{2N}\sum_{\alpha\nu}\Psi_{\alpha\nu}^{\mathbf{Q}}, \tag{3.2}$$

with

$$\gamma_{\mathbf{k}} = 2\sum_{i=2}^{d} cos(\mathbf{k}_i), \tag{3.3}$$

where $d = 1, 2, 3$ is the system dimensionality. The last term in the above equation describes the contribution due to the carrier–magnon scattering. The first three terms on the rhs give the RPA magnon energy provided that $X_{\nu}^{\mathbf{Q}}$ is approximated by its RPA value, obtained for $\Psi^{\mathbf{Q}} = 0$. The third term of Eq. (3.2) gives the super–exchange contribution to the magnon energy. This term has the form of the cosine-like nearest–neighbor Heisenberg ferromagnet discussed in the introduction. We notice that there is not explicit contribution of H_U in the equation of magnon energy as this term of the Hamiltonian includes only itinerant carrier operators. Because of this, the Hubbard repulsion term contributes only to the equation of amplitudes $X^{\mathbf{Q}}$ and $\Phi^{\mathbf{Q}}$. The super–exchange interaction also contributes to equation of $\Psi^{\mathbf{Q}}$, in addition to Eq. (3.2). The equation of $X_{\nu}^{\mathbf{Q}}$ has a form very similar to Eq. (2.17) obtained for the simple double–exchange model. The carrier–magnon scattering renormalizes $X_{\nu}^{\mathbf{Q}}$ as compared to the RPA result:

$$\begin{aligned}\left(JS + nU + \varepsilon_{\nu+\mathbf{Q}} - \varepsilon_{\nu} - \omega_{\mathbf{Q}}\right) X_{\nu}^{\mathbf{Q}} = \;& JS\left[1 + \sum_{\alpha}\Psi_{\alpha\nu}^{\mathbf{Q}}\right] \\ &+ \frac{U}{N}\left[\sum_{\nu'} X_{\nu'}^{\mathbf{Q}} + \sum_{\alpha,\nu'}\Phi_{\alpha\nu'\nu}^{\mathbf{Q}}\right],\end{aligned} \tag{3.4}$$

The first term in the above equation is similar to the minimal double–exchange model. However, the second term is new and is introduced by correlations due to Hubbard repulsion. While the first contribution to the second term is the RPA, the second term $\propto \Phi$ is due to correlations. As we show below this term plays a dominant role on the spin–wave softening.

The RPA is obtained from Eqs. (3.2) and (3.4) after setting $\Psi^{\mathbf{Q}} = \Phi^{\mathbf{Q}} = 0$:

$$\omega_{\mathbf{Q}}^{RPA} = \frac{Jn}{2} - \frac{J}{2N}\sum_{\nu} X_{\nu}^{\mathbf{Q}RPA} + 2J_{AF}S\left(\gamma_{\mathbf{Q}} - \gamma_0\right) \tag{3.5}$$

$$\left(JS + nU + \varepsilon_{\nu+\mathbf{Q}} - \varepsilon_{\nu} - \omega_{\mathbf{Q}}^{RPA}\right) X_{\nu}^{\mathbf{Q}RPA} = JS + \frac{U}{N}\sum_{\nu} X_{\nu}^{\mathbf{Q}RPA}. \tag{3.6}$$

One can simplify the above equations by defining the amplitude

$$F^{\mathbf{Q}} = \frac{1}{N}\sum_{\nu} X_{\nu}^{\mathbf{Q}}, \tag{3.7}$$

which does not depend on momentum ν. In this way one can rewrite Eq. (3.5) and (3.6) as:

$$\omega_{\mathbf{Q}}^{RPA} = \frac{Jn}{2} - \frac{J}{2}F^{\mathbf{Q}} + 2J_{AF}S\left(\gamma_{\mathbf{Q}} - \gamma_0\right) \tag{3.8}$$

$$\left(JS + nU + \varepsilon_{\nu+\mathbf{Q}} - \varepsilon_{\nu} - \omega_{\mathbf{Q}}\right) X_{\nu}^{\mathbf{Q}RPA} \quad = \quad JS + UF^{\mathbf{Q}}, \tag{3.9}$$

The amplitude $F^{\mathbf{Q}}$ can be calculated by substituting Eq. (3.9) into definition Eq. (3.7):

$$F^{\mathbf{Q}}\left(1 - \frac{U}{N}\sum_{\nu}\frac{1}{JS + nU + \varepsilon_{\nu+\mathbf{Q}} - \varepsilon_{\nu} - \omega_{\mathbf{Q}}}\right) = SJ\sum_{\nu}\frac{1}{JS + nU + \varepsilon_{\nu+\mathbf{Q}} - \varepsilon_{\nu} - \omega_{\mathbf{Q}}}. \tag{3.10}$$

Finally, substituting $F^{\mathbf{Q}}$ from this equation in Eq. (3.8) we obtain the RPA result in the form of an integral equation:

$$\omega_{\mathbf{Q}}^{RPA} = \frac{Jn}{2} - \frac{SJ^2}{2N}\frac{\sum_{\nu}\frac{1}{E_{\nu\mathbf{Q}}}}{1 - \frac{U}{N}\sum_{\nu}\frac{1}{E_{\nu\mathbf{Q}}}} + 2J_{AF}S\left(\gamma_{\mathbf{Q}} - \gamma_0\right), \tag{3.11}$$

where we introduce the spin flip excitation energy:

$$E_{\nu\mathbf{Q}} = JS + nU + \varepsilon_{\nu+\mathbf{Q}} - \varepsilon_{\nu} - \omega_{\mathbf{Q}}. \tag{3.12}$$

By setting $U = 0$ in Eq. (3.11) we recover the RPA result for the minimal double–exchange model discussed in the previous chapter. U introduces the enhancement factor described by the denominator in Eq. (3.11). In addition, by setting $J = 0$ in Eq. (3.10) we recover the RPA result for the pure Hubbard model[64]:

$$1 = \frac{U}{N} \sum_{\nu} \frac{1}{nU + \varepsilon_{\nu+\mathbf{Q}} - \varepsilon_{\nu} - \omega_{\mathbf{Q}}}. \tag{3.13}$$

The scattering amplitude $\Psi^{\mathbf{Q}}$ is determined by the variational equation

$$\begin{aligned}\left[\omega_{\mathbf{Q}} - \frac{Jn}{2} + \varepsilon_{\nu} - \varepsilon_{\alpha} - 2J_{AF}S(\gamma_{\mathbf{Q}+\nu-\alpha} - \gamma_0)\right] \Psi^{\mathbf{Q}}_{\alpha\nu} &= \frac{J}{2N}\left(1 - X^{\mathbf{Q}}_{\nu}\right) \\ &+ \frac{J}{2N}\sum_{\alpha'} \Psi^{\mathbf{Q}}_{\alpha'\nu} - \frac{J}{2N}\sum_{\nu'} \Psi^{\mathbf{Q}}_{\alpha\nu'} - \frac{J}{2N}\sum_{\nu'} \Phi^{\mathbf{Q}}_{\alpha\nu'\nu}. \end{aligned} \tag{3.14}$$

We note that this equation does not differ significantly from Eq. (2.18) for double–exchange model. The only new contribution comes from the super–exchange interaction, which simply adds a cosine-line term in the lhs excitation energy. This fact implies that H_{super} does not play an important role in carrier–magnon scattering. The first term on the rhs of the above equation gives the Born scattering approximation contribution to the carrier–magnon scattering amplitude, which is the only one that contributes to $O(1/S^2)$. The next two terms describe the effects of the multiple electron–magnon (second term) and hole magnon (third term) scattering. Finally, the last term comes from the electronic contribution to the scattered magnon, i.e. from the coherent excitation of a spin–$\uparrow$ electron to the spin–$\downarrow$ band.

The amplitude Φ^{Q} is given by the variational equation

$$\begin{aligned}\left(JS + nU + \varepsilon_{\mathbf{Q}+\mu+\nu-\alpha} - \varepsilon_{\mu} + \varepsilon_{\alpha} - \varepsilon_{\nu} - \omega_{\mathbf{Q}}\right) \Phi^{\mathbf{Q}}_{\alpha\nu\mu} &= JS\left(\Psi^{\mathbf{Q}}_{\alpha\nu} - \Psi^{\mathbf{Q}}_{\alpha\mu}\right) \\ &- U\left(X^{\mathbf{Q}}_{\nu} - X^{\mathbf{Q}}_{\mu}\right) \\ &+ \frac{U}{N}\left(\sum_{\nu'} \Phi_{\alpha\mu\nu'} + \sum_{\mu'} \Phi_{\alpha\mu'\nu}\right) - \frac{U}{N}\sum_{\alpha'} \Phi_{\alpha'\mu\nu}. \end{aligned} \tag{3.15}$$

Comparing this equation for the amplitude Φ with the corresponding one for the double–exchange model Eq. (2.19) we note that the above equation includes two additional terms (second and third line in the rhs) of Eq. (3.15) coming from H_U. The existence of those additional rescattering terms in the variational equation of amplitude Φ^{Q} do not allow us to obtain a closed equation for Φ^{Q} in contrast to the minimal double–exchange model considered in the previous chapter. This makes the solution of the set of variational equations impossible numerically since we have to deal with the matrix Φ^{Q} that depends on three momenta. Fortunately,

we can reduce the number of indexes of the variational amplitudes by defining:

$$A^{\mathbf{Q}}_{\mu\alpha} = \frac{1}{N}\sum_{\nu}\Phi^{\mathbf{Q}}_{\alpha\nu\mu}, \tag{3.16}$$

$$C^{\mathbf{Q}}_{\mu\nu} = \frac{1}{N}\sum_{\alpha}\Phi^{\mathbf{Q}}_{\alpha\nu\mu}. \tag{3.17}$$

The importance of these formulas is that we can express Φ and X in terms of A and C:

$$E_{\nu\mathbf{Q}}X^{\mathbf{Q}}_{\nu} = JS\left[1+\sum_{\alpha}\Psi^{\mathbf{Q}}_{\alpha\nu}\right] + \frac{U}{N}\left[\sum_{\nu}X^{\mathbf{Q}}_{\nu'} + \sum_{\alpha}A^{\mathbf{Q}}_{\alpha\nu}\right], \tag{3.18}$$

$$\begin{aligned}\left(JS + nU + \varepsilon_{\mathbf{Q}+\mu+\nu-\alpha} - \varepsilon_{\mu} + \varepsilon_{\alpha} - \varepsilon_{\nu} - \omega_{\mathbf{Q}}\right)\Phi^{\mathbf{Q}}_{\alpha\nu\mu} &= JS\left(\Psi^{\mathbf{Q}}_{\alpha\nu} - \Psi^{\mathbf{Q}}_{\alpha\mu}\right)\\ &-U\left(X^{\mathbf{Q}}_{\nu} - X^{\mathbf{Q}}_{\mu}\right)\\ &+U\left(A^{\mathbf{Q}}_{\nu\alpha} - A^{\mathbf{Q}}_{\mu\alpha}\right) + UC^{\mathbf{Q}}_{\mu\nu}.\end{aligned} \tag{3.19}$$

We can then solve Eq. (3.19) for matrices A and C, which depend on two momenta, rather than for Φ, which depends on three momenta. This transformation allows us to solve the system of equations for fairly large systems ($N \simeq 20-30$). Using the notations (3.16,3.17) and Eq. (3.19) we obtain the set of equations which is satisfied by the new amplitudes:

$$\begin{aligned}A^{\mathbf{Q}}_{\mu\alpha}\left(1+\frac{U}{N}\sum_{\nu}\frac{1}{K_{\mathbf{Q};\mu\nu\alpha}}\right) &= \frac{JS}{N}\sum_{\nu}\frac{\Psi^{\mathbf{Q}}_{\alpha\nu} - \Psi^{\mathbf{Q}}_{\alpha\mu}}{K_{\mathbf{Q};\mu\nu\alpha}}\\ &-\frac{U}{N}\sum_{\nu}(X^{\mathbf{Q}}_{\nu} - X^{\mathbf{Q}}_{\mu})\frac{1}{K_{\mathbf{Q};\mu\nu\alpha}}\\ &+\frac{U}{N}\sum_{\nu}\frac{A^{\mathbf{Q}}_{\nu\alpha} + C^{\mathbf{Q}}_{\mu\nu}}{K_{\mathbf{Q};\mu\nu\alpha}},\end{aligned} \tag{3.20}$$

$$\begin{aligned}C^{\mathbf{Q}}_{\mu\nu}\left(1-\frac{U}{N}\sum_{\alpha}\frac{1}{K_{\mathbf{Q};\mu\nu\alpha}}\right) &= \frac{JS}{N}\sum_{\alpha}\frac{\Psi^{\mathbf{Q}}_{\alpha\nu} - \Psi^{\mathbf{Q}}_{\alpha\mu}}{K_{\mathbf{Q};\mu\nu\alpha}}\\ &-\frac{U}{N}(X^{\mathbf{Q}}_{\nu} - X^{\mathbf{Q}}_{\mu})\sum_{\alpha}\frac{1}{K_{\mathbf{Q};\mu\nu\alpha}}\\ &+\frac{U}{N}\sum_{\alpha}\frac{A^{\mathbf{Q}}_{\nu\alpha} - A^{\mathbf{Q}}_{\mu\alpha}}{K_{\mathbf{Q};\mu\nu\alpha}},\end{aligned} \tag{3.21}$$

where we introduced the excitation energy

$$K_{\mathbf{Q};\mu\nu\alpha} = JS + nU + \varepsilon_{\mathbf{Q}+\mu+\nu-\alpha} - \varepsilon_{\mu} + \varepsilon_{\alpha} - \varepsilon_{\nu} - \omega_{\mathbf{Q}}. \tag{3.22}$$

Summarizing, by using a number of transformations, we reduce the the variational solution of the three–body correlations to the system of variational equations 3.2, 3.14,3.18, 3.20 and 3.21. We solve this system iteratively until full convergence is reached to the magnon energy.

A very useful form of the variational equations can be obtained by substituting the amplitude $X_{\nu}^{\mathbf{Q}}$ from Eq. (3.18) to the variational equation for the magnon energy Eq. (3.2). In this way we obtain:

$$\begin{aligned}
\omega_{\mathbf{Q}} &= 2J_{AF}S\left(\gamma_{\mathbf{Q}} - \gamma_0\right) + \frac{Jn}{2} - \frac{SJ^2}{2N}\frac{\sum_{\nu}\frac{1}{E_{\nu\mathbf{Q}}}}{1 - \frac{U}{N}\sum_{\nu}\frac{1}{E_{\nu\mathbf{Q}}}} \\
&- \frac{SJ^2}{2N}\frac{1}{1 - \frac{U}{N}\sum_{\nu}\frac{1}{E_{\nu\mathbf{Q}}}}\sum_{\alpha\nu}\frac{\Psi_{\alpha\nu}^{\mathbf{Q}}}{E_{\nu\mathbf{Q}}} + \frac{J}{2N}\sum_{\alpha\nu}\Psi_{\alpha\nu}^{\mathbf{Q}} \\
&+ \frac{JU}{2N^2}\frac{1}{1 - \frac{U}{N}\sum_{\nu}\frac{1}{E_{\nu\mathbf{Q}}}}\sum_{\mu}\frac{1}{E_{\mu\mathbf{Q}}}\sum_{\alpha}A_{\mu\alpha}^{\mathbf{Q}}.
\end{aligned} \tag{3.23}$$

The first term of the r.h.s. of Eq. (3.23) gives the RPA magnon energy Eq. (3.5) while the second and third terms give the correlation contribution. More precisely the third term is the contribution of the $\Phi_{\alpha\mu\nu}^{\mathbf{Q}}$ variational amplitude which describes a contribution due to scattering of a spin flip excitation with a Fermi sea electron excitation induced by U. The second term is similar to the minimal Hamiltonian. Therefore, the form of equation 3.23 provides us with an explicit description of the contribution of each one of the variational amplitudes to magnon energy. In this way we are able to assess the role of each one term and also to determine the main origin of our results.

3.2.2 The $1/J_S$ expansion

Before presenting our numerical results, we obtain the spinwave energy at 1^{st} order at $1/J_S$ expansion approximation, where $J_S = SJ + nU$ is the mean–field spin polarized band splitting. This is a reasonable approximation since both J and U are quite large parameters in comparison to the Fermi energy, E_F. An expansion in the above parameter is performed in the literature[11] by Golosov simultaneously with a first order expansion in powers of $1/S$. The purpose of this subsection is to show that our equations recover these results by applying the same kind of expansions. First of all, we suppose that $S \to \infty$ while we keep the

parameters $SJ = \bar{J}$ and $S^2 J_{AF} = \bar{J}_{AF}$ finite. Within this notation the equation of variational amplitude $\Psi_{\alpha\nu}$ becomes:

$$\left[\omega_{\mathbf{Q}} - \frac{\bar{J}n}{2S} + \varepsilon_\nu - \varepsilon_\alpha\right] \Psi^{\mathbf{Q}}_{\alpha\nu} = \frac{\bar{J}}{2NS}\left(1 - X^{\mathbf{Q}}_\nu\right)$$
$$+\frac{\bar{J}}{2NS}\sum_{\alpha'} \Psi^{\mathbf{Q}}_{\alpha'\nu} - \frac{\bar{J}}{2NS}\sum_{\nu'} \Psi^{\mathbf{Q}}_{\alpha\nu'} - \frac{\bar{J}}{2NS}\sum_{\nu'} \Phi^{\mathbf{Q}}_{\alpha\nu'\nu}. \tag{3.24}$$

It becomes clear that $\Psi_{\alpha\nu}$ is of order $O(1/S)$ and thus contributes as $O(1/S^2)$. Therefore $\Psi_{\alpha\nu}$ does not contribute to the $O(1/S)$ magnon energy which subsequently becomes:

$$\omega_{\mathbf{Q}} = \frac{\bar{J}n}{2S} - \frac{\bar{J}^2}{2NS}\frac{\sum_\nu \frac{1}{E_{\nu\mathbf{Q}}}}{1 - \frac{U}{N}\sum_\nu \frac{1}{E_{\nu\mathbf{Q}}}}$$
$$+\frac{\bar{J}U}{2N^2 S}\frac{1}{1 - \frac{U}{N}\sum_\nu \frac{1}{E_{\nu\mathbf{Q}}}}\sum_\mu \frac{1}{E_{\mu\mathbf{Q}}}\sum_\alpha A^{\mathbf{Q}}_{\mu\alpha},$$

where we have to remove magnon energy from $E_{\nu\mathbf{Q}}$, in order to obtain $\omega_{\mathbf{Q}}$ to $O(1/S)$. Thus we obtain: $E_{\nu\mathbf{Q}} = J_S + \varepsilon_{\nu+\mathbf{Q}} - \varepsilon_\nu$. Note also that we have set $\bar{J}_{AF} = 0$ in both equations 3.24 and 3.25. The amplitude $A^{\mathbf{Q}}_{\mu\alpha}$ must be calculated in zeroth order in $1/S$.

$$A^{\mathbf{Q}}_{\mu\alpha}\left(1 - \frac{U}{N}\sum_\nu \frac{1}{K_{\mathbf{Q};\mu\nu\alpha}}\right) = -\frac{U}{N^2}\sum_\nu (X^{\mathbf{Q}}_\mu - X^{\mathbf{Q}}_\nu)\frac{1}{K_{\mathbf{Q};\mu\nu\alpha}}$$
$$-\frac{U}{N}\sum_\nu \frac{A^{\mathbf{Q}}_{\nu\alpha} - C^{\mathbf{Q}}_{\mu\nu}}{K_{\mathbf{Q};\mu\nu\alpha}}, \tag{3.25}$$

where $K_{\mathbf{Q};\mu\nu\alpha} = J_S + \varepsilon_{\mathbf{Q}+\mu+\nu-\alpha} - \varepsilon_\mu + \varepsilon_\alpha - \varepsilon_\nu$. Now what remains to do is an expansion in powers of the splitting energy J_S in the above equations, supposing that the fraction E_F/J_S is a small factor. After some algebra we finally obtained one closed equation. The spinwave energy in the leading–order of both $O(E_F/J_S)$ and $O(1/S)$ is:

$$\omega^{(1)}_{\mathbf{Q}} = \frac{E}{2S}\left(1 + \varepsilon_{\mathbf{Q}}\right)\frac{\bar{J}^2 + \frac{n\bar{J}EU^2}{J_S^2}\left(1 + \varepsilon_{\mathbf{Q}}\right)}{\left[\bar{J} + \frac{EU}{J_S}\left(1 + \varepsilon_{\mathbf{Q}}\right)\right]^2}, \tag{3.26}$$

where $E = \sum_\nu \varepsilon_\nu$ is the total electron energy in the spin$\uparrow$ band and $\varepsilon_{\mathbf{Q}}$ is the electron band energy given by Eq. (2.4) in the previous chapter. The above relation for magnon energy recovers previous results obtained perturbatively in a different way[11]. A comparison between the large–J_S magnon dispersion and stiffness and our 3–body calculation is made in subsection 3.3 and the validity of that approximation is assessed.

3.2.3 The $U \to \infty$ approximation

Owing to the fact that the parameter U/t is the largest energy parameter in the manganese oxides, a reasonable treatment of this interaction is the $U \to \infty$ limit. In this extreme limit, two itinerant electrons cannot occupy the same lattice site, since double occupancy increases dramatically the total energy of the system. In this case all the itinerant electron spins are forced to be parallel with the localized spin in order to minimize the total energy of the system. Therefore by assuming $U \to \infty$ one expects an enhancement of ferromagnetism more pronounced, as compared to the finite U result. Instability of the fully polarized state can occurred only by the interplay of the finite Hubbard interaction with the Hund's rule interaction J. In section 3.3 we examine numerically the validity of this extreme limit by comparing with our finite U results.

In order to obtain the system of variational equations in this limit one has to expand the variational amplitudes in powers of $1/U$:

$$X_{\nu}^{\mathbf{Q}} = X_{\nu}^{0} + \frac{X_{\nu}^{1}}{U} + O(\frac{1}{U^2}) \cdots \tag{3.27}$$

$$\Phi_{\alpha\mu\nu}^{\mathbf{Q}} = \Phi_{\alpha\mu\nu}^{0} + \frac{\Phi_{\alpha\mu\nu}^{1}}{U} + O(\frac{1}{U^2}) \cdots . \tag{3.28}$$

Substituting Eqs (3.27) and (3.28) in Eqs. (3.4) and (3.15) and keeping only the $O(U)$ terms we found that:

$$nUX_{\nu}^{0} = \frac{U}{N}(\sum_{\nu'} X_{\nu'}^{0} - \sum_{\alpha\mu} \Phi_{\alpha\mu\nu}^{0}) \tag{3.29}$$

$$\begin{aligned} nU\Phi_{\alpha\mu\nu}^{0} &= -\frac{U}{N}(X_{\mu}^{0} - X_{\nu}^{0}) \\ &+\frac{U}{N}(\sum_{\nu'} \Phi_{\alpha\mu\nu'}^{0} + \sum_{\mu'} \Phi_{\alpha\mu'\nu}^{0}) \\ &-\frac{U}{N}\sum_{\alpha'} \Phi_{\alpha'\mu\nu}^{0}, \end{aligned} \tag{3.30}$$

We can easily see from Eqs. (3.29-3.31) that the variational amplitudes $X_{\nu}^{\mathbf{Q}}$ and $\Phi_{\mu\nu\alpha}^{\mathbf{Q}}$ in the $U \to \infty$ limit are independent of the momenta α, μ and ν. Taking into account the antisymmetry of Φ with respect to the exchange of the Fermi sea electron momenta ν and μ

$$\Phi_{\alpha\mu\nu}^{\mathbf{Q}} = -\Phi_{\alpha\nu\mu}^{\mathbf{Q}}, \tag{3.31}$$

we find that:

$$\Phi^{0} = -\Phi^{0} \Rightarrow \Phi^{0} = 0. \tag{3.32}$$

This results indicates that only the scattering of the electron–hole pair with a localized spin contributes in the infinite Hubbard repulsion limit. We can understand this result by noting that the variational amplitude $\Phi_{\alpha\mu\nu}$ expresses a processes where the electron–hole pair is scattered by an electron spin$\uparrow$–$\downarrow$ excitation. The creation of such excitation, however, is impossible since the electron band's splitting energy $J_S + nU$ is in this limit infinite. In order to determine the $\mathbf{Q}$–dependence of the amplitude X^0 we use Eq. (3.10), which now can be rewritten as follows

$$F^{\mathbf{Q}} = \frac{1}{N}\sum_{\nu} X^{\mathbf{Q}} = nX^0. \tag{3.33}$$

By expanding $F^{\mathbf{Q}}$ we find that:

$$\begin{aligned} F^{\mathbf{Q}} &= nSJ\frac{N_e + \sum_{\alpha\mu}\Psi^{\mathbf{Q}}_{\alpha\mu}}{\sum_{\mu}(\varepsilon_{\mu+\mathbf{Q}} - \varepsilon_{\mu} + SJ - \omega_{\mathbf{Q}})} \Rightarrow \\ X^0 &= SJ\frac{N_e + \sum_{\alpha\mu}\Psi^{\mathbf{Q}}_{\alpha\mu}}{\sum_{\mu}(\varepsilon_{\mu+\mathbf{Q}} - \varepsilon_{\mu} + SJ - \omega_{\mathbf{Q}})}. \end{aligned} \tag{3.34}$$

Finally, the variational equation of the magnon energy in the $U \to \infty$ limit becomes:

$$\begin{aligned} \omega_{\mathbf{Q}} &= \frac{Jn}{2} - \frac{nJ^2S}{2}\frac{N_e}{\sum_{\mu}(\varepsilon_{\mu+\mathbf{Q}} - \varepsilon_{\mu} + SJ - \omega_{\mathbf{Q}})} \\ &\quad + \frac{J}{2n}\left[1 - \frac{N_eSJ}{\sum_{\mu}(\varepsilon_{\mu+\mathbf{Q}} - \varepsilon_{\mu} + SJ - \omega_{\mathbf{Q}})}\right]\sum_{\alpha\nu}\Psi^{\mathbf{Q}}_{\alpha\nu}. \end{aligned} \tag{3.35}$$

The first line of the r.h.s. of Eq. 3.35 determines the RPA spinwave dispersion while the second line expresses the contribution of the correlation described by the amplitude $\Psi^{\mathbf{Q}}_{\alpha\nu}$, which is given by the equation:

$$\begin{aligned} \Psi^{\mathbf{Q}}_{\alpha\nu}\left(\omega_{\mathbf{Q}} + \varepsilon_{\nu} - \varepsilon_{\alpha} - \frac{Jn}{2}\right) &= \frac{J}{2N}\left[1 - \frac{SJn}{\frac{1}{N}\sum_{\mu}(\varepsilon_{\mu+\mathbf{Q}} - \varepsilon_{\mu} + SJ - \omega_{\mathbf{Q}})}\right] \\ &\quad - \frac{SJ^2}{2N}\frac{\sum_{\beta\mu}\Psi^{\mathbf{Q}}_{\beta\mu}}{\sum_{\mu}(\varepsilon_{\mu+\mathbf{Q}} - \varepsilon_{\mu} + SJ - \omega_{\mathbf{Q}})} \\ &\quad + \frac{J}{2N}\left(\sum_{\beta}\Psi^{\mathbf{Q}}_{\beta\nu} - \sum_{\mu}\Psi^{\mathbf{Q}}_{\alpha\mu}\right). \end{aligned} \tag{3.36}$$

We conclude that in the $U \to \infty$ limit the variational equations simplify considerably and reduce to a system of two equations, Eq. (3.35) and (3.36).

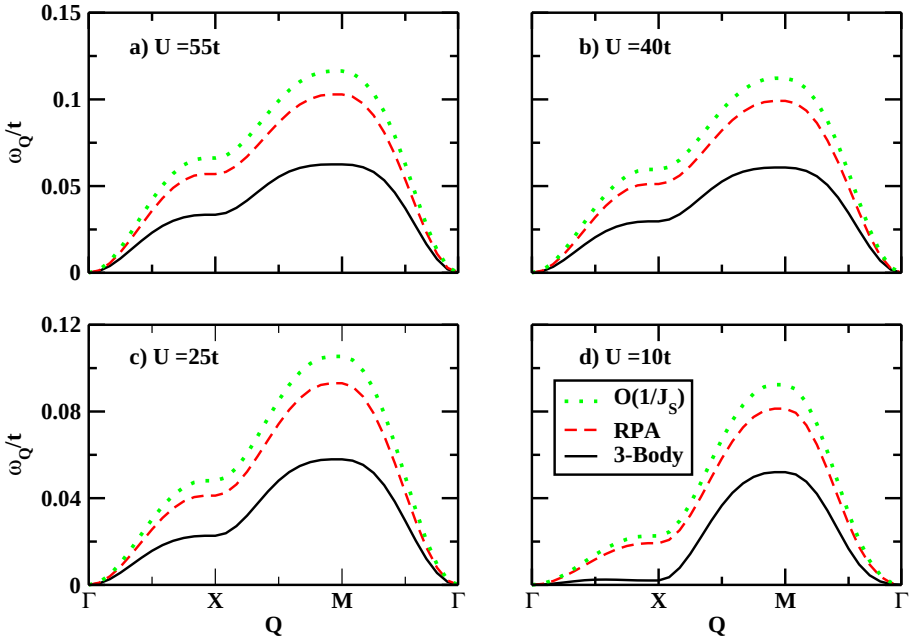

Figure 3.1: Spinwave dispersion along different directions in the Brillouin zone for n=0.6, J =7t, J_{AF} =0.012t and for different values of U/t.

3.3 Numerical results

In this section we present our numerical results obtained by the system of variational equations (Eq. 3.2,3.18, 3.14, 3.20 and 3.21). We perform the numerical calculations in fairly large 2D systems with $N \simeq 20-30$, i.e. N^2 lattice sites, where we obtain satisfying convergence to thermodynamic limit $N \to \infty$.

We start our presentation with the numerical results concerning the effect of Hubbard repulsion on the spin–wave dispersion. Fig.3.1 shows the calculated spinwave dispersion along different directions in the Brillouin zone for values of Hubbard interaction U/t varied from a minimum of $U = 10t$ to a maximum of $U = 55t$. These are typical for the manganese oxides. The double–exchange and super–exchange interaction parameter are fixed to the typical values $J = 7t, J_{AF} = 0.012t$. In addition, in this figure the dispersion is shown within the RPA, using the full three–body calculation, as well as in 1^{st} order in the $1/J_S$ expansion approximation (results of Ref[11]). We notice that with decreasing U/t, the magnon energies take on lower values. The latter applies to all approximations shown in the figure. We conclude that the on–site Coulomb repulsion H_U enhances the spinwave energies and therefore the stability of the ferromagnetic state $|F\rangle$.

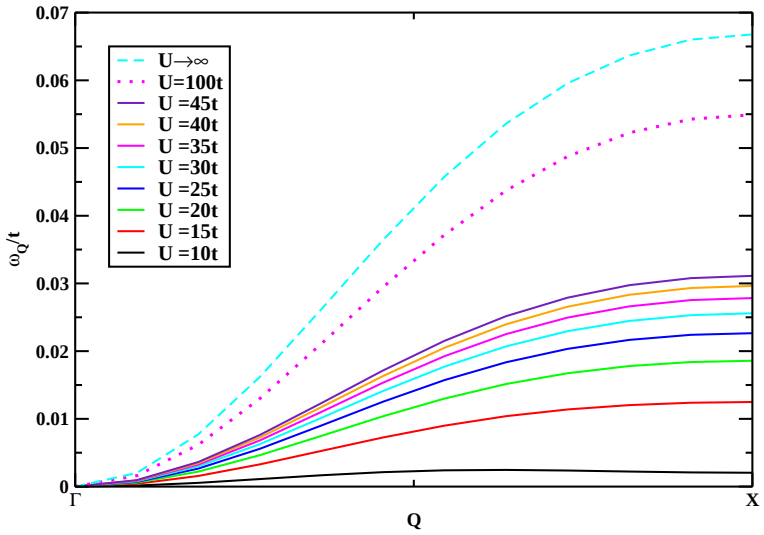

Figure 3.2: Spinwave dispersion along direction $\Gamma - X$ in the Brillouin zone for n=0.6, J =7t, J_{AF} =0.012t and U=(10–45)t in increments of 5t, increasing upward. Dotted line: $U = 100t$, Dashed line: $U \to \infty$. We notice the very slow convergence to the $U \to \infty$ result.

The value of the Hubbard repulsion U relevant to the manganites varies in the literature. In general, the interaction U is the largest energy of the manganese oxides systems as compared to magnetic–exchange J, hopping energy t and super–exchange interaction J_{AF}. Because of this the Hubbard repulsion is usually treated within the Large–U approximation. We examine here the validity of this treatment by comparing the magnon dispersions along the $\Gamma - X$ direction for different U, within the full three–body correlation treatment. These results are shown in the Fig. 3.2 for values of U that differ by a fixed amount $\Delta U = 5t$. The dispersions in this figure are calculated for U/t which takes values in the region:

$$10 \leq \frac{U}{t} \leq \infty. \tag{3.37}$$

We observe that initially the spin–wave energies increase strongly with U. For example, the $U = 15t$ dispersion differs from the result for $U = 10t$ by a factor of five. However, the difference rapidly diminishes as U/t increases. The relative changes in the dispersion decrease with increasing U and finally converge to the $U \to \infty$ result for $U > 45t$. With increasing U/t we also note a change in the zone boundary softening of spin–wave dispersion. For very large U this softening is completely eliminated and the dispersion acquires a cosine–line shape. The latter

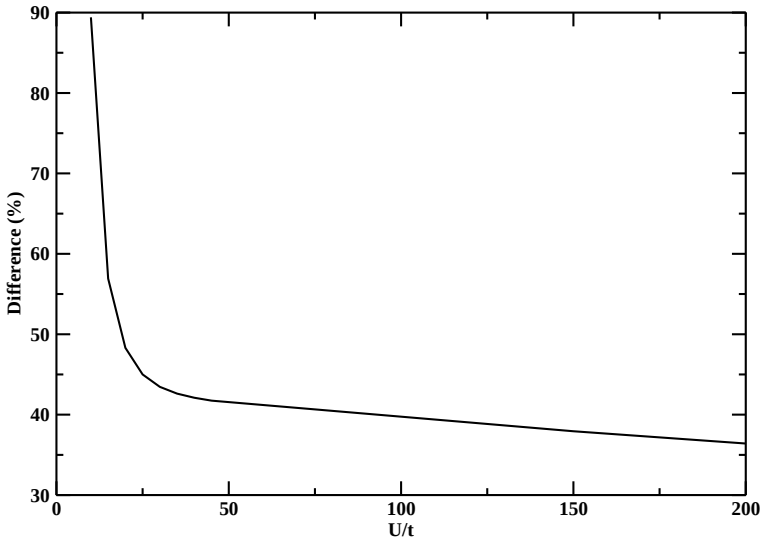

Figure 3.3: Deviations from the RPA at the X–point as a function of Hubbard repulsion U/t. The deviation is slowly converging to the the $U \to \infty$ result.

result indicates that, although the Hubbard interaction U/t is usually larger than the double–exchange interaction J/t, the large–U treatment must be applied with caution. In particular for intermediate U/t, say $U \simeq 20t$, we conclude that the $U \to \infty$ limit is not expected to give a trustworthy description of magnon dispersion. In conclusion, typical values of U quoted in the literature give a dispersion that differs by factor of 3 or larger from the $U \to \infty$ result.

Fig.3.1 also compares our results to the RPA ($\Psi = \Phi = 0$) and to the results of Ref.[11], obtained by expanding the RPA to $O(1/J_S)$, where $J_S = SJ + nU$. While our RPA variational results agree well with Ref.[11], the pair–magnon correlations lead to a strong softening (deviations $\sim$100% from the RPA). While this is maximum along Γ–X ((0,0)$\to(\pi,0)$) it remains strong along the other directions. The latter is in contrast to the U=J_{AF}=0 results[58]. While the relative differences from the RPA decrease with increasing U, they remain quite large as $U \to \infty$. The latter result points the importance of the three–body correlations even in the large–U limit. This can be seen in Fig. 3.3, which shows the percentage deviation from the RPA at the X–point as function of U:

$$R = (1 - \omega/\omega^{RPA}) \tag{3.38}$$

Note that the maximum possible value of this parameter is 100% if the three–body dispersion is so softened near the zone boundary that it is about to turn negative.

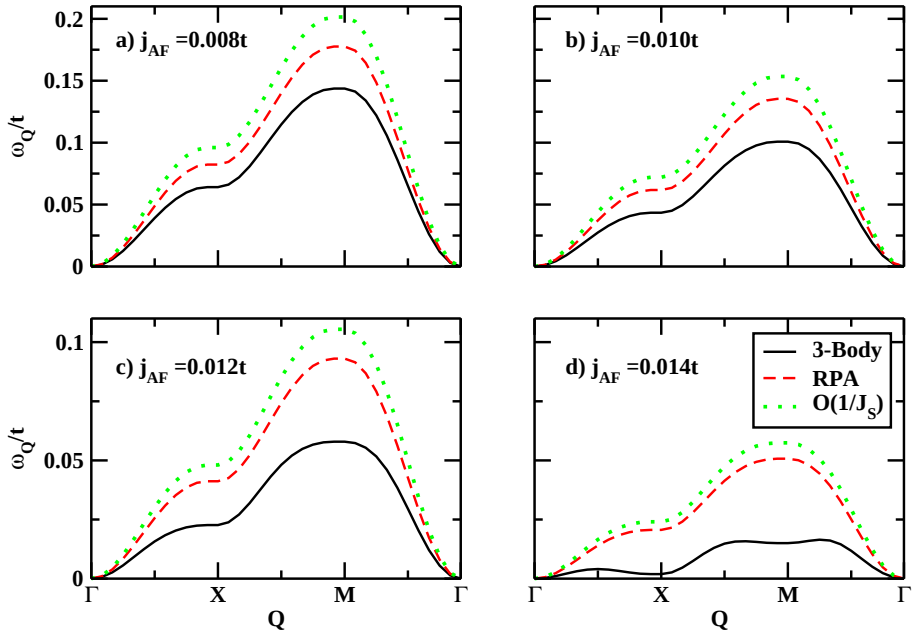

Figure 3.4: Spinwave dispersion along different directions in the Brillouin zone for n=0.6, J =7t, U =25t and for different values of J_{AF}/t.

For Hubbard repulsion equal to this critical value U_C, R takes its maximum value, since for this value the three–body dispersion is exactly equal to zero. We observe that we can distinguish two regions regarding the behaviour of the deviation of the RPA (i.e. the effect of the correlations). For small values of U/t, the percentage deviation from the RPA is decreasing rapidly from its maximum value (100%) with increasing values of parameter U/t. Within the region $10t \lesssim U \lesssim 30t$, $100\% \gtrsim R \gtrsim 45\%$. On the hand, for larger values of Hubbard interaction the deviation is decreasing slowly. Indeed, Fig. (3.3) is characterized by two different slopes. In particular, for a value as large as $U = 100t$, $R \simeq 40\%$ almost equal to that for $U = 50t$. Note that the $U \to \infty$ deviation is about 20%, therefore we have slow convergence to that limit. These results are consistent with the previous discussion about the convergence to the $U \to \infty$ limit. It is expected that for small values of Hubbard repulsion, a small change in U/t affects the dispersion significantly. The effect of increasing U/t on spinwave dispersion becomes less important at the large–U limit. However, full convergence to the $U \to \infty$ results is not achieved even for values as large as $U = 100t$. To conclude, correlations are very strong even in the strong coupling limit ($R \simeq 40\%$ for the largest U quoted in the literature).

Next we continue with the role of super–exchange interaction on spin–wave dispersion. In Fig. (3.4) we plot the magnon dispersion for fixed $J = 7t, U = 25t$ and varied values of J_{AF}/t from $J_{AF} = 0.008t$ to $0.014t$, typical for the systems of interest. We notice an opposite change of dispersion as compared with the Hubbard repulsion. An increase in J_{AF}/t suppresses magnon energies along every direction of the Brillouin zone. Let us note that this suppression does not change the deviation between the RPA and three–body dispersions, which results from correlations. For example at the X–point $\mathbf{Q} = (\pi, 0)$ there is a constant decrease about $\simeq 0.025$ in units of t between these approximations. Taking into account the suppression of magnon energies we see that the increase of J_{AF} magnifies the relative differences. For instance, at the X–point the relative deviation of the three–body dispersion is $\simeq 30\%$ for $J_{AF} = 0.008t$, while it takes a maximum value about 100% for $J_{AF} = 0.014t$, where the correlated dispersion almost turns negative at the zone boundary. The latter applies also to the difference between the RPA and $1/J_S$ dispersion, where however the relative deviation remains very small as these approximations give results very close to each other. We also notice that the increase in J_{AF}/t suppresses equivalently the three–body spinwave along every direction of brillouin zone. We conclude that the super–exchange interaction is of minor importance as compared to the Hubbard interaction since it does not change the spinwave dynamics in a qualitative way. It simply magnifies the effects of Hubbard repulsion.

We now consider the spinwave energies close to the X–point. In the experiments described in Refs.[6, 7, 8] it was shown that the deviations of the nearest–neighbor Heisenberg model dispersion that fits the long–wavelength (small Q) experimental results increase with decreasing n at the zone boundary. The experimental dispersion can be fitted phenomenologically to a Heisenberg model that includes fourth–nearest–neighbor (J_4) and next–nearest–neighbor (J_1) exchange couplings. Along the direction $\Gamma \rightarrow X$ the Heisenberg ferromagnetic dispersion including the fourth–nearest neighbors is:

$$\omega_{\mathbf{Q}}^{Heis.} = 2J_1(1 - cosQ_x) + J_4 sinQ_x{}^2. \tag{3.39}$$

The ratio J_4/J_1, obtained by fitting the experiments, characterizes the magnitude of the zone boundary softening. J_4/J_1 was found to increase linearly with x=1-n for $0.5 \leq n \leq 0.7$ [8, 7]. Our numerical results can be fitted very well to the above J_1–J_4 Heisenberg model dispersion, similar with the experiments. Fig. 3.5 shows $J_4(n)/J_1(n)$ for four different J. We do not show the $1/J_S$ expansion results in this figure as these are very similar to the RPA ones The crucial role of the pair–magnon correlations is clear by comparing to the RPA. The RPA gives a small J_4/J_1, which can be understood by noting that, in the strong coupling limit, it coincides with the nearest–neighbor Heisenberg dispersion [58]. However, the pair–

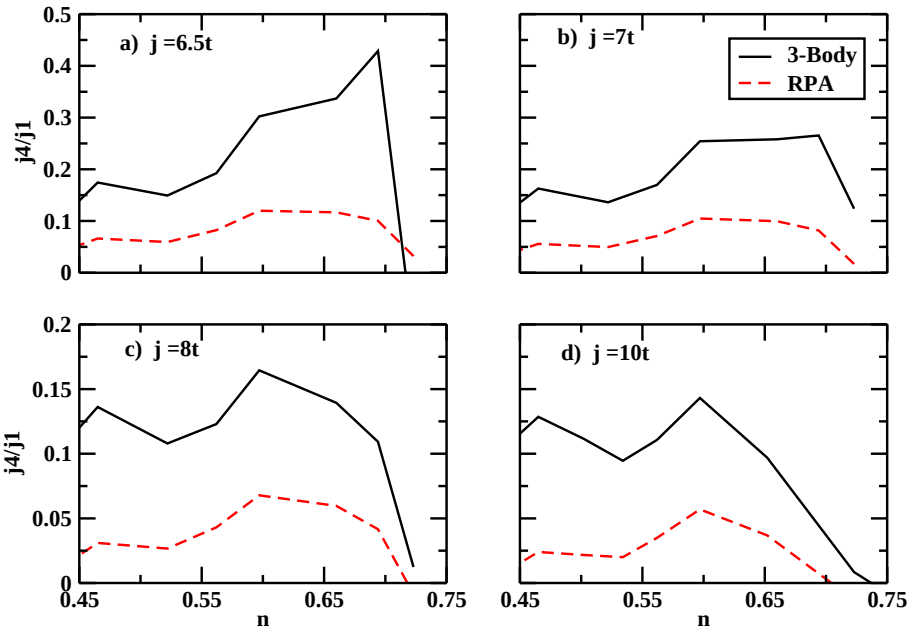

Figure 3.5: $J_4(n)/J_1(n)$ for $J_{AF} = 0.012t, U = 25t$ from the best fit to the 1st+4th nearest neighbor Heisenberg model.

magnon correlations greatly enhance J_4/J_1, typically by a factor 3-4 or higher in Fig. 3.5. The resulting X–point softening increases as we decrease J/t (to as high as J_4/J_1= 0.4 or 40% for the parameters of Fig. 3.5). J_4/J_1 increases with x=1-n until it reaches its maximum value. The range of concentrations within which this increase occurs depends on the interaction parameters. For large J/t (i.e. closer to the strong coupling limit), J_4/J_1 increases more slowly with x, while it increases more sharply for smaller J as the ferromagnetic state becomes less stable (compare Figs. 3.5(a) and 3.5(d)). On the other hand, J_4/J_1 is small (or negative, which implies hardening) for n >0.7. For smaller n, J_4/J_1 decreases with decreasing n and eventually increases again as the antiferromagnetic correlations dominate.

Next we turn to the spinwave dispersion for small momenta Q. Its behaviour is characterized by the spinwave stiffness $D(n)$, obtained by fitting the small–Q numerical dispersion to the quadratic form DQ^2. Golosov[11] showed that, to $O(1/JS)$, the on–site Hubbard repulsion U shifts the maximum value of $D(n)$ to larger concentrations $n > 0.5$. Fig. 3.6(a) compares the $O(1/J_S)$ results of Ref.[11] to Eq.(2.15) and the RPA. The pair–magnon correlations decrease the magnitude of the spinwave stiffness $D(n)$, by as much as ∼100% as compared to Ref.[11] and by as much as ∼50% as compared to the RPA. We note in Fig.3.6(a) that

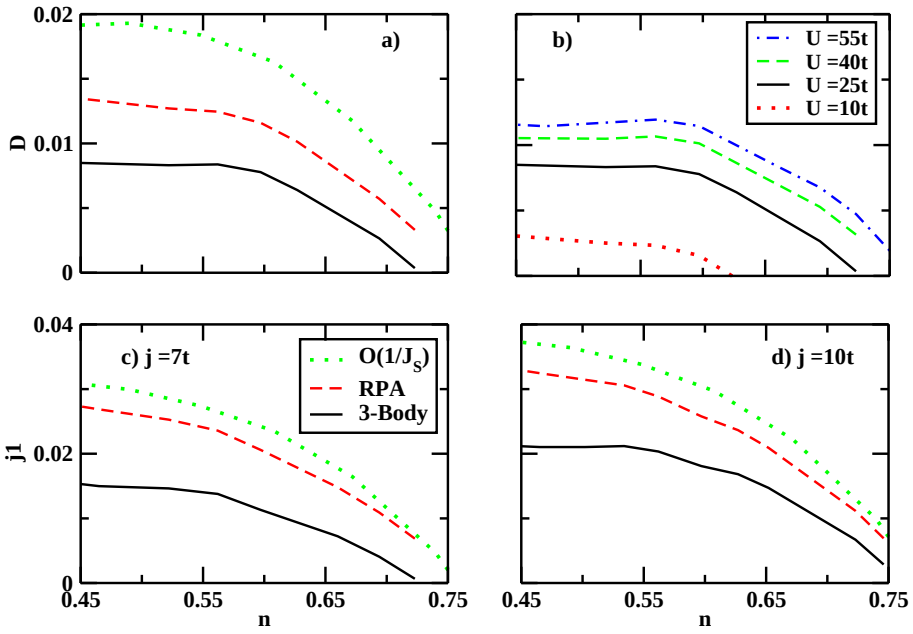

Figure 3.6: Spinwave stiffness D as function of electron concentration n for J_{AF}=0.012t. (a) Comparison to the RPA and $O(1/J_S)$ results for J =7t and U=25t. (b) The effects of U. (c) Comparison of $J_1(n)$ to the RPA and $O(1/JS)$ approximations for J=7t, U=25t. (d) same as (c) for J=10t.

$D(n)$ exhibits a rather broad plateau as a function of n, where it remains fairly constant within a wide range of concentrations relevant to the manganites. The pair–magnon correlations also decrease the dependence of $D(n)$ on n within this concentration range and shift its maximum to higher n as compared to the RPA and Ref.[11]. The above plateau is followed by a regime of decreasing $D(n)$ as the spinwave instability shifts from the zone boundary to small momenta ($D < 0$). The effects of U on $D(n)$ are demonstrated by Fig.3.6(b). The stiffness increases with U and starts to converge to its $U \to \infty$ values for $U > 40t$. U shifts the maximum of $D(n)$ to higher values of n and broadens the concentration range where $D(n)$ remains constant.

Although overall Figs.3.5 and 3.6 after including the correlation effects are consistent with the experiment [7, 8], J_1 increases with decreasing n, unlike in Ref.[8] (Figs.3.6(c) and 3.6(d)). However, the pair–magnon correlations significantly *reduce* J_1 as compared to the RPA prediction, i.e. change its behaviour in the direction of the experiment [8] (Figs.3.5 and 3.6). Given that our calculation was performed in 2D without including bandstructure effects, we speculate

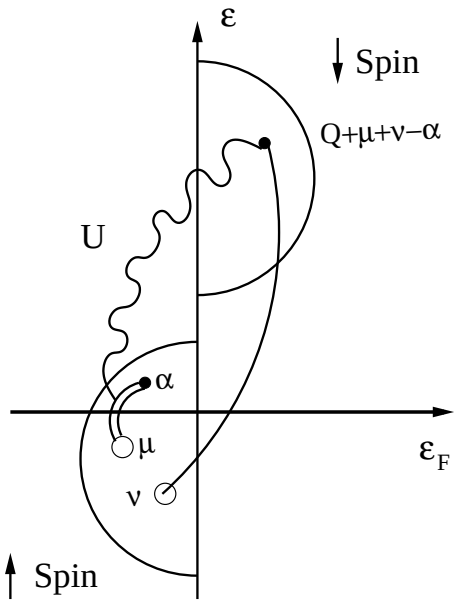

Figure 3.7: The scattering of the spin↑→spin↓ excitation (solid line) with a Fermi sea pair (double line). The interaction takes place via U (wave curve)

that the suppression of $J_1(n)$ by the correlations could be stronger in the realistic system.

We now turn to the origin of the zone boundary softening which is demonstrated above. We show here that it is mainly dominated by strong correlations due to Hubbard repulsion, described by the parameter U. In order to focus on the role of U we set the super–exchange interaction $J_{AF} = 0$. As we discussed, the spin–wave dispersion $\omega_{\mathbf{Q}}$ is determined by the amplitude $X_{\mu}^{\mathbf{Q}}$ Eq. 3.4, which describes the coherent spin↑ spin↓ excitation and $\Psi_{\alpha\nu}$, describing magnon–pair scattering. These processes are expressed by the second and the last term correspondingly of the r.h.s. of Eq. 3.2. Although Ψ also contributes to the minimal model discussed in the previous chapter, the dominant new effect here comes from the renormalization of $X_{\mu}^{\mathbf{Q}}$ by the scattering, due to U, of a spin↑→ spin↓ excitation with a Fermi sea pair. The corresponding interaction process is described by the amplitude Φ in the variational equation of amplitude X Eq. 3.4 and is shown schematically in Fig 3.7. In this figure the spin↑ and spin↓ bands are represented by the two semi–circles and are separated by the energy $SJ + nU$. The spin↑→ spin↓ excitation is presented as a solid line while a double line indicates an electron–hole pair excitation. The Fermi sea pair $(\alpha\mu)$ is created by interacting with the spin–↓ electron via U (wave curve). Such scattering gives a contribution

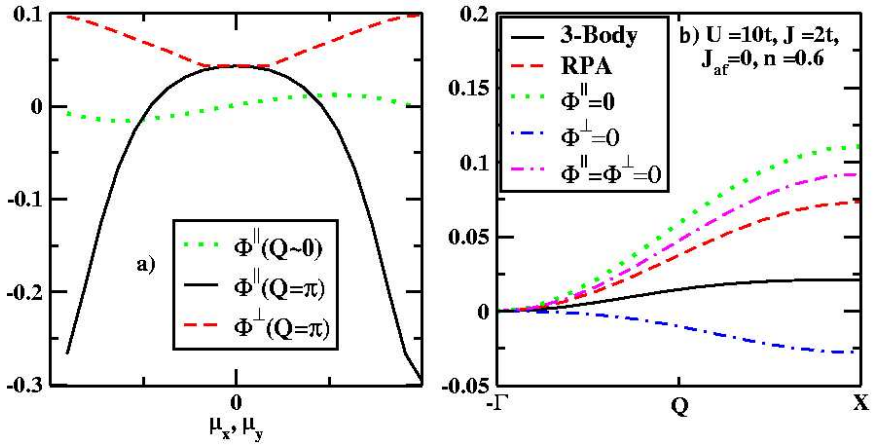

Figure 3.8: (a) Contribution of magnon–pair correlations for different momenta, (b) origin of the X–point softening.

to $X_{\mu}^{\mathbf{Q}}$ which is proportional to $U\sum_{\alpha\nu}\Phi_{\alpha\nu\mu}$ and is expressed by the last term in the r.h.s of Eq. 3.4. In order to assess the contribution of this correlation effect, we define the one–component amplitudes

$$\Phi^{\|} = \sum_{\alpha\nu} \Phi^{(Q_X,0)}_{(\mu_X,0)\nu\alpha} \tag{3.40}$$

$$\Phi^{\perp} = \sum_{\alpha\nu} \Phi^{(Q_X,0)}_{(0,\mu_Y)\nu\alpha}. \tag{3.41}$$

What motivates us to make such definitions is that the three-momentum variational amplitude $\Phi_{\alpha\nu\mu}$ is rather difficult to be plotted, since in a 2D system, for example, it has six components for each lattice momentum $\mathbf{Q}$ and thus even a 3D plot is not enough to provide an appropriate representation of amplitude Φ. Therefore we can not easily understand the properties of Φ and its dependence on the electron momenta. The amplitudes which we defined above are one–variable functions and at the same time contain the most important information provided by Φ. Moreover, they give us a rather satisfying idea of the momentum–dependence of the amplitude Φ of interest here. By plotting these amplitudes versus electron momentum μ_X or μ_Y, for fixed values of Q, we simply plot a particular projection of Φ and therefore its properties can be inferred. In Fig. 3.8(a) we plot this correlation contribution, both for $\mathbf{Q}$ close to the X point and for small $\mathbf{Q}$, as a function of momentum μ_X for $\Phi^{\|}$ and of μ_Y for $\Phi^{\perp}$. As can be seen in Fig. 3.8(a), the largest correlation contribution comes from $\mu \parallel \mathbf{Q}$ close to the Fermi surface (which for the concentrations of interest is close to the zone boundary $\mathbf{Q} = \pi$) and for $\mathbf{Q}$ close to

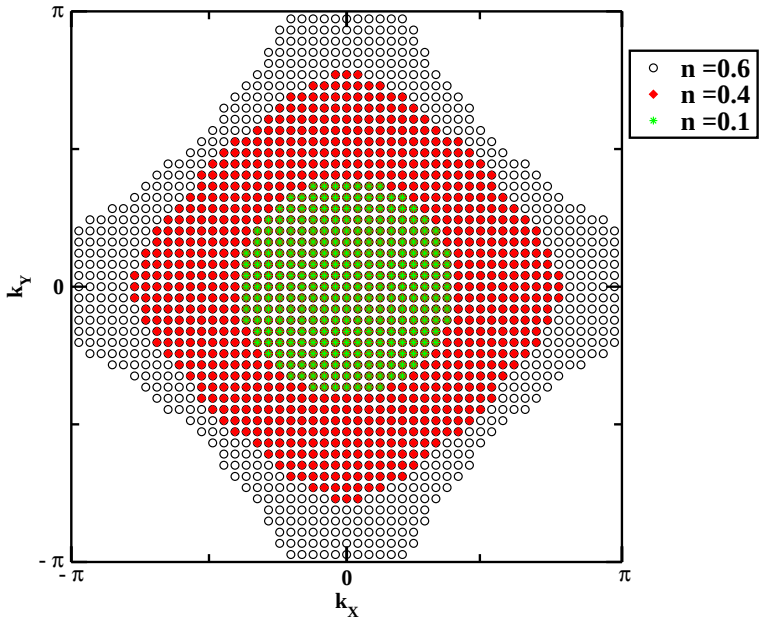

Figure 3.9: Illustration of the Fermi surface for the cosine–like tight binding band for different electron concentrations. Stars :Low concentration $n \simeq 0.1$, fermi sea is in a very good approximation a circle. Diamonds: Intermediate regime the first deviations of the circle are noticed. Open circles: High concentration: The Brillouin zone's boundaries $k = \pi$ are reached for a wide range of momenta.

the zone boundary. The contribution of $\Phi^{\perp}$ is three times smaller than that of $\Phi^{\parallel}$ near the zone boundary. More importantly, it gives a positive contribution while $\Phi^{\parallel}$ contributes a negative contribution to the spin–wave energy. Therefore near the zone boundary $\Phi^{\perp}$ hardens $\omega_{\mathbf{Q}}$ and $\Phi^{\parallel}$ softens it. The contribution of $\Phi^{\parallel}$ to the long wavelength $\mathbf{Q} \simeq 0$ spin wave excitations is also presented in Fig. 3.8. We observe that this behaviour is quite different from that for $\mathbf{Q} \simeq \pi$. $\Phi^{\parallel}$ is a smooth function of momenta since the large zone boundary decrease does not appear for $\mathbf{Q} = 0$. The latter is in agreement with the experimental fact that the softening is confined to the zone boundary. In order to further corroborate our conclusions we can compare spin–wave dispersion from the full calculation with the results obtained by neglecting $\Phi^{\perp}$ and/or $\Phi^{\parallel}$. The latter is shown in Fig. 3.8. First of all, we observe that by removing $\Phi^{\parallel}$ we obtain a dispersion harder than the RPA results while if $\Phi^{\perp}$ is additionally removed an RPA–like dispersion is obtained. On the other hand, by removing $\Phi^{\perp}$ and leaving only the $\Phi^{\parallel}$, we obtain a strongly softened result. This comparison in Fig. 3.8(b) clearly shows that the strong softening of the spin–wave dispersion as compared to the RPA comes from $\Phi^{\parallel}$, i.e.

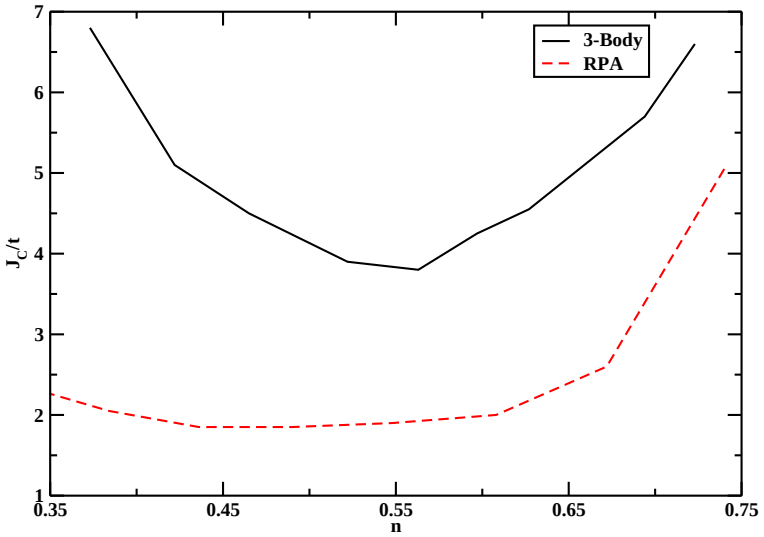

Figure 3.10: $J_c(n)$ for $J_{AF} = 0.012t, U = 25t$. $J < J_c$: the ferromagnetic state is unstable. $J \geq J_c$: phase separation will shift the ferromagnetic phase boundary further up.

from the renormalization of $X_\mu^{\mathbf{Q}}$ by the scattering of a spin $\uparrow\rightarrow$ spin $\downarrow$ excitation with a Fermi sea pair for momenta μ along Γ–X. This effect becomes stronger for momenta near the zone boundary, $\mu \simeq \pi$. Note that due to the cosine–like band of the tight binding model the Fermi–sea electrons are allowed to reach the zone boundary $\mu = \pi$ for a high concentration. This is shown in Fig. 3.9 where the shape of the Fermi surface for three different dopings is plotted. For an itinerant electron concentration $n \simeq 0.6$ (open circles) we note that there is a wide range of momenta where the zone boundary is reached. This explains the strong softening for that density as plotted in Fig. 3.8. For an intermediate concentration $n = 0.4$ (filled diamonds) we note that the pockets of zone boundary momentum start to disappear. Finally for very low electron concentration $n = 0.1$ (stars) we can make two observations. Firstly, the zone boundary is very far from the Fermi surface and thus the effect of the softening, as discussed above, is reduced. We note also that the shape of the Fermi surface differs significantly from that for higher dopings, since it can be easily approximated be a circle with radius equal to the Fermi momentum k_F. Additionally, the Fermi sea is symmetric with respect to momentum and depends solely on the norm of the electron momentum $|\vec{\mu}|$. Therefore, for such dopings it is reasonable to approximate the band energy $\varepsilon_{\vec{\mu}}$ with a parabolic

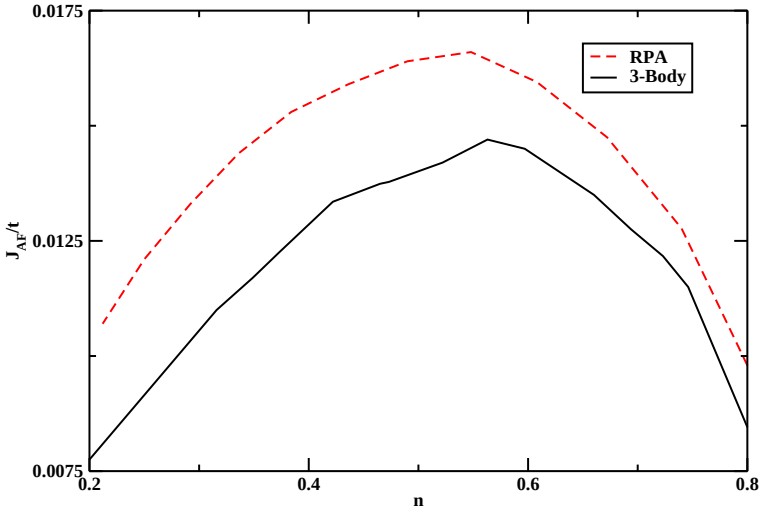

Figure 3.11: J_{AF}^{C} as a function of n for $J = 7t, U = 25t$. For $J_{AF} > J_{AF}^{C}$ the ferromagnetic state is unstable.

function

$$\varepsilon_{\mu} = \frac{\hbar^2 \mu^2}{2m^*}, \tag{3.42}$$

where m^* is the effective band mass. The latter approximation does not apply here since we are interested in the higher concentration regime, where the parabolic approximation is inadequate. We conclude that the inclusion of the Hubbard repulsion changes the physical origin of the zone boundary softening as compared to the minimal model. In particular, we showed above that the scattering introduced by U and shown in Fig. (3.7) is mainly responsible for the softening. Such boundary effects, occur for momenta close to the zone boundary and the Fermi surface. Given that the shape of the Fermi surface changes significantly with n, we conclude that the zone boundary softening has a strong concentration dependence and only occurs for intermediate n. This is consist with the experimental results.

With decreasing J/t, the magnon energy for intermediate n eventually turns negative at the X–point while the magnon stiffness is still positive. This variational result allows us to conclude instability of the ferromagnetic state. It also implies a zone boundary softening larger than that of the small–Q dispersion. On the other hand, for small n, the spinwave energy first turns negative at the (π, π) point (antiferromagnetic correlations). Finally, for larger n, $\omega_{\mathbf{Q}}$ turns negative for small momenta, $D < 0$. By identifying the minimum values of J, $J_c(n)$, where $\omega_{\mathbf{Q}} \geq 0$ for all momenta, we can definitely conclude, due to the variational nature

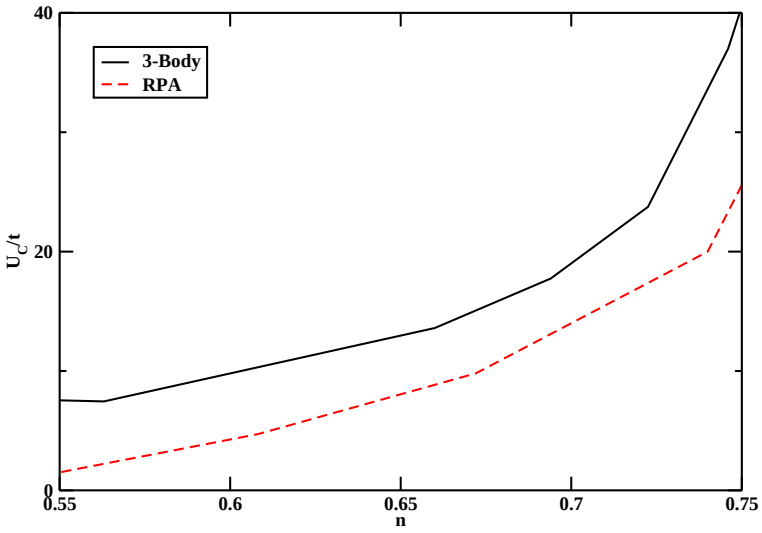

Figure 3.12: U_C as a function of n for $J = 7t, J_{AF} = 0.012t$. For $U < U_C$ the ferromagnetic state is unstable.

of our calculation, that the ground state is not ferromagnetic for $J < J_c$. On the other hand, for $J > J_c$, the stability of $|F\rangle$ is not guaranteed, due to e.g. phase separation [11, 2]. $J_c(n)$ is shown in Fig.3.10. By comparing to the RPA result, it is clear that the pair–magnon correlations lead to a very pronounced upward shift in $J_c(n)$. While for large concentrations the effects of the correlations diminish, and the RPA becomes exact at n=1, for n <0.7 the deviations from the RPA exceed 100%. As n decreases, the RPA fails completely. We can conclude that the RPA grossly overestimates the stability of the ferromagnetism. Even though for some concentrations additional effects such as phase separation will shift the ferromagnetic phase boundary $J_c(n)$ further up as compared to Fig. 3.10, it is clear from our variational calculation that the effects of the pair–magnon correlations are significant in the manganites. Finally, we note that the onsite Coulomb repulsion U decreases the values of $J_c(n)$ and thus enhances the stability of the ferromagnetic state. It is important to note that U changes qualitatively the shape of the critical line (compare Fig. 3.10 with Fig. 2.12) as compared to the minimum model. We therefore conclude that its effect cannot be neglected.

Having examined the role of the magnetic–exchange interaction on the stability of ferromagnetic state, we continue now with the effect of the super–exchange interaction. The Heisenberg-like H_{super} generally narrows the bounds where ferromagnetism is possible since is is an antiferromagnetic contribution which gives an overall suppression of the magnon energy. This means that with increasing

J_{AF}, and fixed U/t and J/t the spin–wave energy lowers for a particular electron density n. There is a critical J_{AF}^C for which magnon energy eventually turns negative. For $J_{AF} \geq J_{AF}^C$ and fixed $U/t, J/t, n$ ferromagnetic order is impossible. In order to determine the critical super–exchange parameter, we fix U/t and J/t and seek the critical point for every electron concentration n. To make the connection with the J–n phase diagram, we fix J to a value which allows the ground state to be ferromagnetic for a wide region of electron concentrations $0.4 \leq n \leq 0.7$. By examining Fig. 3.11 we can conclude that an appropriate value for that parameter is $J/t = 7$. We show the results for the phase diagram with respect to J_{AF}^C as a function of n in Fig. (3.11). Again the $1/J_S$ results are not shown as they are very close to RPA. First, we notice that in this situation three–body effects do not seem to affect so importantly the critical value of U/t as in the J vs n phase diagram. The dependence of J_{AF}^C on n remains rather similar if correlations are included. Within the region of concentrations of interest ($n \geq 0.6$), the RPA J_{AF}^C is similar to the three–body result. For intermediate concentrations ($n \simeq 0.5$), correlations effects start to diminish the critical J_{AF}^C with a suppression of about 20% as compared to the RPA value. This suppression in the correlated critical J_{AF} remains almost constant for lower fillings ($n \leq 0.4$) and because of this the relative difference increases to exceed 60% at the very low doping regime (n$\simeq$ 0.2-0.3).

To complete the presentation of the phase diagrams, we now fix $J/t, J_{AF}/t$ and identify the critical Hubbard interaction U_C as a function of electron filling n. In Fig. (3.12) we present the $U_C(n)$ results, where ferromagnetic order is impossible for $U \leq U_C$. Firstly, we notice that in order to stabilize the ferromagnetic ground state up to electron concentration $n \simeq 0.7$, consistent with the fillings in 2D quasi–layered samples, the parameter U/t must be as large as $U \simeq 25t$. As expected, the three–body correlations increase the critical U as compared to RPA results, since it introduces a ferromagnetic interaction. In Fig. (3.12) we note that within a wide range of concentrations $0.55 \lesssim n \lesssim 0.7$ that the three–body correlations shifts H_U by a constant quantity about $\Delta U = 8t$. The relative deviation between these two approximations increases with lowering n. For the experimentally interesting concentration $n = 0.6$, we have a deviation which exceeds 100%, while for $n = 0.7$ it is also significant, about 25%, as compared to the RPA results. For higher electron fillings such as $n \geq 0.75$ the critical U_C starts to increase rapidly and thus the relative deviation is lower. Although the doping dependence of the critical Hubbard interaction seems not to change strongly by three–body correlations, we find that quantitatively the deviation is large within the experimental interesting regime of n. Moreover the relative deviation between correlated and RPA results is very large in this regime.

To sum up with the phase diagram results, our variational calculation allows us to find stricter bounds where ferromagnetism is possible in manganese oxides.

The critical lines presented here are further shifted up by phase separation effects. We found that the most significant effect of the three–body correlations is on the $J_C(n)$. By fixing U/t and J_{AF}/t we showed that the correlations change the n dependence of the critical Hund's rule coupling, in addition to an extremely large quantitative shift as compared with RPA results. We showed that correlations affect the critical values of the other parameters (U_C and J_{AF}) only quantitatively since the dependence on electron doping n remains similar with that obtained within RPA. However, within the experimentally interesting regime of dopings, the shift for example of U_C, is very large while the deviation of J_{AF} is small. We conclude that the three–body correlation effects on the stability of ferromagnetic ground state are very sensitive to small changes of double–exchange interaction.

3.4 Conclusions

To conclude, in this chapter we presented a variational calculation of the spin-wave excitation spectrum of double–exchange ferromagnets that allows us to study the role of the interplay between the Coulomb, Hund's exchange, and Heisenberg super–exchange interactions in the intermediate coupling regime relevant to the manganites. The motivation of this work is that the Coulomb interaction is the largest energy factor in manganites and therefore it cannot be neglected. Having studied a simplified model in the previous chapter, here we constructed a more realistic description of this kind of systems by including the Coulomb interaction and super–exchange coupling in our model hamiltonian. Our numerical results recover RPA and $1/(SJ+nU)$ expansion as limiting case. Despite of the complexity of our variational system of equations, we could perform the numerical calculation for fairly large 2D systems, where convergence to the thermodynamic limit was satisfyingly achieved.

The main numerical results of this study can be summarized as follows. Firstly, we conclude that nonperturbative long range electron–hole pair–magnon correlations play a very important role in the spin dynamics of the manganites. Most important is the strong zone boundary softening of the spinwave dispersion and additionally the decrease in the stability of the ferromagnetic state. As a result, the 3–body dispersion deviates strongly from the Heisenberg dispersion as the electron concentration decreases. The correlation effects depend sensitively on the on–site Coulomb repulsion, which enhances the ferromagnetism, and on its interplay with the magnetic exchange and super–exchange interactions. The role of the latter super–exchange interaction is of minor importance since it can be expressed as an overall suppression of the magnon dispersion. In addition, we found that three–body correlation effects remains important even in the extreme limit of $U \to \infty$.

The validity of the latter limit as well the $1/J_S$ expansion were examined by comparing to the three–body approximation. We discussed also the possible relevance of our numerical results to experiments in manganites. Our analysis indicates that three–body correlations improve the consistency of the results with experiments in 2D quasi–layered manganese oxides. A comparison with the numerical results of the simple double–exchange hamiltonian of the previous chapter, showing the existence of a zone boundary softening along $\Gamma \rightarrow M$ and $X \rightarrow M$ direction of the Brillouin zone, reveals the importance of on–site Coulomb and super–exchange interactions. The latter result indicates a new possible instability of the ferromagnetic ground state: through the zone boundary softening along $\Gamma \rightarrow M$, (π, π) point, which occurs for low electron dopings. For higher n the $(\pi, 0)$ instability preempts the above spin–wave softening. Finally, our work can be extended to treat other itinerant ferromagnetic systems, such as the III(Mn)V semiconductors. Moreover, the origin of the spin–wave softening near the zone boundary is discussed. We conclude that the main reason which creates that interesting behaviour is the existence of fermi electrons near the zone boundary. The latter becomes possible due to cosine–like band of the tight binding model which causes large deviations of Fermi surface from the circular shape of the simple parabolic band. In this way for electron concentrations within the experimental interesting region, $0.5 \lesssim n \lesssim 0.7$, there are broad pockets of near zone boundary electrons, and therefore the role of three–body correlations on spin–wave excitations is pronounced. We identify a new scattering process between a fermi sea charge excitation and a spin flip electron excitation (described by Φ) which is induced by U and leads to a very pronounced zone boundary softening for concentrations such as the Fermi surface approaches the Brillouin zone boundary. The correlations discussed here should also play an important role in the ultrafast dynamics measured by magneto–optical pump–probe spectroscopy [63].

Chapter 4

Spin–wave damping in Double–Exchange Ferromagnetic Manganites.

4.1 Introduction

In this chapter we show that the variational results for the spin–wave dispersion obtained in the previous chapters can be reproduced by using the double–time Green's function method[54]. Although the connections between the Green's function and variational theory are not apriori clear, here we show that the infinite hierarchy of the Green's function equations of motion can be closed by factorizing the higher order Green's functions in a way that preserves the variational nature of our results. This is important for drawing define conclusions regarding the spin–wave softening and stability of the ferromagnetic phase. At the same time, the Green's function method allows us to calculate dynamical properties such as the lifetime of spin–wave excitations. This is important for studying the magnetization dynamics and relaxation in ferromagnetic systems, which is important for future device applications. The Green's method method has been used before in literature to calculate the magnon's dispersion within RPA[55] and, in conjunction with Monte Carlo (MC) technique to derive results for the manganites phase diagram in small clusters[57]. Here however, our focus is on correlations and therefore the Hartree-Fock Green's function factorization, reproducing the RPA, is not enough. Going beyond the RPA with Green's function is a difficult issue. Here we assess the validity of a truncation method by showing that is reproduces the three–body variational results of the previous chapters. An experiment of particular interest here is the measurement of the spin–wave damping along the main directions in

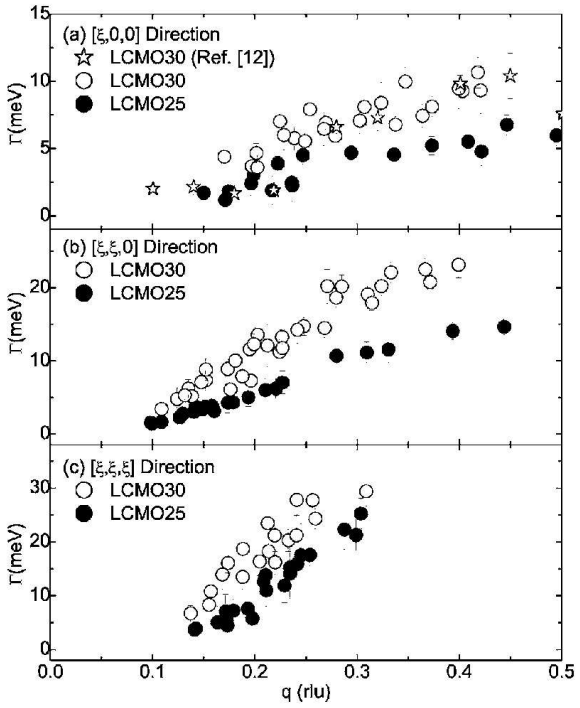

Figure 4.1: Experimental measurement of the spin–wave damping along the main directions in the Brillouin zone taken from Phys. Rev. **B** 75, 144408, (2007)

the Brillouin zone[52]. Although this experiment is concentrated on the high electron doping regime, there are two interesting features obtained by this experiment. Fig. (4.1) shows these results taken from Ref[52]. First, spin–wave damping along the direction $\Gamma \rightarrow X$ in the Brillouin zone is lower as compared to the observed value along the other directions. Additionally, the doping dependence of damping is the following. For the the higher doping (filled circles) spin–wave damping is lower in comparison with the lower doping sample (open circle). Here we examine whether our numerical calculation reproduces these experimental behaviour.

This outline of this chapter is as follows. In section 4.2 the Green's function technique is introduced. More precisely, in subsection 4.2.1 we apply this method to the ferromagnetic double–exchange model. By using a Hartree-Fock factorization procedure we reproduce the RPA result[55] which was obtained variationally in the chapter 2. The next step is the introduction of correlations which is discussed in 4.2.2. Again we prove that a factorization of the higher–order Green's

functions leads to equations similar to the variational results of chapter 2 for the correlated spinwave dispersion. In particular, we calculate the spinwave damping coming from the correlations. The magnon damping is a very interesting experimentally observable property[9, 35, 36, 37, 38, 8, 52] which so far in the literature was treated perturbatively using in $1/S$ expansion[11, 24]. This calculation can be recovered by our three–body results. However, here we calculate damping due to 3–body correlations non–perturbatively in 1/S. In subsections 4.2.3 and 4.2.4 we reproduce that results in both finite and infinite J. Our numerical results is presented and discussed in section 4.3. The last section 4.4 of this chapter contains the conclusions.

4.2 Calculations

We derive the chain of equations of motion which describe spin–wave excitations up to three-body correlations. First, we show that the Green's function method together with an appropriate approximation of the higher order Green's functions leads to the well–known RPA results[25, 55].

Using this result we introduce correlations beyond RPA using a similar factorization technique. In this way we show that the variational results of Chapter 2 is reproduced. Since we reproduce our previous variational treatment of correlations, as well as the $O(1/S)$ expansion, we conclude that the termination of the infinitive chain of equations of motion, unavoidable in strongly correlated systems, by approximating the higher–order Green's functions is a reasonable approximation.

4.2.1 The RPA results

In this subsection we consider the ferromagnetic model which is described by the usual double–exchange hamiltonian:

$$\begin{aligned} H = \quad & \sum_{\mathbf{k}\sigma} \varepsilon_{\mathbf{k}}\ c^{\dagger}_{\mathbf{k}\sigma} c_{\mathbf{k}\sigma} - \frac{J}{2\sqrt{N}} \sum_{\mathbf{kq}\sigma} \sigma S^{z}_{\mathbf{q}}\ c^{\dagger}_{\mathbf{k-q}\sigma} c_{\mathbf{k}\sigma} \\ & - \frac{J}{2\sqrt{N}} \sum_{\mathbf{kq}} \left(S^{-}_{\mathbf{q}}\ c^{\dagger}_{\mathbf{k-q}\uparrow} c_{\mathbf{k}\downarrow} + S^{\dagger}_{\mathbf{q}}\ c^{\dagger}_{\mathbf{k}\downarrow} c_{\mathbf{k+q}\uparrow} \right). \end{aligned}$$

We introduce the double–time local spin Green's function:

$$\begin{aligned} Y^{\mathbf{Q}}(t-t') &= \theta(t-t') \ll S^{\dagger}_{-\mathbf{Q}}(t) | S^{-}_{\mathbf{Q}}(t') \gg \\ &= \theta(t-t') < \left[S^{\dagger}_{-\mathbf{Q}}(t), S^{-}_{\mathbf{Q}}(t') \right] >, \end{aligned} \tag{4.1}$$

where $S^{\dagger}_{-\mathbf{Q}}(t)$ is Heisenberg operators. By taking the derivative of the above equation with respect to t one can easily show that $Y^{\mathbf{Q}}(t-t')$ is given by an equation of motion:

$$\begin{aligned} i\frac{\partial}{\partial t}Y^{\mathbf{Q}}(t-t') &= i\delta(t-t') < \left[S^{\dagger}_{-\mathbf{Q}}(t), S^{-}_{\mathbf{Q}}(t')\right] > + \\ &\ll \left[S^{\dagger}_{-\mathbf{Q}}(t), H\right] | S^{-}_{\mathbf{Q}}(t') \gg . \end{aligned} \tag{4.2}$$

After some algebra we obtain

$$\begin{aligned} i\frac{\partial}{\partial t}Y^{\mathbf{Q}}(t-t') &= 2Si\delta(t-t') \\ &+ \frac{J}{2N}\sum_{\mathbf{kq}\sigma}\sigma \ll S^{\dagger}_{\mathbf{q}-\mathbf{Q}}c^{\dagger}_{\mathbf{k}-\mathbf{q}\sigma}c_{\mathbf{k}\sigma}(t)|S^{-}_{\mathbf{Q}}(t') \gg \\ &- \frac{J}{N}\sum_{\mathbf{kq}} \ll S^{z}_{\mathbf{q}-\mathbf{Q}}c^{\dagger}_{\mathbf{k}-\mathbf{q}\uparrow}c_{\mathbf{k}\downarrow}(t)|S^{-}_{\mathbf{Q}}(t') \gg . \end{aligned} \tag{4.3}$$

We see that the equation of motion for $Y^{\mathbf{Q}}(t-t')$ contains two new Green's functions on the rhs of Eq. (4.3). The simplest strategy to deal with these second-order Green's function is to factorize them in a way which allow us to determine them in term of the lowest order one(Tyablikov decoupling). This strategy leads to the results:

$$\begin{aligned} \ll S^{\dagger}_{\mathbf{q}-\mathbf{Q}}c^{\dagger}_{\mathbf{k}-\mathbf{q}\sigma}c_{\mathbf{k}\sigma}(t)|S^{-}_{\mathbf{Q}}(t') \gg \simeq & < S^{\dagger}_{\mathbf{q}-\mathbf{Q}} > \ll c^{\dagger}_{\mathbf{k}-\mathbf{q}\sigma}c_{\mathbf{k}\sigma}(t)|S^{-}_{\mathbf{Q}}(t') \gg \\ &+ < c^{\dagger}_{\mathbf{k}-\mathbf{q}\sigma}c_{\mathbf{k}\sigma} > \ll S^{\dagger}_{\mathbf{q}-\mathbf{Q}}(t)|S^{-}_{\mathbf{Q}}(t') \gg \end{aligned} \tag{4.4}$$

$$\begin{aligned} \ll S^{z}_{\mathbf{q}-\mathbf{Q}}c^{\dagger}_{\mathbf{k}-\mathbf{q}\uparrow}c_{\mathbf{k}\downarrow}(t)|S^{-}_{\mathbf{Q}}(t') \gg \simeq & < S^{z}_{\mathbf{q}-\mathbf{Q}} > \ll c^{\dagger}_{\mathbf{k}-\mathbf{q}\uparrow}c_{\mathbf{k}\downarrow}(t)|S^{-}_{\mathbf{Q}}(t' \gg \\ &+ < c^{\dagger}_{\mathbf{k}-\mathbf{q}\uparrow}c_{\mathbf{k}\downarrow} > \ll S^{\dagger}_{\mathbf{q}-\mathbf{Q}}(t)|S^{-}_{\mathbf{Q}}(t') \gg \end{aligned} \tag{4.5}$$

Note here that the mean values appearing in the above equations must be calculated in the true ground state of the system. The ferromagnetic Hartree-Fock state, an exact eigenstate of the double–exchange Hamiltonian, is a rather reasonable approximation for the ground state, thus we obtain that:

$$< S^{\dagger}_{\mathbf{q}-\mathbf{Q}} >= 0 \tag{4.6}$$

$$< S^{z}_{\mathbf{q}-\mathbf{Q}} >= \sqrt{N}S\delta_{\mathbf{q},\mathbf{Q}} \tag{4.7}$$

$$< c^{\dagger}_{\mathbf{k}-\mathbf{q}\sigma}c_{\mathbf{k}\sigma} >= \delta_{\mathbf{q},\mathbf{0}}\delta_{\sigma\downarrow}n(\varepsilon_{\mathbf{k}}) \tag{4.8}$$

where $n(\varepsilon_{\mathbf{k}})$ is the Fermi–Dirac distribution for the spin$\uparrow$ itinerant electrons. In this way the second-order Green's functions become:

$$\ll S^{\dagger}_{\mathbf{q}-\mathbf{Q}} c^{\dagger}_{\mathbf{k}-\mathbf{q}\sigma} c_{\mathbf{k}\sigma}(t) | S^{-}_{\mathbf{Q}}(t') \gg \simeq \delta_{\mathbf{q},\mathbf{0}} \delta_{\sigma\downarrow} n(\varepsilon_{\mathbf{k}}) Y^{\mathbf{Q}}(t-t') \tag{4.9}$$

$$\begin{aligned} \ll S^{z}_{\mathbf{q}-\mathbf{Q}} c^{\dagger}_{\mathbf{k}-\mathbf{q}\uparrow} c_{\mathbf{k}\downarrow}(t) | S^{-}_{\mathbf{Q}}(t') \gg \simeq & \sqrt{N} S \delta_{\mathbf{q},\mathbf{Q}} X^{\mathbf{Q}}_{\mathbf{k}}(t-t') \\ & + \delta_{\mathbf{q},\mathbf{0}} \delta_{\sigma\downarrow} n(\varepsilon_{\mathbf{k}}) Y^{\mathbf{Q}}(t-t') \end{aligned} \tag{4.10}$$

where we introduce the Green's function $X^{\mathbf{Q}}_{\mathbf{k}}(t-t')$

$$X^{\mathbf{Q}}_{\mathbf{k}}(t-t') = \ll c^{\dagger}_{\mathbf{k}-\mathbf{Q}\uparrow} c_{\mathbf{k}\downarrow}(t) | S^{-}_{\mathbf{Q}}(t') \gg \tag{4.11}$$

The equation of motion Eq. (4.3) becomes:

$$\begin{aligned} i\frac{\partial}{\partial t} Y^{\mathbf{Q}}(t-t') = & \quad 2Si\delta(t-t') + \frac{Jn}{2} Y^{\mathbf{Q}}(t-t') \\ & - \frac{JS}{\sqrt{N}} \sum_{\mathbf{k}} X^{\mathbf{Q}}_{\mathbf{k}}(t-t') \end{aligned} \tag{4.12}$$

We conclude that although the truncation we used here leads to a quite simple form of equation of motion the existence of a new Green's function cannot be prevailed. One has to write the equation of motion for the new Green's function:

$$\begin{aligned} i\frac{\partial}{\partial t} X^{\mathbf{Q}}_{\mathbf{k}}(t-t') = & \, i\delta(t-t') < [c^{\dagger}_{\mathbf{k}-\mathbf{Q}\uparrow} c_{\mathbf{k}\downarrow}, S^{-}_{\mathbf{Q}}] > \\ & + \ll [c^{\dagger}_{\mathbf{k}-\mathbf{Q}\uparrow} c_{\mathbf{k}\downarrow}, H] | S^{-}_{\mathbf{Q}} \gg \end{aligned} \tag{4.13}$$

Again, after some algebra we obtain the general equation:

$$\begin{aligned} i\frac{\partial}{\partial t} X^{\mathbf{Q}}_{\mathbf{k}}(t-t') &= (\varepsilon_{\mathbf{k}} - \varepsilon_{\mathbf{k}-\mathbf{Q}}) X^{\mathbf{Q}}_{\mathbf{k}}(t-t') \\ &+ \frac{J}{2\,N} \sum_{\mathbf{q}} \ll S^{z}_{\mathbf{q}} \left(c^{\dagger}_{\mathbf{k}-\mathbf{Q}\uparrow} c_{\mathbf{k}+\mathbf{q}\downarrow} + c^{\dagger}_{\mathbf{k}-\mathbf{Q}-\mathbf{q}\uparrow} c_{\mathbf{k}\downarrow} \right)(t) | S^{-}_{\mathbf{Q}}(t') \gg \\ &- \frac{J}{2\,N} \sum_{\mathbf{q}} \ll S^{\dagger}_{\mathbf{q}} \left(c^{\dagger}_{\mathbf{k}-\mathbf{Q}\uparrow} c_{\mathbf{k}+\mathbf{q}\uparrow} - c^{\dagger}_{\mathbf{k}-\mathbf{Q}-\mathbf{q}\downarrow} c_{\mathbf{k}\downarrow} \right)(t) | S^{-}_{\mathbf{Q}}(t') \gg \end{aligned} \tag{4.14}$$

Following the Hartree-Fock truncation procedure as described above we approxi-

mate the new Green's functions in the rhs of Eq. 4.14 as follows:

$$\begin{aligned} &\ll S^z_{\mathbf{q}} \left(c^\dagger_{\mathbf{k-Q}\uparrow} c_{\mathbf{k+q}\downarrow} + c^\dagger_{\mathbf{k-Q-q}\uparrow} c_{\mathbf{k}\downarrow} \right)(t) | S^-_{\mathbf{Q}}(t') \gg \simeq \\ &< S^z_{\mathbf{q}} > \ll \left(c^\dagger_{\mathbf{k-Q}\uparrow} c_{\mathbf{k+q}\downarrow} + c^\dagger_{\mathbf{k-Q-q}\uparrow} c_{\mathbf{k}\downarrow} \right)(t) | S^-_{\mathbf{Q}}(t') \gg \\ &+ < \left(c^\dagger_{\mathbf{k-Q}\uparrow} c_{\mathbf{k+q}\downarrow} + c^\dagger_{\mathbf{k-Q-q}\uparrow} c_{\mathbf{k}\downarrow} \right) > \ll S^z_{\mathbf{q}}(t) | S^-_{\mathbf{Q}}(t') \gg \end{aligned} \tag{4.15}$$

$$\begin{aligned} &\ll S^\dagger_{\mathbf{q}} \left(c^\dagger_{\mathbf{k-Q}\uparrow} c_{\mathbf{k+q}\uparrow} - c^\dagger_{\mathbf{k-Q-q}\downarrow} c_{\mathbf{k}\downarrow} \right)(t) | S^-_{\mathbf{Q}}(t') \gg \simeq \\ &< S^\dagger_{\mathbf{q}} > \ll \left(c^\dagger_{\mathbf{k-Q}\uparrow} c_{\mathbf{k+q}\uparrow} - c^\dagger_{\mathbf{k-Q-q}\downarrow} c_{\mathbf{k}\downarrow} \right)(t) | S^-_{\mathbf{Q}}(t') \gg \\ &+ < \left(c^\dagger_{\mathbf{k-Q}\uparrow} c_{\mathbf{k+q}\uparrow} - c^\dagger_{\mathbf{k-Q-q}\downarrow} c_{\mathbf{k}\downarrow} \right) > \ll S^\dagger_{\mathbf{q}}(t) | S^-_{\mathbf{Q}}(t') \gg \end{aligned} \tag{4.16}$$

Taking into account the properties 4.6–4.8 in addition to the property:

$$< c^\dagger_{\mathbf{q},\sigma} c_{\mathbf{q}',\sigma'} > = \delta_{\mathbf{q},\mathbf{q}'} \delta_{\sigma,\sigma'} < c^\dagger_{\mathbf{q},\sigma} c_{\mathbf{q},\sigma} >, \tag{4.17}$$

we obtain:

$$\ll S^z_{\mathbf{q}} \left(c^\dagger_{\mathbf{k-Q}\uparrow} c_{\mathbf{k+q}\downarrow} + c^\dagger_{\mathbf{k-Q-q}\uparrow} c_{\mathbf{k}\downarrow} \right)(t) | S^-_{\mathbf{Q}}(t') \gg \simeq \sqrt{N} S \delta_{\mathbf{q},\mathbf{0}} X^{\mathbf{Q}}_{\mathbf{k}}(t-t') \tag{4.18}$$

$$\ll S^\dagger_{\mathbf{q}} \left(c^\dagger_{\mathbf{k-Q}\uparrow} c_{\mathbf{k+q}\uparrow} - c^\dagger_{\mathbf{k-Q-q}\downarrow} c_{\mathbf{k}\downarrow} \right)(t) | S^-_{\mathbf{Q}}(t') \gg \simeq \delta_{\mathbf{q},-\mathbf{Q}} n(\varepsilon_{\mathbf{k}}) Y^{\mathbf{Q}}(t-t'). \tag{4.19}$$

Substituting Eqs. 4.18 and 4.19 into Eq. 4.14 we obtain the final form of the equation of motion for the Green's function $X^{\mathbf{Q}}_{\mathbf{k}}(t-t')$

$$i \frac{\partial}{\partial t} X^{\mathbf{Q}}_{\mathbf{k}}(t-t') = (\varepsilon_{\mathbf{k}} - \varepsilon_{\mathbf{k-Q}} + SJ) X^{\mathbf{Q}}_{\mathbf{k}}(t-t') - \frac{J\, n(\varepsilon_{\mathbf{k}})}{2\sqrt{N}} Y^{\mathbf{Q}}(t-t') \tag{4.20}$$

Since all Green's functions depend on $t-t'$ is useful to set $t'=0$ in the equations of motion. Therefore, we seek for the evolution of the Green's functions in time t starting from $t=0$.

In conclusion, by applying a Hartree-Fock truncation procedure to the infinite chain of equations of motion we manage to obtain a simple system of two equations Eq 4.12 and 4.20. By solving this system of equation we can determine the time–evolution of our system. One needs the initial values of the Green's functions 4.1 and 4.11 which can be easily determined as follows:

$$Y^{\mathbf{Q}}(0) = < \left[S^\dagger_{-\mathbf{Q}}(0), S^-_{\mathbf{Q}}(0) \right] > = < \left[S^\dagger_{-\mathbf{Q}}, S^-_{\mathbf{Q}} \right] > = 2S \tag{4.21}$$

$$X^{\mathbf{Q}}_{\mathbf{k}}(0) = < \left[c^\dagger_{\mathbf{k-Q}\uparrow} c_{\mathbf{k}\downarrow}(0), S^-_{\mathbf{Q}}(0) \right] > = < \left[c^\dagger_{\mathbf{k-Q}\uparrow} c_{\mathbf{k}\downarrow}, S^-_{\mathbf{Q}} \right] > = 0. \tag{4.22}$$

It is more convenient to use the Laplace transformation since what we are actually interested in is the dispersion relation of the spinwave excitations described by the above Green's functions:

$$Y^{\mathbf{Q}}(\omega) = \int_0^\infty Y^{\mathbf{Q}}(t) e^{i\omega t - \gamma t} dt \tag{4.23}$$

$$X^{\mathbf{Q}}_{\mathbf{k}}(\omega) = \int_0^\infty X^{\mathbf{Q}}_{\mathbf{k}}(t) e^{i\omega t - \gamma t} dt \tag{4.24}$$

where $\gamma > 0$ ensures convergence at the $t \to \infty$ limit. Using the above definitions we can obtain the Laplace transformation of derivatives:

$$\begin{aligned} \int_0^\infty \frac{\partial}{\partial t} A(t) e^{i\omega t - \gamma t} dt &= \left[A(t) e^{i\omega t - \gamma t} \right] |_0^\infty - (i\omega - \gamma) A(\omega) \Rightarrow \\ \int_0^\infty \frac{\partial}{\partial t} A(t) e^{i\omega t - \gamma t} dt &= -A(0) - (i\omega - \gamma) A(\omega) \end{aligned} \tag{4.25}$$

Substituting the definitions 4.23, 4.24 and 4.25 into the equations of motion 4.12 and 4.20 with $t' = 0$ and the initial conditions 4.21 and 4.22 we finally obtain:

$$\left(\omega - \frac{Jn}{2} + i\gamma \right) Y^{\mathbf{Q}}(\omega) = 4Si + \frac{JS}{\sqrt{N}} \sum_{\mathbf{k}} X^{\mathbf{Q}}_{\mathbf{k}}(\omega) \tag{4.26}$$

$$\left(\omega + \varepsilon_{\mathbf{k}-\mathbf{Q}} - \varepsilon_{\mathbf{k}} - SJ + i\gamma' \right) X^{\mathbf{Q}}_{\mathbf{k}}(\omega) = -\frac{Jn(\varepsilon_{\mathbf{k}-\mathbf{Q}})}{2\sqrt{N}} Y^{\mathbf{Q}}(\omega) \tag{4.27}$$

Substituting $X^{\mathbf{Q}}_{\mathbf{k}}$ from 4.27 into 4.26 we obtain that the Green's function $Y^{\mathbf{Q}}$ has the form:

$$\left[\omega - \frac{Jn}{2} + i\gamma - \frac{J^2 S}{2N} \sum_{\mathbf{k}} \frac{n(\varepsilon_{\mathbf{k}-\mathbf{Q}})}{\omega + \varepsilon_{\mathbf{k}-\mathbf{Q}} - \varepsilon_{\mathbf{k}} - SJ + i\gamma'} \right] Y^{\mathbf{Q}} = 4Si \tag{4.28}$$

The above form indicates that the Green's function $Y^{\mathbf{Q}}$ has a pole when:

$$\omega = \frac{Jn}{2} - i\gamma + \frac{J^2 S}{2N} \sum_{\mathbf{k}} \frac{n(\varepsilon_{\mathbf{k}-\mathbf{Q}})}{\omega + \varepsilon_{\mathbf{k}-\mathbf{Q}} - \varepsilon_{\mathbf{k}} - SJ + i\gamma'} \tag{4.29}$$

Now in order to determine the magnon's energies $\omega_{\mathbf{Q}}$ we have only to take the limits $\gamma \to 0$ and $\gamma' \to 0$ in the above equation for the pole. In this way we find that the spinwave disperses as:

$$\omega_{\mathbf{Q}} = \frac{Jn}{2} + \frac{J^2 S}{2N} \sum_{\mathbf{k}} \frac{n(\varepsilon_{\mathbf{k}-\mathbf{Q}})}{\omega_{\mathbf{Q}} + \varepsilon_{\mathbf{k}-\mathbf{Q}} - \varepsilon_{\mathbf{k}} - SJ} \tag{4.30}$$

This form for the spinwave dispersion is exactly the same to the one obtained in the chapter 2 where the variational theory is applied, and by Green's function method in Ref. [55]. Note that using the above form for the spinwave energies we find that $\omega_{\mathbf{Q}} < \frac{Jn}{2}$. There is also the possibility for spinwave damping $\Gamma_{\mathbf{Q}}$ since the Green's function's pole 4.29 has the general form $\omega = \omega_{\mathbf{Q}} - i\Gamma_{\mathbf{Q}}$ where:

$$\Gamma_{\mathbf{Q}} = \frac{\pi J^2 S}{2N} \sum_{\mathbf{k}} \delta(\omega_{\mathbf{Q}} + \varepsilon_{\mathbf{k}-\mathbf{Q}} - \varepsilon_{\mathbf{k}} - SJ) \tag{4.31}$$

However, owing to the large Zeeman gap energy $\Delta = SJ$ in the delta function and the fact that the spinwave energies are less than $Jn/2$ we conclude that spinwave dispersion is undamped within the RPA. However, damping of a magnon at momentum $\mathbf{Q}$ comes from the scattering with the fermi sea electrons to a lower momentum $\mathbf{Q}'$.

In conclusion, we showed here that the double–time Green's function's method reproduce the spin–wave dispersion within the RPA. Additionally it is shown that the lifetime of the magnons within this approximation is infinite. Despite the fact that a finite life time of magnons for $\mathbf{Q} \neq 0$ is expected since they are not exact eigenvalues of the DE hamiltonian. A non-zero damping can be obtained by considering the spinwave–fermi sea electrons scattering. The latter is the main aim of the next subsection where the Green's function's technique are used to go beyond the RPA.

4.2.2 Three–body correlations

In this subsection we apply the Green's function's method, as introduced previously, in order to study the magnon–fermi sea electron scattering. The role of the scattering on the spinwave dispersion is discussed and the agreement with the variational results obtained in the chapter 2 and 3 is proven. The usefulness of the Green's function's technique is clearly demonstrated when one seeks to determine the spinwave's life time. Let us note that the $\mathbf{Q} = \mathbf{0}$ magnon state is an exact eigenstate of the ferromagnetic double–exchange hamiltonian. Therefore it is expected that this state shows no damping. This however can not apply to the rest of the magnon states with $\mathbf{Q} \neq \mathbf{0}$ since they are not exact eigenstate states of the DE Hamiltonian and thus the life time of these excited states is finite.

The starting point of our calculations in this subsection is the general form of the equation of motion of the local spin Green's function Eq. 4.3. We define the local spin–fermi sea electron Green's function $G^{\mathbf{Q}}_{\mathbf{k},\mathbf{q}}(t)$ as follows:

$$G^{\mathbf{Q}}_{\mathbf{k},\mathbf{q}}(t) = \ll S^{\dagger}_{\mathbf{q}-\mathbf{Q}} \left(c^{\dagger}_{\mathbf{k}-\mathbf{q}\uparrow} c_{\mathbf{k}\uparrow} - \delta_{\mathbf{q},\mathbf{0}} n(\varepsilon_{\mathbf{k}}) \right)(t) | S^{-}_{\mathbf{Q}}(0) \gg . \tag{4.32}$$

This describes the deviations from the RPA result. Using this definition we obtain

$$\begin{aligned} i\frac{\partial}{\partial t}Y^{\mathbf{Q}}(t) &= 2iS\delta(t) \\ &+ \frac{Jn}{2}Y^{\mathbf{Q}}(t) - \frac{JS}{\sqrt{N}}\sum_{\mathbf{k}} X^{\mathbf{Q}}_{\mathbf{k}}(t) \\ &+ \frac{J}{2N}\sum_{\mathbf{k},\mathbf{q}} G_{\mathbf{k},\mathbf{q}}(t), \end{aligned} \tag{4.33}$$

where the last term on the r.h.s. expresses the contribution of the correlations in the local spin Green's function. With the introduction of the new Green's function the equations of motion 4.26 and 4.27 become:

$$\begin{aligned} \left(\omega - \frac{Jn}{2} + i\gamma\right) Y^{\mathbf{Q}}(\omega) &= 4Si - \frac{JS}{\sqrt{N}}\sum_{\mathbf{k}} X^{\mathbf{Q}}_{\mathbf{k}}(\omega) \\ &+ \frac{J}{2N}\sum_{\mathbf{k},\mathbf{q}} G^{\mathbf{Q}}_{\mathbf{k},\mathbf{q}}(\omega) \end{aligned} \tag{4.34}$$

$$\begin{aligned} \left(\omega + \varepsilon_{\mathbf{k}-\mathbf{Q}} - \varepsilon_{\mathbf{k}} - SJ + i\gamma'\right) X^{\mathbf{Q}}_{\mathbf{k}} &= -\frac{Jn(\varepsilon_{\mathbf{k}-\mathbf{Q}})}{2\sqrt{N}} Y^{\mathbf{Q}}(\omega) \\ &- \frac{J}{2\sqrt{N}}\sum_{\mathbf{q}'} G^{\mathbf{Q}}_{\mathbf{k}+\mathbf{q}',\mathbf{q}'+\mathbf{Q}}(\omega). \end{aligned} \tag{4.35}$$

By setting $G = 0$ in Eqs. 4.34 and 4.35 the RPA set of equations 4.12, 4.20 is reproduced. The equation of motion for $G^{\mathbf{Q}}_{\mathbf{k},\mathbf{q}}(t)$ can be obtained similarly to that of $Y^{\mathbf{Q}}(t)$ and $X^{\mathbf{Q}}_{\mathbf{k}}(t)$ although we have the deal with some rather complex commutators:

$$\begin{aligned} i\frac{\partial}{\partial_t} G^{\mathbf{Q}}_{\mathbf{k},\mathbf{q}}(t) = i\delta(0) < \left[S^{\dagger}_{\mathbf{q}-\mathbf{Q}}\left(c^{\dagger}_{\mathbf{k}-\mathbf{q}\uparrow}c_{\mathbf{k}\uparrow} - n(\varepsilon_{\mathbf{k}})\delta_{\mathbf{q},\mathbf{0}}\right), S^{-}_{\mathbf{Q}}\right] > \\ + \ll \left[\left(S^{\dagger}_{\mathbf{q}-\mathbf{Q}}c^{\dagger}_{\mathbf{k}-\mathbf{q}\uparrow}c_{\mathbf{k}\uparrow} - n(\varepsilon_{\mathbf{k}})\delta_{\mathbf{q},\mathbf{0}}\right), H\right] | S^{-}_{\mathbf{Q}}(0) \gg . \end{aligned} \tag{4.36}$$

After some algebra we obtain:

$$
\begin{aligned}
i\frac{\partial}{\partial t}G^{\mathbf{Q}}_{\mathbf{k},\mathbf{q}}(t) &= (\varepsilon_{\mathbf{k}}-\varepsilon_{\mathbf{k}-\mathbf{q}}) \ll S^{\dagger}_{\mathbf{q}-\mathbf{Q}}c^{\dagger}_{\mathbf{k}-\mathbf{q}\uparrow}c_{\mathbf{k}\uparrow}(t)|S^{-}_{\mathbf{Q}}(0) \gg \\
&- \frac{J}{2\sqrt{N}}\sum_{\mathbf{q}'} \ll S^{\dagger}_{\mathbf{q}-\mathbf{Q}}S^{z}_{\mathbf{q}'}\left(c^{\dagger}_{\mathbf{k}-\mathbf{q}\uparrow}c_{\mathbf{k}+\mathbf{q}'\uparrow}-c^{\dagger}_{\mathbf{k}-\mathbf{q}-\mathbf{q}'\uparrow}c_{\mathbf{k}\uparrow}\right)(t)|S^{-}_{\mathbf{Q}}(0) \gg \\
&- \frac{J}{2\sqrt{N}}\sum_{\mathbf{q}'} \ll S^{\dagger}_{\mathbf{q}-\mathbf{Q}}S^{-}_{\mathbf{q}'}c^{\dagger}_{\mathbf{k}-\mathbf{q}\uparrow}c_{\mathbf{k}+\mathbf{q}'\downarrow}(t)|S^{-}_{\mathbf{Q}}(0) \gg \\
&+ \frac{J}{2\sqrt{N}}\sum_{\mathbf{q}'} \ll S^{\dagger}_{\mathbf{q}-\mathbf{Q}}S^{\dagger}_{\mathbf{q}'}c^{\dagger}_{\mathbf{k}-\mathbf{q}-\mathbf{q}'\uparrow}c_{\mathbf{k}\downarrow}(t)|S^{-}_{\mathbf{Q}}(0) \gg \qquad (4.37) \\
&+ \frac{J}{2N}\sum_{\mathbf{k}'\mathbf{q}'\sigma'} \ll S^{\dagger}_{\mathbf{q}-\mathbf{Q}+\mathbf{q}'}c^{\dagger}_{\mathbf{k}'-\mathbf{q}'\sigma'}c_{\mathbf{k}'\sigma'}\left(c^{\dagger}_{\mathbf{k}-\mathbf{q}\uparrow}c_{\mathbf{k}\uparrow}-n(\varepsilon_{\mathbf{k}})\delta_{\mathbf{q},\mathbf{0}}\right)(t)|S^{-}_{\mathbf{Q}}(0) \gg \\
&- \frac{J}{N}\sum_{\mathbf{k}'\mathbf{q}'} \ll S^{z}_{\mathbf{q}-\mathbf{Q}+\mathbf{q}'}c^{\dagger}_{\mathbf{k}'-\mathbf{q}'\uparrow}c_{\mathbf{k}'\downarrow}\left(c^{\dagger}_{\mathbf{k}-\mathbf{q}\uparrow}c_{\mathbf{k}\uparrow}-n(\varepsilon_{\mathbf{k}})\delta_{\mathbf{q},\mathbf{0}}\right)(t)|S^{-}_{\mathbf{Q}}(0) \gg .
\end{aligned}
$$

The above equation of motion seems to be rather complex since it contains a large number of new Green's functions. However, we can treat these Green's functions approximately by factorizing them in a similar way with that discussed above. Note that we have to truncate three–term factors in the general form $\ll ABC|S^{-}_{\mathbf{Q}}(0) \gg$. One must be very careful when applying such a procedure since the result can be different depending on the way of truncation. We adopt here a two–step approximation. Firstly, we treat the factor BC in the Green's function as a simple operator. In this way we factorize the Green's function as previously shown: $\ll ABC|S_{\mathbf{Q}}(0) \gg \simeq < A > \ll BC|S^{-}_{\mathbf{Q}} \gg + < BC > \ll A|S^{-}_{\mathbf{Q}} \gg$. The form of the new Green's functions indicate whether we have to apply a factorization one more time. If $\ll BC|S^{-}_{\mathbf{Q}} \gg$ is a known Green's function, for example $Y^{\mathbf{Q}}$, we do not need to proceed to any further approximation, otherwise the new term is approximated in the same way: $\ll BC|S^{-}_{\mathbf{Q}} \gg \simeq < B > \ll C|S^{-}_{\mathbf{Q}} \gg + < C > \ll C|S_{\mathbf{Q}} \gg$. In this way we can distinguish all the higher–order Green's functions into two categories. The first where all the Green's functions which can be reduced to a lower–order one and the second with the non–reducible ones. We apply now this procedure to each of the higher–order Green's function. First of all, the 1^{st} term on the rhs can be written in terms of of $G^{\mathbf{Q}}_{\mathbf{k},\mathbf{q}}(t)$ and $Y^{\mathbf{Q}}(t)$. Using the definitions 4.1 and 4.32 we easily find that:

$$
\ll S^{\dagger}_{\mathbf{q}-\mathbf{Q}}c^{\dagger}_{\mathbf{k}-\mathbf{q}\uparrow}c_{\mathbf{k}\uparrow}(t)|S^{-}_{\mathbf{Q}} \gg = n(\varepsilon_{\mathbf{k}})\delta_{\mathbf{q}}Y^{\mathbf{Q}}(t) + G^{\mathbf{Q}}_{\mathbf{k},\mathbf{q}}(t). \qquad (4.38)
$$

We observe that this term contributes only to the electron spin flip energy. The 2^{nd} term of Eq. 4.36 is a higher–order Green's function and must be approximated.

First, using the identity 8.16 we rewrite this term as:

$$\begin{aligned}
&\ll S^{\dagger}_{\mathbf{q}-\mathbf{Q}} S^{z}_{\mathbf{q}'} \left(c^{\dagger}_{\mathbf{k}-\mathbf{q}\uparrow} c_{\mathbf{k}+\mathbf{q}'\uparrow} - c^{\dagger}_{\mathbf{k}-\mathbf{q}-\mathbf{q}'\uparrow} c_{\mathbf{k}\uparrow} \right)(t) | S^{-}_{\mathbf{Q}} \gg = \\
&\ll \left(-\frac{1}{\sqrt{N}} S^{\dagger}_{\mathbf{q}'+\mathbf{q}-\mathbf{Q}} + S^{z}_{\mathbf{q}'} S^{\dagger}_{\mathbf{q}-\mathbf{Q}} \right) \left(c^{\dagger}_{\mathbf{k}-\mathbf{q}\uparrow} c_{\mathbf{k}+\mathbf{q}'\uparrow} - c^{\dagger}_{\mathbf{k}-\mathbf{q}-\mathbf{q}'\uparrow} c_{\mathbf{k}\uparrow} \right)(t) | S^{-}_{\mathbf{Q}} \gg \\
&= -\frac{1}{\sqrt{N}} \ll S^{\dagger}_{\mathbf{q}'+\mathbf{q}-\mathbf{Q}} c^{\dagger}_{\mathbf{k}-\mathbf{q}\uparrow} c_{\mathbf{k}+\mathbf{q}'\uparrow}(t) | S^{-}_{\mathbf{Q}} \gg \\
&\quad + \frac{1}{\sqrt{N}} \ll S^{\dagger}_{\mathbf{q}'+\mathbf{q}-\mathbf{Q}} c^{\dagger}_{\mathbf{k}-\mathbf{q}-\mathbf{q}'\uparrow} c_{\mathbf{k}\uparrow}(t) | S^{-}_{\mathbf{Q}} \gg \\
&\quad + \ll S^{z}_{\mathbf{q}'} S^{\dagger}_{\mathbf{q}-\mathbf{Q}} \left(c^{\dagger}_{\mathbf{k}-\mathbf{q}\uparrow} c_{\mathbf{k}+\mathbf{q}'\uparrow} - c^{\dagger}_{\mathbf{k}-\mathbf{q}-\mathbf{q}'\uparrow} c_{\mathbf{k}\uparrow} \right)(t) | S^{-}_{\mathbf{Q}} \gg
\end{aligned}$$

Now we note that the 1^{st} two new terms have exactly the same form as the Green's function $G^{\mathbf{Q}}_{\mathbf{k},\mathbf{q}}(t)$. The only difference is in the momentum–dependence $\mathbf{k}, \mathbf{q}$. Using definition 4.32 we find:

$$\ll S^{\dagger}_{\mathbf{q}'+\mathbf{q}-\mathbf{Q}} c^{\dagger}_{\mathbf{k}-\mathbf{q}\uparrow} c_{\mathbf{k}+\mathbf{q}'\uparrow}(t) | S^{-}_{\mathbf{Q}} \gg = G^{\mathbf{Q}}_{\mathbf{k}+\mathbf{q}',\mathbf{q}+\mathbf{q}'}(t) + n(\varepsilon_{\mathbf{k}+\mathbf{q}'}) \delta_{\mathbf{q}',\mathbf{q}} Y^{\mathbf{Q}}(t) \qquad (4.39)$$

$$\ll S^{\dagger}_{\mathbf{q}'+\mathbf{q}-\mathbf{Q}} c^{\dagger}_{\mathbf{k}-\mathbf{q}-\mathbf{q}'\uparrow} c_{\mathbf{k}\uparrow}(t) | S^{-}_{\mathbf{Q}} \gg = G^{\mathbf{Q}}_{\mathbf{k},\mathbf{q}+\mathbf{q}'}(t) + n(\varepsilon_{\mathbf{q}'}) \delta_{\mathbf{q}',\mathbf{q}} Y^{\mathbf{Q}}(t) \qquad (4.40)$$

Regarding the last term, it is a higher–order Green's function and thus must be approximated. Using the strategy described above in addition with the property 4.7 we find that this term vanishes if we take into account the sum over $\mathbf{q}'$ in the equation of motion:

$$\begin{aligned}
\ll S^{z}_{\mathbf{q}'} \quad & S^{\dagger}_{\mathbf{q}-\mathbf{Q}} \quad \left(c^{\dagger}_{\mathbf{k}-\mathbf{q}\uparrow} c_{\mathbf{k}+\mathbf{q}'\uparrow} - c^{\dagger}_{\mathbf{k}-\mathbf{q}-\mathbf{q}'\uparrow} c_{\mathbf{k}\uparrow} \right)(t) | S^{-}_{\mathbf{Q}}(0) \gg \\
&\simeq \quad < S^{z}_{\mathbf{q}'} > \ll S^{\dagger}_{\mathbf{q}-\mathbf{Q}} \left(c^{\dagger}_{\mathbf{k}-\mathbf{q}\uparrow} c_{\mathbf{k}+\mathbf{q}'\uparrow} - c^{\dagger}_{\mathbf{k}-\mathbf{q}-\mathbf{q}'\uparrow} c_{\mathbf{k}\uparrow} \right)(t) | S^{-}_{\mathbf{Q}}(0) \gg \qquad (4.41) \\
&= \quad \sqrt{N} S \delta_{\mathbf{q}',\mathbf{0}} \ll S^{\dagger}_{\mathbf{q}-\mathbf{Q}} \left(c^{\dagger}_{\mathbf{k}-\mathbf{q}\uparrow} c_{\mathbf{k}\uparrow} - c^{\dagger}_{\mathbf{k}-\mathbf{q}\uparrow} c_{\mathbf{k}\uparrow} \right)(t) | S^{-}_{\mathbf{Q}}(0) \gg \\
&= \quad 0
\end{aligned}$$

Summarizing the above calculations we obtain that the 2^{nd} Green's function in the equation of motion of $G^{\mathbf{Q}}_{\mathbf{k},\mathbf{q}}(t)$ is finally approximated as follows:

$$\begin{aligned}
\ll S^{\dagger}_{\mathbf{q}-\mathbf{Q}} S^{z}_{\mathbf{q}'} \left(c^{\dagger}_{\mathbf{k}-\mathbf{q}\uparrow} c_{\mathbf{k}+\mathbf{q}'\uparrow} - c^{\dagger}_{\mathbf{k}-\mathbf{q}-\mathbf{q}'\uparrow} c_{\mathbf{k}\uparrow} \right)(t) | S^{-}_{\mathbf{Q}} \gg = & \\
-\frac{1}{\sqrt{N}} \left(n(\varepsilon_{\mathbf{k}+\mathbf{q}'}) - n(\varepsilon_{\mathbf{q}'}) \right) \delta_{\mathbf{q},\mathbf{q}'} Y^{\mathbf{Q}}(t) & \qquad (4.42) \\
-\frac{1}{\sqrt{N}} \left(G^{\mathbf{Q}}_{\mathbf{k}+\mathbf{q}',\mathbf{q}+\mathbf{q}'}(t) - G^{\mathbf{Q}}_{\mathbf{k},\mathbf{q}+\mathbf{q}'}(t) \right), &
\end{aligned}$$

which shows that this term introduces rescattering terms in the equation of motion of $G^{\mathbf{Q}}_{\mathbf{kq}}(t)$ since it connects momenta $\mathbf{k}, \mathbf{q}$ with $\mathbf{k}+\mathbf{q}', \mathbf{q}+\mathbf{q}'$ respectively.

Now we turn to the third Green's function appearing in the equation of motion of $G^{\mathbf{Q}}_{\mathbf{k},\mathbf{q}}(t)$ Eq. 4.37. If we consider the local spin operators $S^{\dagger}$ and S^{-} as one operator then we can easily approximate this function as:

$$\begin{aligned} &\ll S^{\dagger}_{\mathbf{q}-\mathbf{Q}} S^{-}_{\mathbf{q}'} c^{\dagger}_{\mathbf{k}-\mathbf{q}\uparrow} c_{\mathbf{k}+\mathbf{q}'\downarrow}(t) | S^{-}_{\mathbf{Q}}(0) \gg = \\ &< S^{\dagger}_{\mathbf{q}-\mathbf{Q}} S^{-}_{\mathbf{q}'} > \ll c^{\dagger}_{\mathbf{k}-\mathbf{q}\uparrow} c_{\mathbf{k}+\mathbf{q}'\downarrow}(t) | S^{-}_{\mathbf{Q}}(0) \gg \\ &+ < c^{\dagger}_{\mathbf{k}-\mathbf{q}\uparrow} c_{\mathbf{k}+\mathbf{q}'\downarrow} > \ll S^{\dagger}_{\mathbf{q}-\mathbf{Q}} S^{-}_{\mathbf{q}'}(t) | S^{-}_{\mathbf{Q}}(0) \gg . \end{aligned} \tag{4.43}$$

Now using the properties 4.7, 4.8 and 8.14 along with the definition 4.11 we finally find:

$$\ll S^{\dagger}_{\mathbf{q}-\mathbf{Q}} S^{-}_{\mathbf{q}'} c^{\dagger}_{\mathbf{k}-\mathbf{q}\uparrow} c_{\mathbf{k}+\mathbf{q}'\downarrow}(t) | S^{-}_{\mathbf{Q}}(0) \gg = 2S \delta_{\mathbf{q}',\mathbf{Q}-\mathbf{q}} X^{\mathbf{Q}}_{\mathbf{k}+\mathbf{q}+\mathbf{Q}}(t). \tag{4.44}$$

We continue with the 4^{th} Green's function appearing in the equation of motion. We observe that this function does not contribute to the dynamics of $G^{\mathbf{Q}}_{\mathbf{k},\mathbf{q}}(t)$ if one approximates it using factorization. This can be easily seen by taking into account the property 4.7 as well as the fact that $< S^{\dagger} >= 0$. In this way we can obtain

$$\begin{aligned} \ll S^{\dagger}_{\mathbf{q}-\mathbf{Q}} S^{\dagger}_{\mathbf{q}'} c^{\dagger}_{\mathbf{k}-\mathbf{q}-\mathbf{q}'\uparrow} c_{\mathbf{k}\downarrow}(t) | S^{-}_{\mathbf{Q}}(0) \gg \; &\simeq \; < S^{\dagger}_{\mathbf{q}-\mathbf{Q}} S^{\dagger}_{\mathbf{q}'} > \ll c^{\dagger}_{\mathbf{k}-\mathbf{q}-\mathbf{q}'\uparrow} c_{\mathbf{k}\downarrow}(t) | S^{-}_{\mathbf{Q}}(0) \gg \\ &+ \; < c^{\dagger}_{\mathbf{k}-\mathbf{q}-\mathbf{q}'\uparrow} c_{\mathbf{k}\downarrow} > \ll S^{\dagger}_{\mathbf{q}-\mathbf{Q}} S^{\dagger}_{\mathbf{q}'}(t) | S^{-}_{\mathbf{Q}}(0) \gg \\ &= \; 0. \end{aligned} \tag{4.45}$$

This might indicate that we must keep this Green's function in Eq. 4.37 motion without any approximation and write its own equation of motion. However, we are interested in the process of scattering between one magnon and one electron. Therefore the Green's function 4.45 can be ignored since it expresses a two electron scattering process.

As far as the fifth term is concerned, it is easy to see that the only non-zero contribution of this term can be written as follows:

$$\begin{aligned} \ll \; & S^{\dagger}_{\mathbf{q}-\mathbf{Q}+\mathbf{q}'} c^{\dagger}_{\mathbf{k}'-\mathbf{q}'\sigma'} c_{\mathbf{k}'\sigma'} \left(c^{\dagger}_{\mathbf{k}-\mathbf{q}\uparrow} c_{\mathbf{k}\uparrow} - n(\varepsilon_{\mathbf{k}}) \delta_{\mathbf{q},\mathbf{0}} \right)(t) | S^{-}_{\mathbf{Q}}(0) \gg \simeq \\ < \; & c^{\dagger}_{\mathbf{k}'-\mathbf{q}'\sigma'} c_{\mathbf{k}'\sigma'} > \times \\ \ll \; & S^{\dagger}_{\mathbf{q}-\mathbf{Q}+\mathbf{q}'} \left(c^{\dagger}_{\mathbf{k}-\mathbf{q}\uparrow} c_{\mathbf{k}\uparrow} - n(\varepsilon_{\mathbf{k}}) \delta_{\mathbf{q},\mathbf{0}} \right)(t) | S^{-}_{\mathbf{Q}}(0) \gg = \delta_{\mathbf{q}'=\mathbf{0}} G^{\mathbf{Q}}_{\mathbf{k},\mathbf{q}}(t), \end{aligned} \tag{4.46}$$

where we used the property 4.7 and the definition 4.32. Eq. 4.46 contributes only to the electron spin–flip energy, similar to the 1^{st} term of the equation of motion as discussed above.

We complete the discussion about the equation of motion of $G^{\mathbf{Q}}_{\mathbf{kq}}$ and the way in which can be approximated with the last term appeared in Eq. 4.37. First of

all, we can make an approximation of this Green's function using the property 4.6. We find that

$$\begin{aligned}
&\ll S^z_{\mathbf{q}-\mathbf{Q}+\mathbf{q}'} c^\dagger_{\mathbf{k}'-\mathbf{q}'\uparrow} c_{\mathbf{k}'\downarrow} \left(c^\dagger_{\mathbf{k}-\mathbf{q}\uparrow} c_{\mathbf{k}\uparrow} - n(\varepsilon_{\mathbf{k}})\delta_{\mathbf{q},\mathbf{0}} \right)(t) | S^-_{\mathbf{Q}}(0) \gg \simeq \\
&< S^z_{\mathbf{q}-\mathbf{Q}+\mathbf{q}'} > \ll c^\dagger_{\mathbf{k}'-\mathbf{q}'\uparrow} c_{\mathbf{k}'\downarrow} \left(c^\dagger_{\mathbf{k}-\mathbf{q}\uparrow} c_{\mathbf{k}\uparrow} - n(\varepsilon_{\mathbf{k}})\delta_{\mathbf{q},\mathbf{0}} \right)(t) | S^-_{\mathbf{Q}}(0) \gg = \\
&\sqrt{N} S \delta_{\mathbf{q}',\mathbf{Q}-\mathbf{q}} \ll c^\dagger_{\mathbf{k}'-\mathbf{Q}+\mathbf{q}\uparrow} c_{\mathbf{k}'\downarrow} \left(c^\dagger_{\mathbf{k}-\mathbf{q}\uparrow} c_{\mathbf{k}\uparrow} - n(\varepsilon_{\mathbf{k}})\delta_{\mathbf{q},\mathbf{0}} \right)(t) | S^-_{\mathbf{Q}}(0) \gg .
\end{aligned}$$

It can be easily shown that a further approximation in the above function leads to a zero contribution to the equation of motion 4.37. Indeed, taking into account the property 4.17 we find that the factorized form of function 4.47 becomes:

$$\begin{aligned}
&\ll c^\dagger_{\mathbf{k}'-\mathbf{Q}+\mathbf{q}\uparrow} c_{\mathbf{k}'\downarrow} \left(c^\dagger_{\mathbf{k}-\mathbf{q}\uparrow} c_{\mathbf{k}\uparrow} - n(\varepsilon_{\mathbf{k}})\delta_{\mathbf{q},\mathbf{0}} \right)(t) | S^-_{\mathbf{Q}}(0) \gg \simeq \\
&< c^\dagger_{\mathbf{k}'-\mathbf{Q}+\mathbf{q}\uparrow} c_{\mathbf{k}'\downarrow} > \ll \left(c^\dagger_{\mathbf{k}-\mathbf{q}\uparrow} c_{\mathbf{k}\uparrow} - n(\varepsilon_{\mathbf{k}})\delta_{\mathbf{q},\mathbf{0}} \right)(t) | S^-_{\mathbf{Q}}(0) \gg \qquad (4.47) \\
&+ < \left(c^\dagger_{\mathbf{k}-\mathbf{q}\uparrow} c_{\mathbf{k}\uparrow} - n(\varepsilon_{\mathbf{k}})\delta_{\mathbf{q},\mathbf{0}} \right) > \ll c^\dagger_{\mathbf{k}'-\mathbf{Q}+\mathbf{q}\uparrow} c_{\mathbf{k}'\downarrow}(t) | S^-_{\mathbf{Q}}(0) \gg = 0.
\end{aligned}$$

The latter indicates that the discussion regarding the fourth term on the r.h.s of Eq. 4.37 can also be applied here. One can keep green's function 4.47 in the equation of motion 4.37 and accordingly, a new equation of motion for this function must be written. A direct comparison between $G^{\mathbf{Q}}_{\mathbf{kq}}$ and the Green's function appearing in the above equation can be made. The latter shows a similarity which becomes clear if one writes again those two Green's functions.

$$\begin{aligned}
G^{\mathbf{Q}}_{\mathbf{k},\mathbf{q}}(t) &= \ll S^\dagger_{\mathbf{q}-\mathbf{Q}} \left(c^\dagger_{\mathbf{k}-\mathbf{q}\uparrow} c_{\mathbf{k}\uparrow} - \delta_{\mathbf{q},\mathbf{0}} n(\varepsilon_{\mathbf{k}}) \right)(t) | S^-_{\mathbf{Q}}(0) \gg \qquad (4.48) \\
&\ll c^\dagger_{\mathbf{k}'-\mathbf{Q}+\mathbf{q}\uparrow} c_{\mathbf{k}'\downarrow} \left(c^\dagger_{\mathbf{k}-\mathbf{q}\uparrow} c_{\mathbf{k}\uparrow} - \delta_{\mathbf{q},\mathbf{0}} n(\varepsilon_{\mathbf{k}}) \right)(t) | S^-_{\mathbf{Q}}(0) \gg . \qquad (4.49)
\end{aligned}$$

As we have said, the Green's function $G^{\mathbf{Q}}_{\mathbf{kq}}$ expresses a scattering process between an fermi sea electron and a local spin. Comparing the form of the new function with that of 4.32 we note that the local spin operator $S^\dagger_{\mathbf{Q}}$ is replaced by $c^\dagger_{\mathbf{k}'-\mathbf{Q}+\mathbf{q}\uparrow} c_{\mathbf{k}'\downarrow}$ of itinerant electron. Consequently it introduces the process of scattering of a fermi sea electron via a spin–flip excitation thus it is a 3–body process. In other words it corresponds to the variational amplitude $\Phi^{\mathbf{Q}}_{\alpha\nu\mu}$ of the Chapter 2 while $G^{\mathbf{Q}}_{\mathbf{kq}}$ corresponds to the amplitude $\Psi^{\mathbf{Q}}_{\alpha\mu}$. Since we are interested in examining the role of correlations on the spinwave excitations up to 3–body process we have to determine the time-dependence of this new Green's function, which is defined as follows

$$H^{\mathbf{Q}}_{\mathbf{p},\mathbf{k},\mathbf{q}}(t) = \ll c^\dagger_{\mathbf{p}+\mathbf{q}-\mathbf{Q}\uparrow} c_{\mathbf{p}\downarrow} \left(c^\dagger_{\mathbf{k}-\mathbf{q}\uparrow} c_{\mathbf{k}\uparrow} - n(\varepsilon_{\mathbf{k}})\delta_{\mathbf{q},\mathbf{0}} \right)(t) | S^-_{\mathbf{Q}}(0) \gg \qquad (4.50)$$

Before this, let us complete the discussion of the local spin–fermi sea electron scattering Green's function $G^{\mathbf{Q}}_{\mathbf{kq}}(t)$. Substituting the approximations 4.38, 4.42, 4.44, 4.45, 4.46 and 4.47 of all the green's functions on the r.h.s of Eq. 4.37 taking also into account the properties 4.6, 4.7, 4.8 and 4.17 we find that the equation of motion of $G^{\mathbf{Q}}_{\mathbf{kq}}(t)$ is transformed into the rather simple form:

$$\begin{aligned} i\frac{\partial}{\partial t}G^{\mathbf{Q}}_{\mathbf{k,q}}(t) &= \frac{J}{2N}\left(n(\varepsilon_{\mathbf{k-q}}) - n(\varepsilon_{\mathbf{k}})\right) Y^{\mathbf{Q}}(t) \\ &- \frac{JS}{\sqrt{N}} X^{\mathbf{Q}}_{\mathbf{k+Q-q}}(t) \\ &+ \left(\varepsilon_{\mathbf{k}} - \varepsilon_{\mathbf{k-q}} + \frac{Jn}{2}\right) G^{\mathbf{Q}}_{\mathbf{k,q}}(t) \\ &+ \frac{J}{2N}\sum_{\mathbf{q'}} \left(G^{\mathbf{Q}}_{\mathbf{k+q',q+q'}}(t) - G^{\mathbf{Q}}_{\mathbf{k,q+q'}}(t)\right) \\ &- \frac{SJ}{\sqrt{N}}\sum_{\mathbf{k'}} H^{\mathbf{Q}}_{\mathbf{k'kq}}(t). \end{aligned} \tag{4.51}$$

The 1^{st} three terms in the r.h.s. of the above equation gives a contribution of order $O(1/S)$ to the Green's function $G^{\mathbf{Q}}_{\mathbf{kq}}$ while higher contributions is introduced by the last two terms. By setting $H = 0$ in Eq. 4.51 one obtains only the local spin–electron scattering, which corresponds to the $\Phi = 0$ approximation in Chapter (2), whereas the full 3–body calculation demands the calculation of the higher–order Green's function $H^{\mathbf{Q}}_{\mathbf{k'kq}}(t)$.

We conclude that, the introduction of a higher–order Green's function which expresses the scattering process of a fermi sea electron and the creation of an electron–hole pair leads to an additional equation of motion which can be treated approximately by expanding all but of one the new terms appearing in the r.h.s. in products of lower–order functions. That terminates the infinite chain of coupled equations which is unavoidable for a strongly correlated system such as the manganites of interest here. However, our approximate method leads to another Green's function (higher–order than $G^{\mathbf{Q}}_{\mathbf{kq}}$) which expresses the creation of an electron–hole pair with the simultaneous flip of an electron's spin. In the rest of this subsection we treat this Green's function in the same approximate way as we adopted for $G^{\mathbf{Q}}_{\mathbf{kq}}$. We show that with the application of that method we finally obtain a finite set of equations since our approximations leaves no new Green's functions in the equation of motion for $H^{\mathbf{Q}}_{\mathbf{k'kq}}(t)$.

Let us continue now with the equation of motion of the spin–flip fermi electron

Green's function. It has the general form:

$$
\begin{aligned}
i\frac{\partial}{\partial t}H^{\mathbf{Q}}_{\mathbf{pkq}}(t) &= i\delta(0) < \left[c^{\dagger}_{\mathbf{p+q-Q}\uparrow}c_{\mathbf{p}\downarrow}\left(c^{\dagger}_{\mathbf{k-q}\uparrow}c_{\mathbf{k}\uparrow} - n(\varepsilon_{\mathbf{k}})\delta_{\mathbf{q},\mathbf{0}}\right), S^{-}_{\mathbf{Q}}\right] > \\
&+ \ll \left[c^{\dagger}_{\mathbf{p+q-Q}\uparrow}c_{\mathbf{p}\downarrow}\left(c^{\dagger}_{\mathbf{k-q}\uparrow}c_{\mathbf{k}\uparrow} - n(\varepsilon_{\mathbf{k}})\delta_{\mathbf{q},\mathbf{0}}\right), H\right](t)|S^{-}_{\mathbf{Q}}(0) \gg \qquad (4.52)
\end{aligned}
$$

which after calculating the commutators in the r.h.s becomes

$$
\begin{aligned}
i\frac{\partial}{\partial t}H^{\mathbf{Q}}_{\mathbf{pkq}}(t) &= (\varepsilon_{\mathbf{p}} - \varepsilon_{\mathbf{p+q+Q}}) \ll c^{\dagger}_{\mathbf{p+q-Q}\uparrow}c_{\mathbf{p}\downarrow}\left(c^{\dagger}_{\mathbf{k-q}\uparrow}c_{\mathbf{k}\uparrow} - n(\varepsilon_{\mathbf{k}})\delta_{\mathbf{q},\mathbf{0}}\right)(t)|S^{-}_{\mathbf{Q}}(0) \gg \\
&+ \frac{J}{2\sqrt{N}}\sum_{\mathbf{q}'} \ll S^{z}_{\mathbf{q}'}\left(c^{\dagger}_{\mathbf{p+q-Q}\uparrow}c_{\mathbf{p+q}'\downarrow} + c^{\dagger}_{\mathbf{p+q-Q-q}'\uparrow}c_{\mathbf{p}\downarrow}\right) \times \\
&\qquad\qquad \left(c^{\dagger}_{\mathbf{k-q}\uparrow}c_{\mathbf{k}\uparrow} - n(\varepsilon_{\mathbf{k}})\delta_{\mathbf{q},\mathbf{0}}\right)(t)|S^{-}_{\mathbf{Q}}(0) \gg \\
&- \frac{J}{2\sqrt{N}}\sum_{\mathbf{q}'} \ll S^{\dagger}_{\mathbf{q}'}\left(c^{\dagger}_{\mathbf{p+q-Q}\uparrow}c_{\mathbf{p+q}'\uparrow} - c^{\dagger}_{\mathbf{p+q-Q-q}'\downarrow}c_{\mathbf{p}\downarrow}\right) \times \\
&\qquad\qquad \left(c^{\dagger}_{\mathbf{k-q}\uparrow}c_{\mathbf{k}\uparrow} - n(\varepsilon_{\mathbf{k}})\delta_{\mathbf{q},\mathbf{0}}\right)(t)|S^{-}_{\mathbf{Q}}(0) \gg \\
&+ (\varepsilon_{\mathbf{k}} - \varepsilon_{\mathbf{k-q}}) \ll c^{\dagger}_{\mathbf{p+q-Q}\uparrow}c_{\mathbf{p}\downarrow}c^{\dagger}_{\mathbf{k-q}\uparrow}c_{\mathbf{k}\uparrow}(t)|S^{-}_{\mathbf{Q}}(0) \gg \qquad (4.53) \\
&- \frac{J}{2\sqrt{N}}\sum_{\mathbf{q}'} \ll c^{\dagger}_{\mathbf{p+q-Q}\uparrow}c_{\mathbf{p}\downarrow}S^{z}_{\mathbf{q}'}\left(c^{\dagger}_{\mathbf{k-q}\uparrow}c_{\mathbf{k+q}'\uparrow} - c^{\dagger}_{\mathbf{k-q+q}'\uparrow}c_{\mathbf{k}\uparrow}\right)(t)|S^{-}_{\mathbf{Q}}(0) \gg \\
&- \frac{J}{2\sqrt{N}}\sum_{\mathbf{q}'} \ll c^{\dagger}_{\mathbf{p+q-Q}\uparrow}c_{\mathbf{p}\downarrow}S^{-}_{\mathbf{q}'}c^{\dagger}_{\mathbf{k-q}\uparrow}c_{\mathbf{k}\downarrow}(t)|S^{-}_{\mathbf{Q}}(0) \gg \\
&+ \frac{J}{2\sqrt{N}}\sum_{\mathbf{q}'} \ll c^{\dagger}_{\mathbf{p+q-Q}\uparrow}c_{\mathbf{p}\downarrow}S^{\dagger}_{\mathbf{q}'}c^{\dagger}_{\mathbf{k-q-q}'\uparrow}c_{\mathbf{k}\uparrow}(t)|S^{-}_{\mathbf{Q}}(0) \gg .
\end{aligned}
$$

This is a rather complex equation which contains a large number of higher–order Green's functions. However, we will show here that by applying the approximate method as described above a quite simple equation can be obtained. First of all, we note that using the definition 4.50 of Green's function $H^{\mathbf{Q}}_{\mathbf{kpq}}(t)$ we rewrite the 1^{st} term as:

$$
\ll c^{\dagger}_{\mathbf{p+q-Q}\uparrow}c_{\mathbf{p}\downarrow}\left(c^{\dagger}_{\mathbf{k-q}\uparrow}c_{\mathbf{k}\uparrow} - n(\varepsilon_{\mathbf{k}})\delta_{\mathbf{q},\mathbf{0}}\right)(t)|S^{-}_{\mathbf{Q}}(0) \gg = H^{\mathbf{Q}}_{\mathbf{kpq}}(t) \qquad (4.54)
$$

and the 4^{th} one as:

$$
\ll c^{\dagger}_{\mathbf{p+q-Q}\uparrow}c_{\mathbf{p}\downarrow}c^{\dagger}_{\mathbf{k-q}\uparrow}c_{\mathbf{k}\uparrow}(t)|S^{-}_{\mathbf{Q}}(0) \gg = n(\varepsilon_{\mathbf{k}})\delta_{\mathbf{q},\mathbf{0}} + H^{\mathbf{Q}}_{\mathbf{kpq}}(t), \qquad (4.55)
$$

where the first term does not contribute to the equation of motion since it is multiplied by zero at $\mathbf{q} = \mathbf{0}$ due to the term $\varepsilon_{\mathbf{k}} - \varepsilon_{\mathbf{k-q}}$. The second term of the

equation of motion is of the general form: $\ll S^z_{\mathbf{q}} A(t)|S^-_{\mathbf{q}}(0) \gg$, which can be approximated as $\ll S^z_{\mathbf{q}} A(t)|S^-_{\mathbf{q}}(0) \gg \simeq < S^z_{\mathbf{q}} > \ll A(t)|S^-_{\mathbf{q}}(0) \gg$. In this way the second term can be written as:

$$\ll S^z_{\mathbf{q}'} \left(c^\dagger_{\mathbf{p+q-Q}\uparrow} c_{\mathbf{p+q'}\downarrow} + c^\dagger_{\mathbf{p+q-Q-q'}\uparrow} c_{\mathbf{p}\downarrow}\right) \left(c^\dagger_{\mathbf{k-q}\uparrow} c_{\mathbf{k}\uparrow} - n(\varepsilon_{\mathbf{k}})\delta_{\mathbf{q},\mathbf{0}}\right)(t)|S^-_{\mathbf{Q}}(0) \gg$$
$$\simeq \sqrt{N} S \delta_{\mathbf{q},\mathbf{Q}} 2H^{\mathbf{Q}}_{\mathbf{kpq}}(t), \quad (4.56)$$

where the property 4.7 is used. The next term in the equation of motion 4.53 gives only one non–zero contribution. This contribution can be written in the form of Green's function G as follows:

$$\ll S^\dagger_{\mathbf{q}'} \left(c^\dagger_{\mathbf{p+q-Q}\uparrow} c_{\mathbf{p+q'}\uparrow} - c^\dagger_{\mathbf{p+q-Q-q'}\downarrow} c_{\mathbf{p}\downarrow}\right) \left(c^\dagger_{\mathbf{k-q}\uparrow} c_{\mathbf{k}\uparrow} - n(\varepsilon_{\mathbf{k}})\delta_{\mathbf{q},\mathbf{0}}\right)(t)|S^-_{\mathbf{Q}}(0) \gg$$
$$\simeq < c^\dagger_{\mathbf{p+q-Q}\uparrow} c_{\mathbf{p+q'}\uparrow} - c^\dagger_{\mathbf{p+q-Q-q'}\downarrow} c_{\mathbf{p}\downarrow} > \times$$
$$\ll S^\dagger_{\mathbf{q}'} \left(c^\dagger_{\mathbf{k-q}\uparrow} c_{\mathbf{k}\uparrow} - n(\varepsilon_{\mathbf{k}})\delta_{\mathbf{q},\mathbf{0}}\right)(t)|S^-_{\mathbf{Q}}(0) \gg, \quad (4.57)$$

which finally, after using the property 4.17 of itinerant electron operators and the definition 4.32, becomes:

$$\ll S^\dagger_{\mathbf{q}'} \left(c^\dagger_{\mathbf{p+q-Q}\uparrow} c_{\mathbf{p+q'}\uparrow} - c^\dagger_{\mathbf{p+q-Q-q'}\downarrow} c_{\mathbf{p}\downarrow}\right) \left(c^\dagger_{\mathbf{k-q}\uparrow} c_{\mathbf{k}\uparrow} - n(\varepsilon_{\mathbf{k}})\delta_{\mathbf{q},\mathbf{0}}\right)(t)|S^-_{\mathbf{Q}}(0) \gg$$
$$\simeq \delta_{\mathbf{q}',\mathbf{q}-\mathbf{Q}} G^{\mathbf{Q}}_{\mathbf{kq}}(t). \quad (4.58)$$

Let us continue now with the fifth term of the equation of motion. It can be seen that this term has a form similar to the second one and therefore can be approximated in the same way. In this way we can see that the contribution of this term vanishes within this approximation. This can be easily seen as follows:

$$\ll c^\dagger_{\mathbf{p+q-Q}\uparrow} c_{\mathbf{p}\downarrow} S^z_{\mathbf{q}'} \left(c^\dagger_{\mathbf{k-q}\uparrow} c_{\mathbf{k}\uparrow} - n(\varepsilon_{\mathbf{k}})\delta_{\mathbf{q},\mathbf{0}}\right)(t)|S^-_{\mathbf{Q}}(0) \gg \simeq$$
$$< S^z_{\mathbf{q}'} > \ll c^\dagger_{\mathbf{p+q-Q}\uparrow} c_{\mathbf{p}\downarrow} \left(c^\dagger_{\mathbf{k-q}\uparrow} c_{\mathbf{k+q'}\uparrow} - c^\dagger_{\mathbf{k-q-q'}\uparrow} c_{\mathbf{k}\uparrow}\right)(t)|S^-_{\mathbf{Q}}(0) \gg =$$
$$\sqrt{N} S \delta_{\mathbf{q}',\mathbf{0}} \ll c^\dagger_{\mathbf{p+q-Q}\uparrow} c_{\mathbf{p}\downarrow} \left(c^\dagger_{\mathbf{k-q}\uparrow} c_{\mathbf{k}\uparrow} - c^\dagger_{\mathbf{k-q}\uparrow} c_{\mathbf{k}\uparrow}\right)(t)|S^-_{\mathbf{Q}}(0) \gg = 0. \quad (4.59)$$

There are two higher–order Green's functions left in the equation of motion Eq. 4.53, which must be approximated in some way. Starting from the sixth term, we can see that by applying a factorization procedure as we have done to the previous Green's functions we do not obtain any contribution from this term. This becomes clear if we write this term in its factorized form:

$$\ll c^\dagger_{\mathbf{p+q-Q}\uparrow} c_{\mathbf{p}\downarrow} S^-_{\mathbf{q}'} c^\dagger_{\mathbf{k-q}\uparrow} c_{\mathbf{k}\downarrow}(t)|S^-_{\mathbf{Q}}(0) \gg \simeq$$
$$< c^\dagger_{\mathbf{p+q-Q}\uparrow} c_{\mathbf{p}\downarrow} > \ll S^-_{\mathbf{q}'} c^\dagger_{\mathbf{k-q}\uparrow} c_{\mathbf{k}\downarrow}(t)|S^-_{\mathbf{Q}}(0) \gg$$
$$+ < S^-_{\mathbf{q}'} > \ll c^\dagger_{\mathbf{p+q-Q}\uparrow} c_{\mathbf{p}\downarrow} c^\dagger_{\mathbf{k-q}\uparrow} c_{\mathbf{k}\downarrow}(t)|S^-_{\mathbf{Q}}(0) \gg \quad (4.60)$$
$$+ < c^\dagger_{\mathbf{k-q}\uparrow} c_{\mathbf{k}\downarrow} > \ll c^\dagger_{\mathbf{p+q-Q}\uparrow} c_{\mathbf{p}\downarrow} S^-_{\mathbf{q}'}(t)|S^-_{\mathbf{Q}}(0) \gg .$$

Now due to the properties 4.6 and 4.17 of the expectation values of itinerant electron operators we obtain that these three contributions vanish. Note that the above Green's function contains spin↑ creation and spin↓ annihilation operators. This explains the fact that this function is vanishing. Whatever truncation we apply, vanishing expectation values (for instance $< c^{\dagger}_{\uparrow} c_{\downarrow} >, < c^{\dagger}_{\uparrow} c^{\dagger}_{\uparrow} >$ e.t.c.) all always obtained. To complete the approximation of the equation of motion of $H_{\mathbf{kpq}}$, we have to examine its last term. Let us notice that this term contains a pair of spin↑ creation–annihilation operators. This indicates the existence of a non–zero contribution of this term after the truncation. One must be very careful when applying such a procedure to that term. As a first step the electron operators must be rearranged in order to have the appearance of the pair $c^{\dagger}_{\uparrow} c^{\dagger}_{\uparrow}$. Note that the operator $c_{\mathbf{k}\uparrow}$ anticommutes with the operators $c_{\mathbf{p}\downarrow}$ and $c_{\mathbf{k-q-q'}\uparrow}$. Therefore we obtain:

$$\begin{aligned} &\ll S^{\dagger}_{\mathbf{q'}} c^{\dagger}_{\mathbf{p+q-Q}\uparrow} c_{\mathbf{p}\downarrow} c^{\dagger}_{\mathbf{k-q-q'}\uparrow} c_{\mathbf{k}\uparrow}(t) | S^{-}_{\mathbf{Q}}(0) \gg = \\ &\ll S^{\dagger}_{\mathbf{q'}} c^{\dagger}_{\mathbf{p+q-Q}\uparrow} c_{\mathbf{k}\uparrow} c_{\mathbf{p}\downarrow} c^{\dagger}_{\mathbf{k-q-q'}\uparrow}(t) | S^{-}_{\mathbf{Q}}(0) \gg . \end{aligned} \tag{4.61}$$

Having written the seventh term of the equation of motion in this form we can finally approximate this term as follows:

$$\begin{aligned} &\ll S^{\dagger}_{\mathbf{q'}} c^{\dagger}_{\mathbf{p+q-Q}\uparrow} c_{\mathbf{k}\uparrow} c_{\mathbf{p}\downarrow} c^{\dagger}_{\mathbf{k-q-q'}\uparrow}(t) | S^{-}_{\mathbf{Q}}(0) \gg \simeq \\ &< c^{\dagger}_{\mathbf{p+q-Q}\uparrow} c_{\mathbf{k}\uparrow} > \ll S^{\dagger}_{\mathbf{q'}} c_{\mathbf{p}\downarrow} c^{\dagger}_{\mathbf{k-q-q'}\uparrow}(t) | S^{-}_{\mathbf{Q}}(0) \gg = \\ &\delta_{\mathbf{q',k-q-p}} n(\varepsilon_{\mathbf{p}}) \ll S^{\dagger}_{\mathbf{k-q-p}} c_{\mathbf{p}\downarrow} c^{\dagger}_{\mathbf{k-q-q'}\uparrow}(t) | S^{-}_{\mathbf{Q}}(0) \gg = \\ &\delta_{\mathbf{q',k-q-p}} n(\varepsilon_{\mathbf{p}}) \left(G^{\mathbf{Q}}_{\mathbf{k,k-q-p+Q}}(t) + n(\varepsilon_{\mathbf{k}}) \delta_{\mathbf{k,q+p-Q}} Y^{\mathbf{Q}}(t) \right) , \end{aligned} \tag{4.62}$$

where in the last step we made use of the definition 4.32 for $G^{\mathbf{Q}}_{\mathbf{k,q}}$. Summarizing the above calculations we obtain the final form of the equation of motion of Green's function $H^{\mathbf{Q}}_{\mathbf{kpq}}(t)$ which does not contain any higher–order Green's function and thus there is not need for extra equation of motions. Substituting the r.h.s Green's functions with their approximate forms Eqs. (4.54–4.56), (4.58–4.60) and (4.62) into the equation of motion 4.53 we obtain:

$$\begin{aligned} i \frac{\partial}{\partial t} H^{\mathbf{Q}}_{\mathbf{pkq}}(t) &= (\varepsilon_{\mathbf{p}} - \varepsilon_{\mathbf{p+q-Q}} + \varepsilon_{\mathbf{k}} - \varepsilon_{\mathbf{k-q}} + SJ)\, H^{\mathbf{Q}}_{\mathbf{kpq}}(t) \\ &+ \frac{J}{2\sqrt{N}} n(\varepsilon_{\mathbf{k}}) \delta_{\mathbf{q,k-p+Q}} Y^{\mathbf{Q}}(t) \\ &- \frac{J}{2\sqrt{N}} \left(n(\varepsilon_{\mathbf{p+q-Q}}) G^{\mathbf{Q}}_{\mathbf{k,q}}(t) - G^{\mathbf{Q}}_{\mathbf{k,k-p+Q-q}}(t) \right) . \end{aligned} \tag{4.63}$$

Now we can write our equations of motion into ω–representation by using the Laplace transformation. For convenience, we set the $\mathbf{k} - \mathbf{q} = \mathbf{p}$ into G. By substituting $X_{\mathbf{k}}$ from Eq. (4.35) into Eqs. (4.34) and (4.37) for Y and G respectively

we obtain a system of two equations. In addition, by setting $G = GY$ into these equations we obtain the pole of green's function Y:

$$\begin{aligned}\omega_{\mathbf{Q}} &= \frac{Jn}{2} + \frac{SJ^2}{2N}\sum_{\mathbf{p}} \frac{n(\varepsilon_{\mathbf{p}})}{\omega_{\mathbf{Q}} + \varepsilon_{\mathbf{p}} - \varepsilon_{\mathbf{p+Q}} - SJ} \\ &+ \frac{J^2}{4N^2}\sum_{\mathbf{kp}} G^{\mathbf{Q}}_{\mathbf{kp}} \left(1 + \frac{SJ}{\omega_{\mathbf{Q}} + \varepsilon_{\mathbf{p}} - \varepsilon_{\mathbf{p+Q}} - SJ}\right), \end{aligned} \tag{4.64}$$

where the Green's function $G^{\mathbf{Q}}_{\mathbf{kp}}$ obeys the equation of motion:

$$\begin{aligned}\left(\omega_{\mathbf{Q}} + \varepsilon_{\mathbf{p}} - \varepsilon_{\mathbf{k}} - \frac{Jn}{2} + i\gamma\right) G^{\mathbf{Q}}_{\mathbf{kp}} &= n(\varepsilon_{\mathbf{p}})\left(1 + \frac{SJ}{\omega_{\mathbf{Q}} + \varepsilon_{\mathbf{p}} - \varepsilon_{\mathbf{p+Q}} - SJ}\right) - n(\varepsilon_{\mathbf{k}}) \\ &+ \frac{J}{2N}\sum_{\mathbf{k'}} G^{\mathbf{Q}}_{\mathbf{k'p}} \left(1 + \frac{SJ}{\omega_{\mathbf{Q}} + \varepsilon_{\mathbf{p}} - \varepsilon_{\mathbf{p+Q}} - SJ}\right) \\ &- \frac{J}{2N}\sum_{\mathbf{p'}} G^{\mathbf{Q}}_{\mathbf{kp'}} - SJ\sum_{\mathbf{p'}} H^{\mathbf{Q}}_{\mathbf{p'kp}}. \end{aligned} \tag{4.65}$$

Up to this point we do not make any discussion about the momentum indexes $\mathbf{k}, \mathbf{q}, \mathbf{p}$ which appeared in the Green's functions $G^{\mathbf{Q}}_{\mathbf{kq}}$ and $H^{\mathbf{Q}}_{\mathbf{kpq}}$. One can suppose that these indexes run all over the Brillouin zone. However, these bounds must be stricter if the physical origin of these Green's functions be taken into account. Green's function $G_{\mathbf{kq}}$ is defined to express the scattering of an electron–hole pair with a localized spin while scattering with spin$\uparrow$–$\downarrow$ excitation is described by $H^{\mathbf{Q}}_{\mathbf{kpq}}$. Keeping in our mind that and noting the definition of G

$$G^{\mathbf{Q}}_{\mathbf{k,q}}(t) = \ll S^{\dagger}_{\mathbf{q-Q}}\left(c^{\dagger}_{\mathbf{k-q}\uparrow} c_{\mathbf{k}\uparrow} - \delta_{\mathbf{q},\mathbf{0}} n(\varepsilon_{\mathbf{k}})\right)(t) | S^{-}_{\mathbf{Q}}(0) \gg, \tag{4.66}$$

we conclude that momentum $\mathbf{k} - \mathbf{q}$ is a fermi electron momentum and thus must run into Brillouin zone. Additionally, momentum $\mathbf{k}$ accounts for the hole and consequently must run out of Brillouin zone. That means that Green's function $G^{\mathbf{Q}}_{\mathbf{kq}}$ is simplified as

$$G^{\mathbf{Q}}_{\mathbf{kq}} = (1 - n(\varepsilon_{\mathbf{k}}))\, n(\varepsilon_{\mathbf{k-q}}) G^{\mathbf{Q}}_{\mathbf{kq}} = G_{\alpha\nu}, \tag{4.67}$$

where the notation of momenta is similar with that of the chapter 2. We use $\mu, \nu, \cdots$ for momenta inside and $\alpha, \beta, \cdots$ for momenta outside the Fermi sea. Using that assumption the above equations of motion become:

$$\begin{aligned}\omega_{\mathbf{Q}} &= \frac{Jn}{2} + \frac{SJ^2}{2N}\sum_{\nu} \frac{1}{\omega_{\mathbf{Q}} + \varepsilon_{\nu} - \varepsilon_{\nu+\mathbf{Q}} - SJ} \\ &+ \frac{J^2}{4N^2}\sum_{\alpha\nu} G^{\mathbf{Q}}_{\alpha\nu} \left(1 + \frac{SJ}{\omega_{\mathbf{Q}} + \varepsilon_{\nu} - \varepsilon_{\nu+\mathbf{Q}} - SJ}\right), \end{aligned} \tag{4.68}$$

and

$$\left(\omega_{\mathbf{Q}}+\varepsilon_\nu-\varepsilon_\alpha-\frac{Jn}{2}+i\gamma\right)G^{\mathbf{Q}}_{\alpha\nu} = 1+\frac{SJ}{\omega_{\mathbf{Q}}+\varepsilon_\nu-\varepsilon_{\nu+\mathbf{Q}}-SJ} + \frac{J}{2N}\left(1+\frac{SJ}{\omega_{\mathbf{Q}}+\varepsilon_\nu-\varepsilon_{\nu+\mathbf{Q}}-SJ}\right)\sum_\beta G^{\mathbf{Q}}_{\beta\nu} - \frac{J}{2N}\sum_\mu G^{\mathbf{Q}}_{\alpha\mu}-SJ\sum_{\mathbf{p}'}H^{\mathbf{Q}}_{\mathbf{p}'\alpha\mu}, \quad (4.69)$$

where

$$\left(\omega_{\mathbf{Q}}+\varepsilon_\mu+\varepsilon_\nu-\varepsilon_{\mathbf{Q}+\mu+\nu-\alpha}-\varepsilon_\alpha-SJ+i\gamma'\right)H_{\mathbf{p}'\alpha\nu} = -\frac{J}{2N}\left(n(\varepsilon_{\mathbf{p}'})G^{\mathbf{Q}}_{\alpha\nu}-\delta_{\mu,p'-Q+\alpha-\nu}G_{\alpha\mu}\right). \quad (4.70)$$

The small imaginary part $i\gamma'$ in the denominator of H does not contribute to the spinwave damping for the same reason with that in the equation of X. Because of the large energy factor SJ these denominators can not be vanished and therefore we can set $\gamma'=0$ in the equation of motion 4.35 and 4.70. If we substitute H from Eq. 4.70 into that of G Eq. 4.69 we obtain the final form of this equation of motion

$$\Delta^{\mathbf{Q}}_{\alpha\nu}G^{\mathbf{Q}}_{\alpha\nu} = 1+\frac{SJ}{\omega_{\mathbf{Q}}+\varepsilon_\nu-\varepsilon_{\nu+\mathbf{Q}}-SJ} + \frac{J}{2N}\left(1+\frac{SJ}{\omega_{\mathbf{Q}}+\varepsilon_\nu-\varepsilon_{\nu+\mathbf{Q}}-SJ}\right)\sum_\beta G^{\mathbf{Q}}_{\beta\nu} - \frac{J}{2N}\sum_\mu\left(1+\frac{SJ}{\omega_{\mathbf{Q}}+\varepsilon_\mu+\varepsilon_\nu-\varepsilon_{\mathbf{Q}+\mu+\nu-\alpha}-SJ}\right)G^{\mathbf{Q}}_{\alpha\mu}, \quad (4.71)$$

where

$$\Delta^{\mathbf{Q}}_{\alpha\nu}=\omega_{\mathbf{Q}}+\varepsilon_\nu-\varepsilon_\alpha - \frac{Jn}{2}+i\gamma - \frac{SJ^2}{2N}\sum_\mu\frac{1}{\omega_{\mathbf{Q}}+\varepsilon_\mu+\varepsilon_\nu-\varepsilon_{\mathbf{Q}+\mu+\nu-\alpha}-SJ}. \quad (4.72)$$

Note that the set of equation Eq. 4.71 and 4.68 is identical with the equations of the chapter 2 obtained variationally.

In conclusion, we have used the double–time Green's function method to describe the role of scattering of a magnon with an electron–hole pair. The infinite chain of equations of motion can be terminated by approximating the second or

the third order Green's functions by factorizing them in a way that they reduce to lower–order functions. The set of equations of motion obtained is similar with that determined by the variational calculation of the same processes of chapter 2. The usefulness of the Green's function method is that an additional result is obtained. This result is the damping $\Gamma_{\mathbf{Q}}$ of the spinwave excitations described by the imaginary part of the magnon energy. Our system of equations is rather complicated and therefore close relations for magnon energy and damping can not be found. However we can solve Eqs. 4.68 and 4.71 using an iterative method similar with that we use in chapters 2 and 3 to solve the system of variational equations. The difference here is that we have complex variables such as $\omega_{\mathbf{Q}} = Re(\omega_{\mathbf{Q}}) - i\Gamma_{\mathbf{Q}}$ and $G^{\mathbf{Q}}_{\mathbf{kp}}$. That means that after calculating the complex variable $\omega_{\mathbf{Q}}$ we can calculate the spinwave energy by taking the real part of it and the damping by the relation $\Gamma_{\mathbf{Q}} = -i\mathrm{Im}(\omega_{\mathbf{Q}})$.

4.2.3 1/S expansion

In this subsection we apply the expansion of the magnon energy in the form of the pole of Green's function $Y^{\mathbf{Q}}$ Eq. 4.68 in powers of $1/S$. In this way we are able to determine the first non–zero contribution to the spinwave damping coming from the localized spin–fermi pair scattering.

In the $1/S$ expansion we suppose that $S \to \infty$ while the band splitting SJ is kept finite. For this reason it is convenient to set $SJ = \bar{J}$ in our equations which in this way become:

$$\begin{aligned} \omega_{\mathbf{Q}} &= \frac{\bar{J}n}{2S} + \frac{\bar{J}^2}{2NS}\sum_{\nu}\frac{1}{\omega_{\mathbf{Q}} + \varepsilon_\nu - \varepsilon_{\nu+\mathbf{Q}} - \bar{J}} \\ &+ \frac{\bar{J}^2}{4N^2S^2}\sum_{\alpha\nu} G^{\mathbf{Q}}_{\alpha\nu}\left(1 + \frac{\bar{J}}{\omega_{\mathbf{Q}} + \varepsilon_\nu - \varepsilon_{\nu+\mathbf{Q}} - \bar{J}}\right), \end{aligned} \tag{4.73}$$

and

$$\begin{aligned} \Delta^{\mathbf{Q}}_{\alpha\nu} G^{\mathbf{Q}}_{\alpha\nu} &= 1 + \frac{\bar{J}}{\omega_{\mathbf{Q}} + \varepsilon_\nu - \varepsilon_{\nu+\mathbf{Q}} - \bar{J}} \\ &+ \frac{\bar{J}}{2NS}\left(1 + \frac{\bar{J}}{\omega_{\mathbf{Q}} + \varepsilon_\nu - \varepsilon_{\nu+\mathbf{Q}} - \bar{J}}\right)\sum_{\beta} G^{\mathbf{Q}}_{\beta\nu} \\ &- \frac{\bar{J}}{2N}\sum_{\mu}\left(1 + \frac{\bar{J}}{\omega_{\mathbf{Q}} + \varepsilon_\mu + \varepsilon_\nu - \varepsilon_{\mathbf{Q}+\mu+\nu-\alpha} - \bar{J}}\right) G^{\mathbf{Q}}_{\alpha\mu}. \end{aligned} \tag{4.74}$$

First of all, let us suppose that the double–exchange interaction becomes $\bar{J} \to \infty$.

By expanding the magnon energy in the $\bar{J} \to \infty$ limit we find

$$\omega_{\mathbf{Q}} = - \frac{1}{2NS} \sum_{\nu} (\omega_{\mathbf{Q}} + \varepsilon_{\nu} - \varepsilon_{\nu+\mathbf{Q}}) \\ \frac{1}{4N^2S^2} \sum_{\alpha\nu} G^{\mathbf{Q}}_{\alpha\nu} (\omega_{\mathbf{Q}} + \varepsilon_{\nu} - \varepsilon_{\nu+\mathbf{Q}}), \tag{4.75}$$

and

$$[\omega_{\mathbf{Q}} + \varepsilon_{\nu} - \varepsilon_{\alpha} - i\gamma + \frac{1}{2NS} \sum_{\mu} (\omega_{\mathbf{Q}} + \varepsilon_{\nu} + \varepsilon_{\mu} - \varepsilon_{\mathbf{Q}+\nu+\mu-\alpha} - \varepsilon_{\alpha})] G^{\mathbf{Q}}_{\alpha\nu} = \\ - (\omega_{\mathbf{Q}} + \varepsilon_{\nu} - \varepsilon_{\nu+\mathbf{Q}}) - \frac{1}{2NS} \sum_{\beta} G^{\mathbf{Q}}_{\beta\nu} (\omega_{\mathbf{Q}} + \varepsilon_{\nu} - \varepsilon_{\nu+\mathbf{Q}}) \\ + \frac{1}{2NS} \sum_{\mu} G^{\mathbf{Q}}_{\alpha\mu} (\omega_{\mathbf{Q}} + \varepsilon_{\nu} + \varepsilon_{\mu} - \varepsilon_{\mathbf{Q}+\nu+\mu-\alpha} - \varepsilon_{\alpha}). \tag{4.76}$$

Now one can determine the leading order $\omega^{(1)}_{\mathbf{Q}}$ of the magnon energy by a $1/S$ expansion:

$$\omega^{(1)}_{\mathbf{Q}} = -\frac{1}{2NS} \sum_{\nu} (\varepsilon_{\nu} - \varepsilon_{\nu+\mathbf{Q}}), \tag{4.77}$$

and the zeroth contribution of $G^{\mathbf{Q}}_{\alpha\nu}$:

$$G^{(0)}_{\alpha\nu} = -\frac{\varepsilon_{\nu} - \varepsilon_{\nu+\mathbf{Q}}}{\varepsilon_{\nu} - \varepsilon_{\alpha} - i\gamma} \tag{4.78}$$

Note here that the Green's function G does not contribute to the 1^{st} order magnon energy. Since the imaginary part of $\omega_{\mathbf{Q}}$ comes from that Green's function we conclude that the spinwave dispersion is undamped at 1^{st} order in $1/S$ expansion. The first non–zero contribution to the damping appears when expanding the magnon energy up to the 2^{nd} order in $1/S$ where G contributes at zeroth order

$$\omega^{(2)}_{\mathbf{Q}} = -\frac{1}{2NS} \sum_{\nu} \omega^{(1)}_{\mathbf{Q}} + \frac{1}{4N^2S^2} \sum_{\alpha\nu} G^{(0)}_{\alpha\nu} (\varepsilon_{\nu} - \varepsilon_{\nu+\mathbf{Q}}), \tag{4.79}$$

which after using relations 4.77 and 4.78 yields:

$$\omega^{(2)}_{\mathbf{Q}} = \frac{n}{4NS^2} \sum_{\nu} (\varepsilon_{\nu} - \varepsilon_{\nu+\mathbf{Q}}) - \frac{1}{4N^2S^2} \sum_{\alpha\nu} \frac{(\varepsilon_{\nu} - \varepsilon_{\nu+\mathbf{Q}})^2}{\varepsilon_{\nu} - \varepsilon_{\alpha} - i\gamma}. \tag{4.80}$$

The imaginary part of the magnon energy, coming from the second term of the above relation, can be easily determined using the relation

$$\frac{1}{x \pm i\gamma} = \frac{1}{x} \mp i\pi\delta(x). \tag{4.81}$$

In this way we find that the 2^{nd} order contribution of spinwave damping is:

$$\Gamma^{(2)}_{\mathbf{Q}} = \frac{\pi}{4N^2S^2}\sum_{\alpha\nu}(\varepsilon_\nu - \varepsilon_{\nu+\mathbf{Q}})^2\delta(\varepsilon_\nu - \varepsilon_\alpha) \tag{4.82}$$

However, this contribution is also zero, owing to the form of the delta function. Notice that there is no overlap between band energy ε_ν and ε_α since we have that $\varepsilon_\nu \leqq E_F$ and $\varepsilon_\alpha > E_F$. Therefore in order to determine the first non–zero contribution of the spinwave damping one must expand $\omega_{\mathbf{Q}}$ up to 3^{rd} order in $1/S$. Fortunately, the 3^{rd} order term of spinwave energy is rather easily determined by using equation (4.75) to be:

$$\begin{aligned}\omega^{(3)}_{\mathbf{Q}} &= -\frac{1}{4NS}\sum_\nu \omega^{(2)}_{\mathbf{Q}} + \frac{1}{4N^2S^2}\sum_{\alpha\nu} G^{(0)}_{\alpha\nu}\omega^{(1)}_{\mathbf{Q}} \\ &+ \frac{1}{4N^2S^2}\sum_{\alpha\nu} G^{(1)}_{\alpha\nu}(\varepsilon_\nu - \varepsilon_{\nu+\mathbf{Q}}),\end{aligned} \tag{4.83}$$

which after substituting $\omega^{(1)}_{\mathbf{Q}}$, $\omega^{(2)}_{\mathbf{Q}}$ and $G^{(0)}_{\alpha\nu}$ from eqs 4.77, 4.80 and 4.78 respectively we finally find:

$$\begin{aligned}\omega^{(3)}_{\mathbf{Q}} &= -\frac{n^2}{16NS^3}\sum_\nu(\varepsilon_\nu - \varepsilon_{\nu+\mathbf{Q}}) + \frac{n}{16N^2S^3}\sum_{\alpha\nu}\frac{(\varepsilon_\nu - \varepsilon_{\nu+\mathbf{Q}})^2}{\varepsilon_\nu - \varepsilon_\alpha - i\gamma} \\ &+\frac{1}{8N^3S^3}\sum_\mu(\varepsilon_\mu - \varepsilon_{\mu+\mathbf{Q}})\sum_{\alpha\nu}\frac{\varepsilon_\nu - \varepsilon_{\nu+\mathbf{Q}}}{\varepsilon_\nu - \varepsilon_\alpha - i\gamma} \\ &+\frac{1}{4N^2S^2}\sum_{\alpha\nu} G^{(1)}_{\alpha\nu}(\varepsilon_\nu - \varepsilon_{\nu+\mathbf{Q}}),\end{aligned} \tag{4.84}$$

where the imaginary contribution clearly comes from the forth term since the denominators of the second and third term give again an imaginary part of the form $\delta(\varepsilon_\alpha - \varepsilon_\nu)$ which as we said vanishes. In order to determine $\Gamma^{(3)}_{\mathbf{Q}}$ we have to extract the first order contribution of $G^{\mathbf{Q}}_{\alpha\nu}$ from Eq. 4.76. We can do that by substituting $\omega_{\mathbf{Q}}$ with $\omega^{(1)}_{\mathbf{Q}}$ from Eq. (4.77) in both sides of Eq. (4.76) and by substituting $G_{\alpha\nu}$ with $G^{(0)}_{\alpha\nu}$ from Eq. (4.78) in the right side. In this way second–order terms are obtained on the right side which must be removed. Finally by

gathering the same order terms together we find that:

$$\begin{aligned}[\omega^{(1)}_{\mathbf{Q}} - \omega^{(1)}_{\mathbf{Q}+\nu-\alpha} + \left(1+\frac{n}{2S}\right)(\varepsilon_\nu - \varepsilon_\alpha) - i\gamma] G^{\mathbf{Q}}_{\alpha\nu} = \\ -(\varepsilon_\nu - \varepsilon_{\nu+\mathbf{Q}}) - \frac{1}{2NS}\sum_\nu (\varepsilon_\nu - \varepsilon_{\nu+\mathbf{Q}}) \\ +\frac{1}{2NS}(\varepsilon_\nu - \varepsilon_{\nu+\mathbf{Q}})^2 \sum_\beta \frac{1}{\varepsilon_\nu - \varepsilon_\beta - i\gamma} \\ -\frac{1}{2NS}\sum_\mu \frac{\varepsilon_\mu - \varepsilon_{\mu+\mathbf{Q}}}{\varepsilon_\mu - \varepsilon_\alpha - i\gamma}(\varepsilon_\nu + \varepsilon_\mu - \varepsilon_{\mathbf{Q}+\nu+\mu-\alpha} - \varepsilon_\alpha),\end{aligned} \tag{4.85}$$

where we use Eq. 4.77 to substitute the term:

$$\frac{1}{2NS}\sum_\mu (\varepsilon_\mu - \varepsilon_{\mathbf{Q}+\nu+\mu-\alpha}) = \omega^{(1)}_{\mathbf{Q}+\nu-\alpha}. \tag{4.86}$$

Note that the imaginary part of the rescattering terms in the r.h.s of the above equation is zero since it is of the form $\sim \delta(\varepsilon_\nu - \varepsilon_\alpha)$. Therefore the damping of the magnon energy 4.84 comes solely from the denominator of the Eq. 4.85 which at $O(1/S^3)$ is:

$$\Gamma^{(3)}_{\mathbf{Q}} = \frac{1}{4N^2S^2}\sum_{\alpha\nu}\frac{(\varepsilon_\nu - \varepsilon_{\nu+\mathbf{Q}})^2}{\omega^{(1)}_{\mathbf{Q}} - \omega^{(1)}_{\mathbf{Q}+\nu-\alpha} + \varepsilon_\nu - \varepsilon_\alpha - i\gamma}, \tag{4.87}$$

which after taking the limit $\gamma \to 0$ yields:

$$\Gamma^{(3)}_{\mathbf{Q}} = \frac{\pi}{4N^2S^2}\sum_{\alpha\nu}(\varepsilon_\nu - \varepsilon_{\nu+\mathbf{Q}})^2\,\delta(\omega^{(1)}_{\mathbf{Q}} - \omega^{(1)}_{\mathbf{Q}+\nu-\alpha} + \varepsilon_\nu - \varepsilon_\alpha). \tag{4.88}$$

This recovers the result of Ref[11, 24].

In conclusion by applying a $1/S$ expansion in the strong coupling limit $J \to \infty$ we are able to recover the first contribution to the spinwave damping which is of order $O(1/S^3)$. We show also that the rescattering processes of Green's function G contribute only at higher order of $1/S$ expansion. In the next subsection we focus on the finite J case. It is expected that in this limit the rescattering processes contribution to the spinwave damping is not vanishing at $O(1/S^3)$. Therefore a question about the importance of this terms reasonably arises.

4.2.4 1/S expansion at finite double–exchange interaction J.

Starting from Eqs. 4.73 and 4.76 we can easily determine the first non-zero contribution to the magnon damping for the finite double–exchange interaction $\bar{J}$ case.

First of all, we show here that this contribution is of third order with respect to $1/S$. For this purpose we have to determine magnon energy up to $O(1/S^2)$ which clearly is:

$$\begin{aligned}\omega_{\mathbf{Q}}^{(2)} &= \frac{\bar{J}n}{2S} + \frac{\bar{J}^2}{2NS}\sum_{\nu}\frac{1}{\omega_{\mathbf{Q}}^{(1)} + \varepsilon_\nu - \varepsilon_{\nu+\mathbf{Q}} - \bar{J}} \\ &+ \frac{\bar{J}^2}{4N^2S^2}\sum_{\alpha\nu}\left(1 + \frac{\bar{J}}{\varepsilon_\nu - \varepsilon_{\nu+\mathbf{Q}} - \bar{J}}\right)^2 \frac{1}{\varepsilon_\nu - \varepsilon_\alpha - i\gamma},\end{aligned} \tag{4.89}$$

where

$$\omega_{\mathbf{Q}}^{(1)} = \frac{\bar{J}n}{2S} + \frac{\bar{J}^2}{2NS}\sum_{\nu}\frac{1}{\varepsilon_\nu - \varepsilon_{\nu+\mathbf{Q}} - \bar{J}}. \tag{4.90}$$

is the leading order in $1/S$ magnon energy. The zeroth order of $G_{\alpha\nu}^{\mathbf{Q}}$ is also inserted in Eq. 4.89. Note again that up to second order of $1/S$ expansion magnon dispersion appeared to be undamped as in the $\bar{J} \to \infty$ limit. Therefore the first non-zero contribution to the magnon damping comes from the imaginary part of the first order contribution of the Green's function $G_{\alpha\nu}^{\mathbf{Q}}$ to the magnon energy which is of the form:

$$\Gamma_{\mathbf{Q}}^{(3)} = \frac{\bar{J}^2}{4N^2S^2}\sum_{\alpha\nu}\mathrm{Im}(G_{\alpha\nu}^{(1)})\left(1 + \frac{\bar{J}}{\varepsilon_\nu - \varepsilon_{\nu+\mathbf{Q}} - \bar{J}}\right). \tag{4.91}$$

This contribution of $G_{\alpha\nu}^{\mathbf{Q}}$ can be easily determined by the relation:

$$\mathrm{Im}(G_{\alpha\nu}^{(1)}) = \left(1 + \frac{\bar{J}}{\varepsilon_\nu - \varepsilon_{\nu+\mathbf{Q}} - \bar{J}}\right)\mathrm{Im}(\frac{1}{\Delta_{\alpha\nu}}), \tag{4.92}$$

where the complex denominator is:

$$\begin{aligned}\Delta_{\alpha\nu} = \omega_{\mathbf{Q}}^{(1)} + \varepsilon_\nu - \varepsilon_\alpha &- \frac{\bar{J}n}{2S} - i\gamma \\ &- \frac{\bar{J}^2}{2NS}\sum_{\mu}\frac{1}{\varepsilon_\mu + \varepsilon_\nu - \varepsilon_{\mathbf{Q}+\mu+\nu-\alpha} - \varepsilon_\alpha - \bar{J}}\end{aligned} \tag{4.93}$$

There are some additional terms which contribute at this order, but they are real and therefore do not contribute to the imaginary part of $G_{\alpha\nu}^{\mathbf{Q}}$. Normally, one has to take the limit $\gamma \to 0$ in order to determine the magnon damping which in this way is of the form: $\Gamma_{\mathbf{Q}}^{(3)} \sim \sum_{\alpha\nu}\delta(\omega_{\mathbf{Q}}^{(1)} + \varepsilon_\nu - \varepsilon_\alpha - \frac{\bar{J}n}{2S} + \frac{1}{S}f_{\alpha\nu})$. Note that, the existence of function $f_{\alpha\nu}$ prevents the explicit calculation of the delta function and thus the $\gamma \to 0$ limit result can not be easily obtained. However the calculation of magnon

damping can be well performed by using a small value for parameter γ that the calculated dispersion is not affected by that small imaginary part of denominator. The parameter γ must be comparable with the spacing $\Delta\epsilon$ between energy levels. For values of γ larger than $\Delta\epsilon$ the obtained damping does not represent the actual damping of magnon, while for an extremely small γ, which approaches zero we obtain vanishing damping. Therefore the first non–zero contribution to magnon damping with respect to $1/S$ is determined by the relation:

$$\Gamma^{(3)}_{\mathbf{Q}} = \frac{\bar{J}^2}{4N^2S^2}\sum_{\alpha\nu}\left(1+\frac{\bar{J}}{\varepsilon_\nu-\varepsilon_{\nu+\mathbf{Q}}-\bar{J}}\right)^2 \mathrm{Im}\left(\frac{1}{\Delta_{\alpha\nu}}\right). \tag{4.94}$$

Note also, the above relation recover the result 4.88 by taking the limit $\bar{J}\to\infty$.

4.3 Numerical results

In this section we present our numerical results for the spinwave damping. We make a comparison of the approximations presented above and also discuss the role of double–exchange interaction and itinerant electron concentration on magnon damping. The connection between strong spinwave softening and short lifetime near the zone boundary is also made[56].

First of all, we discuss the effect of the phenomenological relaxation parameter γ of electron–hole pair. One must be very careful in choosing the value of that free parameter since it depends strongly on the number of the lattice sites. If the spacing between two adjacent energy levels is $\Delta\epsilon$ then γ must be comparable with that energy. For $\gamma \ll \Delta\epsilon$ we cannot determine spin–wave damping since the magnon pole obtained is real. On the other hand, a very large value of γ, in comparison with $\Delta\epsilon$, creates a large imaginary part which does not corresponds to the actual spin–wave damping. Since we perform our numerical calculation in finite size systems the energy spacing is finite. This means that we have to assume a non–zero value for the parameter γ in order to determine spin–wave damping. In this chapter we perform our numerical calculations is 2D systems with number of sites about $N = 20\times 20$. For such systems energy spacing varies as $\Delta\epsilon \simeq 0.5 - 0.1$. In Fig. 4.2 we plot the real part of the pole, which describes spin–wave excitations, as a function of the parameter γ. We note that the spin–wave dispersion does not depend strongly on the particular value of γ. The deviations are pronounced along the $\Gamma \to X$ direction where the magnon energies are smaller. For this reason we choose to fix the phenomenological parameter at an intermediate value $\gamma = 0.2$ for the rest of this chapter.

We continue the presentation of our numerical results with Fig. (4.3) which shows the 2D spinwave dispersion (a) and damping (b) obtained with the different

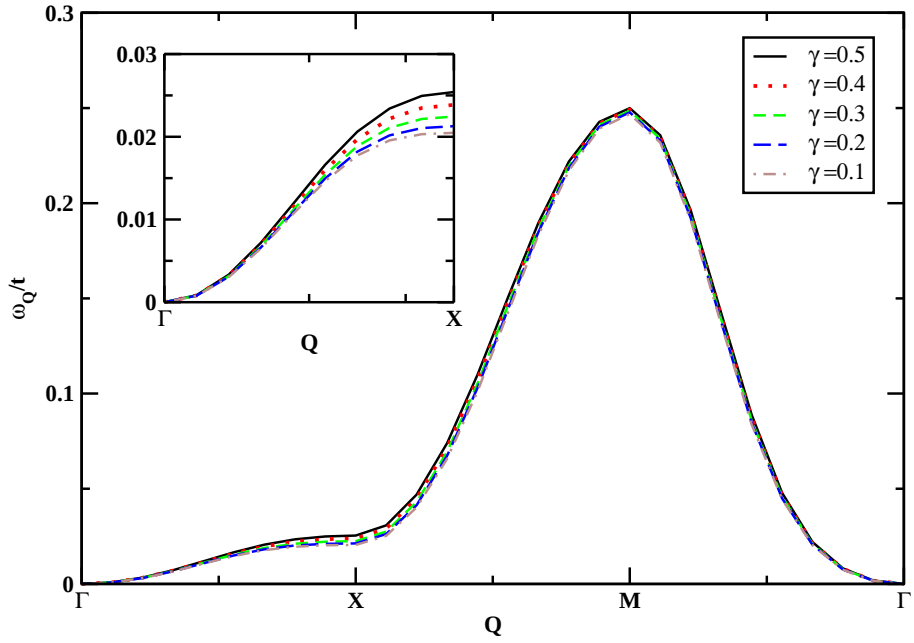

Figure 4.2: The real part of magnon's pole as a function of phenomenological parameter γ. Inset: spin–wave dispersion along $\Gamma \rightarrow X$ direction in Brillouin zone.

approximations along the main directions in the Brillouin zone. The parameters $(n = 0.7, J = 8t)$ we use here are typical in the manganites, and are the same with these of chapter 2. In this way we can make a comparison with the variational results of that chapter. Let us notice that the $\mathbf{Q} = 0$ state is an exact eigenstate of the double–exchange Hamiltionian. Therefore the damping of this state is equal to zero. On the other hand, every magnon state with $\mathbf{Q} \neq 0$ must have a finite lifetime, $\Gamma_{\mathbf{Q}} \neq 0$, since they are not exact eigenstates. First, we note in Fig. 4.3 that within the three–body approximation and along the direction $\Gamma \rightarrow X$ the spinwave damping is about 25% of the real part of the pole, i.e. the magnon energies. The latter is due to the strong softening effect of spinwave dispersion along that direction which indicates that magnons are short–lived excited states. On the other hand along the other main directions this ratio is as small as 5%. Furthermore, for $H_{\mathbf{kpq}} = 0$ damping is very small as compared with the three–body result, since the damping within that approximation is about 20% of the full three–body one. The latter indicates the importance of the spin $\uparrow$–$\downarrow$ excitations described by Green's function $H_{\mathbf{kpq}}$. The main contribution to magnon relaxation seems to be its scattering with a spin$\uparrow$–spin$\downarrow$ excitation. The scattering with solely

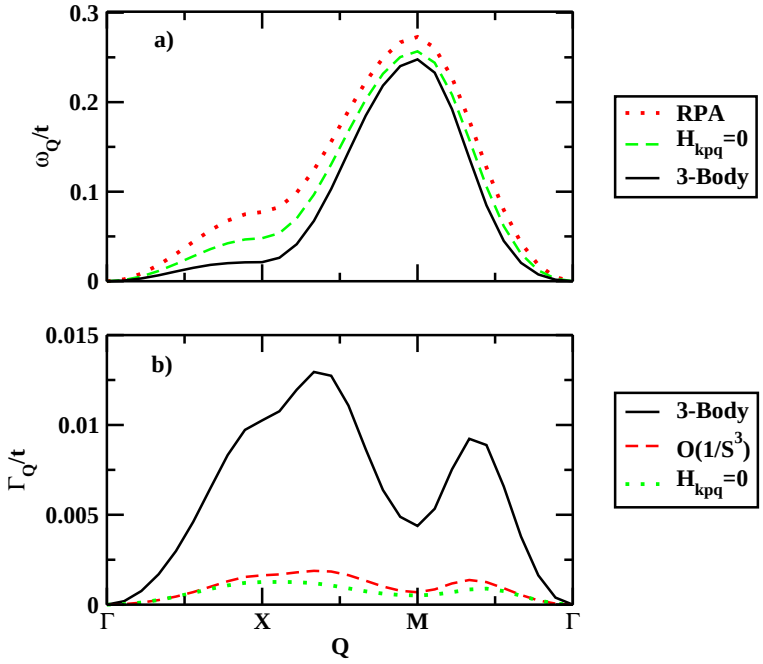

Figure 4.3: Real (a) and imaginary (b) part of magnon's pole along the different different directions in Brillouin zone for $n = 0.7, J = 8t, \gamma = 0.2$: Comparison of the different approximations.

localized spins, $H_{\mathbf{kpq}} = 0$ approximation, gives a rather weak relaxation rate and magnon can be well considered as undamped states with infinite lifetime within this approximation. This is consistent with the fact that the $H_{\mathbf{kpq}} = 0$ dispersion shows no strong softening as we discussed previously, and fails to describe the spin–wave dispersion. The first deviations from the $H_{\mathbf{kpq}} = 0$ result appear when the first contribution in $1/S$ expansion is considered. We showed is Sec. 4.2 that this contribution is of order $O(1/S^3)$. We note first, that the spin–wave damping to $O(1/S^3)$ is approximately close to the $H_{\mathbf{kpq}} = 0$ result. This means that the perturbative treatment of the spin $\uparrow$–$\downarrow$ excitations fails to describe spin–wave damping mechanism. Meanwhile, our full three–body calculation gives a strong magnon damping and therefore finite lifetime. Apart from that discrepancy, $1/S$ expansion fails also to reproduce another behaviour which the full three–body calculation exhibits. This is the appearance of sharp peaks in the damping which for the parameters used here takes place near the point $(\pi, \pi/2)$, while a minimum at $\mathbf{Q} = (\pi, \pi)$ also appears. That result implies that magnon relaxes very fast within this momentum region. This is an important feature since it

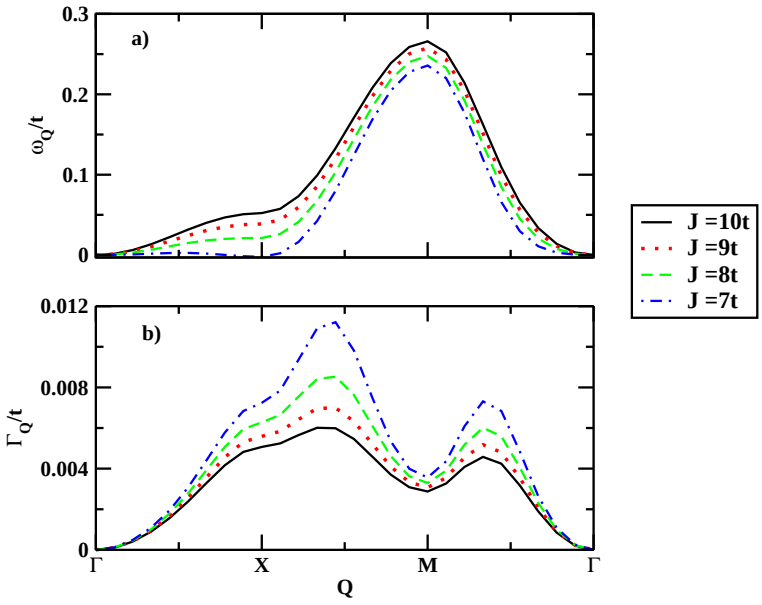

Figure 4.4: The role of double–exchange interaction: Three–body spin–wave dispersion (a) and damping (b) for $n = 0.7$ and different values of double–exchange parameter J/t.

predicts a strong dependence of lifetime on the direction we observe the magnon. The corresponding $O(1/S^3)$ and $H_{\mathbf{kpq}} = 0$ value does not differ significantly from the values of damping along the direction $\Gamma \rightarrow X$. The smooth behaviour of damping indicates the inadequacy of these approximations to describe the spin–wave lifetime. The latter enhances the importance of 3–body correlations. A direct comparison between the real part (Fig. 4.3(a)) and imaginary part (Fig. 4.3(b)) of the magnon pole indicates a connection of this behaviour with the softening effects of the magnon's dispersion. First of all, the behaviour of magnon's damping at M point can be explained by the fact that the spin–wave dispersion is well described by the RPA result and the softening is extremely weak. Therefore, within momentum regions where 3–body correlations are not important, the spin–wave damping is also small. The behaviour along the direction $\Gamma \rightarrow X$ in the Brillouin zone, where the spin–wave softening is pronounced, is rather complicated. Fig. 4.3 shows that the appearance of strong softening is connected with large values of spin–wave damping. However this is not a direct connection since damping remains large within the momentum region $(\pi, 0) \rightarrow (\pi, \pi/2)$ while the dispersion's softening is rather weak.

Let us examine now the role of double–exchange interaction on spinwave damp-

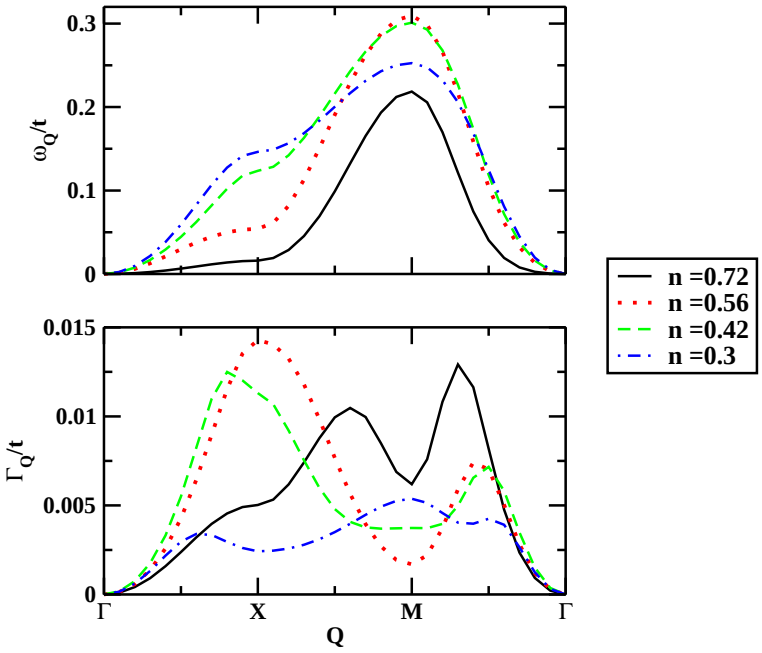

Figure 4.5: The role itinerant electron concentration: Three–body spin–wave dispersion (a) and damping (b) for $J = 8t$ and different electron dopings

ing. Fig. 4.3(a)–(b) shows spinwave dispersion and damping within three–body approximation for electron concentration $n = 0.7$ and different values of double–exchange parameter $J/t = 10 - 7$. Firstly, we note that the position of the momentum points where an extremum appears is unaffected by the strength of double–exchange parameter. We will show that the position of $\mathbf{Q}_C$ points depends solely on itinerant electron concentration, and therefore has to do with the Fermi surface. Fig. 4.4 also shows that the damping is increasing while J/t is diminishing. More precisely, the smaller the parameter J/t the more pronounced is the peak of the damping. For example, we note that spin–wave dispersion for $J = 7t$ (solid-dotted line) shows such a strong softening that it almost turns negative at Γ point, indicating that the fully polarized ferromagnetic state is unstable. For that value of J/t we note that the maximum of damping becomes extremely large, actually it is larger than the magnon energy, indicating that the magnon is not a well defined state for this parameter. This is a reasonable result since the life time of an excited state with $\omega_{\mathbf{Q}} \simeq 0$ it expected to be very short. For lower values of the J/t spin–wave damping is as small as 10% of magnon energy.

We discuss now the dependence of extremum points of damping as a function

of itinerant electron concentration. It is shown in Fig. 4.4 that this behaviour of damping does not depend on the strength of magnetic–exchange interaction. Fig. 4.5 shows dispersion and damping for fixed $J = 8t$ and different electron dopings. We note first in Fig. 4.5(a) that softening effects along $\Gamma \rightarrow X$ direction are minimized while electron concentration is diminishing. For a high electron concentration $n = 0.72$, the spin–wave damping exhibits two maximum points; at $\mathbf{Q} = (\pi, \pi/2)$ and $\mathbf{Q} \simeq (\pi, \pi/2)$, in the middle of $X \rightarrow M$ and $M \rightarrow \Gamma$ direction respectively. For a lower electron doping, $n = 0.56$, we note that the first minimum starts to approach the X–point while the second one is slightly shifted nearer to the middle of $M \rightarrow \Gamma$ direction. This effect becomes clear within the low electron concentration regime, $n \simeq 0.3 - 0.4$, where the maximum appears at $\mathbf{Q} \lesssim (\pi, 0)$. In addition, Fig. 4.5 shows that within the intermediate electron concentration regime, $0.4 \lesssim n \lesssim 0.6$, the spin–wave damping becomes extremely large along the $\Gamma \rightarrow X$ direction in the Brillouin zone, while along the other main directions it takes comparatively low values. On the contrary, for low $n \lesssim 0.3$ and very high $n \gtrsim 0.7$, the spin–wave damping exhibits a contrasting behaviour since it is rather low along $\Gamma \rightarrow X$. We conclude that spin–wave magnons have a very low lifetime along $\Gamma \rightarrow X$ direction within the intermediate concentrations regime. Let us note that the latter result is in disagreement with experiments[52], which show lower damping along $\Gamma \rightarrow X$ as compared with the other directions. Moreover spin–wave damping appears to be lower for a higher doping. That indicates a discrepancy in our simplified model hamiltonian, which can be alleviated by including Hubbard repulsion in our hamiltonian as we show in the next chapter. Spin–wave dispersion exhibits strong softening along that direction and for these concentrations. These two effects, therefore, are connected by the fact that a very softened magnon state, with very low excitation energy, can be easily damped and thus its lifetime is short. On the other hand along directions in the Brillouin zone where softening effects are weak lifetime is reasonably long, for example the M–point in Fig. 4.5.

4.4 Conclusion

To conclude, in this chapter we present an application of the double–time Tyablikov Green's function method to a double–exchange ferromagnetic system which describes manganese oxides. In order to terminate the infinite chain of equations of motion a decoupling scheme is used. This approximate method consists of the factorization of the higher–order Green's function. In this way the variational results of chapter 2 is reproduced, where spin–wave dispersion is described up to 3–body correlations, and therefore the factorization technique is justified. Moreover the method presented here allows us to determine spin–wave damping due

to scattering of a magnon with a Fermi electron–hole pair. Our equations recover also the previous obtained results where a perturbative treatment of local spin is used and spin–wave damping is obtained in $O(1/S^3)$ order. We show that this approximation underestimates damping by a significant factor and thus gives a rough description of spin–wave excitations in the double–exchange model. Since we consider here the minimal double–exchange hamiltonian, which we have shown is rather inadequate to describe manganites, we focus on the role of double–exchange interaction on spin–wave damping. We show that for values of double–exchange parameter near to critical value J_C spin–wave damping becomes extremely large as compared with magnon energy. For intermediate electron concentrations damping also becomes large along the direction $\Gamma \rightarrow X$ in the Brillouin zone. The latter is in agreement with the appearance of spin–wave softening as discussed in the previous chapter. Therefore we show here that these two results must be considered as a two–side effect of correlations on spin–wave excited states. Finally, a comparison of the 3–body damping with that obtained by assuming scattering only with localized spins ($H_{\mathbf{kpq}} = 0$ or equivalently $\Phi_{\alpha\mu\nu}$=0 of the variational calculation), shows the importance of the scattering with the spin↑–↓ excitation. The latter process seems to be the main origin of the effects of correlations on the real (softening) and the imaginary part (short lifetime) of the magnon's pole.

Chapter 5

The effects of the on-site Hubbard repulsion on Spin–Wave damping of Ferromagnetic Manganites.

5.1 Introduction

This chapter discusses the role of the local Hubbard and super–exchange interaction on the spin–wave damping. In contrast with the previous chapter where the minimal model of double–exchange Hamiltonian is studied, here we focus on the on–site Hubbard repulsion between itinerant electrons on the same lattice site. Additionally, we include an antiferromagnetic Heisenberg–like interaction between neighboring localized spins constructing that way a rather reliable model for the Ferromagnetic Manganites of interest here. This model is discussed in chapter (3) where a variational treatment of spin–waves excitation energies is presented. There was shown that the Hubbard repulsion affects significantly the spin–waves. We show in Chapter (3) that the on–site Hubbard interaction between itinerant electrons enhances ferromagnetism which becomes stable in the concentration regime relevant to the experiments. Therefore it must be included in a hamiltonian which is used to model manganites. In this chapter we discuss the effect of these additional interactions, H_U and H_{AF}, on the spin–wave damping. The Green's function method, as discussed in the previous chapter, is used in order to determine the magnon's pole. The infinite chain of equations of motion is terminated by performing a factorization procedure similar to that of the previous chapter. The fact that this method reproduces the variational results of chapter (2) also applies here, and establishes the validity of our factorization approximation.

In the next section we derive briefly the equations of motion which describe

spin–waves up to three–body correlations. We show that by assuming mean values in the fully–polarized state the variational equations of (3) is reproduced. Sec. (5.3) contains our numerical results. Here we fix the Hund' rule coupling to experimentally relevant values and study the role of Hubbard U/t and super–exchange J_{AF}/t interaction on spin–wave damping. The doping dependence of the damping is also examined and in this way a connection with the dispersion's softening effects is made. In the previous chapter the crucial role of the three–body correlations is emphasized, due to strong contribution of electron–hole pair scattering effects on the spin–wave damping. In order to solidify that conclusion, a comparison between the carrier–localized spin and the full three–body result is also presented. We close this chapter with the conclusions.

5.2 Calculations

In this section we derive the equations of motion for the Green's functions that describe the spin–wave excitations. These Green's functions were defined in the previous chapter where, the chain of equation of motion for the minimal double–exchange model was presented. What we do here is to add to these equations the new terms coming from the additional interactions of our model. We suppose here the full hamiltonian which describes manganese oxides

$$H = H_{exch} + H_U + H_{super}. \tag{5.1}$$

Here, H_{exch} is the magnetic exchange coupling studied variationally in chapter (2) and using Green's functions in (4). We add now in our model hamiltonian two new terms: the on-site Hubbard repulsion described by the term:

$$H_U = \frac{U}{N} \sum_{\mathbf{k}\mathbf{k}'\mathbf{q}} c^{\dagger}_{\mathbf{k}\uparrow} c_{\mathbf{k}'\uparrow} c^{\dagger}_{\mathbf{q}\downarrow} c_{\mathbf{q}+\mathbf{l}-\mathbf{k}'\downarrow}, \tag{5.2}$$

and the Heisenberg–like antiferromagnetic super–exchange interaction:

$$H_{super} = J_{AF} \sum_{\mathbf{k}} \gamma_{\mathbf{k}} S^z_{\mathbf{k}} S^z_{-\mathbf{k}} + \frac{J_{AF}}{2} \sum_{\mathbf{k}} \gamma_{\mathbf{k}} (S^{\dagger}_{\mathbf{k}} S^-_{-\mathbf{k}} + S^-_{\mathbf{k}} S^{\dagger}_{-\mathbf{k}}), \tag{5.3}$$

where $\gamma_{\mathbf{k}} = -\varepsilon_{\mathbf{k}}/2$. We start the derivation of the new equations with the equation of motion for the local spin Green's function $Y^{\mathbf{Q}}(t) = \ll S^{\dagger}_{-\mathbf{Q}}(t) \mid S^-_{\mathbf{Q}}(0) \gg$. It is clear that only the term H_{AF} contributes to this equation since the commutator $[H_U, S^-]$ vanishes. This non–zero contribution can be determined by using the relation 8.25. In this way the equation of $Y^{\mathbf{Q}}(t)$ yields:

$$\begin{aligned} i\frac{\partial}{\partial t} Y^{\mathbf{Q}}(t) = i\delta(t) < S^z_0 > \; &+ \; \ll [S^{\dagger}_{-\mathbf{Q}}(t), H_{exch}] \mid S^-_{\mathbf{Q}}(0) \gg \\ &+ \; 2J_{AF} S(\gamma_{\mathbf{Q}} - \gamma_0) Y^{\mathbf{Q}}(t), \end{aligned} \tag{5.4}$$

where the first line comes from the double–exchange hamiltonian of the previous chapter while the second line is the new term added by the super–exchange interaction. Similarly, the Green's function $G^{\mathbf{Q}}_{\mathbf{kq}}(t) = \ll S^{\dagger}_{q-Q}(c^{\dagger}_{\mathbf{k-q}\uparrow}c_{\mathbf{k}\uparrow} - n(\varepsilon_{\mathbf{k}})\delta_{\mathbf{q},\mathbf{0}}) \mid S^{-}_{\mathbf{Q}}(0) \gg$ is described:

$$\begin{aligned} i\frac{\partial}{\partial t}G^{\mathbf{Q}}_{\mathbf{kq}}(t) &= i\delta(t) < [S^{\dagger}_{q-Q}(c^{\dagger}_{\mathbf{k-q}\uparrow}c_{\mathbf{k}\uparrow} - n(\varepsilon_{\mathbf{k}})\delta_{\mathbf{q},\mathbf{0}}), S^{-}_{\mathbf{Q}}] > \\ &+ \ll [S^{\dagger}_{q-Q}(c^{\dagger}_{\mathbf{k-q}\uparrow}c_{\mathbf{k}\uparrow} - n(\varepsilon_{\mathbf{k}})\delta_{\mathbf{q},\mathbf{0}}), H_{exch}] \mid S^{-}_{\mathbf{Q}}(0) \gg \\ &+ \ll S^{\dagger}_{\mathbf{q-Q}}[c^{\dagger}_{\mathbf{k-q}\uparrow}c_{\mathbf{k}\uparrow}, H_U] \mid S^{-}_{\mathbf{Q}}(0) \gg \\ &+ \ll [S^{\dagger}_{\mathbf{q-Q}}, H_{AF}](c^{\dagger}_{\mathbf{k-q}\uparrow}c_{\mathbf{k}\uparrow} - n(\varepsilon_{\mathbf{k}})\delta_{\mathbf{q},\mathbf{0}}) \mid S^{-}_{\mathbf{Q}}(0) \gg . \end{aligned} \tag{5.5}$$

which after using commutators 8.26 and 8.27 becomes:

$$\begin{aligned} i\frac{\partial}{\partial t}G^{\mathbf{Q}}_{\mathbf{kq}}(t) &= i\delta(t) < [S^{\dagger}_{\mathbf{q-Q}}(c^{\dagger}_{\mathbf{k-q}\uparrow}c_{\mathbf{k}\uparrow} - n(\varepsilon_{\mathbf{k}})\delta_{\mathbf{q},\mathbf{0}}), S^{-}_{\mathbf{Q}}] > \\ &+ \ll [S^{\dagger}_{\mathbf{q-Q}}(c^{\dagger}_{\mathbf{k-q}\uparrow}c_{\mathbf{k}\uparrow} - n(\varepsilon_{\mathbf{k}})\delta_{\mathbf{q},\mathbf{0}}), H_{exch}] \mid S^{-}_{\mathbf{Q}}(0) \gg \\ &+ \frac{U}{N}\sum_{\mathbf{k'q'}} \ll S^{\dagger}_{q-Q}c^{\dagger}_{\mathbf{k-q}\uparrow}c_{\mathbf{k'}\uparrow}c^{\dagger}_{\mathbf{q'}\downarrow}c_{\mathbf{q'+k-k'}\downarrow} \mid S^{-}_{\mathbf{Q}}(0) \gg \\ &- \frac{U}{N}\sum_{\mathbf{k'q'}} \ll S^{\dagger}_{\mathbf{q-Q}}c^{\dagger}_{\mathbf{k'}\uparrow}c_{\mathbf{k}\uparrow}c^{\dagger}_{\mathbf{q'}\downarrow}c_{\mathbf{q'+k'-k+q}\downarrow} \mid S^{-}_{\mathbf{Q}}(0) \gg \\ &- \frac{J_{AF}}{\sqrt{N}}\sum_{\mathbf{k'}}\gamma_{\mathbf{k'}} \\ &\ll \left(S^{z}_{\mathbf{k'}}S^{\dagger}_{\mathbf{q-Q-k'}} + S^{\dagger}_{\mathbf{q-Q+k'}}S^{z}_{\mathbf{-k'}}\right)(c^{\dagger}_{\mathbf{k-q}\uparrow}c_{\mathbf{k}\uparrow} - n(\varepsilon_{\mathbf{k}})\delta_{\mathbf{q},\mathbf{0}}) \mid S^{-}_{\mathbf{Q}}(0) \gg \\ &+ \frac{J_{AF}}{\sqrt{N}}\sum_{\mathbf{k'}}\gamma_{\mathbf{k'}} \\ &\ll \left(S^{\dagger}_{\mathbf{k'}}S^{z}_{\mathbf{q-Q-k'}} + S^{\dagger}_{\mathbf{k'}}S^{z}_{\mathbf{q-Q-k'}}\right)(c^{\dagger}_{\mathbf{k-q}\uparrow}c_{\mathbf{k}\uparrow} - n(\varepsilon_{\mathbf{k}})\delta_{\mathbf{q},\mathbf{0}}) \mid S^{-}_{\mathbf{Q}}(0) \gg . \end{aligned} \tag{5.6}$$

The additional terms must be approximated using the method discussed in the previous chapter. First, we note that after factorizing the third and forth term in the r.h.s., which come from Hubbard repulsion, these term vanishes since they are proportional to the expectation value $< c^{\dagger}_{\downarrow}c_{\downarrow} >$ which is zero if evaluated in the fully–polarized state. On the other hand, the last two terms which express the super–exchange contribution can be approximated by using the property4.7. In this way the equation of motion yields:

$$\begin{aligned} i\frac{\partial}{\partial t}G^{\mathbf{Q}}_{\mathbf{kq}}(t) &= i\delta(t) < [S^{\dagger}_{\mathbf{q-Q}}(c^{\dagger}_{\mathbf{k-q}\uparrow}c_{\mathbf{k}\uparrow} - n(\varepsilon_{\mathbf{k}})\delta_{\mathbf{q},\mathbf{0}}), S^{-}_{\mathbf{Q}}] > \\ &+ \ll [S^{\dagger}_{\mathbf{q-Q}}(c^{\dagger}_{\mathbf{k-q}\uparrow}c_{\mathbf{k}\uparrow} - n(\varepsilon_{\mathbf{k}})\delta_{\mathbf{q},\mathbf{0}}), H_{exch}] \mid S^{-}_{\mathbf{Q}}(0) \gg \\ &+ 2J_{AF}S\left(\gamma_{\mathbf{q-Q}} - \gamma_0\right)G^{\mathbf{Q}}_{\mathbf{kq}}. \end{aligned} \tag{5.7}$$

We conclude that the equation of motion of Green's function $G^{\mathbf{Q}}_{\mathbf{kq}}(t)$ for the full hamiltonian (5.1) differs from that obtained for the simple double–exchange model by only a term which shifts the source energy by a cosine–like term. We continue now with the equation of motion of Green's function $X^{\mathbf{Q}}_{\mathbf{k}}(t) = \ll c^{\dagger}_{\mathbf{k}-\mathbf{Q}\uparrow} c_{\mathbf{k}\downarrow} \mid S^{-}_{\mathbf{Q}}(0) \gg$. Due to the form of this Green's function only the Hubbard interaction term H_U gives an additional contribution apart from the double–exchange Hamiltonian H_{DE} of the previous chapter:

$$\begin{aligned} i\frac{\partial}{\partial t} X^{\mathbf{Q}}_{\mathbf{k}}(t) &= i\delta(0) < [c^{\dagger}_{\mathbf{k}-\mathbf{Q}\uparrow} c_{\mathbf{k}}, S^{-}_{\mathbf{Q}}] > \\ &+ \ll [c^{\mathbf{Q}}_{\mathbf{k}-\mathbf{Q}\uparrow} c_{\mathbf{k}\downarrow}, H_{exch}] \mid S^{-}_{\mathbf{Q}}(0) \gg \\ &+ \ll [c^{\mathbf{Q}}_{\mathbf{k}-\mathbf{Q}\uparrow} c_{\mathbf{k}\downarrow}, H_U] \mid S^{-}_{\mathbf{Q}}(0) \gg, \end{aligned} \tag{5.8}$$

where we have to evaluate the non–zero commutator $[c^{\mathbf{Q}}_{\mathbf{k}-\mathbf{Q}\uparrow} c_{\mathbf{k}\downarrow}, H_U]$. Using the relation (8.28) we obtain that the equations of motion for Green's function $X^{\mathbf{Q}}_{\mathbf{k}}(t)$ can be written in the form:

$$\begin{aligned} i\frac{\partial}{\partial t} X^{\mathbf{Q}}_{\mathbf{k}}(t) &= i\delta(0) < [c^{\dagger}_{\mathbf{k}-\mathbf{Q}\uparrow} c_{\mathbf{k}}, S^{-}_{\mathbf{Q}}] > \\ &+ \ll [c^{\mathbf{Q}}_{\mathbf{k}-\mathbf{Q}\uparrow} c_{\mathbf{k}\downarrow}, H_{exch}] \mid S^{-}_{\mathbf{Q}}(0) \gg \\ &- \frac{U}{N} \sum_{\mathbf{k}'\mathbf{q}'} \ll c^{\dagger}_{\mathbf{k}'\uparrow} c_{\mathbf{k}\uparrow} c^{\dagger}_{\mathbf{q}'\downarrow} c_{\mathbf{q}'+\mathbf{k}'-\mathbf{k}-\mathbf{Q}\downarrow} \mid S^{-}_{\mathbf{Q}}(0) \gg \\ &+ \frac{U}{N} \sum_{\mathbf{k}'\mathbf{q}'} \ll c^{\dagger}_{\mathbf{k}'\uparrow} c_{\mathbf{q}'\uparrow} c^{\dagger}_{\mathbf{k}-\mathbf{Q}\uparrow} c_{\mathbf{k}+\mathbf{k}'-\mathbf{q}'\downarrow} \mid S^{-}_{\mathbf{Q}}(0) \gg . \end{aligned} \tag{5.9}$$

Note again that due to the term $< c^{\dagger}_{\downarrow} c_{\downarrow} >$ the third term of the above equation does not contribute if approximated by a factorization. The only non–zero contribution comes from the last term which after using anticommutator properties between electron's operators yields the result:

$$\begin{aligned} \ll c^{\dagger}_{\mathbf{k}'\uparrow} c_{\mathbf{q}'\uparrow} c^{\dagger}_{\mathbf{k}-\mathbf{Q}\uparrow} c_{\mathbf{k}+\mathbf{k}'-\mathbf{q}'\downarrow} \mid S^{-}_{\mathbf{Q}}(0) \gg &= \ll c^{\dagger}_{\mathbf{k}-\mathbf{Q}\uparrow} c_{\mathbf{k}+\mathbf{k}'-\mathbf{q}'\downarrow} c^{\dagger}_{\mathbf{k}'\uparrow} c_{\mathbf{q}'\uparrow} \mid S^{-}_{\mathbf{Q}}(0) \gg \\ &+ \delta_{\mathbf{q}',\mathbf{k}-\mathbf{Q}} \ll c_{\mathbf{k}'\uparrow} c_{\mathbf{k}+\mathbf{k}'-\mathbf{q}'\downarrow} \mid S^{-}_{\mathbf{Q}}(0) \gg, \end{aligned} \tag{5.10}$$

which using the definition of the Green's function $H^{\mathbf{Q}}_{\mathbf{kpq}}(t)$ and $X^{\mathbf{Q}}_{\mathbf{k}}(t)$ of the previous chapter can be simplified as follows:

$$\begin{aligned} \ll c^{\dagger}_{\mathbf{k}'\uparrow} c_{\mathbf{q}'\uparrow} c^{\dagger}_{\mathbf{k}-\mathbf{Q}\uparrow} c_{\mathbf{k}+\mathbf{k}'-\mathbf{q}'\downarrow} \mid S^{-}_{\mathbf{Q}}(0) \gg &= H^{\mathbf{Q}}_{\mathbf{k}+\mathbf{k}'-\mathbf{q}',\mathbf{q}',\mathbf{q}'-\mathbf{k}'}(t) \\ &+ n(\varepsilon_{\mathbf{q}'}) \delta_{\mathbf{q}',\mathbf{k}'} X^{\mathbf{Q}}_{\mathbf{k}}(t) \\ &+ \delta_{\mathbf{q}',\mathbf{k}-\mathbf{Q}} X^{\mathbf{Q}}_{\mathbf{k}'+\mathbf{Q}}(t). \end{aligned} \tag{5.11}$$

Therefore, we conclude that the Hubbard repulsion contributes to the dynamics of the Green's function $X^{\mathbf{Q}}_{\mathbf{k}}(t)$ with a term which is proportional to $X^{\mathbf{Q}}_{\mathbf{k}}(t)$ and additionally creates a coupling between that Green's function and $H^{\mathbf{Q}}_{\mathbf{k+k'-q',q',q'-k'}}(t)$. We derive now the final form of the equation of $X^{\mathbf{Q}}_{\mathbf{k}}(t)$. By substituting the result for the truncated Green's function $\ll c^{\dagger}_{\mathbf{k'}\uparrow} c_{\mathbf{q'}\uparrow} c^{\dagger}_{\mathbf{k-Q}\uparrow} c_{\mathbf{k+k'-q'}\downarrow} \mid S^{-}_{\mathbf{Q}}(0) \gg$ from Eq. (5.12) into Eq. (5.9) we finally obtain:

$$\begin{aligned} i\frac{\partial}{\partial t} X^{\mathbf{Q}}_{\mathbf{k}}(t) &= i\delta(0) < [c^{\dagger}_{\mathbf{k-Q}\uparrow} c_{\mathbf{k}}, S^{-}_{\mathbf{Q}}] > + \ll [c^{\mathbf{Q}}_{\mathbf{k-Q}\uparrow} c_{\mathbf{k}\downarrow}, H_{exch}] \mid S^{-}_{\mathbf{Q}}(0) \gg \\ &+ \frac{U}{N} \left(\sum_{\mathbf{k'}} X^{\mathbf{Q}}_{\mathbf{k'+Q}}(t) + \sum_{\mathbf{k'q'}} H^{\mathbf{Q}}_{\mathbf{k+k'-q',q',q'-k'}}(t) \right) \\ &+ nU X^{\mathbf{Q}}_{\mathbf{k}}(t). \end{aligned} \tag{5.12}$$

Let us now derive the additional terms into the equation of motion for $H^{\mathbf{Q}}_{\mathbf{k'kq}}(t) = \ll c^{\dagger}_{\mathbf{k'+q-Q}\uparrow} c_{\mathbf{k'}\downarrow} \left(c^{\dagger}_{\mathbf{k-q}\uparrow} c_{\mathbf{k}\uparrow} - n(\varepsilon_{\mathbf{k}}) \delta_{\mathbf{q},\mathbf{0}} \right) \mid S^{-}_{\mathbf{Q}}(0) \gg$ which come solely from Hubbard interaction H_U since $H^{\mathbf{Q}}_{\mathbf{k'kq}}(t)$ does not contain any localized spin operator. This equation has the form:

$$\begin{aligned} i\frac{\partial}{\partial t} H^{\mathbf{Q}}_{\mathbf{k'kq}}(t) &= i\delta(t) < [c^{\dagger}_{\mathbf{k'+q-Q}\uparrow} c_{\mathbf{k'}\downarrow} \left(c^{\dagger}_{\mathbf{k-q}\uparrow} c_{\mathbf{k}\uparrow} - n(\varepsilon_{\mathbf{k}}) \delta_{\mathbf{q},\mathbf{0}} \right), S^{-}_{\mathbf{Q}}] > \\ &+ \ll [c^{\dagger}_{\mathbf{k'+q-Q}\uparrow} c_{\mathbf{k'}\downarrow} \left(c^{\dagger}_{\mathbf{k-q}\uparrow} c_{\mathbf{k}\uparrow} - n(\varepsilon_{\mathbf{k}}) \delta_{\mathbf{q},\mathbf{0}} \right), H_{exch}] \mid S^{-}_{\mathbf{Q}}(0) \gg \\ &+ \ll [c^{\dagger}_{\mathbf{k'+q-Q}\uparrow} c_{\mathbf{k'}\downarrow} \left(c^{\dagger}_{\mathbf{k-q}\uparrow} c_{\mathbf{k'}\uparrow} - n(\varepsilon_{\mathbf{k}}) \delta_{\mathbf{q},\mathbf{0}} \right), H_U] \mid S^{-}_{\mathbf{Q}}(0) \gg, \end{aligned}$$

which, by expanding the commutators in the r.h.s Green's functions using the relation (8.17), takes the form:

$$\begin{aligned} i\frac{\partial}{\partial t} H^{\mathbf{Q}}_{\mathbf{k'kq}}(t) &= \ll [c^{\dagger}_{\mathbf{k'+q-Q}\uparrow} c_{\mathbf{k'}\downarrow} \left(c^{\dagger}_{\mathbf{k-q}\uparrow} c_{\mathbf{k}\uparrow} - n(\varepsilon_{\mathbf{k}}) \delta_{\mathbf{q},\mathbf{0}} \right), H_{exch}] \mid S^{-}_{\mathbf{Q}}(0) \gg \\ &+ \ll c^{\dagger}_{\mathbf{k'+q-Q}\uparrow} c_{\mathbf{k'}\downarrow} [c^{\dagger}_{\mathbf{k-q}\uparrow} c_{\mathbf{k}\uparrow}, H_U] \mid S^{-}_{\mathbf{Q}}(0) \gg \\ &+ \ll [c^{\dagger}_{\mathbf{k'+q-Q}\uparrow} c_{\mathbf{k'}\downarrow}, H_U] \left(c^{\dagger}_{\mathbf{k-q}\uparrow} c_{\mathbf{k}\uparrow} - n(\varepsilon_{\mathbf{k}}) \delta_{\mathbf{q},\mathbf{0}} \right) \mid S^{-}_{\mathbf{Q}}(0) \gg \end{aligned} \tag{5.13}$$

Using the results (8.27) and (8.29) we can calculate the last two terms of the above equation. In this way we obtain:

$$
\begin{aligned}
i\frac{\partial}{\partial t}H^{\mathbf{Q}}_{\mathbf{k'kq}}(t) &= \ll [c^{\dagger}_{\mathbf{k'+q-Q}\uparrow}c_{\mathbf{k'}\downarrow}\left(c^{\dagger}_{\mathbf{k-q}\uparrow}c_{\mathbf{k}\uparrow}-n(\varepsilon_{\mathbf{k}})\delta_{\mathbf{q},\mathbf{0}}\right), H_{exch}] \mid S^{-}_{\mathbf{Q}}(0)\gg \\
&+ \frac{U}{N}\sum_{\mathbf{k''q'}} \ll c^{\dagger}_{\mathbf{k'+q-Q}\uparrow}c_{\mathbf{k'}\downarrow}c^{\dagger}_{\mathbf{k-q}\uparrow}c_{\mathbf{k''}\uparrow}c^{\dagger}_{\mathbf{q'}\downarrow}c_{\mathbf{q'+k-k''}\downarrow} \mid S^{-}_{\mathbf{Q}}(0)\gg \\
&- \frac{U}{N}\sum_{\mathbf{k''q'}} \ll c^{\dagger}_{\mathbf{k'+q-Q}\uparrow}c_{\mathbf{k'}\downarrow}c^{\dagger}_{\mathbf{k''}\uparrow}c_{\mathbf{k}\uparrow}c^{\dagger}_{\mathbf{q'}\downarrow}c_{\mathbf{q'+k''-k+q}\downarrow} \mid S^{-}_{\mathbf{Q}}(0)\gg \qquad (5.14)\\
&- \frac{U}{N}\sum_{\mathbf{k''q'}} \\
&\ll c^{\dagger}_{\mathbf{k''}\uparrow}c_{\mathbf{k'}\downarrow}c^{\dagger}_{\mathbf{q'}\downarrow}c_{\mathbf{q'+k''-k'-q-Q}\downarrow}\left(c^{\dagger}_{\mathbf{k-q}\uparrow}c_{\mathbf{k}\uparrow}-n(\varepsilon_{\mathbf{k}})\delta_{\mathbf{q},\mathbf{0}}\right) \mid S^{-}_{\mathbf{Q}}(0)\gg \\
&+ \frac{U}{N}\sum_{\mathbf{k''q'}} \\
&\ll c^{\dagger}_{\mathbf{k''}\uparrow}c_{\mathbf{q'}\uparrow}c^{\dagger}_{\mathbf{k'+q-Q}\uparrow}c_{\mathbf{k'+k''-q'}\downarrow}\left(c^{\dagger}_{\mathbf{k-q}\uparrow}c_{\mathbf{k}\uparrow}-n(\varepsilon_{\mathbf{k}})\delta_{\mathbf{q},\mathbf{0}}\right) \mid S^{-}_{\mathbf{Q}}(0)\gg
\end{aligned}
$$

Now the only step left to obtain the finite chain of equations of motion is the approximation of the r.h.s. Green's functions applying the usual factorization method to the last four terms of the above equation. Let us start from the first of those terms which after using anticommutators properties for the electron operators yields:

$$
\begin{aligned}
&\ll c^{\dagger}_{\mathbf{k'+q-Q}\uparrow}c_{\mathbf{k'}\downarrow}c^{\dagger}_{\mathbf{k-q}\uparrow}c_{\mathbf{k''}\uparrow}c^{\dagger}_{\mathbf{q'}\downarrow}c_{\mathbf{q'+k-k''}\downarrow} \mid S^{-}_{\mathbf{Q}}(0)\gg= \\
&\ll c_{\mathbf{k'}\downarrow}c^{\dagger}_{\mathbf{q'}\downarrow}c^{\dagger}_{\mathbf{k'+q-Q}\uparrow}c^{\dagger}_{\mathbf{k-q}\uparrow}c_{\mathbf{k''}\uparrow}c_{\mathbf{q'+k-k''}\downarrow} \mid S^{-}_{\mathbf{Q}}(0)\gg .
\end{aligned}
$$

In this form the Green's function can be easily factorized as follows:

$$
\begin{aligned}
&\ll c_{\mathbf{k'}\downarrow}c^{\dagger}_{\mathbf{q'}\downarrow}c^{\dagger}_{\mathbf{k'+q-Q}\uparrow}c^{\dagger}_{\mathbf{k-q}\uparrow}c_{\mathbf{k''}\uparrow}c_{\mathbf{q'+k-k''}\downarrow} \mid S^{-}_{\mathbf{Q}}(0)\gg\simeq \\
&< c_{\mathbf{k'}\downarrow}c^{\dagger}_{\mathbf{q'}\downarrow} >\ll c^{\dagger}_{\mathbf{k'+q-Q}\uparrow}c^{\dagger}_{\mathbf{k-q}\uparrow}c_{\mathbf{k''}\uparrow}c_{\mathbf{q'+k-k''}\downarrow} \mid S^{-}_{\mathbf{Q}}(0)\gg= \qquad (5.15)\\
&\delta_{\mathbf{k'},\mathbf{q'}}\left(H^{\mathbf{Q}}_{\mathbf{k},\mathbf{k'},\mathbf{k'-k+q}}(t)+n(\varepsilon_{\mathbf{k'}})\delta_{\mathbf{k'},\mathbf{k-q}}X^{\mathbf{Q}}_{\mathbf{k}}(t)\right),
\end{aligned}
$$

where in the last step the definition of Green's functions is used. Similarly, the second term becomes:

$$
\begin{aligned}
&\ll c^{\dagger}_{\mathbf{k'+q-Q}\uparrow}c_{\mathbf{k'}\downarrow}c^{\dagger}_{\mathbf{k''}\uparrow}c_{\mathbf{k}\uparrow}c^{\dagger}_{\mathbf{q'}\downarrow}c_{\mathbf{q'+k''-k+q}\downarrow} \mid S^{-}_{\mathbf{Q}}(0)\gg= \\
&\ll c_{\mathbf{k'}\downarrow}c^{\dagger}_{\mathbf{q'}\downarrow}c^{\dagger}_{\mathbf{k'+q-Q}\uparrow}c^{\dagger}_{\mathbf{k''}\uparrow}c_{\mathbf{k}\uparrow}c_{\mathbf{q'+k''-k+q}\downarrow} \mid S^{-}_{\mathbf{Q}}(0)\gg\simeq \\
&< c_{\mathbf{k'}\downarrow}c^{\dagger}_{\mathbf{q'}\downarrow} >\ll c^{\dagger}_{\mathbf{k'+q-Q}\uparrow}c^{\dagger}_{\mathbf{k''}\uparrow}c_{\mathbf{k}\uparrow}c_{\mathbf{q'+k''-k+q}\downarrow} \mid S^{-}_{\mathbf{Q}}(0)\gg= \qquad (5.16)\\
&\delta_{\mathbf{k'},\mathbf{q'}}\left(H^{\mathbf{Q}}_{\mathbf{k'+k''-k+q},\mathbf{k},\mathbf{k'-k''}}(t)-n(\varepsilon_{\mathbf{k}})\delta_{\mathbf{k''},\mathbf{k}}X^{\mathbf{Q}}_{\mathbf{k'+q}}(t)\right). \qquad (5.17)
\end{aligned}
$$

Finally, the last two terms become:

$$\ll c^{\dagger}_{\mathbf{k''}\uparrow}c_{\mathbf{k'}\downarrow}c^{\dagger}_{\mathbf{q'}\downarrow}c_{\mathbf{q'+k''-k'-q-Q}\downarrow}\left(c^{\dagger}_{\mathbf{k-q}\uparrow}c_{\mathbf{k}\uparrow}-n(\varepsilon_{\mathbf{k}})\delta_{q,0}\right)\mid S^{-}_{\mathbf{Q}}(0)\gg\simeq$$
$$<c_{\mathbf{k'}\downarrow}c^{\dagger}_{\mathbf{q'}\downarrow}>\ll c^{\dagger}_{\mathbf{k''}\uparrow}c_{\mathbf{q'+k''-k'-q-Q}\downarrow}\left(c^{\dagger}_{\mathbf{k-q}\uparrow}c_{\mathbf{k}\uparrow}-n(\varepsilon_{\mathbf{k}})\delta_{\mathbf{q},\mathbf{0}}\right)\mid S^{-}_{\mathbf{Q}}(0)\gg= \quad (5.18)$$
$$\delta_{\mathbf{k'},\mathbf{q'}}H^{\mathbf{Q}}_{\mathbf{k''-q+Q},\mathbf{k},\mathbf{q}}(t),$$

and

$$\ll c^{\dagger}_{\mathbf{k''}\uparrow}c_{\mathbf{q'}\uparrow}c^{\dagger}_{\mathbf{k'+q-Q}\uparrow}c_{\mathbf{k'+k''-q'}\downarrow}\left(c^{\dagger}_{\mathbf{k-q}\uparrow}c_{\mathbf{k}\uparrow}-n(\varepsilon_{\mathbf{k}})\delta_{\mathbf{q},\mathbf{0}}\right)\mid S^{-}_{\mathbf{Q}}(0)\gg\simeq$$
$$<c^{\dagger}_{\mathbf{k''}\uparrow}c_{\mathbf{q'}\uparrow}>\ll c^{\dagger}_{\mathbf{k'+q-Q}\uparrow}c_{\mathbf{k'+k''-q'}\downarrow}\left(c^{\dagger}_{\mathbf{k-q}\uparrow}c_{\mathbf{k}\uparrow}-n(\varepsilon_{\mathbf{k}})\delta_{\mathbf{q},\mathbf{0}}\right)\mid S^{-}_{\mathbf{Q}}(0)\gg \quad (5.19)$$
$$\delta_{\mathbf{p'},\mathbf{k''}}n(\varepsilon_{\mathbf{p'}})H^{\mathbf{Q}}_{\mathbf{k'},\mathbf{k},\mathbf{q}}(t).$$

Substituting relations 5.15,5.16, 5.18 and 5.19 into Eq. 5.14 we obtain the final form of the equation of motion which governs the dynamics of $H^{\mathbf{Q}}_{\mathbf{k'kq}}(t)$.

$$\begin{aligned} i\frac{\partial}{\partial t}H^{\mathbf{Q}}_{\mathbf{k'kq}}(t) &= \ll [c^{\dagger}_{\mathbf{k'+q-Q}\uparrow}c_{\mathbf{k'}\downarrow}\left(c^{\dagger}_{\mathbf{k-q}\uparrow}c_{\mathbf{k}\uparrow}-n(\varepsilon_{\mathbf{k}})\delta_{\mathbf{q},\mathbf{0}}\right),H_{exch}]\mid S^{-}_{\mathbf{Q}}(0)\gg \\ &+ nUH^{\mathbf{Q}}_{\mathbf{k'kq}}(t)+\frac{U}{N}\left(n(\varepsilon_{\mathbf{k-q}})X^{\mathbf{Q}}_{\mathbf{k}}(t)-n(\varepsilon_{\mathbf{k}})X^{\mathbf{Q}}_{\mathbf{k'+Q}}(t)\right) \\ &+ \frac{U}{N}\left(\sum_{\mathbf{k'}}H^{\mathbf{Q}}_{\mathbf{k},\mathbf{k'},\mathbf{k'-k+q}}(t)-\sum_{\mathbf{k''}}H_{\mathbf{k''+k'-k+q},\mathbf{k},\mathbf{k-k''}}\right) \quad (5.20) \\ &- \frac{U}{N}\sum_{\mathbf{k''}}H_{\mathbf{k''-q+Q},\mathbf{k},\mathbf{q}}(t). \end{aligned}$$

Now we transform Eqs. 5.4, 5.12, 5.7 and 5.20 into frequency domain using the Laplace transformation as defined in relations 4.23 and 4.24. Also, using the results of the previous chapter we substitute the contribution of H_{exch} in the above equations. Similar with the previous chapter, we set stricter bounds for momentum indexes. That means that our Green's functions must be written as: $X^{\mathbf{Q}}_{\mathbf{k}}(\omega)=n(\varepsilon_{\mathbf{k}})X^{\mathbf{Q}}_{\mathbf{k}}(\omega)=X^{\mathbf{Q}}_{\nu}(\omega)$, $G_{\mathbf{kq}}=(1-n(\varepsilon_{\mathbf{k}}))n(\varepsilon_{\mathbf{k-q}})G^{\mathbf{Q}}_{\mathbf{kq}}(\omega)=G^{\mathbf{Q}}_{\alpha\nu}(\omega)$ and $H^{\mathbf{Q}}_{\mathbf{k'kq}}(\omega)=n(\varepsilon_{\mathbf{k'}})n(\varepsilon_{\mathbf{k}})(1-n(\varepsilon_{\mathbf{q}}))H^{\mathbf{Q}}_{\mathbf{k'kq}}(\omega)=H^{\mathbf{Q}}_{\mu\nu\alpha}(\omega)$. Additionally, it is more convenient to write equations of motion for Green's functions of the form: $X=\frac{J}{2\sqrt{N}}XY$, $G=\frac{J}{2N}GY$ and $H=\frac{J^2}{4N\sqrt{N}}HY$. In this way we achieve two goals: every sum is of order $O(1)$, therefore appropriate for numerical evaluation. More importantly the equation of Y becomes:

$$\left(\omega-\frac{Jn}{2}-2J_{AF}S(\gamma_{\mathbf{Q}}-\gamma_0)-\frac{J^2S}{2N}\sum_{\nu}X^{\mathbf{Q}}_{\nu}(\omega)\right.$$
$$\left.-\frac{J^2}{4N^2}\sum_{\alpha\nu}G^{\mathbf{Q}}_{\alpha\nu}(\omega)+i\gamma\right)Y^{\mathbf{Q}}(\omega)=4Si, \quad (5.21)$$

which in the limit $\gamma \to 0$ give us an explicit form of the pole of this Green's function

$$\omega_{\mathbf{Q}} = \frac{Jn}{2} + \frac{J^2 S}{2N} \sum_{\nu} X_{\nu}^{\mathbf{Q}}(\omega) + \frac{J^2}{4N^2} \sum_{\alpha\nu} G_{\alpha\nu}(\omega) + 2J_{AF} S(\gamma_Q - \gamma_0), \qquad (5.22)$$

which describes the spin–wave excitations. The Green's functions X, G and H obey the equations:

$$\begin{aligned} (\omega + \varepsilon_{\nu-\mathbf{Q}} - \varepsilon_{\nu} + SJ + nU)\, X_{\nu}^{\mathbf{Q}}(\omega) &= -1 - \frac{J}{2N} \sum_{\alpha} G_{\alpha\nu}^{\mathbf{Q}}(\omega) \qquad (5.23) \\ &+ \frac{U}{N} \left(\sum_{\mu} X_{\mu}^{\mathbf{Q}}(\omega) + \sum_{\mu\alpha} H_{\mu\nu\alpha}^{\mathbf{Q}}(\omega) \right), \end{aligned}$$

$$\begin{aligned} \left(\omega + \varepsilon_{\nu} - \varepsilon_{\alpha} - \frac{Jn}{2} + i\gamma - 2J_{AF} S(\gamma_{\alpha-\nu-Q} - \gamma_0) \right) G_{\alpha\nu}^{\mathbf{Q}}(\omega) &= 1 - SJ X_{\nu}^{\mathbf{Q}}(\omega) \\ + \frac{J}{2N} \left(\sum_{\beta} G_{\beta\nu}^{\mathbf{Q}}(\omega) - \sum_{\mu} G_{\alpha\mu}^{\mathbf{Q}}(\omega) \right) \qquad (5.24) \\ + \frac{J^2 S}{2N} \sum_{\mu} H_{\mu\nu\alpha}^{\mathbf{Q}}(\omega), \end{aligned}$$

$$\begin{aligned} (\omega_{\mathbf{Q}} + \varepsilon_{\mu} + \varepsilon_{\nu} - \varepsilon_{\mathbf{Q}+\mu+\nu-\alpha} - \varepsilon_{\alpha} - SJ - nU)\, H_{\mu\nu\alpha} &= JS \left(G_{\alpha\nu}^{\mathbf{Q}}(\omega) - G_{\alpha\mu}^{\mathbf{Q}}(\omega) \right) \\ - \frac{U}{N} \left(X_{\nu}^{\mathbf{Q}}(\omega) - X_{\mu}^{\mathbf{Q}}(\omega) \right) \qquad (5.25) \\ + \frac{U}{N} \left(\sum_{\nu'} H_{\mu\nu'\alpha}^{\mathbf{Q}}(\omega) + \sum_{\mu'} H_{\mu'\nu\alpha}^{\mathbf{Q}}(\omega) \right) - \frac{U}{N} \sum_{\alpha'} H_{\mu\nu\alpha'}^{\mathbf{Q}}(\omega). \end{aligned}$$

A comparison between Eqs. (5.21–5.25) with the variational equations of chapter 3 proves that these two different methods, arrive at the same equations which describe spin–wave excitation energies up to three–body correlations. The validity of approximation we discuss here, i.e. the factorization of higher order Green's functions, is in this way proved.

5.3 Numerical results

Now we present our numerical results concerning spin–wave damping and its dependence on the large Hubbard repulsion and the weaker super–exchange interaction. The role of double–exchange interaction is discussed in the previous chapter

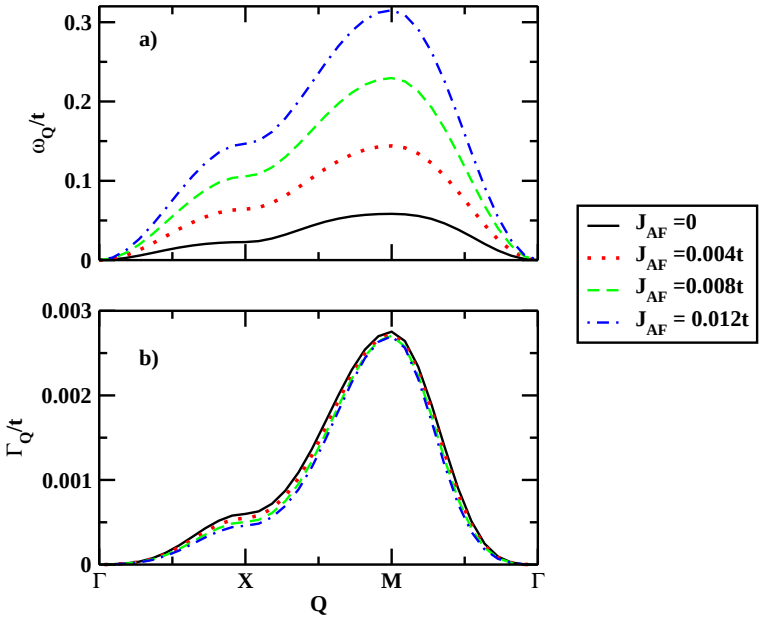

Figure 5.1: The role of the super–exchange interaction on spin–wave dispersion (a) and damping (b) for $J = 7t, U = 25t, n = 0.6, \gamma = 0.2$

within the simple double–exchange hamiltonian. For that reason we fix now parameter J/t to values which are relevant to these quoted in the literature[22]. Moreover the phenomenological damping γ is fixed to the same value $\gamma = 0.2$ of the previous chapter. For that value of γ the real part of spin–wave pole, which describe the magnon excited energies, are equivalent with our variational results[59] as presented in Chapter (3). Our numerical calculations is performed in a 2D fairly large system with $N \simeq 20 \times 20$ lattice sites.

We start the presentation of our numerical results with the effect of the super–exchange interaction. Fig. (5.1) shows spin–wave dispersion (a) and damping (b) along the main directions in the Brilouin zone for different values of J_{AF}/t within the region $0 \leq J_{AF} \leq 0.012t$. We fix the other free parameters as $n = 0.6, J = 7t, U = 25t$. The real part of the magnon's pole is strongly suppressed while J_{AF}/t is increasing, something which is in agreement with the discussion in Chapter (3). On the other hand, super–exchange interaction only slightly affect the spin–wave damping. While the magnon dispersion varies from $\sim 0.05t$ to $\sim 0.3t$ in M–point the deviation of damping is rather insignificant. Taking also into account the small value of spin–wave damping as compared with magnon energy we conclude that for realistic values of energy parameters J/t and U/t

H_{super} plays a minor role on the spin–wave dynamics. Although the suppression of the spin–wave dispersion due to super–exchange interaction is rather large and thus not negligible, we can suppose that the properties of spin–wave damping and thus spin–wave excitations is exclusively governed by the double–exchange mechanism and the on–site Hubbard repulsion. We can understand the latter results by examining the system of equations of motion Eqs. (5.22–5.25). We note that there is no contribution of the super–exchange interaction, H_{super}, to the equation of $H_{\mu\nu\alpha}$ Eq. (5.25) which describes the scattering effects with a Fermi sea electron–hole pair. The main contribution is in Eq. (5.22) of the magnon pole which is the origin of the large suppression of the real part of the pole. The only imaginary contributions comes from Eq. (5.24) of Green's function $G_{\alpha\nu}$ which is not enough to significantly affect spin–wave damping due to low strength of the super–exchange interaction. Therefore we conclude that H_{AF} contributes solely on spin–wave dispersion.

As we discussed the spin–wave excited states relax by scattering with an electron–hole pair. In our calculations this process consists of two independent channels with different relaxation rates. The first one is obtained if the electronic contribution to scattered magnon is neglected, which corresponds to set the $H^{\mathbf{Q}}_{\mathbf{kpq}} = 0$. We now assess the contribution of the Fermi electrons, described by Green's function $H^{\mathbf{Q}}_{\mathbf{kpq}}$, to the spin–wave damping. The affects of that process on spin–wave dispersion is strong as is shown in Chapter (3) since it can qualitatively explain the softening near the zone boundary. In Fig. (5.2) we plot spin–wave dispersion (a) and damping (b) along every main direction in the Brilouin zone. The values of the parameters is chosen so that the zone boundary softening is strong. Focusing on direction $\Gamma \rightarrow X$ we note in Fig. (5.2)(b) that the three–body damping is only 30% of the result obtained by considering only localized spin scattering. Although three–body spin–wave dispersion exhibits a strong zone boundary softening the corresponding lifetime seems to be long. However damping must be directly compared with spin–wave energy in order to draw define conclusions about lifetime. In this way three–body damping is about 5% of magnon's energy, while the $H_{\mathbf{kpq}} = 0$ percentage is as small as 0.5%. That means that the magnon lifetime within three–body approximation is about 10 times shorter as compared with the result obtained by neglecting electronic contribution to scattering process. Moreover considering damping along the other directions we note that the $H_{\mathbf{kpq}} = 0$ fails also to reproduce the behavior of the spin–wave damping observed in recent experiments[52]. Magnon damping along the diagonal direction is sufficiently larger as compared with the result along x–axis. We observe that this behavior is qualitatively reproduced only when three–body correlations are taken into account. Additionally in the previous chapter we show the failure even of the three–body correlated damping to reproduce that experimental result within the

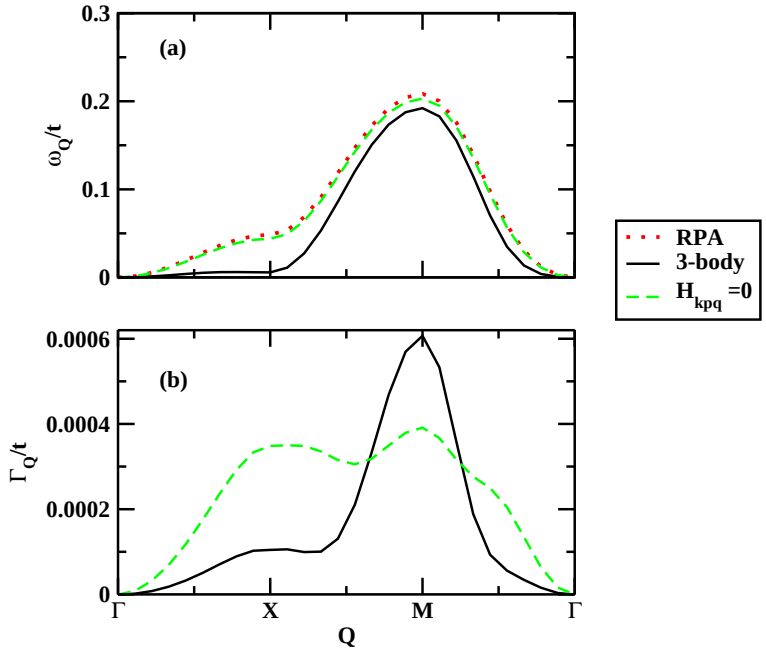

Figure 5.2: Spin–wave dispersion (a) and damping (b) for $n = 0.7, J = 2t, U = 10t, J_{AF} = 0.0, \gamma = 0.2$: A comparison between the different approximations.

simplified double–exchange model. The fact that the right behavior is recovered by including the on–site Hubbard repulsion in our model hamiltonian, indicates the important role of H_U in the dynamics of the manganites.

Experimental studies on the damping of highly doped manganites[52] show a strong dependence on itinerant electron concentration. More precisely, the higher the electron doping the lower is the spin–wave damping. In order to examine the nature of that numerical result we plot spin–wave dispersion and damping for two different electron concentrations, $n \simeq 0.55$ and $n = 0.6$ and for the typical values $J = 7t, U = 25t, J_{AF} = 0.012t$. Fig. (5.3) shows these results where spin–wave dispersion is plotted within RPA and three–body approximation. For the higher density we note in Fig. (5.3)(c) that along $\Gamma \rightarrow X$ direction damping is about only 5% of spin–wave dispersion while along the other directions it is $2-3\%$. This means that spin–wave excitations are rather long–lived for that electron concentration. At the same time, Fig. (5.3)(d) shows that for a lower electron doping along $\Gamma \rightarrow X$ we have a damping about 15% of the magnon energy while becomes slightly larger along $X \rightarrow M$ and $M \rightarrow \Gamma$. The latter indicates the appearance of short lifetime of magnons, which can be associated with the larger softening of the spin–wave

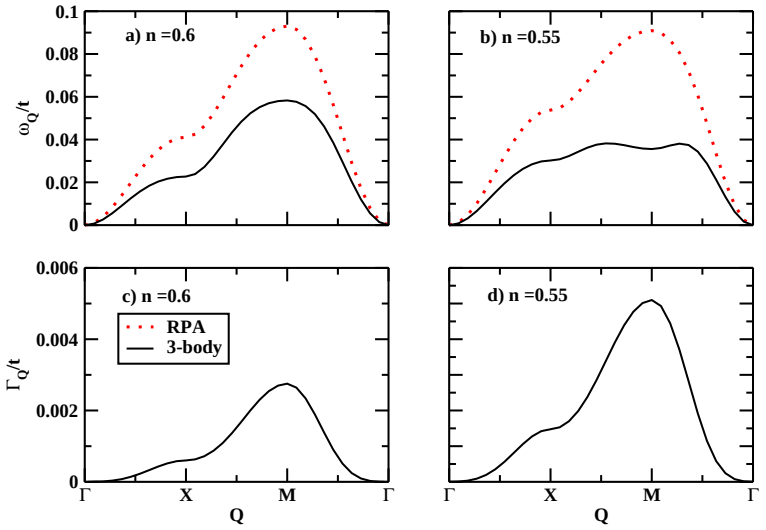

Figure 5.3: The role of itinerant electron concentration for $J = 7t, U = 25t, J_{AF} = 0.012t, \gamma = 0.2$.

dispersion as shown in Fig. (5.3)(a)–(b). A direct comparison between spin–wave damping in (a) and (b) shows that the higher doping system exhibits lower spin–wave damping. Furthermore, damping is lower along the $\Gamma \rightarrow X$ direction as compared with the other directions. That result stands for every main direction in the Brilouin zone and is in agreement with the experimental results. In addition, we note that for $n = 0.55$ the large damping at the $M = (\pi, \pi)$ point is directly connected with a strong softening of spin–wave dispersion, similar with the result of the previous chapter.

We discuss now further the role of Hubbard repulsion on the spin–wave damping. Fig. (5.4) shows again spin–wave dispersion (a) and damping (b) within three–body approximation for the experimentally interesting electron doping $n = 0.7$ and for values of U/t which lie in the region $10t \leq U \leq 55t$, while we fix the rest of the parameters as $J = 2t, J_{AF} = 0$. In this figure a strikingly large softening of spin–wave dispersion along $\Gamma \rightarrow X$ direction for low U/t is noticed. The effect of U/t on magnon energy along the other directions is rather weak. On the contrary damping along $\Gamma \rightarrow X$ direction seems to be slightly affected by increasing U/t, while the diminishing Hubbard repulsion affects significantly damping along $X \rightarrow M$ and $M \rightarrow \Gamma$ directions. For instance at the point $\mathbf{Q} = M = (\pi, \pi)$ damping for $U = 10t$ is about 50% lower than that for $U = 55t$. Spin–wave energy along $\Gamma \rightarrow X$ increases with an extremely larger rate as compared to the increasing of

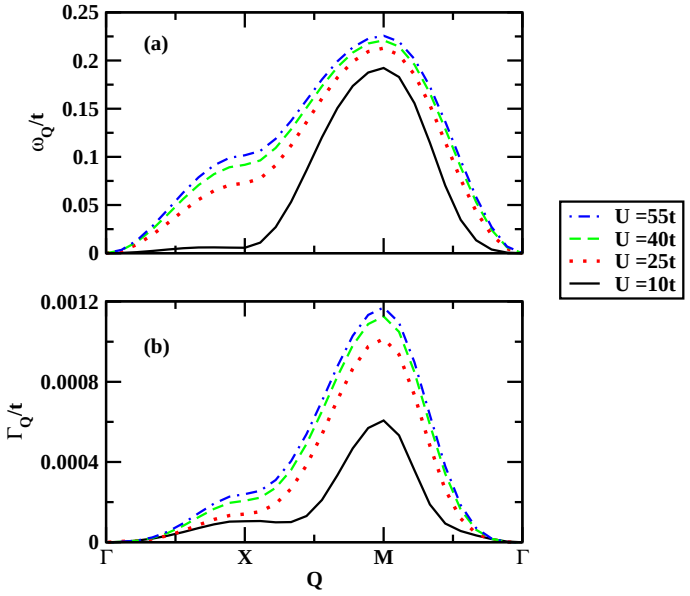

Figure 5.4: The role of Hubbard repulsion on the spin–wave damping: $n = 0.7, J = 2t, J_{AF} = 0.0, \gamma = 0.2$.

damping. The latter indicates a significant increase of spin–wave's lifetime with increasing U/t along that direction. This result can be understood in this way. The strength of the scattering between the electron–hole pair with the spin$\uparrow$–$\downarrow$ excitation is proportional to U. That means that for a very large value of U/t the latter process is very difficult to take place. This is consistent with the result that $H^{\mathbf{Q}}_{\mathbf{kpq}} = 0$ in the limit $U \to \infty$. The latter is discussed in chapter (3) within the variational method and applies also here since these two methods give equivalent results. These result that increasing U/t diminishes the role of $H_{\mathbf{kpq}}$ along with the fact that the $H_{\mathbf{kpq}} = 0$ approximation gives long–lived magnons, explains the effect of Hubbard repulsion on spin–wave's lifetime. The larger is the parameter U/t, the smaller is the role of $H_{\mathbf{kpq}}$ and the longer the magnon's lifetime.

5.4 Conclusions

In conclusion, we apply the double–time Green's function method to a model which is believed to provide a rather realistic description of the ferromagnetic manganites. This method along with an appropriate decoupling procedure reproduces our previous results obtained by a variational treatment of the three–body correla-

tions on spin–wave excitations. In this way we are able to determine magnon's lifetime something that is impossible without Green's functions. We examine here the role of the different interactions, included in our hamiltonian, on the spin–wave damping and also discuss the concentration –dependence of our numerical results. The minor important of the super–exchange interaction on the damping is showed, while this term gives a rather strong contribution (suppression) of the real part of the magnon's pole. On the other hand, the crucial role of the local Hubbard repulsion is proved. First, a comparison between the damping for different doping samples shows a qualitative agreement with the corresponding experimental behavior, within the three–body approximation. Moreover, we show that by including the Hubbard interaction in our model Hamiltonian, the experimentally observed behavior of the damping along the different directions in the Brilouin zone is also recovered. The importance of the three–body correlations on the spin–wave dynamics is enhanced by our results. More precisely we show that the scattering process between the spin$\uparrow$–$\downarrow$ excitation with a Fermi sea pair affects significantly magnon's lifetime by shortening it considerably.

Chapter 6

Long–wavelength spin–wave dynamics of III(Mn)V semiconductors.

6.1 Introduction

In the previous chapters we presented a study of the three–body correlation effects on spin–wave excitations in manganites. We introduced two different ways which was shown produce equivalent results. We wish now to apply the same methods to another kind of carrier–induced ferromagnetic systems; the III(Mn)V diluted magnetic semiconductors. Unfortunately, the variational treatment of spin–waves as discussed in Chapter (2) leads to a failure, since here the Goldstone theorem ($\omega_{\mathbf{Q}=0} = 0$) is not satisfied. The existence of a non–zero energy at $\mathbf{Q} = 0$ can be explained by the fact that the choice of Hartree–Fock state $|F>$ as a reference state within variational theory is not a proper selection. In order to derive spin–wave excitations in magnetic semiconductors we seek another method that satisfies the Goldstone theorem. For that reason we employ the Green's functions method as described in chapters (4) and (5). We showed there this method reproduces the variational results in the manganites. It also reproduces the $1/S$ expansion result contained in our full three-body calculation. Additionally it satisfies Goldstone theorem without any assumption on the ground state. The latter is due to the fact that the Green's function method describes excitations energies and treats better the ground state effects as compared to the variational treatment. Therefore, by applying the Green's function method to ferromagnetic III(Mn)V semiconductors of interest here we recover Goldstone theorem is automatically satisfied. In this way we derive the equations of motion which describe the spin–wave

spectrum within RPA and also the effects of correlations. Moreover, since this method reproduces the $1/S$ expansion results in the manganites we can very well perform that expansion in the DMS. Note that, due to large value of impurity spin's amplitude $S = 5/2$ the expansion up to $O(1/S^2)$ may be enough to describe the effects of correlations.

This chapter is organized as follows. In the next Section the application of the Green's function method to the spin–waves excited spectrum is presented. We reproduce the variational RPA results and additionally the green's function, which describes correlations, is introduced. We also obtain the correlation results for the spin–wave dispersion. Since we are interested in the long–wavelength magnons, we determine the spin–wave stiffness within RPA and also the correlated results. A phenomenologically description of spin–wave damping is given by the so–called Gilbert damping coefficient α which is discussed is subsection (6.2.4). Our numerical results are presented and discussed in Sec. (6.3). Finally, we close with our conclusions in Sec. (6.4).

6.2 Calculations

Now we derive green's functions equations of motion which describe spin–waves in the model Hamiltonian (2.1). We adopt here the magnetic–exchange Hamiltonian

$$H = K + H_{exch}, \tag{6.1}$$

where K expresses the kinetic energy of the s–p valence band holes

$$K = \sum_{\mathbf{k}\sigma} \varepsilon_{\mathbf{k}} a^{\dagger}_{\mathbf{k}\sigma} a_{\mathbf{k}\sigma}. \tag{6.2}$$

which interact with the localized impurity spins via the magnetic–exchange interaction

$$\begin{aligned} H_{exch} &= \frac{J}{2\sqrt{N}} \sum_{\mathbf{kq}\sigma} \sigma\, S^z_{\mathbf{q}}\; a^{\dagger}_{\mathbf{k-q}\sigma} a_{\mathbf{k}\sigma} \\ &+ \frac{J}{2\sqrt{N}} \sum_{\mathbf{kq}} \left(S^-_{\mathbf{q}}\; a^{\dagger}_{\mathbf{k-q}\uparrow} a_{\mathbf{k}\downarrow} + S^{\dagger}_{\mathbf{q}}\; a^{\dagger}_{\mathbf{k}\downarrow} a_{\mathbf{k+q}\uparrow} \right), \end{aligned} \tag{6.3}$$

where N is the number of lattice sites, each occupied by a localized impurity spin S, and $\sigma = 1$ for spin $\uparrow$ and $\sigma = -1$ for spin $\downarrow$. Due to the s–p nature of the valence band hole kinetic energy is given by the so–called effective mass approximation

$$\varepsilon_{\mathbf{k}} = \frac{\hbar^2 \mathbf{k}^2}{2m_h}. \tag{6.4}$$

As a result, the magnetic interaction is smaller than the bandwidth unlike the manganites.

We employ here a simple two–band description to model the valence bands. Within that simplification we focus on the role of correlations on DMS properties. Our calculations can be generalized by taking into account band structure details and spin–orbit coupling [75, 89] that are believed to play an important role on Mn–doped III–V semiconductors. The calculations are rather similar with that appeared in Chapters (4) and (5) where the same method is applied to a Ferromagnetic model of manganese oxides. For that reason here we present very briefly the intermediate algebra since its repetition provides the reader with none new information.

6.2.1 RPA results

We start with the definition of the local spin green's function

$$Y^{\mathbf{Q}}(t) = \theta(t) < [S^{\dagger}_{\mathbf{Q}}(t), S^{-}_{-\mathbf{Q}}(0)] >= \ll S^{\dagger}_{\mathbf{Q}}(t) \mid S^{-}_{-\mathbf{Q}}(0) \gg . \tag{6.5}$$

After some algebra we obtain that the Fourier transformation of $Y_{\mathbf{Q}}(t)$ within RPA obeys the equation of motion

$$\left(\omega - \frac{Jp}{2} + i\gamma_0\right) Y^{\mathbf{Q}}(\omega) = 4Si + \frac{SJ^2}{2N} \sum_{\mathbf{k}} X^{\mathbf{Q}}_{\mathbf{k}}(\omega), \tag{6.6}$$

where p is hole fraction. The equation of motion of the Green's function

$$X^{\mathbf{Q}}_{\mathbf{k}}(t) = \ll a^{\dagger}_{\mathbf{k}-\mathbf{Q}\uparrow} a_{\mathbf{k}\downarrow}(t) \mid S^{-}_{-\mathbf{Q}}(0) \gg \tag{6.7}$$

can be easily shown to be

$$\left(\omega + \varepsilon_{\mathbf{k}-\mathbf{Q}} - \varepsilon_{\mathbf{k}} + SJ + i\gamma_1\right) X^{\mathbf{Q}}_{\mathbf{k}} = -n(\varepsilon_{\mathbf{k}}) Y^{\mathbf{Q}}. \tag{6.8}$$

Eq. (6.6) by substituting $X^{\mathbf{Q}}_{\mathbf{k}}$ from Eq. (6.8) yields

$$\left[\omega - \frac{Jp}{2} + i\gamma_0 + \frac{SJ^2}{2N} \sum_{\nu} \frac{1}{\omega + \varepsilon_{\nu-\mathbf{Q}} - \varepsilon_{\nu} + SJ + i\gamma_1}\right] Y^{\mathbf{Q}} = 4Si. \tag{6.9}$$

We finally obtain the well–known non–interacting RPA magnon dispersion[20] which is given by the pole of green's function $Y^{\mathbf{Q}}$ in the limit $\gamma_0, \gamma_1 \to 0$

$$\omega^{RPA}_{\mathbf{Q}} = \frac{Jp}{2} - \frac{SJ^2}{2N} \sum_{\nu} \frac{1}{\omega^{RPA}_{\mathbf{Q}} + \varepsilon_{\nu-\mathbf{Q}} - \varepsilon_{\nu} + SJ}. \tag{6.10}$$

Note now that the III(Mn)V ferromagnetic semiconductors of interest here lies within the low doping regime $p \simeq 0.1$, and therefore ,as discussed in Chapter (3), Fermi surface can be considered as spherical and the band energy $\varepsilon_{\mathbf{k}}$ is well approximated by a parabolic form $\varepsilon_{\mathbf{k}} = \frac{\hbar k^2}{2m_h}$. Within that approximation the sum in Eq. (6.10) can be transformed to an integral using the relation

$$\frac{1}{N}\sum_{\mathbf{k}} = \frac{1}{(2\pi)^d C_{Mn}} \int d^d\vec{k}, \tag{6.11}$$

where $d = 1, 2, 3$ is the dimensionality of our system and C_{Mn} is the density of Mn impurity spins. Therefore in a 2D system magnon's dispersion within RPA becomes:

$$\omega_{\mathbf{Q}}^{RPA} = \frac{\Delta p}{2S} - \frac{\Delta}{2S(2\pi)^2 C_{Mn}} \int_{|\vec{k}|\leq k_F} d^2\vec{k} \frac{1}{\omega_{\mathbf{Q}}^{RPA} + \varepsilon_{\mathbf{k}-\mathbf{Q}} - \varepsilon_{\mathbf{k}} + \Delta}, \tag{6.12}$$

where $\Delta = SJ$ is the Zeeman splitting energy. Fermi momentum k_F for a 2D system with hole's density C_h satisfies the equation:

$$\pi k_F^2 = (2\pi)^2 C_h. \tag{6.13}$$

The RPA result can be expanded to $O(1/S)$ by removing the magnon energy from the r.h.s. of Eq. (6.12). Therefore, the leading order spin–wave energy in $O(1/S)$ expansion is given by the formula

$$\omega_{\mathbf{Q}}^{(1)} = \frac{\Delta p}{2S} - \frac{\Delta}{2S(2\pi)^2 C_{Mn}} \int_{|\vec{k}|\leq k_F} d^2\vec{k} \frac{1}{\varepsilon_{\mathbf{k}-\mathbf{Q}} - \varepsilon_{\mathbf{k}} + \Delta}. \tag{6.14}$$

The integral in Eq. (6.14) can be easily performed leading to the result

$$\omega_{\mathbf{Q}}^{(1)} = \frac{\frac{p}{2S}}{1 - \frac{p}{2S}} (1 - \frac{E_{\mathbf{F}}}{\Delta}) \varepsilon_{\mathbf{Q}}. \tag{6.15}$$

This result was obtained in Ref[83] with an application of the path–integral formulation along with a Holstein–Primakoff representation of bosonic degrees of freedom, while Eq. (6.12) is more general.

6.2.2 The correlated dispersion

To go beyond RPA carrier–magnon scattering processes must be taken into account. Similar with Chapter 4 we define the Green's function $G_{\mathbf{k},\mathbf{p}}^{\mathbf{Q}}(t)$ which describes localized spin–Fermi pair scattering

$$G_{\mathbf{kp}}(t) = \ll S_{\mathbf{k}-\mathbf{p}-\mathbf{Q}}^{\dagger} \left(a_{\mathbf{p}\downarrow}^{\dagger} a_{\mathbf{k}\downarrow} - n(\varepsilon_{\mathbf{k}}) \delta_{\mathbf{k},\mathbf{p}} \right)(t) \mid S_{\mathbf{Q}}^{-}(0) \gg . \tag{6.16}$$

Performing the approximate method of factorization as described in the previous chapters we obtain, after some algebra, the equation of motion for the Fourier transformation of $G^{\mathbf{Q}}_{\mathbf{k},\mathbf{p}}$

$$\begin{aligned}\left(\omega+\varepsilon_{\mathbf{p}}-\varepsilon_{\mathbf{k}}-\frac{\Delta p}{2S}+i\gamma_2\right)G^{\mathbf{Q}}_{\mathbf{kp}} &= n(\varepsilon_{\mathbf{p}})-n(\varepsilon_{\mathbf{k}})\left(1-\frac{\Delta}{\omega+\varepsilon_{\mathbf{k}-\mathbf{Q}}-\varepsilon_{\mathbf{k}}+\Delta}\right)\\ &+ \frac{\Delta}{2NS}\left(1-\frac{\Delta}{\omega+\varepsilon_{\mathbf{k}-\mathbf{Q}}-\varepsilon_{\mathbf{k}}+\Delta}\right)\sum_{\mathbf{p}'}G^{\mathbf{Q}}_{\mathbf{kp}'}\\ &- \frac{\Delta}{2NS}\sum_{\mathbf{k}'}G^{\mathbf{Q}}_{\mathbf{k}'\mathbf{p}} \qquad (6.17)\\ &+ O(H),\end{aligned}$$

Here we have substituted the contribution of $X^{\mathbf{Q}}_{\mathbf{k}}$ and therefore a self–consistent equation for $G^{\mathbf{Q}}_{\mathbf{kp}}$ is obtained. Note also that we do not include $O(H)$ contributions of higher–order green's function's. As we showed in the case of the manganites the $H=0$ approximation is in a very good agreement with the full three–body result within the low doping regime. Therefore, since in the case of the III(Mn)V semiconductors we are interested in such densities the above approximation is reasonable. Moreover, the equation of motion for green's function $Y^{\mathbf{Q}}$, if correlations are included, becomes

$$\begin{aligned}&\left[\omega-\frac{\Delta p}{2S}+\frac{\Delta^2}{2NS}\sum_{\nu}\frac{1}{\omega+\varepsilon_{\nu-\mathbf{Q}}-\varepsilon_{\nu}+\Delta+i\gamma_1}\right.\\ &\left.-\frac{\Delta^2}{4S^2}\sum_{\mathbf{k},\mathbf{p}}G^{\mathbf{Q}}_{\mathbf{kp}}\left(1-\frac{\Delta}{\omega+\varepsilon_{\mathbf{k}-\mathbf{Q}}-\varepsilon_{\mathbf{k}}+\Delta+i\gamma_1}\right)+i\gamma_0\right]Y^{\mathbf{Q}}=4Si, \qquad (6.18)\end{aligned}$$

where again the contribution of green's function $X^{\mathbf{Q}}_{\mathbf{k}}$ is substituted by using its equation of motion. Moreover by supposing that the true ground state can be approximated by the Hartree-Fock state we conclude that momentum indexes $\mathbf{k}$ and $\mathbf{p}$ is transformed to $\alpha > k_F$ and $\nu \leq k_F$ correspondingly. Subsequently, we obtain magnon's pole from that equation by taking the limit $\gamma_0 \to 0$

$$\begin{aligned}\omega &= \frac{\Delta p}{2S}-\frac{\Delta^2}{2NS}\sum_{\nu}\frac{1}{\omega+\varepsilon_{\nu-\mathbf{Q}}-\varepsilon_{\nu}+\Delta}\\ &+ \frac{\Delta^2}{4S^2}\sum_{\alpha\nu}G^{\mathbf{Q}}_{\alpha\nu}\left(1-\frac{\Delta}{\omega+\varepsilon_{\alpha-\mathbf{Q}}-\varepsilon_{\alpha}+\Delta}\right). \qquad (6.19)\end{aligned}$$

Using relation (6.11) the sum over occupied states is transformed to an integral. By defining a Debye cut–off momentum p_c the sum over unoccupied states is also

evaluated as an integral. In this way Eq. (6.19) yields

$$\omega = \frac{\Delta p}{2S} - \frac{\Delta}{2S(2\pi)^2 C_{Mn}} \int_{|\vec{\nu}|\leq k_F} d^2\vec{\nu} \frac{1}{\omega + \varepsilon_{\nu-\mathbf{Q}} - \varepsilon_\nu + \Delta} \tag{6.20}$$
$$+ \frac{\Delta^2}{4S^2[(2\pi)^2 C_{Mn}]^2} \int_{k_F\leq|\vec{\alpha}|\leq p_C} \int_{|\vec{\nu}|\leq k_F} d^2\vec{\alpha} d^2\vec{\nu} G^{\mathbf{Q}}_{\alpha\nu} \left(1 - \frac{\Delta}{\omega + \varepsilon_{\alpha-\mathbf{Q}} - \varepsilon_\alpha + \Delta}\right),$$

while green's function $G^{\mathbf{Q}}_{\alpha\nu}$ obeys the equation of motion

$$\left(\omega + \varepsilon_\nu - \varepsilon_\alpha - \frac{\Delta p}{2S} + i\gamma_2\right) G^{\mathbf{Q}}_{\alpha\nu} = 1 - \frac{\Delta}{2S} R^{\mathbf{Q}}_\nu \tag{6.21}$$
$$+ \frac{\Delta}{2S}\left(1 - \frac{\Delta}{\omega + \varepsilon_{\alpha-\mathbf{Q}} - \varepsilon_\alpha + \Delta}\right) H^{\mathbf{Q}}_\alpha,$$

where we define the hole

$$R^{\mathbf{Q}}_\nu = \frac{1}{(2\pi)^2 C_{Mn}} \int_{k_F\leq|\vec{\alpha}|\leq p_C} G^{\mathbf{Q}}_{\alpha\nu} d^2\alpha \tag{6.22}$$

and electron

$$H^{\mathbf{Q}}_\alpha = \frac{1}{(2\pi)^2 C_{Mn}} \int_{|\vec{\nu}|\leq k_F} G^{\mathbf{Q}}_{\alpha\nu} d^2\nu, \tag{6.23}$$

contribution to the rescattering process Using the Eqs. (6.21–6.23) the equations of motion for that the Green's functions are obtained as follows

$$R^{\mathbf{Q}}_\nu \left[1 - \frac{\Delta}{2S} I^{\mathbf{Q}}_\nu\right] = I^{\mathbf{Q}}_\nu \tag{6.24}$$
$$- \frac{\Delta}{2S(2\pi)^2 C_{Mn}} \int_{k_F\leq|\vec{\beta}|\leq p_C} \left(1 - \frac{\Delta}{\omega + \varepsilon_{\beta-\mathbf{Q}} - \varepsilon_\beta + \Delta}\right) \frac{H^{\mathbf{Q}}_\beta}{\Delta^{\mathbf{Q}}_{\beta\nu}} d^2\beta$$

and

$$H^{\mathbf{Q}}_\alpha \left[1 + \frac{\Delta}{2S}\left(1 - \frac{\Delta}{\omega + \varepsilon_{\alpha-\mathbf{Q}} - \varepsilon_\alpha + \Delta}\right) I^{\mathbf{Q}}_\alpha\right] = I^{\mathbf{Q}}_\alpha \tag{6.25}$$
$$+ \frac{\Delta}{2S} \frac{1}{(2\pi)^2 C_{Mn}} \int_{|\vec{\mu}|\leq k_F} \frac{R^{\mathbf{Q}}_\mu}{\Delta^{\mathbf{Q}}_{\alpha\mu}} d^2\mu,$$

where we introduce the integrals

$$I^{\mathbf{Q}}_\alpha = \frac{1}{(2\pi)^2 C_{Mn}} \int_\mu \frac{1}{\Delta^{\mathbf{Q}}_{\alpha\mu}} d^2\mu, \quad I^{\mathbf{Q}}_\nu = \frac{1}{(2\pi)^2 C_{Mn}} \int_\beta \frac{1}{\Delta^{\mathbf{Q}}_{\beta\nu}} d^2\beta, \tag{6.26}$$

with $\Delta^{\mathbf{Q}}_{\alpha\nu} = \omega + \varepsilon_\nu - \varepsilon_\alpha - \frac{\Delta p}{2S} + i\gamma_2$. These green's function are one–component functions something that allows us to perform numerical calculations in a more convenient way as compared to the multiple–index function $G^{\mathbf{Q}}_{\alpha\nu}$. Using the definitions of green's function $H^{\mathbf{Q}}_{\alpha}$ magnon's energy Eq. (6.20) becomes

$$\begin{aligned} \omega &= \frac{\Delta p}{2S} - \frac{\Delta}{2S(2\pi)^2 C_{Mn}} \int_{|\vec{\nu}|\leq k_F} d^2\vec{\nu} \frac{1}{\omega + \varepsilon_{\nu-\mathbf{Q}} - \varepsilon_\nu + \Delta} \\ &+ \frac{\Delta^2}{4S^2(2\pi)^2 C_{Mn}} \int_{k_F \leq |\vec{\alpha}| \leq p_C} d^2\vec{\alpha} H^{\mathbf{Q}}_{\alpha} \left(1 - \frac{\Delta}{\omega + \varepsilon_{\alpha-\mathbf{Q}} - \varepsilon_\alpha + \Delta}\right), \end{aligned} \tag{6.27}$$

Similar with Fermi momentum k_F Debye momentum is determined by the relation

$$\pi p_C^2 = (2\pi)^2 C_{Mn}, \tag{6.28}$$

which ensures that the correct total number of states is included in Eq. (6.20). Note that since the III(Mn)V semiconductors are in the weak–coupling limit , only momenta close to $\mathbf{Q} = 0$ contributes. The latter allows us to focus on the long–wavelength spin–wave excitations, describing by the spin–wave stiffness. Moreover, the spin–wave stiffness is directly connected with the critical temperature T_C of magnetic semiconductors[76]. T_C is proportional to spin–wave stiffness D obtained by the formula $\omega_{\mathbf{Q}} = D\mathbf{Q}^2$ in the limit $\mathbf{Q} \to 0$. Therefore the calculation of spin–wave stiffness provides us with the determination of a very interesting physical quantity such us the critical temperature[77, 78, 79, 80, 81, 82] of the systems of interest. In the next subsection spin–wave stiffness is calculated within RPA and additionally the effect of correlations on long–wavelength magnons is discussed.

6.2.3 Long–wavelength Spin–wave: Stiffness

In this subsection spin–wave stiffness constant D is determined as a function of hole doping. Since critical temperature is proportional to that constant an estimation of T_C can be made. We start with the RPA result. The long–wavelength magnon within RPA can be easily determined by Eq. (6.12). At the limit $\mathbf{Q} \to 0$ magnon dispersion behaves as a parabolic function of $\mathbf{Q}$. Therefore by setting $\omega^{RPA}_{\mathbf{Q}} = D^{RPA}\mathbf{Q}^2$ in Eq. (6.12) and expanding the r.h.s we easily obtain spin–wave stiffness within RPA

$$D^{RPA} = \frac{\frac{p}{2S}}{1 - \frac{p}{2S}} \varepsilon_0 (1 - \frac{E_{\mathbf{F}}}{\Delta}), \tag{6.29}$$

where $\varepsilon_0 = \frac{\hbar^2}{2m_h}$. We continue now with the correlated spin–wave stiffness. In order to determine the $O(Q^2)$ contribution of the second term in Eq. (6.20) we

have to expand $H_\alpha^{\mathbf{Q}}$ up to 1^{st} in Q using Eq. (6.25). After some algebra we find that the expansion of $R_\nu^{\mathbf{Q}}$ consists only of even powers since the $O(Q^{2n+1})$ orders vanish. Therefore the first order of $H_\alpha^{\mathbf{Q}}$ is regulated by the zeroth order of $R_\nu^{\mathbf{Q}}$

$$R_\nu^{(0)} = I_\nu^{(0)}\left[1 - \frac{J}{2} I_\nu^{(0)}\right]^{-1}, \tag{6.30}$$

and is given by

$$H_\alpha^{(1)} = \left[I_\alpha^{(0)} + \frac{\Delta}{2S(2\pi)^2 C_{Mn}} \int d^2\vec{v} \frac{I_\nu^{(0)}}{\left(\varepsilon_\nu - \varepsilon_\alpha - \frac{\Delta p}{2S}\right)\left(1 - \frac{\Delta}{2S} I_\nu^{(0)}\right)}\right] \times \left(1 + \frac{\varepsilon_0 \alpha_x}{S} I_\alpha^{(0)} Q\right). \tag{6.31}$$

The zeroth order of integrals (6.26) can be easily evaluated since they are transformed to simple integrals of norms

$$I_\alpha^{(0)} = \frac{1}{2\pi C_{Mn}} \int_0^{k_F} \frac{\nu d\mu}{\varepsilon_\nu - \varepsilon_\alpha - \frac{\Delta p}{2}} = \frac{1}{4\pi C_{Mn}\varepsilon_0} \ln \frac{\varepsilon_\alpha - E_F + \frac{\Delta p}{2S}}{\varepsilon_\alpha + \frac{\Delta p}{2S}}, \tag{6.32}$$

$$I_\nu^{(0)} = \frac{1}{2\pi C_{Mn}} \int_{k_F}^{p_C} \frac{\alpha d\alpha}{\varepsilon_\nu - \varepsilon_\alpha - \frac{\Delta p}{2}} = -\frac{1}{4\pi C_{Mn}\varepsilon_0} \ln \frac{-\varepsilon_\nu + \frac{\Delta p}{2S} + E_C}{-\varepsilon_\nu + \frac{\Delta p}{2S} + E_F}. \tag{6.33}$$

We finally obtain the correlated result for the spin–wave stiffness

$$D\left[1 - \frac{p}{2S} - \frac{\Delta}{8\pi S^2 C_{Mn}} \int_{k_F}^{p_C} \alpha V_\alpha d\alpha\right] = \frac{p}{2S}\varepsilon_0\left(1 - \frac{E_{\mathbf{F}}}{\Delta}\right) + \frac{\Delta\varepsilon_0}{8\pi S^2 C_{Mn}} \int_{k_F}^{p_C} \alpha V_\alpha \left[1 - 2\frac{\varepsilon_0 \alpha^2}{\Delta}\left(1 + \frac{\Delta}{2S} I_\alpha^{(0)}\right)\right] d\alpha, \tag{6.34}$$

where we introduced the function

$$V_\alpha = I_\alpha^{(0)} + \frac{\Delta}{4\pi S C_{Mn}} \int_0^{k_F} d\nu \frac{\nu I_\nu^{(0)}}{\left(\varepsilon_\nu - \varepsilon_\alpha - \frac{\Delta p}{2S}\right)\left(1 - \frac{\Delta}{2S} I_\nu^{(0)}\right)}. \tag{6.35}$$

Note that by removing the second term on the r.h.s. in Eq. (6.35) we determine the spin–wave stiffness at $O(1/S^2)$ order. Also RPA result (6.29) is reproduced if $V_\alpha = 0$.

6.2.4 Spin–wave damping: Gilbert damping coefficient.

The dynamics of the magnetization dynamics in III(Mn)V magnetic semiconductors is well described by the so-called Landau–Lifshitz–Gilbert (LLG) equation.

The dimensionless coefficient Gilbert damping α describes phenomenologically the relaxation rate of collective magnetization [88, 89, 90, 91]. Within (LLG) classical theory of collective magnetization dynamics Gilbert coefficient measures the damping of magnetization and energy dissipation in the system. In our theory the mechanism of that phenomenon is originated by the spin–exchange interaction between localized Mn spin and the itinerant holes and therefore a Gilbert coefficient can be determined. LLG theory can be used to derive a phenomenological susceptibility whose inverse imaginary part is proportional to $\alpha\omega$. Here we identify coefficient α by comparing the quantum transverse susceptibility with that semiclassical result [88, 91]. We start with the determination of quantum susceptibility which can be connected with our local spin green's function $Y^{\mathbf{Q}}$ as follows

$$Y^{\mathbf{Q}}_{+-}(\omega) = i\theta(t) < [S^{\dagger}_{\mathbf{Q}}(t), S^{-}_{-\mathbf{Q}}(0)] >= iY^{\mathbf{Q}}(\omega). \tag{6.36}$$

In order to establish the connection with the semiclassical linear response we suppose that $Y^{\mathbf{Q}}_{+-}$ is of the form

$$\frac{1}{Y^{\mathbf{Q}}_{+-}(\omega)} = -\frac{1}{4S}[\omega - \omega_0(\omega, \mathbf{Q}) + i\alpha(\omega, \mathbf{Q})\omega]. \tag{6.37}$$

where α is the Gilbert damping we wish to determine. Now by solving Eq. (6.37) with respect to α we find that Gilbert damping is defined by the relation

$$\alpha(\omega \to 0, \mathbf{Q}) = -4S \lim_{\omega \to 0} \partial_{\omega} Im \left(\frac{1}{Y^{\mathbf{Q}}_{+-}(\omega)} \right), \tag{6.38}$$

where since we emphasized on the uniform limit we set $\mathbf{Q} = 0$ into above relation.

We derive now the Gilbert damping within RPA. Using definition (6.36) and RPA result (6.9) we obtain that the inverse susceptibility of the system is given by

$$\frac{1}{Y^{\mathbf{Q}}_{+-}(\omega)} = -\frac{1}{4S}\left(\omega - \frac{\Delta p}{2S} + \frac{\Delta^2}{2S(2\pi)^2 C_{Mn}} \int \frac{d^2\nu}{\omega + \varepsilon_{\nu-\mathbf{Q}} - \varepsilon_{\nu} + \Delta + i\Gamma}\right) \tag{6.39}$$

where Γ is the intrinsic damping of the system coming from the spin–flip excited states. After a straightforward application of definition (6.38) we obtain that Gilbert damping α^{RPA} within RPA to the uniform limit is determined by

$$\alpha^{RPA} = \frac{p}{2S}\left[\frac{\frac{\Gamma}{\Delta}}{1 + (\frac{\Gamma}{\Delta})^2} - \frac{(\frac{\Gamma}{\Delta})^3}{[1 + (\frac{\Gamma}{\Delta})^2]^2}\right] \tag{6.40}$$

Note that the second term in Eq. (6.40) is a $O(\frac{\Gamma}{\Delta})^3$ contribution to Gilbert damping. The value of the ratio $\frac{\Gamma}{\Delta}$ quoted in the literature[89] is 0.1 and therefore the

third ordered term is a small contribution which can be neglected. In this way the mean–field result[89] is reproduced. Moreover Gilbert damping within RPA is of the first order in $1/S$ expansion, while correlations contribute to higher order.

Let us continue with the effects of correlations on Gilbert damping. The inverse susceptibility now becomes

$$\frac{1}{Y^{\mathbf{Q}}_{+-}(\omega)} = -\frac{1}{4S}\Bigg[\omega - \frac{\Delta p}{2S} + \frac{\Delta^2}{2S(2\pi)^2 C_{Mn}}\int \frac{d^2\nu}{\omega + \varepsilon_{\nu-\mathbf{Q}} - \varepsilon_\nu + \Delta + i\Gamma} - \frac{\Delta^2}{4S^2(2\pi)^2 C_{Mn}}\int d^2\vec{\alpha} H^{\mathbf{Q}}_\alpha \Big(1 - \frac{\Delta}{\omega + \varepsilon_{\alpha-\mathbf{Q}} - \varepsilon_\alpha + \Delta + i\Gamma}\Big)\Bigg], \quad (6.41)$$

Here the first line gives the RPA result, while correlations are introduced by the second line. In order to treat correlations at $O(1/S)$ we set

$$H_\alpha = \frac{1}{(2\pi)^2 C_{Mn}}\int_\mu \frac{d^2\mu}{\omega + \varepsilon_{\nu-\mathbf{Q}} - \varepsilon_\nu + \Delta + i\gamma}, \quad (6.42)$$

where γ is an additional phenomenological intrinsic damping of Fermi sea pair excitations. It is reasonable to assume that γ cannot be as large as Γ which is about 10% of the Zeeman energy Δ. A typical value of spin$\uparrow$–$\downarrow$ pair's energy is Δ while the electron–hole upper bound energy is about $\frac{\Delta p}{2S} \simeq 0.05\Delta$ for the hole doping of interest here. Therefore a consistent choice for electron–hole pair damping is $\gamma = 0.005\Delta$. From now on we use dimensionless intrinsic damping parameters $\bar{\Gamma} = \frac{\Gamma}{\Delta} \simeq 0.1$ and $\bar{\gamma} = \frac{\gamma}{\Delta} \simeq 0.005$. Within that assumptions, we use definition (6.38) to derive a beyond mean–filed result for the Gilbert damping. In this way we assess the role of the carrier–localized spin scattering process, treated at $1/S$ order. After some algebra we obtain the result

$$\alpha = \alpha^{RPA} + \frac{\Delta}{4S^2}\Bigg[\frac{\bar{\Gamma}^2 - 1}{(\bar{\Gamma}^2+1)^2} I_2(\omega \to 0) - \frac{\Delta\bar{\Gamma}^2}{\bar{\Gamma}^2+1}\partial_\omega I_2(\omega \to 0) + 2\frac{\bar{\Gamma}}{(\bar{\Gamma}^2+1)^2} I_3(\omega \to 0) - \frac{\Delta\bar{\Gamma}}{\bar{\Gamma}^2+1}\partial_\omega I_3(\omega \to 0)\Bigg], \quad (6.43)$$

where the integral I_2, I_3 and their derivatives with respect to frequency ω are as

follows

$$I_2(\omega \to 0) = \frac{\bar{\gamma}}{(2\pi)^4 C_{Mn}^2 \Delta} \int\int d^2\alpha d^2\nu \frac{1}{(\varepsilon_\nu - \varepsilon_\alpha)^2 + \bar{\gamma}^2}, \tag{6.44}$$

$$I_3(\omega \to 0) = \frac{\bar{\gamma}}{(2\pi)^4 C_{Mn}^2 \Delta} \int\int d^2\alpha d^2\nu \frac{\varepsilon_\nu - \varepsilon_\alpha}{(\varepsilon_\nu - \varepsilon_\alpha)^2 + \bar{\gamma}^2}, \tag{6.45}$$

$$\partial_\omega I_2(\omega \to 0) = -\frac{2\bar{\gamma}}{(2\pi)^4 C_{Mn}^2 \Delta^2} \int\int d^2\alpha d^2\nu \frac{\varepsilon_\nu - \varepsilon_\alpha}{[(\varepsilon_\nu - \varepsilon_\alpha)^2 + \bar{\gamma}^2]^2}, \tag{6.46}$$

$$\partial_\omega I_3(\omega \to 0) = \frac{\bar{\gamma}}{(2\pi)^4 C_{Mn}^2 \Delta^2} \int\int d^2\alpha d^2\nu \frac{\bar{\gamma}^2 - (\varepsilon_\nu - \varepsilon_\alpha)^2}{[(\varepsilon_\nu - \varepsilon_\alpha)^2 + \bar{\gamma}^2]^2}. \tag{6.47}$$

6.3 Numerical results

We start the presentation of our numerical results with the long–wavelength magnon dispersion in a 2D system. Spin–wave stiffness is defined by the real part of magnon's pole. The intrinsic damping rates γ and Γ affects trivially the stiffness since the dependence on carrier doping is independent of their values. For simplicity we have set $\gamma = 0$ and $\Gamma = 0$ in the derivation of the stiffness. Fig. (6.1) shows our numerical result within the approximations discussed in Sec. (6.2.3). Spin–wave stiffness is plotted within RPA Eq. (6.29), by using Eq. (6.34) as well as to second order in the $O(1/S)$ expansion, for a variety of parameters J and C_{Mn} quoted in the literature. Note also that the stiffness constant is measured in units of the constant $\varepsilon_0 = \frac{\hbar^2}{2m_h}$. First of all, we note that the correlated result does not deviate strongly from $O(1/S^2)$ expansion result. The latter is expected, since within the low doping regime the $1/S$ expansion is in good agreement with the full three–body result as showed in the case of the manganites. We note that this deviation becomes maximum for a low Mn–concentration $(C_{Mn}) = 1nm^{-2}$ and for large spin–exchange interaction $(J = 150meV)$. However, even that difference is small enough to conclude that $1/S$ expansion describes well the long–wavelength spin–wave dynamics. Moreover, a comparison between RPA and correlated results shows a strong deviation, indicating the importance of the correlations. Spin–wave stiffness with respect to the hole doping p exhibits the following behavior. The latter is governed by the interplay between two factors; the local antiferromagnetic coupling between Mn–spins with the valence–band carriers and the kinetic energy of itinerant spins. On the other hand, for intermediate hole dopings an increase in stiffness is observed. For a particular J there is a hole doping p_M where the stiffness becomes maximum and thus ferromagnetic order is well established. For dopings higher than p_M the antiferromagnetic interaction between impurity spins and itinerant carriers starts to suppress the stiffness which finally becomes negative. The latter indicates that ferromagnetism is impossible for very high dop-

ings. This behavior of stiffness can be understood is this way. Due to the kinetic energy degree of freedom the itinerant–carrier spin is fully polarized. This mediates long–range ferromagnetic order via the interaction H_{exch} with the localized spins for intermediate hole–dopings. The latter is consistent with the increase in the spin–wave stiffness within these dopings. On the hand, for higher dopings, itinerant–carrier spin polarization is destroyed by double–occupancy effects and therefore ferromagnetic order is suppressed. We discuss now the effect of correlations on stiffness. Note that the deviation between RPA and correlated results is being pronounced when hole doping is increasing. More precisely correlations shift p_M towards higher dopings as compared with the RPA results. Therefore correlations widen the doping regime where ferromagnetism is possible. For example, the increase of stiffness for an experimentally relevant doping $p = 0.1$ and for $J = 150meV, C_{Mn} = 3nm^{-2}$, see Fig. (6.1a), exceeds the RPA result by 100%. This deviation weakens for lower impurity densities and becomes about 40% for $C_{Mn} = 1nm^{-2}$ at p_M. On the contrary by comparing Figure (a) with (b) and (c) with (d) we understand that correlations play a more important role for lower strength of exchange interaction J. The effect of lowering J is not so strong as that of the increasing impurity density. However the lower value of the local magnetic exchange interaction strength is in better agreement with recent experimental estimations for J. However the effects of correlations remain strong even for that low density of Mn impurities. We can view that result considering the critical temperature of magnetic semiconductors. As we mentioned T_C is regulated by long–wavelength excitations and is proportional to the stiffness. Therefore a 100% increase in spin–wave stiffness can be translated to a large enhancement in the critical temperature. We conclude that correlations enhances T_C of diluted magnetic semiconductors by a significant factor which in some cases can reaches 100%. Moreover our model predicts that enhanced T_C can be obtained by increasing carrier doping to our sample. Although a calculation of critical temperature is rather challenging a rough estimation of T_C can be obtained by using our $T = 0$ result of stiffness D. By assuming that the total spin of the ground state equals the number of magnons at a particular temperature[76] one obtains the simple formula

$$k_B T_C = \frac{2S+1}{6} D p_C^2 , \tag{6.48}$$

where p_C is the Debye cut–off wave vector given by (6.28). Using that formula, we obtain upper bounds for T_C. For experimental relevant parameters $J = 100meV, C_{Mn} = 1 - 3nm^{-2}$ we obtain that within the RPA T_C can not be higher than $100K$ whereas the correlated bound is $200K$. We remind you again that result (6.48) sets only an upper bound to critical temperature and cannot be used to determine the exact T_C of a DMS system such as the III(Mn)V. However, its evaluation to our case gives a quantitatively assessment of the correlation ef-

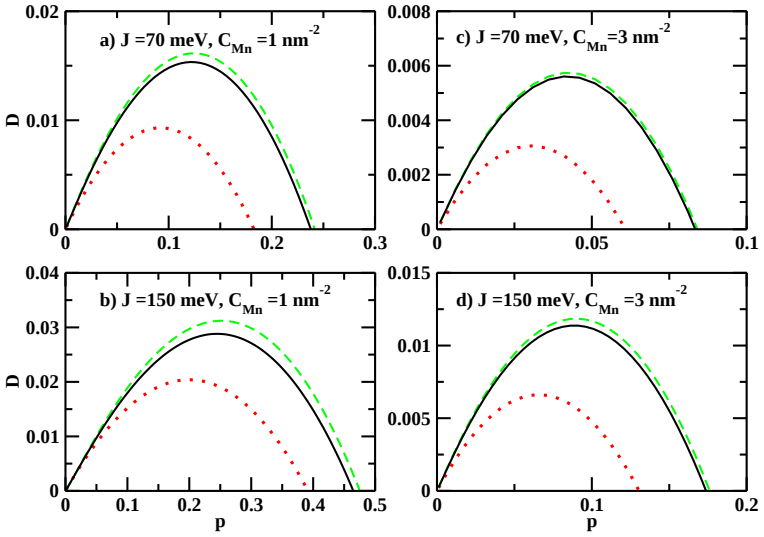

Figure 6.1: Spin–Wave stiffness as a function of hole doping and for different J and C_{Mn}. Solid line: The correlated result of Eq. (6.34), Dotted line: The RPA and Dashed line: The $O(1/S^2)$ result.

fects on the long–range ferromagnetic order. Moreover, this result was obtained within a simple two–band model. In ref. [75], it was shown that relevant results can be obtained by employing a six–band model. We show here that even within the simple two–band approach a significant enhancement of critical temperature can be predicted, while by extending our calculations to a six–band model a more robust description of the effects of correlations on T_C can be derived.

Having discussed the role of correlations on the real part of the magnon's pole (spin–wave spectrum) we continue now with the effects on the relaxation of that excited states. As we discussed in Sec. (6.2.4) the long–range magnetization dynamics is well described by the phenomenological Gilbert coefficient α. Here we present our numerical results concerning coefficient α within RPA, and also we discuss the effects of correlations treated perturtatively in $1/S^2$ order. The latter expansion, which allows us to derive results for the correlated α in a closed form, is consistent with our previous discussion where showed that the spin–wave stiffness is well approximated by an up to second order expansion in $1/S$. The Gilbert damping coefficient is usually plotted as a function of intrinsic damping Γ. We fix now the Mn–impurity density as $C_{Mn} = 1nm^{-2}$ and exchange interaction as $J = 150meV$. For these values we see in Fig. (6.1a) that ferromagnetic order is possible for a wide range of hole–dopings while the effects of J are fairly strong.

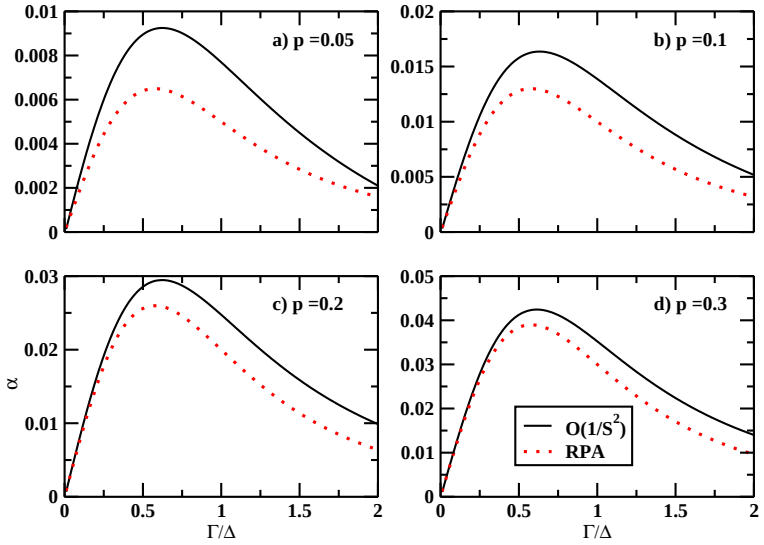

Figure 6.2: Gilbert damping for different hole dopings and for $J = 150meV, C_{Mn} = 1nm^{-2}$. Solid line: $1/S^2$ result, Dotted line: RPA

In order to examine the role of hole–doping on α, we fix now the parameters J, C_{Mn} to these values and plot the Gilbert damping coefficient as a function of Γ in Fig. (6.2). First of all, we observe that, in general, correlations enhance the the Gilbert damping as compared with RPA results. We note that within the very low doping regime ($p \simeq 0.05$) the deviation between the mean–field result (RPA) and the correlated one is large. For example, at the value of Γ that α becomes maximum, correlations increase the damping by a factor about 35% of the RPA value. For higher values of the intrinsic damping the deviations diminish. Examining Fig. (6.2) we note that the effects of correlations on the damping is lowering as the hole–doping increases. For a rather high hole–doping, $p = 0.3$, deviation is about 10% of the RPA result, therefore still significant. However the absolute difference between RPA and correlated result $\alpha^{RPA} - \alpha^{CORR}$ as a function of p is relatively increasing. This difference for $p = 0.05$ is about 0.003 whereas for $p = 0.3$ becomes 0.005 and therefore is enhanced. Since Gilbert damping is decreasing for lower dopings, the deviation as percentage of RPA values becomes larger and consequently the role of correlations is pronounced.

We continue now with the role of Mn–density. Fig. (6.3) shows the Gilbert damping as a function of hole–doping and for different impurity dopings. First of all, we note that the RPA result Eq. (6.40) is independent of Mn–doping. The Gilbert damping within RPA is a function only of ratio $p = \frac{C_h}{C_{Mn}}$. More precisely,

α^{RPA} displays an increasing behavior with p. On the other hand, the correlated result is explicitly affected by C_{Mn} due to integrals (6.44). It is clear that at the extreme limits $p = 0$ and $p = 1$ these integrals vanish since either integration over ν or over α is zero. Therefore, the correlated damping equals the RPA result when hole density is almost zero or is equal to the Mn density. Let us see what happen for intermediate values of p. We note that correlations enhance a as expected. The enhancement becomes large for a low impurity density ($C_{Mn} = 0.5nm^{-2}$). The deviation of the RPA result is rather constant for a wide range of dopings and is about $\Delta\alpha \simeq 0.015$. This deviation becomes more significant within the low doping regime where damping is low. For example, for $p = 0.1$ the correlated damping is two times larger than the RPA result whereas the corresponding result for a high doping, $p = 0.8$, is about 20% of the RPA value. Apart from that significant quantitative contribution of correlations on Gilbert damping we note also that correlations destroy the linear behavior of α with respect to p. More significant is the fact that the non–linear trend occurs within the experimental relevant regime of low hole–dopings. The latter result proves the importance of carrier–localized spin scattering to the relaxation dynamics of elementary spin–wave excited states. The mean–field (RPA) result fails completely to describe the spin–wave damping. The role of Mn density becomes clear for a higher value ($C_{Mn} = 1nm^{-2}$). In this case damping is well described by the RPA result since the contribution of the correlations is rather negligible. Moreover the non–linear behavior weakens. We conclude that correlations effect qualitatively spin–wave damping within the low impurity doping regime.

6.4 Conclusion

In conclusion, we presented here an application of the green's function method to the magnetic excitation spectrum of the III(Mn)V diluted magnetic semiconductors. We employed a simplified two–band description to model valence–band holes while we neglect spin–orbit coupling and band–structure effects. Our purpose here is the study of the many–body correlations, beyond the mean field RPA approach, expressed by the scattering of a magnon by an electron–hole pair. By trying to describe correlation effects on spin–waves using a variational method similar to that in the case of manganites we arrived to the conclusion that a better treatment must be used since Goldstone theorem of excited states was not satisfied. The ground state of the III(Mn)V ferromagnetic semiconductors of interest here is typically approximated by the Hartree–Fock variational state, obtained by treating the localized Mn spins as classical. Nevertheless, that assumption within the variational approach leads to the violation of the Goldstone theorem as mentioned

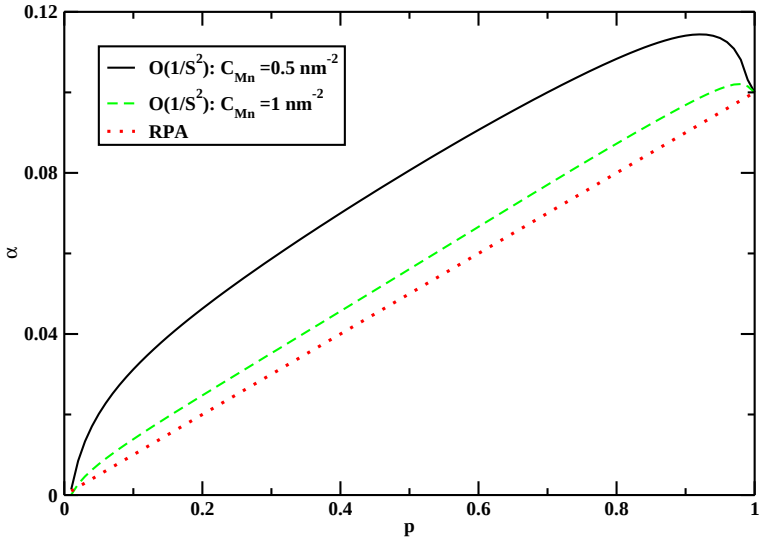

Figure 6.3: Gilbert damping as a function of hole doping for different Mn–densities and for $J = 150meV, \bar{\Gamma} = 1, \bar{\gamma} = 0.005$.

above. This is due to the fact that variational theory is rather sensitive to the initial choice of the reference state employing to excite magnons. Fortunately, the calculations we presented here derive a Goldstone–mode branch that describes well the spin–wave excitation spectrum. This is the great advantage of green's function method in comparison with the variational treatment; the Green's functions describe, by definition, the excitation spectrum and therefore any ground state contributions are removed. Moreover the analysis of the Chapters (4) and (5) proves that green's function method reproduce the variational results in the manganites. Therefore any result that is recovered by our variational treatment can be also re–derived by green's function method. In this way we are able to treat many–body correlation perturbatively in $1/S$ expansion. We show here that the carrier–localized spin scattering approximation is in very good agreement with the $1/S^2$ results. This justifies our assumption to neglect the three–body carrier–fermi pair scattering process. The effects of correlations on long–wavelength spin–wave excitations is shown to be of significant importance. We show that the enhancement on spin–wave stiffness due to correlations can reach a strong value such as 100% of RPA result. The connection between spin–wave stiffness and critical temperature allows us to conclude that RPA underestimates strongly T_C. The latter results are obtained for parameters relevant to these estimated experimentally, indicating the importance of the local correlations to the spin–wave dynamics.

Furthermore, although, the effects of carrier–localized spin scattering process on the damping of magnetic semiconductors is relatively weaker as compared to the effects on the stiffness, we show here that their role is of major importance. We found a $30-10\%$ increase on Gilbert damping for a variety of parameters relevant to experiments. Most significant is the effect on Gilbert damping appeared within the very low impurity doping regime where the linear p–dependence is altered for experimentally relevant hole–dopings. This proves that the carrier–localized spin scattering process studied here plays also a significant role on the long–wavelength spin–wave dynamics of DMS.

6.5 Closing remarks

The work presented in this chapter is highly prospective. As far as the first part of this dissertation is concerned we believe that our results are rather conclusive since there are little remaining works to do for the case of manganites apart from including bandstructure effects and orbital degrees of freedom. Nevertheless, there seems to be a wide range of open questions regarding the diluted magnetic semiconductors studied here. First of all, that our results are obtained in a simplified two–band model without taking into account band–structure effects and spin–orbit coupling indicates two facts. Although a six–band approach seems to be rather realistic we obtain here qualitatively similar with that model results. Moreover our model can be extended in a way that incorporates band–structure and spin–orbit effects. That can be achieved by employing the so–called Kohn–Luttinger Hamiltonian to model valence band holes of DMS. This is a potential work that will improve the reliability of our model. Furthermore the three–body contributions to the spin–wave damping is also an open issue to be study elsewhere. Finally our study is relevant to the ultrafast relaxation dynamics studied by ultrafast spectroscopy. That opens another potential pathway for future extension of our work with plenty of experimental results relevant to theoretical study.

Chapter 7

Numerical methods

7.1 Introduction

In this chapter we present the numerical methods we use in this dissertation. The numerical problems we have to deal with can be divided in two general categories. The first and main one is the solving of a system of variational equation. This kind of problem can be solved by applying an iterative method Finally, the second category of numerical problems also important with the first one is the root finding of a single equation. Of course, this problem can be solved by using the iterative method but in some cases this is not the appropriate way of deal with that problem.

7.2 Iterative method

Our method is based on the iterative method of solving linear equations or linear sets of equations. Firstly, let us suppose a problem which consists of a single equation of the general form:

$$x = f(x) \tag{7.1}$$

We do not suppose any particular form of the function $f(x)$ in the rhs of the equation. Let us notice that the RPA equation for the magnon energy has exactly the form (7.1). In addition, this form applies for the finding of the Fermi energy of a system with N_e itinerant carriers, which is also an unknown parameter of our problem and can be determined only numerically. A iterative solution of Eq. (7.1) demands to rewrite the equation in the form:

$$x_{i+1} = f(x_i) \tag{7.2}$$

Now, using an initial *guess* for x_0 one can take an *improved* value for x. By successively replacing x_i by its *improved* value x_{i+1} in rhs of Eq. (7.2) and examining the difference D:

$$D = \mid x_i - x_{i+1} \mid \tag{7.3}$$

we can achieve full convergence of x to the solution of equation (7.1) until the desired tolerance D. In order to improve the speed of convergence we can generalize Eq. (7.2) so that each step x_{i+1} is replaced by a mixture of its value and some of the previous step's results:

$$x_{i+1} \rightarrow x'_{i+1} = (1 - w_1 - w_2)x_{i-1} + w_1 x_i + w_2 x_{i+1} \cdots \tag{7.4}$$

This formula is known as *Anderson mixing* and the value of parameters w_i varies from 0 to 1. Although, we can include a large number of previous x_i's in the above mixing, the larger number of parameters w_i used here is usually 2. Therefore we mix two *old* x_{i+1} with the *improved* one. Notice that for $w_2 = 1$ and $w_1 = 0$ we return to the unmixed formula. Also when convergence is achieved formula 7.4 is satisfied.

The above strategy can be extended to a system of equations, which is a more interesting problem. Firstly, let us note that we do not gain any speed of convergence by applying the Anderson mixing in the equation of magnon energy, because of the large number of equations. Thus we use the equation of energy in its simple unmixed form:

$$\omega_{\mathbf{Q}} = f^0(X, \Psi, \cdots) \tag{7.5}$$

where f^0 is a known function which depends only on the variational amplitudes X, Ψ included in the system of equations. For example, within $\Phi = 0$ approximation the f^0 is a function only of X and Ψ. Now, the Anderson mixing is applied at each equation of the variational amplitudes. The equation of $X_\nu^{\mathbf{Q}}$, for a particular value of momentum $\mathbf{Q}$ and ν is written:

$$X_{i+1} = (1 - w_1^1 - w_2^1)X_{i-1} + w_1^1 X_i + w_2^1 f^1(\omega_{\mathbf{Q}}, X_i, \cdots) \tag{7.6}$$

We apply a similar transformation on all equations of the system, using a different set of mixing parameters w_i^k, $i = 1, 2$ for each equation.

The optimal choice of w_i^k parameters can be predicted analytically in some simple problems. In our complex problem the only choice we have is to test some set of values performing the iterative method in a system with a small number of sites, where convergence is fast. Afterward, we use the optimal set of these parameters in order to solve our full system of equation. We have tested a variety

of values for parameters w_i and found that the optimal set of the relaxation parameters is $w_i \simeq 0.7 - 0.8$. Using these values we can achieve convergence within about 10-20 iterations per lattice momentum $\mathbf{Q}$.

The next step is the choice of an initial guess for the variational amplitudes and for energy. It is appropriate to use the RPA results as our initial values of energy and amplitude $X_\nu^{\mathbf{Q}}$. Within this assumption the rest of the amplitudes are set equal to zero. It is better to use the above guess than random initial values of the unknown parameters as in this way we lead the iterative procedure to the solution of the system. Another choice of initial guess will cause slow convergence or even divergence of the solution. The iterative solution of the system of variational equation for any momentum $\mathbf{Q}$ within the Brillouin zone consists of the steps:

1. Calculation of a new value energy ω_{NEW} by using Eq. (7.5) and the initial guess of the amplitudes.
2. Using the energy ω_{NEW} we calculate improved values the the amplitudes using their equations in the mixed form.
3. Using again Eq. (7.5) and the improved amplitudes from the last step, we calculate a second value for energy ω'_{NEW}.
4. We apply the criterion of convergence $\mid (\omega'_{NEW} - \omega_{NEW}) \mid \leq TOL$, where TOL is the tolerance we ask the program to calculate the magnon energy. If this criterion is satisfied the program stops, otherwise the steps 1-4 are repeated until the convergence of magnon energy within the desired tolerance.

We repeat the above procedure for any momentum $\mathbf{Q}$ and along any direction within the Brillouin zone.

7.3 Calculation of Fermi energy

Regardless to say that a single equation problem such the above can be easily solved by another way. Eq. 7.1 can be written:

$$x - f(x) = 0 \tag{7.7}$$

In this way one can solve the problem by finding the roots of the above equation using, for instance, the brent's method. We use this strategy in order to calculate the Fermi energy of a system with n concentration of itinerant carriers. In a particular temperature T the concentration n of itinerant carriers is defined as:

$$n = \frac{1}{N} \sum_{\mathbf{k}} \frac{1}{e^{(\varepsilon_k - \varepsilon_F)/k_B T} - 1} \tag{7.8}$$

where ε_F is the Fermi energy of the system. For a known Fermi energy and temperature one can calculate the concentration n using the above formula. However this is not the usual problem since these parameters are usually external constants and we give the values by hand. In general, what we do not known in such numerical problems is the Fermi energy which depends on the band structure and the temperature. In order to calculate the Fermi energy we rewrite the Eq. (7.8) in the form:

$$n - \frac{1}{N}\sum_{\mathbf{k}} \frac{1}{e^{(\varepsilon_k - x)/k_B T} - 1} = 0, \tag{7.9}$$

Now becomes clear that this relations is of the form 7.7 and therefore can be solved by using the brent's method of root's finding.

7.4 Numerical integration

One of the main numerical problems throughout this dissertation is the numerical calculation of multiple integrals. The usual treatment of the calculation of such integrals is by using the Monte Carlo method. These methods are more sufficient for high dimension integrals as compared to a quadratic method such as the Simpson's Rule. However, the integrals we deal with here is usually 3D or 2D integrals. The evaluation of such integrals by Monte Carlo method is not adequate. For this reason, the quadratic formula of Simpson's rule is used in order to numerically evaluate the high dimension integrals. Simpson's rule for a simple 1D integral is:

$$\int_a^b f(x)dx = \frac{h}{6}\sum_{i=1}^{N-1}[f(x_i) + 4f(x_i + \frac{h}{2}) + f(x_i + h)], \tag{7.10}$$

where h is the step length, given by $h = \frac{b-a}{N}$. In order to apply that formula to a 2D integral it is convenient to rewrite (7.10) as follows:

$$\int_a^b f(x)dx = \frac{h}{6}\sum_{i=1}^{N-1}\sum_{l=1}^{3} Z_l f(x_i + m_l h), \tag{7.11}$$

where the matrices Z_l and m_l are:

$$\mathbf{Z} = \begin{pmatrix} 1 \\ 4 \\ 1 \end{pmatrix}, \mathbf{m} = \begin{pmatrix} 0 \\ 1/2 \\ 1 \end{pmatrix}.$$

Now in order to derive a formula for the 2D integral we apply Simpson's formula (7.11) for every variable x, y of integration. In this way we obtain the formula

$$\int_a^b \int_c^d f(x,y)dxdy = \frac{h_X h_Y}{36} \sum_{i,j=1}^{N-1} \sum_{l,l'=1}^{3} \mathbf{Z}_l \mathbf{Z}_{l'} f(x_i + \mathbf{m}_l h_X, y_j + \mathbf{m}_{l'} h_Y), \quad (7.12)$$

which evaluates a 2D integral using the Simpson's rule.

Chapter 8

Appendices

8.1 Variational theory

In this section we introduce the variational theory we adopt in the chapters 2 and 3 in order to determine the spinwave dispersion. Our starting point is the state which describes a magnon with lattice momentum $\mathbf{Q}$. This state $|\mathbf{Q}\rangle$ is of the general form

$$|\mathbf{Q}\rangle = M^{\dagger}_{\mathbf{Q}}|F\rangle, \tag{8.1}$$

where the operator $M^{\dagger}_{\mathbf{Q}}$ excites the magnon from the reference state $|F\rangle$. The state $|F\rangle$ is chosen to be the fully polarized ferromagnetic state where all itinerant and localized spins are parallel. So that its energy is $E_G = \sum_{\mathbf{k}} \varepsilon_{\mathbf{k}} + \frac{SJn}{2}$. Note that this state is an exact eigenstate of the double–exchange hamiltonian. The later can be easily obtained by acting with the Hamiltonian H to $|F\rangle$, then we find $H|F\rangle = E_G|F\rangle = E$. As we saw the operator $M^{\dagger}_{\mathbf{Q}}$ can be generally written in the form

$$M^{\dagger}_{\mathbf{Q}} = \sum_i c_i M^{\dagger}_i = f(\{c_i\}), \tag{8.2}$$

where $\{c_i\}$ is the set of variational variables. This set, in general complex number, contains, for example, the amplitudes $X^{\mathbf{Q}}_{\mathbf{k}}$, $\Psi^{\mathbf{Q}}_{\alpha\nu}$ and $\Phi^{\mathbf{Q}}_{\alpha\mu\nu}$. The energy $E_{\mathbf{Q}}$ of the system is determined by the mean value of the hamiltonian, therefore:

$$E_{\mathbf{Q}} = \frac{\langle \mathbf{Q}|H|\mathbf{Q}\rangle}{\langle \mathbf{Q}|\mathbf{Q}\rangle}, \tag{8.3}$$

where we divide with $\langle \mathbf{Q}|\mathbf{Q}\rangle$ since the magnon state is not normalized. Substituting 8.2 in 8.3 we find the magnon energy:

$$E_{\mathbf{Q}} = \frac{\sum_{ij} c_i^* c_j \langle F|M_i H M_j^\dagger|F\rangle}{\sum_i |c_i|^2} \tag{8.4}$$

as a function of the set of variational variables. Subsequently, in the framework of the variational theory, minimization of energy demands:

$$\frac{\partial E_{\mathbf{Q}}}{\partial c_i} = 0 = \frac{\partial E_{\mathbf{Q}}}{\partial c_i^*}. \tag{8.5}$$

It can be easily proven that by satisfying one of the above equalities the other is automatically satisfied. If we select the second one and take into account that only $\langle \mathbf{Q}|$ depends on c_i^*, then the derivation of that relation gives:

$$\left(\frac{\partial\langle \mathbf{Q}|}{\partial c_i^*} H|\mathbf{Q}\rangle - \frac{\langle \mathbf{Q}|H|\mathbf{Q}\rangle}{\langle \mathbf{Q}|\mathbf{Q}\rangle}\frac{\partial\langle \mathbf{Q}|}{\partial c_i^*}|\mathbf{Q}\rangle\right)\frac{1}{\langle \mathbf{Q}|\mathbf{Q}\rangle} = 0. \tag{8.6}$$

The derivative of the magnon state $\langle \mathbf{Q}|$ is

$$\frac{\partial\langle \mathbf{Q}|}{\partial c_i^*} = \langle F|\frac{\partial}{\partial c_i^*} M_{\mathbf{Q}}^\dagger = \langle F|M_i^\dagger. \tag{8.7}$$

Therefore substituting 8.7 into 8.6 we obtain:

$$\frac{\langle F|M_i H|\mathbf{Q}\rangle}{\langle \mathbf{Q}|\mathbf{Q}\rangle} - \frac{\langle \mathbf{Q}|H|\mathbf{Q}\rangle}{\langle \mathbf{Q}|\mathbf{Q}\rangle^2}\langle F|M_i H|\mathbf{Q}\rangle = 0, \tag{8.8}$$

after using 8.3 we find:

$$\langle F|M_i H|\mathbf{Q}\rangle - E_{\mathbf{Q}}\langle F|M_i H|\mathbf{Q}\rangle = 0, \tag{8.9}$$

which by substituting the magnon state $|\mathbf{Q}\rangle$ from Eq. 8.1 yields:

$$\langle F|M_i\left[H, M_{\mathbf{Q}}^\dagger\right]|F\rangle = (E_{\mathbf{Q}} - E_F)\langle F|M_i M_{\mathbf{Q}}^\dagger|F\rangle, \tag{8.10}$$

where we use the commutator $[H, M_{\mathbf{Q}}^\dagger] = H M_{\mathbf{Q}}^\dagger - M_{\mathbf{Q}}^\dagger H$. Since we are interested here in the excitation spectrum of magnon it is more convenient to define magnon energy as $\omega_{\mathbf{Q}} = E_{\mathbf{Q}} - E_G$. Notice also that we set $\hbar = 1$, thus energy is the same with frequency in this system of units. In this way the variational equation 8.10 becomes:

$$\langle F|M_i\left[H, M_{\mathbf{Q}}^\dagger\right]|F\rangle = \omega_{\mathbf{Q}}\langle F|M_i M_{\mathbf{Q}}^\dagger|F\rangle, \tag{8.11}$$

where for $\mathbf{Q} = 0$ we have $\omega_{\mathbf{Q}} = 0$ as must be for Goldstone modes. The later simply means that at zero momentum $\mathbf{Q}$ the excitation energy is also zero. Now we can determine the equation which governs a particular variational amplitude by substituting the corresponding component M_i in the above equation. In this way a coupled system of variational equations is obtained. The procedure we use here is the following. Firstly, one has to determine the commutator $\left[H, M^{\dagger}_{\mathbf{Q}}\right]$ appeared in the l.h.s. of Eq. 8.11. The results of that calculation is presented in the next appendices. Then by acting with M_i and taking expectation values in $|F\rangle$ state we obtain the variational equation for amplitude c_i.

8.2 General properties of operators

In this Appendix we present a list of some useful relations regarding the localized spin and electron operators appearing in this thesis.

The localized spin operators in momentum space satisfies the useful relations:

$$S^z_q|HF\rangle = \sqrt{N}S\delta_{q,0}|HF\rangle \tag{8.12}$$

$$[S^+_q, S^-_{q'}] = \frac{2}{\sqrt{N}}S^z_{q+q'}, \tag{8.13}$$

$$(S^-_Q)^{\dagger} = S^+_{-Q} \tag{8.14}$$

Now we present some useful properties regarding commutation and anticommutation relations of general operators.

$$[[H, A], B] + [[B, H], A] + [[A, B], H] = 0, \tag{8.15}$$

holds for any operators A and B,

$$[B, CD] = \{B, C\}D - C\{B, D\} \tag{8.16}$$

$$[AB, C] = A[B, C] + [A, C]B \tag{8.17}$$

$$[AB, C] = A\{B, C\} - \{A, C\}B \tag{8.18}$$

8.3 Calculation of commutators

In this section we present the results for the commutators appeared in our calculations. We choose not to incorporate this calculations in the main body of the dissertation due to complexity of those commutators.

We start with the calculation of the commutator appeared in the variational calculations of chapter 2 and 3. This commutator can be written as follows:

$$[H, M^{\dagger}_{\mathbf{Q}}] = [K, M^{\dagger}_{\mathbf{Q}}] + [H_{exch}, M^{\dagger}_{\mathbf{Q}}] + [H_U, M^{\dagger}_{\mathbf{Q}}] + [H_{AF}, M^{\dagger}_{\mathbf{Q}}], \tag{8.19}$$

where each one of the above commutators is:

$$\begin{aligned}
[K, M^{\dagger}_{\mathbf{Q}}] &= \frac{1}{\sqrt{N}} \sum_{\nu} \left(\varepsilon_{\nu+\mathbf{Q}} - \varepsilon_{\nu}\right) X^{\mathbf{Q}}_{\nu} c^{\dagger}_{\nu+\mathbf{Q}\uparrow} c_{\nu\uparrow} \\
&\quad + \sum_{\alpha\nu} \Psi^{\mathbf{Q}}_{\alpha\nu} \left(\varepsilon_{\alpha} - \varepsilon_{\nu}\right) S^{\dagger}_{\mathbf{Q}+\nu-\alpha} c^{\dagger}_{\alpha\uparrow} c_{\nu\uparrow} \\
&\quad + \frac{1}{2\sqrt{N}} \sum_{\alpha\mu\nu} \Phi^{\mathbf{Q}}_{\alpha\mu\nu} \left(\varepsilon_{\mathbf{Q}+\mu+\nu-\alpha} - \varepsilon_{\nu} + \varepsilon_{\alpha} - \varepsilon_{\mu}\right) c^{\dagger}_{\mathbf{Q}+\mu+\nu-\alpha\downarrow} c_{\nu\uparrow} c^{\dagger}_{\alpha\uparrow} c_{\mu\uparrow},
\end{aligned} \tag{8.20}$$

$$\begin{aligned}
[H_{exch}, M^{\dagger}_{\mathbf{Q}}] &= \left(\frac{Jn}{2} - \frac{J}{2N} \sum_{\nu} X^{\mathbf{Q}}_{\nu} + \frac{J}{2N} \sum_{\alpha\nu} \Psi^{\mathbf{Q}}_{\alpha\nu}\right) S^{-}_{\mathbf{Q}} \\
&\quad + \frac{JS}{\sqrt{N}} \sum_{\nu} \left(-1 + X^{\mathbf{Q}}_{\nu} - \sum_{\alpha} \Psi_{\alpha\nu}\right) c^{\dagger}_{\nu+\mathbf{Q}\downarrow} c_{\nu\uparrow} \\
&\quad + \frac{J}{2N} \sum_{\beta\mu} \left(\sum_{\alpha} \Psi^{\mathbf{Q}}_{\alpha\mu} - \sum_{\nu} \Psi^{\mathbf{Q}}_{\beta\nu} + N_e \Psi^{\mathbf{Q}}_{\beta\mu} + 1 - X^{\mathbf{Q}}_{\mu} - \sum_{\nu} \Phi^{\mathbf{Q}}_{\mu\nu\beta}\right) \times \\
&\qquad S^{-}_{\mathbf{Q}+\mu-\beta} c^{\dagger}_{\beta\uparrow} c_{\mu\uparrow} \\
&\quad + \frac{JS}{2\sqrt{N}} \sum_{\alpha\mu\nu} \left(-2\Psi^{\mathbf{Q}}_{\alpha\mu} + \Phi^{\mathbf{Q}}_{\mu\nu\alpha}\right) c^{\dagger}_{\mathbf{Q}+\mu+\nu-\alpha\downarrow} c_{\nu\uparrow} c^{\dagger}_{\alpha\uparrow} c_{\mu\uparrow},
\end{aligned} \tag{8.21}$$

$$[H_U, M^{\dagger}_{\mathbf{Q}}] = \frac{U}{N^{3/2}} \sum_{\nu\mathbf{kq}} X^{\mathbf{Q}}_{\nu} c^{\dagger}_{\mathbf{k}\uparrow} c_{\mathbf{q}+\mathbf{k}-\nu-\mathbf{Q}\uparrow} c^{\dagger}_{\mathbf{q}\downarrow} c_{\nu\uparrow} \tag{8.22}$$

$$+ \frac{U}{2N^{3/2}} \sum_{\alpha\mu\nu\mathbf{kq}} \Phi^{\mathbf{Q}}_{\mu\nu\alpha} c^{\dagger}_{\mathbf{k}\uparrow} c_{\mathbf{q}+\mathbf{k}-\nu+\alpha-\mu-\mathbf{Q}\uparrow} c^{\dagger}_{q\downarrow} c_{\nu\uparrow} c^{\dagger}_{\alpha\uparrow} c_{\mu\uparrow}, \tag{8.23}$$

$$[H_{AF}, M^{\dagger}_{\mathbf{Q}}] = 2J_{AF} S(\gamma_{\mathbf{Q}} - \gamma_0) S^{-}_{\mathbf{Q}} + 2J_{AF} S \sum_{\alpha\mu} \left(\gamma_{\mathbf{Q}+\mu-\alpha} - \gamma_0\right) c^{\dagger}_{\alpha\uparrow} c_{\mu\uparrow}. \tag{8.24}$$

We continue now with the presentation of the commutators appearing in the application of the Green's function method.

$$[S^{\dagger}_{-\mathbf{Q}}, H_{super}] = - \frac{J_{AF}}{\sqrt{N}} \sum_{k} \gamma_k \left(S^z_k S^{\dagger}_{-Q-k} + S^{\dagger}_{-Q+k} S^z_{-k} \right) + \frac{J_{AF}}{\sqrt{N}} \left(S^{\dagger}_k S^z_{-Q-k} + S^{\dagger}_k S^z_{-Q-k} \right). \quad (8.25)$$

$$[S^{\dagger}_{\mathbf{q}-\mathbf{Q}}, H_{super}] = - \frac{J_{AF}}{\sqrt{N}} \sum_{k} \gamma_k \left(S^z_k S^{\dagger}_{q-Q-k} + S^{\dagger}_{q-Q+k} S^z_{-k} \right) + \frac{J_{AF}}{\sqrt{N}} \left(S^{\dagger}_k S^z_{q-Q-k} + S^{\dagger}_k S^z_{q-Q-k} \right). \quad (8.26)$$

$$[c^{\dagger}_{k-q\uparrow} c_{k\uparrow}, H_U] = \frac{U}{N} \sum_{k'q'} \left(c^{\dagger}_{k-q\uparrow} c_{k'\uparrow} c^{\dagger}_{q'\downarrow} c_{q'+k-k'\downarrow} - c^{\dagger}_{k'\uparrow} c_{k\uparrow} c^{\dagger}_{q'\downarrow} c_{q'+k'-k+q\downarrow} \right). \quad (8.27)$$

$$[c^{\dagger}_{k-Q\uparrow} c_{k\downarrow}, H_U] = \frac{U}{N} \sum_{k'q'} \left(-c^{\dagger}_{k'\uparrow} c_{k\uparrow} c^{\dagger}_{q'\downarrow} c_{q'+k'-k-Q\downarrow} + c^{\dagger}_{k'\uparrow} c_{q'\uparrow} c^{\dagger}_{k-Q\uparrow} c_{k+k'-q'\downarrow} \right). \quad (8.28)$$

$$[c^{\dagger}_{k'+q-Q\uparrow} c_{k'\downarrow}, H_U] = \frac{U}{N} \sum_{k''q'} (c^{\dagger}_{k''\uparrow} c_{q'\uparrow} c^{\dagger}_{k'+q-Q\uparrow} c_{k'+k''-q'\downarrow} - c^{\dagger}_{k''\uparrow} c_{k'\downarrow} c^{\dagger}_{q'\downarrow} c_{q'+k''-k'-q-Q\downarrow}). \quad (8.29)$$

Bibliography

[1] See e.g. E. L. Nagaev, Phys. Rep. **346**, 387 (2001) and references therein.

[2] See e.g. *Colossal Magnetoresistance Oxides*, ed. Y. Tokura (Gordon Breach, Singapore, 2000); E. Dagotto, T. Hotta, and A. Moreo, Phys. Rep. **344**, 1 (2001); D. M. Edwards, Adv. Phys. **51**, 1259 (2002).

[3] See e.g. J. König *et. al.* in *Electronic Structure and Magnetism of Complex Materials*, eds. J. Singh and D. A. Papaconstantopoulos (Springer-Verlag, Berlin, 2002).

[4] Y. Matsumoto, *et. al.* Science **291**, 854 (2001)

[5] S. A. Wolf *et. al.*, Science **294**, 1488 (2001).

[6] H. Y. Hwang *et. al.*, Phys. Rev. Lett. **80**, 1316 (1998); P. Dai *et. al.*, Phys. Rev. B **61**, 9553 (2000); L. Vasiliu-Doloc *et. al.*, Phys. Rev. B **58**, 14913 (1998); T. Chatterji, L. P. Regnault, and W. Schmidt, Phys. Rev. B **66**, 214408 (2002).

[7] Y. Endoh, H. Hiraka, Y. Tomioka, Y. Tokura, N. Nagaosa, and T. Fujiwara, Phys. Rev. Lett. **94**, 017206 (2005).

[8] F. Ye *et. al.*, Phys. Rev. Lett. **96**, 047204 (2006).

[9] T. G. Perring, G. Aeppli, S. M. Hayden, S. A. Carter, J. P. Remeika, and S.-W. Cheong, Phys. Rev. Lett. **77**, 711 (1996).

[10] G. Khaliullin and R. Kilian, Phys. Rev. B **61**, 3494 (2000).

[11] D. I. Golosov, Phys. Rev. Lett. **84**, 3974 (2000); Phys. Rev. B **71**, 014428 (2005); and references therein.

[12] I. V. Solovyev and K. Terakura, Phys. Rev. Lett. **82**, 2959 (1999).

[13] S–S Feng and M. Mochena, J. Phys. Cond. Matt. **17**, 3895 (2005); F. Mancini, N. B. Perkins, and N. M. Plakida, Phys. Lett. A **284**, 286 (2001).

[14] K. Wang *et. al.*, AIP Conf. Proc. **772**, 333 (2005).

[15] L. D. Landau, E. M. Lifshitz, and L. P. Pitaeviski, Statistical Physics, Part 2 (Pergamon, Oxford, 1980)

[16] H. Ohno *et. al.* App. Phys. Lett. **69**, 3, (1996)

[17] E. L. Nagaev, Phys. Rev. B **58**, 827 (1998)

[18] E. L. Nagaev, Sov. Physics Solid State, **11** (1970)

[19] See e.g. J. König, J. Schliemann, T. Jungwirth, and A. H. MacDonald, in *Electronic Structure and Magnetism of Complex Materials*, eds. J. Singh and D. A. Papaconstantopoulos (Springer-Verlag, Berlin, 2002).

[20] M. Berciu and R. N. Bhatt, Phys. Rev. B **66**, 085207 (2002); P. M. Krstajic, F. M. Peeters, V. A. Ivanov, V. Fleurov, and K. Kikoin, Phys. Rev. B **70**, 195215 (2004).

[21] See e.g. *Colossal Magnetoresistance Oxides*, ed. Y. Tokura (Gordon Breach, Singapore, 2000) and references therein.

[22] E. Dagotto, T. Hotta, and A. Moreo, Phys. Rep. **344**, 1 (2001).

[23] C. S. Zener, Phys. Rev. **82**, 403 (1951); P. W. Anderson and H. Hasegawa, Phys. Rev. **100**, 675 (1955); P. G. de Gennes, Phys. Rev. **100**, 564 (1955); K. Kubo and N. Ohata, J. Phys. Soc. Jpn. **33**, 21 (1972).

[24] N. Shannon and A. V. Chubukov, Phys. Rev. B **65**, 104418 (2002); J. Phys. Cond. Matt. **14**, L235 (2002).

[25] X. Wang, Phys. Rev. B **57**, 7427 (1998).

[26] J. Zang. H. Röder, A. R. Bishop, and S. A. Trugman, J. Phys. Cond. Matt. **9**, L157 (1997).

[27] T. A. Kaplan and S. D. Mahanti, J. Phys. Cond. Matt. **9**, L291 (1997).

[28] T. A. Kaplan and S. D. Mahanti, Phys. Rev. Lett. **86**, 3634 (2000).

[29] T. Okabe, Phys. Rev. B **57**, 403 (1998).

[30] T. Okabe, Theor. Phys. **97**, 21 (1997).

[31] P. Wurth and E. Müller-Hartmann, Eur. Phys. J. B **5**, 403 (1998).

[32] L. M. Roth, Phys. Rev. Lett. **20**, 1431 (1968); Phys. Rev. **186**, 428 (1969); Phys. Rev. **184**, 451 (1969); J. Phys. Chem. Solids **28**, 1549 (1967).

[33] B. S. Shastry, H. R. Krishnamurthy, and P. W. Anderson, Phys. Rev. B **41**, 2375 (1990).

[34] W. von der Linden and D. M. Edwards, J. Phys. : Condens. Matter **3**, 4917 (1991).

[35] H. Y. Hwang, P. Dai, S.-W. Cheong, G. Aeppli, D. A. Tennant, and H. A. Mook, Phys. Rev. Lett. **80**, 1316 (1998).

[36] P. Dai, H. Y. Hwang, J. Zhang, J. A. Fernandez-Baca, S.-W. Cheong, C. Kloc, Y. Tomioka, and Y. Tokura, Phys. Rev. B **61**, 9553 (2000).

[37] L. Vasiliu-Doloc, J. W. Lynn, A. H. Moudden, A. M. de Leon-Guevara, and A. Revcolevschi, Phys. Rev. B **58**, 14913 (1998).

[38] T. Chatterji, L. P. Regnault, and W. Schmidt, Phys. Rev. B **66**, 214408 (2002).

[39] T. Chatterji, L. P. Regnault, P. Thalmeier, R. Suryanarayanan, G. Dhalenne, and A. Revcolevschi, Phys. Rev. B **60**, R6965 (1999).

[40] N. Shannon, T. Chatterji, F. Ouchni, and P. Thalmeier, Eur. Phys. J. B **27**, 287 (2002).

[41] J. Igarashi, M. Takahashi, and T. Nagao, J. Phys. Soc. Jpn **68**, 3682 (1999); J. Igarashi, J. Phys. Soc. Jpn **54**, 260 (1985).

[42] I. E. Perakis and Y.–C. Chang, Phys. Rev. B **47**, 6573 (1993); *ibid* **44**, 5877 (1991); and references therein.

[43] J. F. Mueller, A. E. Ruckenstein, and S. Schmitt–Rink, Phys. Rev. B **45**, 8902 (1992); A. E. Ruckenstein and S. Schmitt–Rink, Phys. Rev. B **35**, 7551 (1987); and references therein.

[44] T. G. Perring, D. T. Adroja, G. Chaboussant, G. Aeppli, T. Kimura, and Y. Tokura, Phys. Rev. Lett. **87**, 217201 (2001).

[45] Y. Moritomo, A. Asamitsu, H. Kuwahara, and Y. Tokura, Nature **380**, 141 (1996); H. Martinho, C. Rettori, D. L. Huber, J. F. Mitchell, and S. B. Oseroff, Phys. Rev. B **67**, 214428 (2003).

[46] See e.g. Y. Endoh and K. Hirota, J. Phys. Soc. Jpn **66**, 2264 (1997).

[47] M. Marder, N. Papanicolaou, and G. C. Psaltakis, Phys. Rev. B **41**, 6920 (1990); L. R. Mead and N. Papanicolaou, Phys. Rev. B **28**, 1633 (1983).

[48] J. Chovan, E. G. Kavousanaki, and I. E. Perakis, cond-mat/0508178; Phys. Rev. Lett. (to be published).

[49] Y. H. Ren, X. H. Zhang, G. Lüpke, M. Schneider, M. Onellion, I. E. Perakis, Y. F. Hu, and Q. Li, Phys. Rev. B **64**, 144401 (2001).

[50] M. Vomir, L. H. F. Andrade, L. Guidoni, E. Beaurepaire, and J.-Y. Bigot, Phys. Rev. Lett. **94**, 237601 (2005); J.-Y. Bigot, L. Guidoni, E. Beaurepaire, and P. N. Saeta, Phys. Rev. Lett. **93**, 077401 (2004).

[51] N. Furukawa, J. Phys. Soc. Jpn. **65**, 1174 (1996). E. L. Nagaev, Phys. Rev. B **58**, 827 (1998).

[52] F. Ye *et. al.*, Phys. Rev. B. **75**, 144408 (2007).

[53] N. Shannon *et. al.*, Eur. Phys. J. B **27**, 287 (2002); Hirota *et. al.*, Phys. Rev. B **65**, 64414 (2002); T. Chatterji *et. al.*, Phys. Rev. B **60**, R6965 (1999).

[54] S. V. Tyablikov, *Methods in the quantum theory of magnetism*, (Plenum press, New York, 1967)

[55] S.–J. Sun, W.–C. Lu, H. Chou, Physica B 324 (2002).

[56] G. Khaliullin and R. Kilian, Phys. Rev. B **61**, 3494 (2000); I. V. Solovyev and K. Terakura, Phys. Rev. Lett. **82**, 2959 (1999); N. Furukawa, J. Phys. Soc. Jpn. **68**, 2522 (1999); Y. Motome and N. Furukawa, Phys. Rev. B **71**, 014446 (2005).

[57] H. Aliaga, Phys. Rev. B 71, 184404 (2005).

[58] M. D. Kapetanakis, A. Manousaki, and I. E. Perakis, Phys. Rev. B, **73**, 174424, (2006).

[59] M. D. Kapetanakis, and I. E. Perakis, Phys. Rev. B, **75**, 140401(R) (2007).

[60] J. Zang. *et. al.*, J. Phys. Cond. Matt. **9**, L157 (1997).

[61] P. Wurth and E. Müller-Hartmann, Eur. Phys. J. B **5**, 403 (1998); T. Okabe, Prog. Theor. Phys. **97**, 21 (1997); Phys. Rev. B **57**, 403 (1998).

[62] A. E. Ruckenstein and S. Schmitt–Rink, Int. J. Mod. Phys. B **3**, 1809 (1989); J. F. Mueller, A. E. Ruckenstein, and S. Schmitt–Rink, Phys. Rev. B **45**, 8902 (1992); I. E. Perakis and Y.–C. Chang, Phys. Rev. B **47**, 6573 (1993).

[63] J. Chovan, E. G. Kavousanaki, and I. E. Perakis, Phys. Rev. Lett. **96**, 057402 (2006); T. V. Shahbazyan, I. E. Perakis, and M. E. Raikh, Phys. Rev. Lett. **84**, 5896 (2000); M. Vomir *et. al.*, Phys. Rev. Lett. **94**, 237601 (2005).

[64] L. M. Roth, J. Phys. Chem. Solids **28**,1549-1555, (1967).

[65] J. M. C. Chen, J. W. Clark, and D. G. Sandler, Z. Phys. A **305**, 223 (1982).

[66] D. J. Thouless, *The Quantum Mechanics of Many-Body Systems* (Academic Press, New York, 1961).

[67] D. J. Rowe, Nucl. Phys. **80**, 209 (1966).

[68] D. J. Rowe, Nucl. Phys. A **107**, 99 (1968).

[69] S.-R. Eric Yang and A. H. MacDonald, Phys. Rev. B 67, 155202 (2003); and references therein

[70] G. Alvarez, M. Mayr, and E. Dagotto, Phys. Rev. Lett. 89, 277202 (2002).

[71] D. J. Rowe, Rev. Mod. Phys. **40**, 153 (1968); D. J. Rowe, *Nuclear Collective Motion: Models and Theory* (Methuen, London, 1970).

[72] J.-P. Blaizot and G. Ripka, *Quantum Theory of Finite Systems* (The MIT Press, Cambridge, 1986).

[73] E. Krotscheck, Phys. Rev. A **26**, 3536 (1982).

[74] T. Chakraborty and P. Pietilainen, *The Quantum Hall Effects: Fractional and Integral* (Springer, Berlin, 1995).

[75] J. König, T. Jungwirth, and A. H. MacDonald, Phys. Rev. B **64**, 184423 (2001).

[76] J. Schliemann and J. König, H.–H. Lin, A. H. MacDonald, Appl. Phys. Lett. **78**, 11, (2001)

[77] T. Jungwirth, W. A. Atkinson, B. H. Lee, and MacDonald, Phys. Rev. B **59**, 9818 (1999)

[78] M. Adolfath, T. Jungwirth, J. Brum, and A. H. MacDonald, Phys. Rev. B, **63**, 054418 (2001)

[79] J. Schliemann, J. König, and A. H. MacDonald, Phys. Rev. B, **64**, 165201 (2001)

[80] S.–J. Sun, H.–H. Lin, Phys. Lett. A 327 73–77 (2004)

[81] T. Jungwirth *et. al.*, Phys. Rev. B **72**, 165204 (2005)

[82] D. J. Priour, E. H. Hwang, and S. D. Sarma, Phys. Rev. Lett. **95**, 037201 (2005)

[83] J. König, H–H Lin and A. H. MacDonald, Phys. Rev. Lett. **84**, 5628, (2000)

[84] C. Yannouleas, Phys. Rev. C **35**, 1159 (1987); S. Drozdz, S. Nishizaki, J. Speth, and J. Wambach, Phys. Rep. **197**, 1 (1990).

[85] E. Feenberg, *Theory of Quantum Fluids* (Academic Press, New York, 1969)

[86] R. P. Feynmann, *Statistical Mechanics: A Set of Lectures* (Benjamin/Cummings, Massachusetts, 1972)

[87] B. Sriram Shastry and D. C. Mattis, Phys. Rev. B **24**, 5340 (1981)

[88] J. Sinova *et. al.*, Phys. Rev. **B** 69, 085209 (2004)

[89] Y. Tserkovnyak, G. A. Flete, and B. I. Halperin, Appl. Phys. Lett. **84**, 25 (2004)

[90] Y. Tserkovnyak, A. Brataas, G. E. W. Bauer, and B. I. Halperin, Rev. Mod. Phys. 77, 1375 (2005)

[91] H. J. Skadsem, Y. Tserkovnyak, A. Brataas, and G. E. W. Bauer, cond-mat/0611588

List of Figures

Acknowledgements

It is a great pleasure to thank my advisor, Ilias Perakis, for an effective collaboration during the years of my doctorate.

Also, I would like to thank the members of my committee, Profesors Nicolaos Papanicolaou and Norman Tolk, for very useful discussions.

Also, I would like to thank my best friends Christos Doudoulakis (DouDou) and Giorgos Tamiolakis (Tam). Their support and friendship during the years of our studies in The Physics Department of the University of Crete was sincere and help me to overcome many difficulties.

This thesis is dedicated to my family. To my mother Irini for her love and patience all these years, to my older brother Michael for his love and support and to his wife Athina. Finally, I would like to dedicate this thesis to my late father Dimitrios.

I would like to thank the Physics Department of the University of Crete for its warm hospitality and financial support all these years. Also, I would like to acknowledge the support of the ministry of education and the EU through the program IRAKLITOS.